

https://dspace.org/

Beneficiating high ash coal using wind sifter

Alade, Jimmy Joanah

2021
https://hdl.handle.net/10539/32946

Downloaded from a DSpace repository. https://dspace.org/

UNIVERSITY OF THE
WITWATERSRAND,
JOHANNESBURG

Beneficiating High Ash Coal Using Wind Sifter

A Masters dissertation submitted to Faculty of Engineering and the Built Environment, University of the Witwatersrand, Johannesburg, South Africa, in fulfilment of the requirements for the degree of Master of Science in Engineering

by

Jimmy Joanah Alade (1914799)

Submitted to:

The School of Chemical and Metallurgical Engineering, Faculty of Engineering and the Built Environment, University of the Witwatersrand, Johannesburg, South Africa.

Supervisor: Dr. Samson Bada

Co-supervisor: Prof. Walter Schmitz

DECLARATION

I declare that this dissertation is my own unaided work. It is being submitted for the degree of Master of Science in Engineering to the University of the Witwatersrand, Johannesburg, South Africa. It has not been submitted before for any degree or examination to any other University.



……
(Signature of Candidate)

……..30th …day of ……November……2020

(Day) / (Month) / (Year)

ABSTRACT

The concept of wind sifting for particle separation has been successfully implemented for various concentration purposes. Separators of diverse configuration have been fabricated for many decades based on this principle in various fields such as the food and furniture industries, waste management (sorting municipal solid wastes) to name a few. The wind-sifter principle is very effective for particle separation as it is based on the separation of lighter particles from heavier ones. This present study entails an investigation using a computer simulation technique, with the aid of the Lagrangian particle tracking method to observe the effectiveness of wind-sifter principle in the designing and fabrication of a dry separator. This present study details the novel application of the principle in designing and fabricating the wind sifter separator for dry coal beneficiation.

The separator was designed with the aid of Autodesk Inventor, and simulated using Star-CCM+^{TM}. The simualtion tests were performed for different particle sizes (-6.7 mm + 3.36 mm), (-3.36 mm + 1 mm) and (-1 mm), at different feed rates and air velocities. The simulation test results show that at a cut-point of 1.5 RD, a yield of 29.1%, 54.3% and 99.4% were attained at different optimum velocities for -6.7+3.36 mm, -3.36+1 mm and -1 mm particle size fraction, respectively. The optimal velocities for this study at a cut point of 1.6 g/cm^3 were 6.0 m/sec, 4.2 m/sec and 1.7 m/sec for the -6.7 + 3.36 mm, -3.36 + 1 mm and -1 mm, respectively. It was also observed from the simulation test that the size and particle density play a significant role in the separation process. To that effect, the designed separator showed great flexibility to cut at any desired relative density.

A laboratory scale wind sifter separator was fabricated based on the results from the simulation test, which served as the first applied prototype in the field of dry coal beneficiation. It was observed from both the experimental and simulation studies that most of the material feed were recovered for all particle sizes from the 4th and the 6th bin of chamber 1 and 2, respectively. The major reason for this constraint was finding an appropriate air jet angle into the first chamber, whilst maintaining adequate sifting of the incoming air to transport the lighter particles. The study had shown that with a proper air jet angle, particles can settle in their designated bins, as they achieved their terminal/settling velocities based on their size and density. It was also observed that the cumulative yield (%) from the experimental test for all fractions were higher when compared

to the simulation. This was because of the assumption made during the initial design that all the particles are perfectly spherical. A clean coal product of 16.75% ash and 27 MJ/kg was produced from a feed coal of about 31% ash content and calorific value of 21 MJ/kg dry (adb) using this separator. A novel wind-sifter separator based on the results obtained from the simulation test has been fabricated with its schematic provided in this dissertation.

ACKNOWLEDGEMENTS

To God be the eternal gratitude!

My sincerest gratitude goes to my supervisors Dr. Samson Bada and Professor Walter Schmitz for their ever present guidance and support throughout the completion of this research. I will also like to appreciate Professor Rosemary Falcon for her impactful guidance throughout the research as well as the team at CFW for helping me fabricate the separator used in this study.

I am eternally grateful to Coaltech Research Association for the financial support of as well as the DSI/NRF South Africa's SARChI Clean coal technology grant (Grant Number: 86421), and also the Clean Coal Technology Research Group of the University of the Witwatersrand. I will also like to acknowledge the School of Chemical and Metallurgical Engineering for access to research facilities.

My sincerest gratitude also goes to my darling wife Mary, my siblings, parents of blessed memories, relatives and friends for their steadfast prayers and encouragement. I also wish to in particular, appreciate Mr. Takudwa Rupere, Mr. Ayodimeji Biobaku, Mr. Andy Morgan, Mr. Damilola Macgregor, Dr. Michael Tosin Bodurin, Dr. Moshood Onifade and Dr. Jibril Abdusalam, I truly appreciate you all.

PRESENTATIONS

The following presentation on this research was made:

I. J. Alade and S.O. Bada. BENEFICIATING HIGH ASH COAL USING WIND-SIFTER SEPARATION. URL: https://coaltech.co.za/wp-content/uploads/2020/09/Coaltech-2020-Annual-Report.pdf

II. J. Alade, S.O.Bada and W. Schmitz. BENEFICIATING HIGH ASH COAL USING WIND-SIFTER SEPARATION. Oral Presentation. The South African Coal Processing Society Conference Novemeber 26th , 2020.

III. Jimmy Alade, Samson O. Bada, and Walter Schmitz. Computer-Aided Design and Fabrication of a Dry Wind-Sifter Separator. *ACS Omega*. https://pubs.acs.org/doi/10.1021/acsomega.1c02192

LIST OF ACRONYMS

adb	Air Dry Basis
ADMFB	Air Dense Medium Fluidized Bed
DMC	Dense Medium Cyclone
DMVFB	Dense Medium Vibrated Fluidized Bed
E_p	Ecart Probable or Probable Error of Seperation
EU	European Union
FGX	Fuhe Ganfa Xuanmei
HD	Heavy Duty
RC	Reflux Classifier
RD	Relative Density
ROM	Run of Mine
USD	United States Dollar
SA	South Africa
SIU	Southern Illinois University
USD	United States Dollar
VFB	Vibrated Fluidized Bed

TABLE OF CONTENT

DECLARATION i
ABSTRACT ii
ACKNOWLEDGEMENTS iv
PRESENTATION v
LIST OF ACRONYMS vi
TABLE OF CONTENT vii
LIST OF TABLES x
LIST OF FIGURES xi
CHAPTER 1: INTRODUCTION 1
1.1. BACKGROUND AND MOTIVATION 1
1.2. PROBLEM STATEMENT 4
1.3. RESEARCH AIM AND OBJECTIVES 5
1.4. RESEARCH QUESTIONS 5
1.5. LAYOUT OF THE DISSERTATION 6
CHAPTER 2: LITERATURE REVIEW 8
2.1. INTRODUCTION 8
2.2. OVERVIEW OF COAL (ORIGIN AND FORMATION) 8
2.3. COAL BENEFICIATION 9
2.3.1. WET BENEFICIATION 10
2.4. DRY BENEFICIATION 19
2.4.1. DRY FLUIDIZED BED 20
2.4.2. AIR DENSE-MEDIUM FLUIDIZED BED (ADMFB) 20
2.4.3. DENSE MEDIUM VIBRATED FLUIDIZED BED (DMVFB) OR VIBRATED FLUIDIZED BED (VFB) 25
2.4.4. MAGNETICALLY STABILIZED FLUIDIZED BED (MSFB) 26
2.4.5. AIR TABLE 27
2.4.6. AIR JIG 28
2.4.7. DRY MAGNETIC SEPARATION 30
2.4.8. FUHE GANFA XUANMEI (FGX)DRY SEPARATOR 31
2.4.9. TRIBO-ELECTROSTATIC SEPARATOR 32
2.5. WIND-SIFTER 36
2.6. THE SOUTH AFRICAN COAL MARKET 38
2.7. SUMMARY 41

CHAPTER 3: RESEARCH METHODOLOGY 42
3.1. INTRODUCTION 42
3.2. EXPERIMENTAL PROCEDURE 42
3.3. DESIGN AND SIMULATION OF THE SEPARATOR 43
3.3.1. GEOMETRY DESIGN OF THE SEPARATOR 43
3.3.2. THE SIMULATION PROCESS 49
3.4. WIND SIFTER SEPARATOR 53
3.4.1. OPERATING PRINCIPLE 55
3.4.2. CALIBRATION OF THE COAL FEEDER 56
3.5. FLOAT AND SINKANALYSIS 57
3.6. ANALYTICAL TECHNIQUES 59
3.6.1. PROXIMATE ANALYSIS 59
3.6.2. ULTIMATE AND TOTAL SULPHUR ANALYSIS 59
3.6.3. CALORIFIC VALUE DETERMINATION 59
3.7. SUMMARY 60
CHAPTER 4: RESULTS AND DISCUSSION 61
4.1. INTRODUCTION 61
4.2. SIMULATION RESULTS 61
4.2.1. EFFECT OF AIR VELOCITY 62
4.2.2. EFFECT OF INDIVIDUAL PARTICLES WITHIN THE PARTICLE SIZE DISTRIBUTION ON THE MASS YIELD 64
4.2.3. PARTICLE MISPLACEMENT IN THE SEPARATOR 67
4.3. BENEFICIATION RESULTS 73
4.3.1. CHARACTERIZATION AND WASHABILITY OF THE FEED COAL 73
4.3.2. DRY WIND SIFTER SEPARATION TEST 76
4.3.3 INFLUENCE OF AIR VELOCITY ON THE WIND SIFTER SEPARATION 79
4.3.4. REPEATABILITY TESTS AND SAMPLE LOSSES OBSERVED FOR EACH PARTICLE SIZE FRACTION 83
4.3.5. INFLUENCE OF MASS FLOWRATE ON THE WINDSIFTER SEPARATOR 87
4.4. COMPARISON BETWEEN SIMULATION AND EXPERIMENTAL RESULTS 90
4.5. SUMMARY 91
CHAPTER 5: CONCLUSION AND RECOMMENDATION 92
5.1. CONCLUSION 92
5.2. RECOMMENDATIONS 93
REFERENCES 96

APPENDIX A: WASHABILITY DATA OF ALL THREE PARTICLE SIZE FRACTION FOR FLOAT AND SINK ANALYSIS AND DRY BENEFICIATION PROCESS 111

APPENDIX B: WASHABILITY PLOTS OF ALL THREE PARTICLE SIZE FRACTION FOR FLOAT AND SINK ANALYSIS AND DRY BENEFICIATION PROCESS 115

APPENDIX C: DESIGN OF THE WIND-SIFTER SEPARATOR FROM AUTODESK INVENTOR SOFTWARE. 121

LIST OF TABLES

Table 3-1: The assigned particle diameters for each particle size fractions..... 53

Table 4 - 1: Physico-chemical properties of the feed coal.....73

Table 4 - 2: Results of proximate analysis for the feed coal of -6.7+3.36 mm particle size fraction 75

Table 4 - 3: Results of proximate analysis for the feed coal of -3.36 + 1 mm particle size fraction 76

Table 4 - 4: Results of proximate analysis for the feed coal of -1 mm particle size fraction..... 76

Table A - 1: Float and sink test result for -6.7+3.36 mm size fraction of the feed coal.....111

Table A - 2: Wind sifter separation test result for -6.7+3.36 mm size fraction at 6.0 m/sec 111

Table A - 3: Wind sifter separation test result for -6.7+3.36 mm size fraction at 4.5 m/sec 111

Table A - 4: Wind sifter separation test result for -6.7+3.36 mm size fraction at 4.0 m/sec 112

Table A - 5: Float and sink test result for -3.36+1 mm size fraction of the feed coal 112

Table A - 6: Wind sifter separation test result for -3.36+1 mm size fraction at 4.2 m/sec 112

Table A - 7: Wind sifter separation test result for -3.36+1 mm size fraction at 3.0 m/sec 113

Table A - 8: Wind sifter separation test result for -3.36+1 mm size fraction at 2.5 m/sec 113

Table A - 9: Wind sifter separation test result for -3.36+1 mm size fraction at 2.0 m/sec 113

Table A - 10: Float and sink test result for -1 mm size fraction of the feed coal..... 114

Table A - 11: Wind sifter separation test result for -1 mm size fraction at 1.7 m/sec 114

Table A - 12: Wind sifter separation test result for -1 mm size fraction at 1.0 m/sec 114

LIST OF FIGURES

Figure 2 - 1: Principle of float-sink separation adapted from Meyer, (2010) 11

Figure 2 - 2: Basic Working principle of the Dense Medium Cyclones. Image from Parnaby Cyclones, (2015) 13

Figure 2 - 3: Working Principle of the Reflux Classifier TM. Image from Rio Suerte, (2021) 15

Figure 2 - 4: Working principle of the wet jig (adapted from England et al., 2002) 17

Figure 2 - 5: Schematic diagram of the FGX dry separator and its processing system (Courtesy of FGX Sep. Tech, LLC, USA) 31

Figure 2 - 6: Principle tribo-electrostatic separator and sampling rule (Xin-xi et al., 2009) 34

Figure 2 - 7: South African coalfields (taken from Hancox and Götz, 2014) 39

Figure 3 - 1:Summary of Experimental methodology 42

Figure 3 - 2: Flow boundaries of the first chamber with its collection bins 46

Figure 3 - 3: Flow boundaries of the second chamber with its collection bins 46

Figure 3 - 4: The full separator assembly 47

Figure 3 - 5: The designed assembly of chamber 1 to depict contact regions 48

Figure 3 - 6: The designing of the chamber 2 48

Figure 3 - 7:The designed assembly of chamber 2 to depict contact regions 49

Figure 3 - 8:Mesh generated for chamber 1 and 2, respectively. 50

Figure 3 - 9: Prism layer in the first chamber 50

Figure 3 - 10: Prism layers in the second chamber 51

Figure 3 - 11: Contact regions in the first chamber 51

Figure 3 - 12: Contact regions in the second chamber 52

Figure 3 - 13: The proposed wind sifter separator assembly 54

Figure 3 - 14: The Fabricated Wind Sifter Separator 56

Figure 3 - 15: The Vibratory feeder Assembly 57

Figure 4 - 1:Effect of Air velocity and optimal velocity determination for (-6.7 + 3.36 mm) size fraction 62

Figure 4 - 2: Effect of Air velocity and optimal velocity determination for (-3.36+1 mm) size fraction ... 63

Figure 4 - 3: Effect of Air velocity and optimal velocity determination for (-1 mm) size fraction 63

Figure 4 - 4: Mass yields from the 3 particle size fractions at their respective optimal velocities 64

Figure 4 - 5:Mass yield(s) of individual particle in the particle size distribution of (-6.7 + 3.36 mm) as a function of relative density. 65

Figure 4 - 6: Mass yield(s) of individual particle at particle size distribution of (-3.36 + 1 mm)..... 66

Figure 4 - 7: Mass yield(s) of individual particle at particle size distribution of (-1 mm)..... 66

Figure 4 - 8: Particle tracks for -6.7 + 3.36 mm at RD of 1.3 in both chambers at 6.0 m/sec 68

Figure 4 - 9: Particle tracks for -6.7 + 3.36 mm at RD of 1.4 in both chambers at 6.0 m/sec 68

Figure 4 - 10: Particle tracks for -6.7 + 3.36 mm at RD of 1.5 in both chambers at 6.0 m/sec 68

Figure 4 - 11: Particle tracks for -6.7 + 3.36 mm at RD of 1.6 in both chambers at 6.0 m/sec 69

Figure 4 - 12: Particle recoveries in each bin in the first chamber for -6.7+3.36 mm 70

Figure 4 - 13: Particle recoveries in each bin in the second chamber for -6.7 + 3.36 mm..... 70

Figure 4 - 14: Particle recoveries in each bin in the first chamber for -3.36 + 1 mm 71

Figure 4 - 15: Particle recoveries in each bin in the second chamber for -3.36 + 1 mm 71

Figure 4 - 16: Particle recoveries in each bin in the first chamber for -1 mm 72

Figure 4 - 17: Particle recoveries in each bin in the second chamber for -1 mm..... 72

Figure 4 - 18: Relative density versus Cumulative Ash (%) of all three-particle sizes 74

Figure 4 - 19: Relative density versus Cumulative mass (%) of all three-particle sizes..... 75

Figure 4 - 20: Calibration of the vibratory feeder for the separation of -6.7+3.36 mm fraction..... 77

Figure 4 - 21: Calibration of the separator for -3.36+1 mm particle size fraction..... 78

Figure 4 - 22: Calibration of the separator for -1 mm particle size fraction 78

Figure 4 - 23: Cumulative Ash content for – 6.7 + 3.36 mm at different air stream velocities 79

Figure 4 - 24: Cumulative mass yield for – 6.7 + 3.36 mm at different air stream velocities 80

Figure 4 - 25: Cumulative Ash content for – 3.36 + 1 mm at different air stream velocities 81

Figure 4 - 26: Cumulative mass yield for – 3.36 + 1 mm at different air stream velocities 81

Figure 4 - 27: Cumulative Ash content for – 1 mm at different air stream velocities 82
Figure 4 - 28: Cumulative mass yield for – 1 mm at different air stream velocities..... 83
Figure 4 - 29: Repeatability test of -6.7+3.36 mm particle size fraction at 6.0 m/sec 84
Figure 4 - 30: Repeatability test of -3.36+1 mm particle size fraction at 4.2 m/sec 84
Figure 4 - 31: Repeatability Test of -1 mm particle size fraction at 1.7 m/sec 85
Figure 4 - 32: Cumulative yield (g) of all seven bins for each particle size fractions at their respective highest velocities 86
Figure 4 - 33: Cumulative yield (g) of all seven bins for each particle size fractions at their respective lowest velocities 86
Figure 4 - 34: Cumulative ash content at different mass flowrates and constant air velocity for -6.7+3.36 mm 88
Figure 4 - 35: Cumulative yield at different mass flowrates and constant velocity for -6.7+3.36 mm 88
Figure 4 - 36: Cumulative ash content (%) at different mass flowrates for -3.36+1 mm 89
Figure 4 - 37: Cumulative wt. (%) at different mass flowrates for -3.36 + 1 mm 89
Figure 4 - 38: Comparison between the Simulation and Experimental results 90
Figure 5 - 1: The particles deposition observed during repeatability testing 94
Figure 5 - 2: Identified areas in the wind sifter pointed out for optimization 95
Figure B - 1: Washability plot for the float and sink analysis of (-6.7+3.36 mm) size fraction of feed coal 115
Figure B - 2: Washability plot for the dry process of (-6.7+3.36 mm) size fraction at 6.0 m/sec 115
Figure B - 3: Washability plot for the dry process of (-6.7+3.36 mm) size fraction at 4.5 m/sec 116
Figure B - 4: Washability plot for the dry process of (-6.7+3.36 mm) size fraction at 4.0 m/sec 116
Figure B - 5: Washability plot for the float and sink analysis of (-3.36+1 mm) size fraction of feed coal 117
Figure B - 6: Washability plot for the dry process of (-3.36+1 mm) size fraction at 4.2 m/sec 117
Figure B - 7: Washability plot for the dry process of (-3.36+1 mm) size fraction at 3.0 m/sec 118

Figure B - 8: Washability plot for the dry process of (-3.36+1 mm) size fraction at 2.5 m/sec 118
Figure B - 9: Washability plot for the dry process of (-3.36+1 mm) size fraction at 2.0 m/sec 119
Figure B - 10: Washability plot for the float and sink analysis of (-1 mm) size fraction of feed coal..... 119
Figure B - 11: Washability plot for the dry process of (-1 mm) size fraction at 1.7 m/sec..... 120
Figure B - 12: Washability plot for the dry process of (-1 mm) size fraction at 1.0 m/sec..... 120
Figure C - 1: The three-dimensional Cartesian planes when starting a new drawing..... 121
Figure C - 2: XY plane slected to draw the first chamber 121
Figure C - 3: Selecting the “Sketch” tab and then “Circle”to draw the first circle..... 122
Figure C - 4: The first circle of 50 mm in dimension, representing the outlet of the first chamber 1 drawn on the XY plane. 122
Figure C - 5: lines drawn on the YZ plane to represent the outlet pipe. 123
Figure C - 6: The circle and the line drawn to create the outlet pipe of chamber 1 123
Figure C - 7: Creating the outlet of the first chamber using the “Sweep” tool 124
Figure C - 8: Outlet pipe created..... 124
Figure C - 9: Base part of the Chamber 1-outlet pipe is lifted to draw the design transition piece. 125
Figure C - 10: Circle drawn and the base of the Outlet Pipe 125
Figure C - 11: Another work plane to draw the base part of the transition piece 126
Figure C - 12: The first nozzle-transition piece designed using the “Loft” tool. 126
Figure C - 13: Line drawn to create the zigzag section..... 127
Figure C - 14: The zigzag section once the sweep is completed..... 127
Figure C - 15: Line for the raw coal-feed inlet 128
Figure C - 16: Customized workplane to draw for the raw coal inlet..... 128
Figure C - 17: Square drawn on a work plane to serve as raw coal inlet..... 129
Figure C - 18: The Design of the inlet pipe for the coal feed using the “Sweep” tool..... 129
Figure C - 19: Work plane to create the second nozzle-transition piece..... 130
Figure C - 20: The second part of the second second nozzle for chamber 1 131

Figure C - 21: Second loft completed for the second nozzle transition piece 131
Figure C - 22: The line for the bin compartment of chamber 1 132
Figure C - 23: The bin compartment for chamber 1 using “Extrusion” tool 133
Figure C - 24: Drawing of the Air-Inlet into the separator 133
Figure C - 25: Work plane for the designing of the inner section 134
Figure C - 26: The circle on the work plane extruded backwards and the circle for the inlet 134
Figure C - 27: Using the “loft” tool to design the Air inlet nozzle 135
Figure C - 28: The completed Air inlet section 135
Figure C - 29: The Drawing of the bin compartment at the base of the first chamber (Upside down view of the Chamber 1) 136
Figure C - 30: Extruding the drawn line inwards 136
Figure C - 31: Creating the remaining bin section using the “Repeated Rectangular Pattern” tool 137
Figure C - 32: Drawing a section to cut the base part away and then attach the collecting bins. 137
Figure C - 33: Cutting away the base part of the bin compartment to attach the bins 138
Figure C - 34: The first chamber, cut off to attach the collection bins 5, 6 and 7 138
Figure C - 35: Drawing of Each collecting bin to attach to the cut-off version and create contact regions 139
Figure C - 36: Attaching the bins as an assembly 139
Figure C - 37: The completed chamber 1 140
Figure C - 38: Circle of 50 mm for the Inlet Diffuser for the second chamber 140
Figure C - 39: Drawing of the Inlet diffuser-transition piece of the second chamber 141
Figure C - 40: First diffuser transition piece created using the “loft” tool 141
Figure C - 41: Drawing the first loft of the second chamber 142
Figure C - 42: Second loft for second chamber 142
Figure C - 43: Third loft for the second chamber 143
Figure C - 44: Fourth loft for the second chamber 143

Figure C - 45: Fifth loft for the second chamber 144
Figure C - 46: Circular Outline for the circular transition piece in the second chamber 144
Figure C - 47: Circlular loft for the second chamber 145
Figure C - 48: XZ plane selected to draw the pipes of the second chamber 145
Figure C - 49: Extrusion of the pipe for the collection bin of the second chamber 146
Figure C - 50: Using “Repeated Pattern” tool to design the remaining pipes for the collection bins 146
Figure C - 51: The partly completed section of the second chamber 147
Figure C - 52: Drawing of the filter section 147
Figure C - 53: Completing the filter section using the “Sweep” tool. 148
Figure C - 54: Designing the nozzle-transition piece for the Air outlet 148
Figure C - 55: Completing the nozzle-transition piece for the Air outlet 149
Figure C - 56: Designing outlet port 149
Figure C - 57:Completing the outlet port using the “Sweep” tool. 150
Figure C - 58: Designing the base section of the collecting bins 150
Figure C - 59: Outline for the connecting pipes of the base section 151
Figure C - 60: The Extruded outline 151
Figure C - 61:Drawing of the remaining connecting pipes using the “Rectangular Pattern” 152
Figure C - 62: The completed bottom section for the second chamber 152
Figure C - 63: The second chamber after assembling 153

CHAPTER 1: INTRODUCTION

1.1. BACKGROUND AND MOTIVATION

As the world's largest single source of electricity (37%), coal is predicted to globally contribute about 22% in the year 2040 and 39 % in the South East Asian electricity market, in the same year (World Coal Association, 2020). Coal contributes 70% of the world steel industries, 90% of the cement industries, 61% of the energy used to make aluminium and forms the backbone of ferro-alloys, making it a major component needed for the social and economic development and building of modern societies (World Coal Association, 2021). It is an integral commodity that will play an integral role in the economic development of nations endowed with this resource (Dwari and Rao, 2007; Yu *et al*., 2016). Globally known to be one of the fundamental fossil fuel energy resource, coal is a significant mainstay of the South-African economy as it supplies nearly all of the nation's electricity generation demands and coal contributed 38% of the global electricity generation in 2018 and 40% in 2019 (de Korte, 2010; Xia *et al*., 2015; IEA, 2018; IEA, 2019). South Africa (SA) is the 7th largest coal producer (Statistical Review of World Energy, 2021) and according to Eskom, (2021), the nation produces approximately 224 million tons of coal with 25% being exported. In an ESKOM 2018 report, 221,936 GWh of electricity was generated in South-Africa with 91% being produced from coal fired power plants (Eskom Report, 2018; Isaac and Bada, 2020; Ndou *et al*., 2020), and coal is still projected to supply about 26% to the global electricity demand in 2040 (Ko and Chang, 2008; Isaac and Bada, 2020). South Africa is at the forefront of nations producing petrochemicals from coal (Schobert and Song, 2002; de Korte, 2010; Duan *et al*., 2015) and had a collective lion share alongside natural gas and petroleum (Levi and Cullen, 2018). Coal accounted for 59% of the total primary energy supply in the year 2018 (Ratshomo and Nembahe, 2018) and presently meets 70% of installed power generation capacity (IEA-Coal-SA, 2020).

A total of USD 118.5 billion in 2019 was realized from worldwide trade of coal export with Republic of South Africa being the 7th largest producer with a revenue of USD 4.8 billion (Workman, 2020). In a report released by Vegter, (2019), it was stated that coal contributed about 24.4%, PGMs (23.5%) and gold (16.0%) to the total mineral sales in South Africa. Vegter, (2019) also indicated that approximately 465,000 workers are directly employed by the sector, and almost 1.4 million jobs created in other industries (Mineral Council of South Africa, 2017). Thus, based

on this fact and breadwinner/dependants ratio assumption, the estimated number of South African depending on this sector, "directly or indirectly for education, rents, healthcare, food etc," will be around 19.9 million (Vegter, 2019). In Mpumalanga, the Witbank coalfields possess South Africa's largest coal reserves supplying coal for local consumption and around half the saleable coal of the country for some time now (Chagwedera, 2017).

With the above-mentioned facts, coal will remain a valuable resource to SA and the entire world. The continuous decline in coal quality necessitates the need for research into more efficient beneficiation approaches (for both wet and dry techniques) to improve the coal quality and meet different applications. Coal is abundant in South Africa; the estimated reserves indicate that enough coal remains to last more than a century, assuming the current rates of usage and production remains the same (Mineral Council SA, 2019). Though, alternative energy sources like natural gas, nuclear, solar energy, etc. are projected to be progressively added to the country's total energy mix, coal will remain a the key energy source into the future because of its relative abundance and minimal cost (World Coal Association, 2020). The coal in South African is of Gondwanan origin and these coal types are known for their significant ash content. This is owing to the fact that the raw coal contains intricate mixture of mineral matter with the clean coal, making them lower ranked coal (Falcon 1986; Bada *et al*., 2010).

Coal is the most important energy source in South Africa, and it is the foundation for the metallurgical industry and feedstock for petrochemical applications (Prevost, 2003). Like every fossil fuel, coal is a carbon-rich substance originating from dead decaying biomass and similar to crude oil and gas, they originate from the anaerobic decomposition of dead flora and fauna creatures (James, 1982). Most coals are formed in a stratified sedimentary deposit, and its classification and quality changes with coalification. The beneficiation of coal is a clean coal technology (CCT) option, which produces coal of different grades for different areas of application through the removal of impurities from the valuable organic fraction. For example, it is important to separate the inorganics in the coal prior to combustion in a boiler, as these causes undue wear, heat absorption and give rise to slagging and fouling.

The Witbank coalfield is known to be South Africa's largest coal reserves as it has supplied around 50% of the nation's coal for export and local markets over a long period of time (Chagwedera,

2017). Owing to continuous production from the reserves, there has been a depletion of high quality coal in the coalfield with coal of lower quality left behind. This has led to the shift in coal mining interests of several mining companies to the Waterberg coalfield (Chagwedera, 2017; Africa Mining iQ, 2019). In a study conducted by Hancox and Götz. (2014), the Waterberg coalfield was projected to contain around 40-50% of the mineable coal left in the country and this put the reserve in a very important position for the coal mining companies. Wet beneficiation processes are very much well received within the mineral processing industry since they accomplish a higher quality product with high recovery. Some of these processes include dense/heavy media separation, hydro-cyclone, spiral, froth flotation, jig, etc. Nevertheless, there are challenges facing the wet beneficiation techniques, some of these include the use of large quantities of water which is a challenge in areas plagued with water scarcity like the Waterberg coalfield. Other problems with the wet beneficiation include dewatering and drying, the handling of slurries generated and managing of effluents produced from the process (Chagwedera, 2017). With the above-mentioned difficulties associated with wet beneficiation techniques, dry beneficiation is increasingly becoming the process of choice however, further research is required to increase its efficiency, particularly when upgrading the smaller size fractions of coal. In addition, energy is not utilized in drying the coal and this means that its calorific value does not change (Dwari and Rao, 2007).

The dry processes for coal beneficiation depend on the physical properties of coal and its associated mineral matter. Numerous researches have been conducted on dry coal beneficiation, based on the physical properties of the coal such as shape, size, density, electrical conductivity, and magnetism (Bada *et al*., 2010a; Bada *et* al., 2010b; Bada *et* al., 2012; Charan *et al*., 2016; Chagwedera, 2017; He *et al*., 2017; Chagwedera *et* al., 2018). In this research, we seek to upgrade the quality of high ash coal less than 6.7 mm, as this proportion is generated in millions of tons due to mechanized mining in South Africa with the use of wind-sifter technology. The wind sifter technology is a relatively new dry beneficiation technique, in which the principle has been applied successfully in the separation of municipal solid waste, opal sandstone, mica, food and other organic materials (Ericsson 1991; Redemann *et al*., 2008; Pettinari and Simone, 2015; Ragaert *et al*., 2017). The the first chamber of the separator designed for this study was adapted from an existing *Wind-sifter luchtscheiding* made by Trennso Technik, (**2018**)and this principle will be

applied in this research, with a new separator designed and fabricated for beneficiating South African coal.

1.2. PROBLEM STATEMENT

In recent times, the Run-of-Mine (ROM) coal quality found in South Africa is increasingly declining and this resource cannot be used without beneficiating it for certain applications. Coal with more than 40% ash is being mined in-situ in South Africa, and to meet different applications or customer's specification, the quality has to be improved. The wet beneficiation process has been the main technique utilized for many decades, producing clean coal with lower ash content and higher yield compared to dry processes. There is however an increase in the demand for dry beneficiation due to the scarcity of water, large amounts of reagents and high operational cost associated with wet beneficiation processes like dewatering and control of acid mine drainage (AMD).

The separation of particles under dry beneficiation process is based on the physical properties of the ore, and this includes the shape, size, density, electrical conductivity/resistivity, frictional coefficient and magnetic property. The complex and near density nature of coal, are responsible for the difficulty faced in separating coal efficiently, particularly South African coal with high quantity of near density materials. In order to remove the inherent inorganic minerals present in coal with the wind sifter technology, the influence of the above-mentioned coal properties will be investigated in this research.

The size, density and shape of the particles could influence the separation efficiency of coal particles in an air stream. The wider the particle size or range, the more likely particles experience different drag forces, leading to different particle velocities in the air stream. In designing a separator for an efficient separation of particles in an air stream, factors such as the flow rate and velocity of the air, drag-force, and particle size distribution, shape, and density of the coal materials must be critically observed by using computational fluid dynamics (CFD). Another factor that might influence the separation of particles under this approach is gravity and air. Since coal will be fed directly into the separator under gravity, the minerals and organic content of coal will assume different parabolic movement or particle trajectories when they interact with the air stream.

This will have an impact on the separation of the particles in the air stream in the first separation chamber. The particle density will also have an effect on separation efficiency, coal dominated with higher density particles (lower grade coal), will be prone to shorter distance and travel velocities in the air stream compared to lower density particles.

The impact of settling velocity in association with the particle density will also be considered and investigated, with more emphasis on its influence on the separation of particles in the second chamber of the separator. This research will therefore focus on designing, fabricating and beneficiating coal through the wind sifter technology based on the operational factors such as coal feed rate, air velocity and flowrate, air-jet angle in the chamber, particle size fraction, particle density, drag force, near gravity materials, static and dynamic pressure, etc.

1.3. RESEARCH AIM AND OBJECTIVES

The aim of this research is to apply Wind Sifter Technology for the dry beneficiation of South African coal, and the objectives of the research are:

I. To design and simulate the wind sifter process for dry coal beneficiation using software tools which include Autodesk Inventor and Star CCM, respectively.
II. To fabricate a laboratory scale of a prototype wind sifter separator.
III. To conduct sample runs using the fabricated unit and compare with the simulation results.
IV. To determine the impact of different particle size fractions ranging from – 6.7 + 3.36 mm, -3.36 mm + 1 mm and -1 mm on the yield and efficiency of the separator; comparing those results to that from sink/float tests.

1.4. RESEARCH QUESTIONS

The most important question in this research is “Will the separation efficiency of this dry beneficiation technique be viable enough?” This leads to four (4) sub-questions:

I. At what particle size range will highest efficiency be attained, and to what extent will the coal particle size influence the separation of the organic matter from the high ash mineral-rich particles?

II. What influence will factor such as drag force ($F_D = \frac{C \times \rho_p \times A \times u^2}{2}$), gravitational force($F_G = m \times g$) and buoyant force ($F_B = \rho_f \times V \times g$), have on the separation of particles in an air stream?

Where;

F_D is the drag force

F_B is the buoyant force

F_G is the gravitational force

C is the coefficient of drag

$c\ is\ coefficient\ of\ drag$

$\rho_p\ is\ density\ of\ particle$

$\rho_f\ is\ density\ of\ fluid(air)$

$A = cross - sectional\ area$

$u = velocity$

$F_G\ is\ the\ garvitational\ force$

$m\ is\ the\ mass$

$g\ is\ the\ acceleration\ due\ to\ gravity.$

III. How will this process affect properties such as the ash content, volatile matter, carbon content, etc.?

IV. How would the performance of the wind sifter compare to that of the sink and float analysis?

1.5. LAYOUT OF THE DISSERTATION

There are five chapters in this thesis, and they comprise of the following:

I. Chapter One which introduces this research with a background and motivation for this research. The aim and objectives of the research are also presented in this chapter.

II. Chapter Two which details the available of literature associated with the wet and dry techniques of coal beneficiation, and also on the wind sifter technique.

III. Chapter Three which gives a detailed research methodology. In this chapter, a meticulous look at how the simulation study and the experimental study, which includes both the sink

and float tests, as well as the dry beneficiation process are executed. It also includes the standards that were followed in this research.

IV. Chapter 4 presents the results of the research as well as the discussions on these results to illustrate the importance of the research. These results comprise the results of the simulation and experimental studies.

V. Chapter five presents the conclusions drawn from the study, as well as the recommendations required to optimize the dry recovery process used in this study.

CHAPTER 2: LITERATURE REVIEW

2.1. INTRODUCTION

The need for coal beneficiation cannot be overemphasized as it encompasses a series of operations performed on the run-of-mine (ROM) coal to meet specific end user needs, some of which include feed coal fired boiler, coke oven, etc. Although wet beneficiation techniques of coal give superb separation efficiency there has, in recent times been a renewed interest in the techniques of dry coal beneficiation. A few reasons of this include;

I. The elimination of the need for large amount of water used in wet beneficiation process which will ultimately lead to significantly large amounts of effluents (waste water) from the process. These effluents seep into the water table and cause environmental degradation for man, animal and plants.
II. The mitigation of the challenges faced from tailings streams disposal and water pollution under wet processes.
III. The elimination of high cost of drying of coal before utilization. This ensures the retention of the thermal value of the coal.
IV. The capital and operating expenditure for the dry beneficiation plants are far much less when compared to the wet beneficiation plants. According to Korte, (2014), the operating expenditure of dry processing plants can be as low as half of that of wet beneficiation plants while the capital expenditure can be as low as one third.

In this chapter, an overview of the origin and significance of coal was discussed. The impact of beneficiation techniques (both wet and dry) on coal quality, with emphasis on the dry coal beneficiation along with the fundamental principles driving these techniques was discussed. Lastly, information on global and local coal market was briefly discussed in order to emphasize more on the importance of coal to the world economy.

2.2. OVERVIEW OF COAL (ORIGIN AND FORMATION)

Coal seams which are currently mined in South Africa were formed roughly 200 million years ago (England *et al*., 2002). Its formation commenced during the first coal age (Carboniferous Period) at around 360 million to 290 million years ago, with the coal seams forming from the death and

putrefaction of vegetable matter from densely populated tropical forest (Wills and Napier-Munn, 2006; WCA, 2015). The dead plant materials are bio-chemically transformed into peat and under appropriate conditions (swampy conditions), formation of thick layers peats occurs (England *et al*., 2002). A typical example showing peat occurrence in South Africa can be found in St. Lucia in KwaZulu-Natal (Scholtz *et al*., 2015). The continuous accumulation and burial of these flora entities beneath the earth's crust over these periods caused the vegetation to be subjected to elevated pressures and temperatures and the flora materials goes through a metamorphosis, transforming to coal.

Coal as explained above, is a solid stratified rock and a natural fossil fuel, formed many millions of years ago from the remains of decaying trees and vegetation and occurs in layers in the earth's crust. The various conditions prevailing during the period of the flora accumulation and transformation of the vegetation, along with the extent of coalification resulted in coal with different grades, types and ranks, which influence the different area of application or utilization (England *et al*., 2002). The complex (organic and inorganic matters) and heterogeneous nature of coal, along with the condition of its formation are responsible for the difficulty faced in beneficiating coal. The run of mine (ROM) coal requires the separation of its ash forming minerals from its organic matter to produce clean coal product of higher quality for different specific application. In South Africa, clean coal products (washed coal product) with ash content less than 15% are mostly exported, while those with higher ash content, the low grades are utilized locally, especially for power generation (Jeffery *et al*., 2014).

2.3. COAL BENEFICIATION

In the area of coal utilization, especially combustion, High Efficiency Low Emissions (HELE) technologies, assist in increasing coal combustion efficiency at the same time reducing emission of pollutants. With this in mind, and the high cost implication of this technology, the coal processing industries globally must take on the challenge (declining coal quality) imposed by the consumption of this fossil fuel (Reid, 2017). With the immense contribution of coal both on the local stage and on the global stage, the inorganic minerals in coal which results in ash and gaseous emissions such as SO_X and NO_X will continue to have have damaging effects on the environment (Onifade *et al*., 2019). The quality of coal mined in South Africa and globally has reduced

overtime, a study by Mills, (2016) showed that average gross calorific value (GCV) of coal supplied from India and the USA during the last half a century, decreased from 24.7 MJ/kg to 14.7 MJ/kg and 28 MJ/kg to 20 MJ/kg respectively. Coal is predominantly composed of organic and inorganic matter which occur as macerals and minerals respectively making the coal majorly heterogeneous in nature. It is of utmost importance to reduce the inorganic minerals present in the coal to acceptable levels as this helps to improve the economic value of the coal.

All the techniques employed in coal beneficiation for the removal of these ash-bearing minerals in coal from its organic component is based on the differences in the physicochemical characteristics of the coal such as specific gravity, surface and electrical properties, particle size and grindability/friability. In spite of the research in this field over many decades, there are still challenges impacting on the recovery and the quality of the products to be overcome. Some of these challenges are due to the inadequate liberation of the coal minerals from the organic coal matrix, the coal origin etc. The following sections described the two main beneficiation techniques for coal, which involves wet beneficiation and dry coal beneficiation.

2.3.1. WET BENEFICIATION

The wet beneficiation process involves the use of water or other liquid separating medium, in beneficiating ROM coal into clean coal product and gangue material by utilizing density separation on accounts of the heterogeneity of the raw coal. In comparison to the water-only plant, the dense/heavy medium processing of coal over the years has proven to deliver more precise and accurate separation, efficient and effective automatic control with its ability to perform standalone processing. Owing to its adaptability in handling diverse coal qualities and particle fractions in the feed, it is a far more recommended technique than the water-only plant (Wills and Naper-Munn, 2006; Langner, 2016). The wet beneficiation techniques in this literature review include the float and sink technique, the dense medium cyclones (DMC), the reflux classifiers, and wet jigs, as well as chemical flotation (Langner, 2016).

2.3.1.1. FLOAT AND SINK

The float-sink technique for coal beneficiation is a technique used to partition raw coal into two or more relative densities by means different RD solution(s) and can used to determine coal properties (England *et al*., 2002; Meyer, 2010). . In this technique, the principle of gravity separation is the principal factor that facilitates the partitioning of the coal feed. England *et al*. (2002) pointed out that there is a relationship between ash content of a piece of coal and the specific gravity implying that ash content can be controlled by washing the coal at a particular specific gravity. The author(s) also stated that the shape and size of the particle play almost no part in the stationary medium, thus making it a very effective means of coal separation. Meyer. (2010) illustrates this technique in the figure below

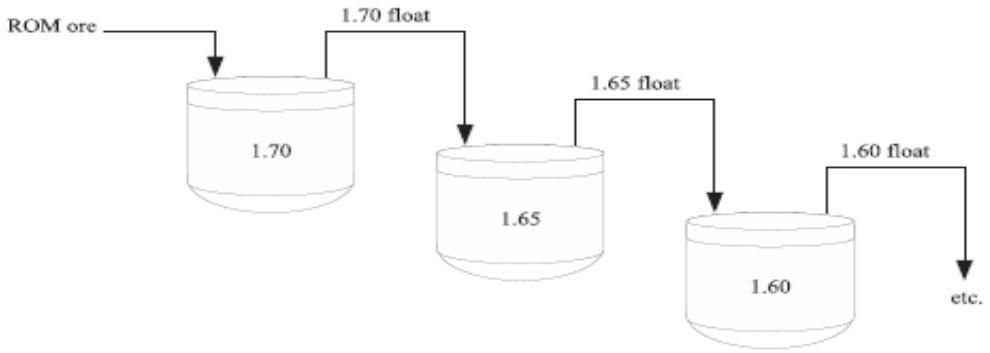


Figure 2 - 1: Principle of float-sink separation adapted from Meyer, (2010)

Killmeyer *et al*. (1992) led an inter-laboratory test program held by Pittsburgh Energy Technology Center (PETC) involving nine (9) laboratories for the upgrading coal fine coal of (-217+83 µm), (-83+48 µm) , (-48+14 µm) and (-14 µm) particle size fractions with the finest of the coal samples sent to all but one laboratory. A centrifugal float-sink technique was deployed to beneficiate coal samples from Pittsburgh Bed, Belmont County in Ohio at relative densities of 1.3, 1.4 and 1.6. In this study, two samples weighing 200 grams each were sent to the eight member laboratories and a brief summary of the results from the study showed a higher mass yield of floats as the particle size fraction was reduced. A low percentage yield was recovered (1-20%) of the 1.3 RD coal at (-14 µm) particle size fraction using organic heavy liquid medium by each laboratory involved.

Aktaş *et al*. (1998) conducted a coal beneficiation study using a centrifuge float-sink equipment to upgrade lignite coal samples from Tunçbilek and Soma–Merkez collieries. A bituminous coal

sample from Zonguldak colliery, crushed to -5 mm particle size fraction was also utilized in the study. In-organic dense medium such as Zinc Chloride ($ZnCl_2$), and organic dense medium comprising of a mixture of isopropyl alcohol (IPA) and carbon tetra-chloride (CCl_4) was used. The zinc chloride solution and the mixture of isopropyl alcohol (IPA) and carbon tetra-chloride (CCl_4) solutions were prepared at relative densities of (1.30, 1.35, 1.4, 1.45 and 1.5) and at room temperature. Also, for this study, two non-ionic surfactants (Triton X-100 and Brij-35), were used to reduce the surface tension of the dense media. The centrifuge was operated for a duration for a duration of 15 minutes at a speed of 5000 rpm and results from the study show a corresponding increase and decrease in yield and grade respectively as the liquid density was increased. As the relative density of the solution was increased from 1.30 to 1.50, the ash content of the floats (bituminous coal) increased from 1.60% to 4.52%, while the ash content of the lignite coal from Soma–Merkez and Tunçbilek collieries went from 1.31% to 5.38% and 2.20% to 9.58% respectively. The mass yield for the bituminous coal from Zonguldak increases from 54% to 90%, 4.5% to 96% for the Soma–Merkez and 4.40% to 94% for the Tunçbilek coal. The author concluded that the difference in the grade achieved between the lignite coal samples and the bituminous coal samples was as a result of the liberation difference between the two coal samples. Another study was conducted by Çetinkaya and Bayat, (2020) on low quality lignite coal from the Çanakkale lignite coalfield in Turkey at (-10+0.5 mm) particle size fraction using the float and sink technique. The total sulphur and ash content of the feed coal was reduced from 6.94% to 6.14% and 39.69% to 16.46%, respectively at a relative density of 1.6. With the float-sink technique, the responsiveness of a coal can be predetermined, as well as its amenability to gravity separation.

2.3.1.2. DENSE MEDIUM CYCLONE (DMC)

The dense-medium cyclone separation process is a well-known process in the processing of coal and is known to be one of the most efficient processes for removing inorganic minerals from run-of-mine coal. The principle of the dense medium separation (Figure 2-2) is a technique which works based on differences in density and has stood the test of time in effectively separating mineral matter from raw coal (England *et al*., 2002; Honaker *et al*., 2000).



Figure 2 - 2: Basic Working principle of the Dense Medium Cyclones. Image from Parnaby Cyclones, (2015)

Honaker *et al*. (2000) discovered that fine coal of (-1 mm) can be efficiently separated by increasing the centrifugal force which can be done by applying feed at high pressure into the dense medium cyclones. This phenomenon was also supported by Suresh *et al*. (2010) and Napier-Munn, (2018), that the efficiency of a dense medium cyclone for beneficiating fine coal of (-1 mm) is noted to depend on the high-pressure feed injection, which provides significantly high centrifugal force in the unit. The use of a pilot scale medium cyclone separator to upgrade coal of (-6+2 mm) was conducted by Suresh *et al.* (2010) under different operating parameters such as the coal feed inlet flowrate, pressure and relative density. The result from this study shows that at a relative density of 1.6, a clean coal product of 12.5% ash content with a recovery yield of 52% is achievable from a feed coal of 32% ash. The same author likewise stated that a further 5% increase in yield is attainable when the air core in the unit is suppressed compared to the air core unsuppressed

A study which integrated a pump storage system (PSS) to a dense medium cyclone coal preparation plant was carried out by Zhang *et al*. (2014) to improve energy efficiency of the plant while continuing to maintain the required supply of the medium. It was observed that the circulation loop of the medium would in turn reduce the associated energy consumption and ultimately, the cost of separating coal using this unit. A life cycle cost analysis also conducted by the author ascertain the effectiveness of the PSS approach using the operation status quo of the dense medium cyclone

plant, and the result showed that with a 160 m^3 storage tank a +50% energy cost reduction is achievable. Another scenario showed that 38% overall cost reduction with a 2.7 years payback period was attainable. The use of dense medium cyclones (DMC) and spirals are well known for upgrading coal and a combination of the two techniques was used by Ma *et al*. (2018) in a study to upgrade coal of (-1+0.125 mm). In this study, the presence of near gravity materials (NGMs) in the coal feed was minimal and the results from this study shows that a clean coal yield of 37.39%, organic recovery of 47.76% and ash content of 8.31% with a Probable Error value (E_P) of 0.150 was gotten from the spiral while the dense medium cyclone gave more acc*ep*table results with clean coal yield of 62.98%, ash content of 8.31%, organic recovery boosting to 80.84% with an E_P of 0.118.

2.3.1.3. REFLUX CLASSIFIER™ (RC™)

The Reflux classifier is an advanced type of gravity separator which has been used in the mineral and coal processing industries and has been efficient in upgrading coal of (-8 mm) and can go as low as 250 µm (Gavin *et al*., 2010; Kopparthi *et al*., 2019). The Reflux Classifier (RC™) as seen in fugure 2-3, separates fine particles based on a difference in density or particle size. In addition, it combines a conventional fluidised bed separator with a set of parallel inclined plates that form lamella channels. A coal beneficiation study using the reflux classifier technique to upgrade coal was by carried out by Gavin *et al*. (2010). In this study, the effectiveness of upgrading coal at -8 mm was critically investigated and it was observed that the process effectively produces a clean coal product with significantly low ash content. Four (4) runs of the process was carried out and separation results show that for Run 1, product mass yield of 80.3% with ash content reduced from 18.0% in the feed to 8.5% in the product. Run 2 saw a 73.7% mass yield with ash content reduced from 16.1% in the feed to 7.4% while for Run 3, product mass yield of 87.9% as 18.0% ash content in the feed coal was reduced to 10.4% in the product and for the run 4, 90.4% yield was realized with ash content brought down to 10.2% in the product from 17.3% in the feed coal.

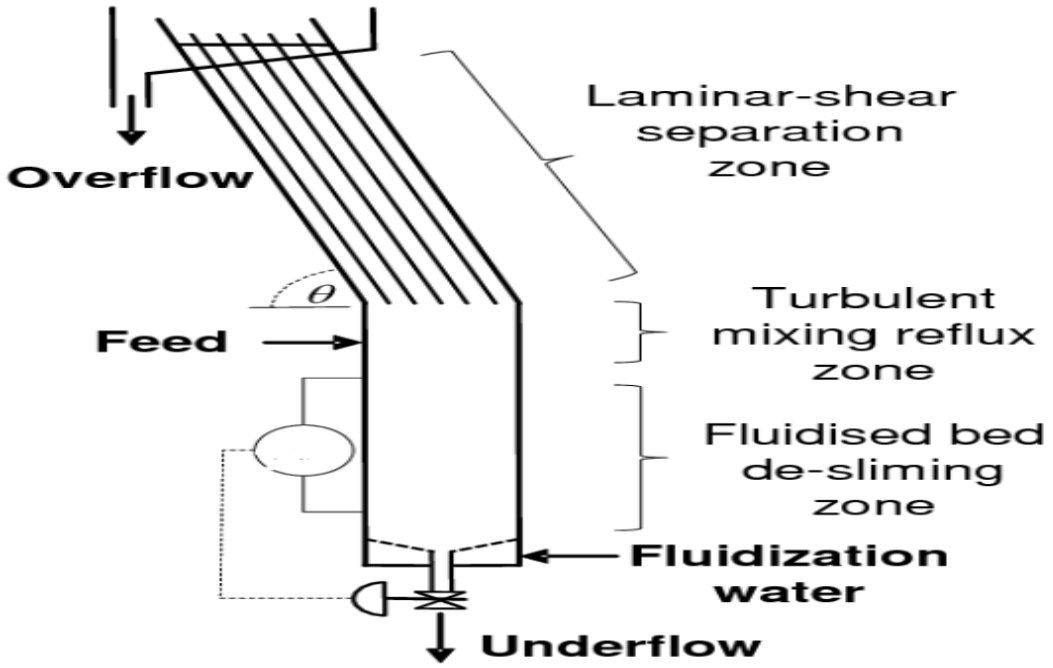


Figure 2 - 3: Working Principle of the Reflux Classifier TM. Image from Rio Suerte, (2021)

Campbell *et al*. (2015) used the reflux classifier to upgrade fine coal samples of (-1400+150 µm) from Waterberg coalfield, Limpopo. A laboratory scale reflux classifier (105 × 105 mm), with 23 steel plates arranged at a 70° angle and 3.5 mm apart was designed and built to investigate the water-only coal fractionation. The sample density was determination using a Quantachrome SPY-4 helium stereo pycnometer while a Malvern Master-sizer 2000 laser diffraction particle size analyzer was used to determine the sample size fraction. Magnetic density tracers 1 mm in size and relative densities from 1.3 - 2.0 at a 0.1 increment was also mixed in some of the test with the coal samples and used in calibrating the relationship between the fluidizing water entering the classifier and the density cut-point. The water flowrate was varied between 25-80 L/min and it was observed that turbulence was prevalent in the channels of the unit which caused unstable results when the flowrate got higher than 50 L/min The coal sample was then used alone, partitioned into (-1180+850 µm, -850+600 µm, -600+355 µm, and -355+150 µm) particle size fractions. The water flowrate was set to 35 L/min and a cut-point of relative density 1.45 was attained for the (1180+850 µm) size fraction, while cut-point of 1.55 RD was obtained for the remaining size fraction. The ash content achieved in the clean coal product was less than 25% using the separator.

Kopparthi *et al*. (2019) conducted a coal beneficiation studies on high ash coking coal fines of (-2+0.25 mm) particle size fraction. For this study, the influence of parameters such as the set-point of the bed, the fluidization velocity of water in the reflux classifier and the feed rate of the feed coal were observed. The results owing to varying operational parameters show that the coal-feed was de-ashed from 28% to a range between 7.9 - 20% ash content in the clean coal. The mass yield of the clean coal product ranged between 31 - 64% with $E_P$value ranging from 0.07 to 0.1 as separation densities varied between 1.34 - 1.7 RD. A recent study to upgrade coal using the reflux classifier was carried out by Iveson *et al*. (2019). Coal of (-6 mm) was upgraded and a comparison was made between the dense medium cyclone (DMC) which processed (-6+4 mm) and the RC^{TM} at (-4+0.5 mm). Sixteen (16) runs was carried out with the volumetric flowrate of the feed ranging from 210 – 368 m^3/h and pulp density ranging from 16 – 37 wt%. The results from the study shows that at a relative density ranging from 1.2 – 1.575, mass yield of the products ranging from 35.7 – 93.9% was obtained. Ash content in the feeds ranging from 55.6% to 11.5% was reduced to ash content ranging from 11.5% to 4.3% in the products and maximum E_P value of 0.1 was obtained.

Rautenbach *et al*. (2019) also used the reflux classifier to separate the organic matter in the coal from its inorganic mineral. 100 kg of feed coal (-75+1.7 mm) size fraction was collected from three different South African power plants. Analyses such as QEMSCAN (Quantitative Evaluation of Materials by Scanning Electron Microscopy), X-Ray Fluorescence (XRF), X-Ray Diffraction (XRD) were carried out on the coal feed sample and the clean coal products to determine their petrographic, chemical and mineralogical properties. The results from this study shows that the three coal samples utilized A, B and C have an ash content of 35.9%, 32.9% and 25%, respectively. These ashes were then reduced to 7.8% in coal A, 12.4% in coal B and 10.5% in coal C. As for the mass yield of the clean coal products, 46% for coal A, 41% for coal B and 59% for coal C was obtained.

2.3.1.4. WET JIG

Jigging is a long-lived and effective gravity separation method to upgrade large arrays of unwrought minerals such as gold (unwrought), raw coal, etc., having approximately 20% near

gravity matter (Ashish *et al*., 2011). As pointed out by England *et al*. (2002), wet jigging works on the same principle as the fluidized bed. In this separation technique, raw coal is fed on the washing deck of the jig and particles of various relative densities are partitioned based on the vertical water pulsation and factors such as viscosity effects and particle sizes also play an important role in the separation process (England *et al*., 2002; Terblanche, 2013). Langner, (2016) pointed out that remixing can occur as pulsation strength increases. A representation of the jigging process is given below by England *et al*. (2002).

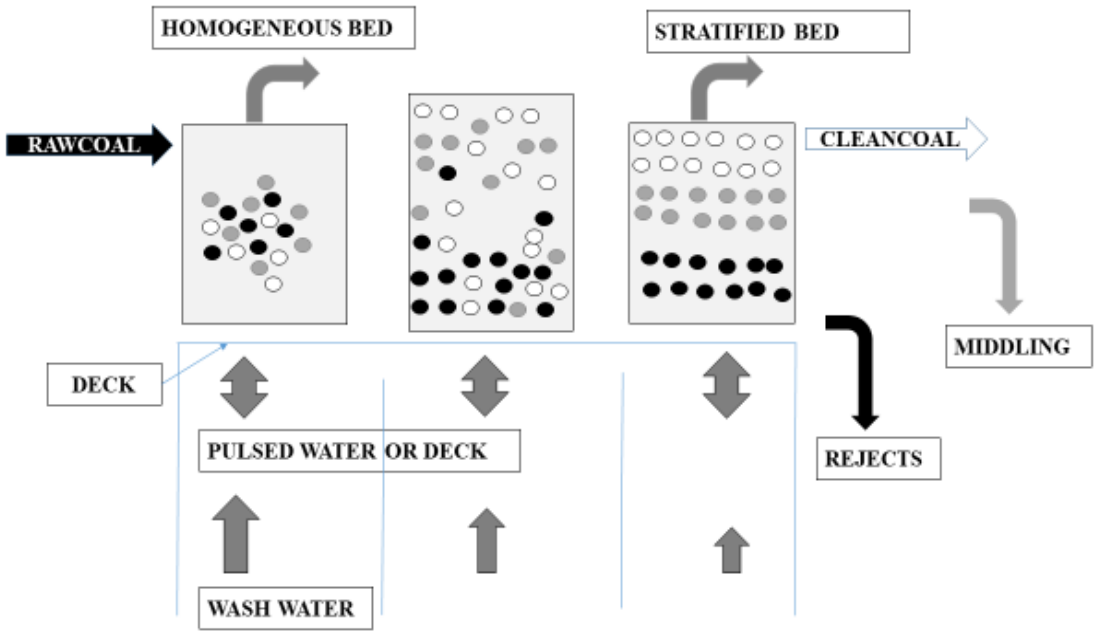


Figure 2 - 4: Working principle of the wet jig (adapted from England *et al*., 2002)

The wet jig technique was used by Rao *et al*. (2006) to upgrade (-10+6.3 mm), (-6.3+4.0 mm), (-4.0+1.0 mm) and (-1.0 mm) sample size of coking coal from Assam. The results from the study show that a clean coal product of 2.67% and 70.7% mass yield was obtained from coal sample with particle size of -10+6.3 mm. The (-6.3+4.0 mm) size fraction gave the lowest ash content of 1.89% with the highest yield of 73.7%, while for the (-4.0+1.0 mm), ash content and recovery yield of 3.29% and 64.9% were realized respectively. Tripathy *et al*. (2016) upgraded non-coking coal of (-3+2 mm, and -2+1 m) using the laboratory scale Denver mineral wet jig by varying operating parameters such as the feed rate, the water flow rate and the feed particle size. Statistical

analysis was carried out to ascertain the jig performance (combustible recovery and ash content of the clean coal product) and from this analysis, the Nelder-Mead multidimensional pattern was used for an optimization investigation of the process. The results from this study shows that 64.15% combustible recovery and ash content of 22.6% can be achieved at optimized condition.

Another study was carried out by Kumar and Venugopal (2017) using the wet jig on coal sample with (-10 mm) size fraction. The coal was screened into different particle sizes of (-10+6.73 mm, -6.73+4.73 mm, -4.73+3 mm, -3+0.5 mm and -0.5 mm). Operating parameters such as jigging time, bed height and water flowrate were varied during this study and the Box-Behnken experimental design, a test program which uses a completely randomized three level factorial design was used to optimize the operating parameter and to improve the separator performance. The result obtained show that the height of the bed was the major factor influencing the ash content and yield of the clean coal product. It was observed that at a jigging time of 10 minutes and 2 liters per minute (L/min) water flowrate, the ash content of 24.32% in the feed can be reduced up to 16.55% in the clean coal product.

2.3.1.5. FROTH FLOTATION

The froth flotation process is based on contrast in surface properties of the materials in the raw coal (Han, 1983). Several parameters (air bubbles, particles sizes and oil droplets) involved in this technique concurrently interface with each other and other species like the molecules that boost reagent and ions that dissolve in water (Polat *et al*., 2003). Air bubbles that will selectively float the clean coal products from the water slurry are created and these bubbles are attached to the clean coal particles due to their hydrophobic nature (Han, 1983). The bubbles lift the hydrophobic material to the top of the water suspension in which they are collected by skimming while the gangue is left behind in the water suspension (Lynch *et al*., 1981; Han, 1983).

A recent study to beneficiate flotation tailings was carried out by Shi *et al*. (2019) using the floatation technology. For this study, a comparison of the performance for four different collectors was carried out. The depressant used was hexa-metaphosphate and parameters such as collector dosage, the rate of inflation of the pulp concentration of the pulp, revolving speed, frother dosage as well as the depressant mechanism were all investigated. Result from the study shows at process

parameters of 300 g/t collector dosage, pulp inflation rate of 0.25 $m^3/(m^2.\text{mins})$, 4000 g/t of depressant, 500 g/t frother dosage, revolving speed of 2200 rpm and a pulp concentration of $100g/L$, optimal flotation condition was achieved. At the above stated parameters, ash content of 62.01% in the feed coal was reduced to 10.64% and a 71.88% mass yield was realized.

Cheng *et al*. (2020) recently upgraded a coking coal of (-500 µm) size fraction, using the froth flotation technique. The coal sample for this study was collected from Linhuan coal preparation plant in the province of Anhui, China. The coal samples were screened into (-500+250 µm), (-250+75 µm), (-75+45 µm) and (-45 µm) and the influence of three (3) flotation systems: the jet, countercurrent and cyclone systems were investigated. The separation result shows that the countercurrent system was very effective for the (-500+250 µm) size fraction, the cyclone for the (-250+45 µm) size fraction while the jet system was effective for the -45 µm fraction. The author noted that factors such as the environment of the flow field as well as the degree of turbulence (the turbulent kinetic energy and turbulent dissipation rate) were responsible for this observation. It was also indicated by the author that turbulent kinetic energy and the different turbulence intensities resulted in different bubble sizes, as well as the collision, detachment and attachment of the different bubble and particle sizes. The countercurrent system showed the least turbulent kinetic energy and dissipation rate while the jet flow system displayed the maximum of the three systems. The clean coal product for (-500+250 µm) size fraction showed that ash content lower than 10% and combustible recovery in the range of 62.34 - 66.16% was obtained while for the (-250+75 µm), combustible matter in the range of 49.19 – 84.09% with an ash content lower than 11%. Ash content lower than 12.5% and recovery in the range of 32.62 – 73.03% was obtained for the (-75+45 µm), while (-45 µm) saw a combustible recovery in the range of 30 – 64.54% and ash content lower than 14.5%.

2.4. DRY BENEFICIATION

The dry beneficiation techniques explore the differences in the physical properties of coal and its inherent mineral matter which include the shape, density, size, magnetic susceptibility tendencies, lustrous nature, and electrical conductivity for coal separation (Dwari and Rao, 2007; Bada *et* al., 2010a; Charan *et al*., 2016; Chagwedera, 2017). Numerous techniques have been used for the dry beneficiation of coal such as air tables and pneumatic separation, air dense medium fluidized bed,

electrostatic separators, air jigging and a few innovative approaches (Chen and Wei, 2003; Bada *et al*., 2010a; Bada *et al*., 2010b; Bada *et al*., 2012; Scholtz *et al*., 2015; Chagwedera *et al*., 2018).

2.4.1. DRY FLUIDIZED BED

There are different types of dry fluidized bed techniques which will be discussed below, they include Air Dense Medium Fluidized Bed (ADMFB), Dense Medium Vibrated Fluidized Bed (DMVFB) and Magnetically Stabilized Fluidized Bed (MSFB).

2.4.2. AIR DENSE-MEDIUM FLUIDIZED BED (ADMFB)

The Air Dense-Medium Fluidized Bed (ADMFB) is a major technique used in the beneficiation of dry coal and is deemed to be one of the most efficient methods for dry coal beneficiation (Fu *et al*., 2019). It makes use of a fluid-like mixture of the blend of a dense medium (magnetite powder) and fine coal powder as the separating medium and the separation of the coal is attained through vertical stratification (Chagwedera, 2017), and skimmers are used to remove middling and clean coal fractions along the table length (Kretzschmar, 2010). This phenomenon is similar to the sink-float process which is dependent on Archimedes' principle (Sahu *et al.,* 2009; Zhao *et al.,* 2014; Meshram *et al*., 2015).

An investigation was carried out by Choung *et al*. (2006) using the ADMFB to upgrade subbituminous coal samples from Genesee, EPCOR (Alberta, Canada). The effects of parameters such as bed height, the particle size fraction of the coal feed as well as the magnetite were investigated to assess their influence on separation efficiency. Coal sample size of (-6+1 mm) was used in this study and was crushed and partitioned into (-6+5.66 mm, -5.66+3.35 mm, -3.35+1 mm, -1+0.42 mm, -0.42+0.25 mm, -0.25+0.04 mm, and -0.04 mm) and the particle sizes of the magnetite used were (-300+150 µm, -106+45 µm, -75+45 µm, -53+45 µm and -45 µm) with the bed density at 1.6 g/cm^3. Separation results show that for (-5.66+3.35 mm) coal size, ash content of 14% in the clean coal product was achieved for magnetite of (-300+150 µm) size at air velocity of 23.5 m/sec, however the ash content was reduced to 6% with a mass yield at 90% when the particle size of magnetite was reduced to (106+45 µm) at velocity of 4 m/sec, with little to no significant improvement in the separation performance when using magnetite of (-75+45 µm) at a velocity of 2.9 m/sec. For the (-3.35+1 mm), when magnetite of (-106+75 µm) was used the ash

content of 7% in the clean coal with a yield of 70% was achieved as the bed density was lowered from 1.6g/cm^3 to 1.4g/cm^3. Separation performance for the (-1+0.42 mm) coal size fraction was very meager and it was decided that the limitation of this beneficiation process was for coal of (+1 mm).

A study was carried out by Luo *et al*. (2007) by deploying the air dense medium fluidized bed technique on raw coal of (-50+6 mm) particle size distribution. The effect of low density cut point was studied using magnetic pearls as the solid medium. The formation of microbubbles was also investigated, and the fluidization characteristics of the pearls were established for a precise particle size fraction. The results showed that the process produced a clean coal product of 90.80% mass yield with ash content of 13.95% while the ash content in the tailings was 56.82%. Prashant *et al*. (2010) carried out a study on the influence of operating parameters such as fluidizing velocity, separating time and media type on separation performance in both continuous and batch ADMFB separators. Run of mine coal of (-6+2 mm) particle size range and 25% ash content were beneficiated, and results of separation show that clean coal of 10% ash content and 80% yield was realized. Dave, (2012) carried out a study using the continuous air dense medium fluidized bed. High ash coal (-22 mm) from Genesee Mine, Alberta, Canada was used as samples for this research. The result display an 80% recovery yield with 10% ash content from a feed coal of 26% ash content. Sahu *et al*. (2009, 2011, 2013) carried out an investigation on the upgrading of high ash Indian coal using the Air Dense Medium Fluidized Bed (ADMFD) separator at (-25+6 mm) particle size fraction. A 600 kg/h capacity continuous ADMFD separator with nano-bubbling condition was fabricated by observing the fluidization stability and this characteristic was an important factor in the separation process. The result from these investigations show that yield in the range of 60-72% of clean coal product was realized as the ash content from the feed coal of 40% was reduced to a range between 32-35.5% with an E_P of 0.12.

A study also was conducted by He et al. (2013) on South African coal using the dense gas-solid fluidized bed technique. In this study, the particle size utilized was (-50+6 mm) with 78.20% of the cumulative mass distribution being 1.6g/cm^3. Simulation and experimental results of the hydro-mechanical and density distribution stability indicated that under stable operating conditions, the dense gas-solid fluidized bed gives steady separation with steady fluctuations in density. The results obtained showed with the application of this technique, feed coal sample was

separated into three product streams; clean coal product with 73.25% mass yield. Ash content of 9.59% was achieved in the concentrate, while the middling of 11.31% and gangue material of 15.44%. An ADMFB was used to beneficiate Canadian low rank coal by Azimi *et al*. (2013) where in exhaustive studies were carried out to investigate how factors such as the bed height, residence time, and superficial air velocity affects the separation performance of lignite coal with low ash content. The results from the study showed a clean coal product of 95.63% yield, 10.60% ash content and 15.29% separation efficiency achieved while working at optimal operating conditions of 150 mm bed height, superficial air velocity of 0.15 m/sec and residence time of 90 seconds. The author also observed that with an increase feed rate, a lower ash clean coal product at higher yield can be achieved.

A research was conducted by Zhao *et al*. (2015), deploying the ADMFB to upgrade coal of (-6+3 mm) size fraction. The influence of particle size of the solid medium was studied: varying size fractions of magnetite of (-0.4+0.3 mm), (-0.3+0.225 mm), (-0.225+0.15 mm), and (-0.15+0.074 mm) were investigated. The results from this research showed that the (-0.15+0.074 mm) size fraction of magnetite was most effective to achieve optimality and coal products with ash content(s) of 19.55% and 60% were realized at the top and bottom layers of the fluidizing bed respectively. Fu *et al*. (2016) carried out a similar investigation on a coal samples of (-6+3 mm) size from Northwest China, using the same particle size range of magnetite as used by Zhao *et al*. (2015) and obtaining similar result. The result from the study showed that clean coal of 31.29% ash content and a mass yield of 27.33% was achieved from the feed coal with 45.9% ash content. The total sulphur content was reduced from 3.02 – 2.57% while the calorific value increased from 13.74 – 19.40 MJ/kg.

Duan *et al*. (2015) conducted a dry beneficiation studies on (-6+1 mm) coal particle size fraction by utilizing a pulsating air dense medium fluidized bed (PADMFB) which introduces pulsating air into the air dense medium fluidized bed. For this study, the time ratio and the largest distance between equal sized falling particles were each utilized as an index to analyze the separation feasiblity of the coal based on density, and also the influence of particle size in the beneficiation process. Equations showing relationship between the time ratio and the largest distance between two equal-falling particles as they sink from the top of the bed to the bottom were derived. The

result from the study shows a feed coal de-ashed from 56.15% to 33.69, with an E_P of 0.085 at pulsation frequency of 1.82 Hz.

A study which deployed a novel air dense medium fluidized bed (ADMFB) was conducted by Zhao *et al*. (2017) from the University of Mining and Technology in China, using a binary mixture of magnetite of (0.3+0.06 mm) and fine coal (-1 mm) as the heavy medium to upgrade coal feed of (-100+6 mm). The industrial application of the approach made it the World's first ADMFB modularized dry separator and the results show clean coal with organic efficiency of 95%, ash content of 3.46% and 67.88% yield with an E_P 0.055 can be achieved. Although a 0.42 kg loss per ton of the heavy medium occurred, but less than 2 dollars was spent was spent for the separation of a ton of coal feed. Chagwedera *et* al. (2018) carried out an investigation to find an alternative dense media to magnetite with potential for use on (-13+6 mm) South African coal using ADMFB. In this study, silica sand, pyrrhotite, magnetite, coal discards and granulated blast furnace slag were investigated. The author reported that magnetite and pyrrhotite gave the most uniform and stable bed density, with a variation in the bed density under 0.7% and standard deviation under $0.0025 kg/m^3$. At 100% magnetite bed, a clean coal product of 25.24 MJ/kg and 20.30% ash content from a feed coal of 39.27% ash was achieved. From a bed of 40% pyrrhotite and 60% magnetite blend, a coal product with an ash content of 14.5% and higher calorific value of 27.3MJ/kg was also obtained. The total sulfur content of the product was also reduced from 2.49% in the feed to approximately 0.41% in the cleaner coal, and E_p value of 0.083 was achieved.

Further investigation on the blending of different medium to form a singular binary medium was investigated by He *et al*. (2018) in upgrading -13+6 mm coal. The two mediums of (-0.20 + 0.15 mm) of magnetite powder and quartz sand of (-0.35+0.25 mm) was investigated. Optimal separation result was achieved when the quartz sand was between 10-20% of the binary media. A high-grade coal product of 10.12% ash content, and 68.29% yield was achieved. The combustible material recovery of 92.09% and E_P of 0.085 was also achieved which indicate that this process has high separation efficiency. Fu *et al*. (2019) similarly used a binary mixture as heavy medium material comprising of fine coal and magnetite, both of 1.5 and 4.6 relative densities respectively and both of (-1+0.045 mm) size fraction. Run-of-mine coal samples of four (4) different coal particle size fractions of (-50+25 mm), (-25+13 mm), (-13+6 mm) and (-6+2 mm) was beneficiated separately by deploying the air dense medium fluidized bed (ADMFB) technique and results from

this study showed that the E_P and cut-point or separation density(ρ_{50}) increases with decreasing size of the coal feed and to further get a lower cut-point, the composition of fine coal in the heavy medium must be increased. The author also observed that the former three coal particle size fractions can be upgraded further.

Zhou *et al*. (2019) used the air dense medium fluidized bed for the beneficiation of run of mine coal of (-6+3 mm) size fraction. In this study, a laboratory scale ADMFB was used and the investigation was carried out with and without a micro-pore sponge. The micro-pore sponge was used to enhance the quality of the characteristics of fluidization. It was observed that the maximum pressure drop fluctuation decreased to 0.16 from 0.23 with the micro-pore sponge, showing a significant boost in the stability of the bed density. The results show that with the aid of the micro-pore sponge showed that an ash rejection from 23.83% to 10.70% with E_P of 0.12 was achieved. The author also deduced from the result that the efficiency of fine coal beneficiation with the ADMFB using the micro-pore sponge was greatly improved. A recent study by Fan *et al*. (2020) was conducted on a modified air dense medium fluidized bed which has been tapered. A magnetite of (-0.5+0.074 mm) medium material was used. The author observed that as the tapered angle increases, the separation efficiency also increased, while a further increase in the tapered angle was seen leading to the deterioration of the separation efficiency. With this modification, an optimal separation efficiency was attained at a tapered angle of 10°, ash content was brought down to 12.33% from 31.82% and the E_P value of 0.11 was attained. This indicated that the tapered fluidized bed boosted the separation efficiency of the fluidized bed for fine coal beneficiation.

Diedericks *et al*. (2020) also used an air dense medium fluidized bed separator to beneficiate South African coal of (-13.2+5.6 mm) size fraction. In this research, magnetite of (-300 µm) was used as the medium and the author exhaustively investigated the effect of vibration, particle size fraction, and medium to ore ratio on the beneficiation process. The result shows that clean coal with mass yield ranging between (82.21% - 83.93%) could be achieved with an ash content ranging between 13% - 17.6%. The author also noted that a medium of coal and magnetite greatly improved the bed stability and minimum fluidization velocity.

2.4.3. DENSE MEDIUM VIBRATED FLUIDIZED BED (DMVFB) OR VIBRATED FLUIDIZED BED (VFB)

Over time the ADMFB has been relatively efficient in upgrading coal of (+ 6 mm) particle size, however, it has been relatively inefficient for (-6 mm). The DMVFB separator is a fluidized bed which utilizes an external vibrating force to upgrade coal of -6 mm (Luo *et al*., 2008). Series of investigations have been carried out on this technique, which include, the understanding of the energy transfer mechanism and the agitation effect on the bed characteristics (Wang *et al*., 2002; Luo *et al*., (2008); Yang *et al*., 2013; Wang *et al*., 2016). The investigations carried out by Luo *et al*. (2008) portrayed the imperfections of the technique as are as following;

I. Increase in back-mixing when the vibration intensity increases, leading to downside in forming a stable bed.
II. Occurrence of unevenly transmitted vibrational forces owing to significant adhesive frictional force which resides between the particles and walls of the bed.

Luo *et al*. (2008) carried out a study deploying the DMVFB to beneficiate (-6 mm) particle size of coal. The bubble breaking mechanism in this study was exhaustively studied and the results showed that at optimal conditions, the coal of (-0.6 mm) with a lower limit of 0.05 mm was effectively beneficiated with an Ep of $0.07 t/m^3$ and proved to be more effective compared to wet jig which gave an E_P of $0.11 t/m^3$. An experimental study was carried out by Yang *et al*. (2013a, b) deploying the VFB to upgrade coal of (-6 mm) particle size and the results show that the E_P values of 0.190-0.225 and 0.175-0.195 were attained for the particle size fractions of (-6+3 mm) and (-3+1 mm) respectively, showing that this process is very effective for upgrading coal of (-6 mm). Yang *et al*. (2015) utilized the vibrated fluidized bed which was continuous operation for this study for the beneficiation of fine coal of (-3+1 mm). For this study, a thorough and methodical investigation of the fluidization and kinematic characteristics was carried out. Results from the study showed an E_P of 0.23.

An exhaustive investigation was carried out by He *et al*. (2015) using the vibrated fluidized bed to upgrade lignite coal of (-6+1 mm) particle size distribution. The homogenous transfer vibrational energy in the separator and the interaction between vibrations and the gas phase makes the process attain uniform density distribution and stable state of fluidization. The promising separation results were achieved for the (-6+1 mm) however, the coal samples were also split into (-6+3 mm), (-3+1

mm) gave more significant yields with the cut-points of 1.68 and 1.75 RD and Ep values of 0.065 and 0.055 were achieved. Mass yield of 84.46% and ash content reduction from 23.52% in the feed to 10.40% was achieved in the clean coal product for the (-6+3 mm) size fraction and the (-3+1 mm) size fraction saw a mass yield of 76.91% and ash reduction from 28.79% from the coal feed to 11.43% in the product. In summary, it could be deduced that the dusting the vibrated fluidized bed enhanced the effective beneficiation of lignite coal of (-6+1 mm) size distribution.

Fu *et al*. (2017) used the vibrated fluidized bed technique to upgrade lignite coal of (-6 mm) particle size distribution. The particles were partitioned into different sizes (-6+4 mm, -4+2 mm, -2+0.5mm, and -0.5 mm). It was observed that good separation was achieved when the (-2+0.5 mm) size fraction of the lignite was at 13% in the coal feed. Optimal separation results for the (-6+0.5 mm) was obtained at operational parameters of 0.646 m/s air velocity, fluidization time of 360 seconds, static initial height of the bed being 129.3 mm and sample feed rate of 1 kg per test. The separation results from this study show that a clean coal product with a yield of 82% and 23% ash content was realized while a yield of 18% yield and 45% ash content was realized in the tailing. The author also observed that the separator was not effective to upgrade coal of (-0.5 mm) size fraction.

2.4.4. MAGNETICALLY STABILIZED FLUIDIZED BED (MSFB)

The MSFB uses both air and magnetic field for the beneficiation of fine coal and the generated magnetic field suppresses the formation of bubbles with the increase in gas velocity while being able to suppress back mixing of the solid or gas (Fan *et al*., 2001). An experimental investigation was conducted by Fan *et al*. (2001) using this approach to upgrade coal of (-6+1 mm) size fraction and magnetic pearls of 98 µm. The separation result show that the process can effectively cut coal at a RD of 1.5 with $E_P$value of approximately 0.07. Another coal beneficiation study was performed by Fan *et al*. (2006) to upgrade ROM coal at a top size of (-50 mm). The coal particles were split into three size fractions (-50+ 6 mm), (-6+0.5 mm) and (-0.5 mm) and subjected to three different beneficiation techniques: air dense medium fluidized bed, the magnetic stabilized fluidized bed and the electro-static technology respectively. The ADMFB was very effective in upgrading the (-50+6 mm) coal, however, for the -6+0.5 mm coal, there was excessive back mixing and bubbling, therefore the magnetic stabilized fluidized bed was used for this fraction. Three

magnetic beads, the Fushun, Shiliquan and Zouxian beads, were used independently in this study, to observe the bead with the highest magnetic stability in the fluidized bed, free of bubbles or pulsation. The Zouxian beads was chosen as it was the most suited for the stated requirements for this MSFB when the magnetic field was applied. An optimal separation efficiency was achieved with an air velocity of 12.3 m/s and 30 oersted magnetic field intensity. A clean coal product of 14.6% ash and an $E_P$value of 0.066 was achieved at a separation density of 1.52g/cm^3.

A study was carried out by Song *et al*. (2012a, b) utilizing a crossflow MSFB separator to beneficiate coal of (-6+0.5 mm) size fraction, using magnetite of (-0.074+0.045 mm) size fraction. A significant separation efficiency was achieved by the author with an E_P of around (0.068-0.095). The author also stated that as the particle size of the coal decreases below 0.5 mm, the separation efficiency of the separator was seen declining continuously.

2.4.5. AIR TABLE

The stratification of particles based on the difference in their density and terminal velocities is used in air table separation technology. The air table possesses a flat deck with apertures and riffles which are uniformly distributed. Filtered air enters the deck to fluidize the coal and stratifies the coal particles depending on the particles terminal velocities. Particulate layer is formed with the lighter particles move to the top and then travel down the slope towards the discharge open while the heavier particles travel to the bottom, in the direction of the deck's vibration along the riffles (Zhao *et al*., 2014). Material in the air table moves in different directions and separation is achieved through vertical stratification of the coal particles. Skimmers are used to remove fractions of clean coal and middlings along the table's length (Kretzschmar, 2010). Çicek (2008) investigated on the technical and economic feasibility of dry beneficiation of coal using air table. Two coal feed samples (A & B) and of three different particle size ranges (-8+5 mm), (-5+3 mm) and (-3+1 mm) were upgraded and the results showed that the coal feed of (-3+1 mm) size fraction portrayed the best results, as the ash content of the coal feed A & B were reduced from 42.36% and 29.72% to 21.82% and 17.94 %, with an E_P of 0.09 and 0.20 respectively.

A study to ascertain the effects of operating parameters i.e. frequency of the table and the transverse and longitudinal angles on the yields of the clean coal products by making use of

statistical design experiments was carried out by Patil and Parekh (2011). Results from this investigation shows that the mass yield of the clean coal was around 75%-80% while ash content was reduced from 27% of the raw coal to 10%-12%. It was concluded clean coal yield decreases as the table frequency increases, however increases as the transverse inclination increases. Chalavadi and Das, (2015) used an air table separator to beneficiate fine coal at (-1 mm) size fraction. The research was done from a theoretical and an experimental point of view. Feed coal of 43% ash content was upgraded using the air table as the experiment was performed according to Response Surface Method. From the results of the separation, it was established that 10% (absolute) ash reduction with a significantly high amount of clean coal product was achieved. Using the force balance approach, a set of mathematical equations was used to describe the separation of the fine coal in the air table and it was discovered that the two key factors responsible for the separation are the horizontal segregation as well as the vertical layering. The trajectories of the particles with various particle sizes and densities on the surface of the deck were identified using simulation which then led to the product's mass yield and ash content being computed. The author discovered that the data computed and the observations from the experiment were in concurrence with very minimal discrepancies.

A modified air table, known as Southern Illinois University (SIU) air table, was utilized by Akbari *et al*. (2017) to upgrade coal at (-6.35+1 mm) size fraction. The separator was integrated with a novel deck and air distribution channel for fluidizing fine coal particles. In this study the efficiency of the SIU air table for coal beneficiation was optimized and the performance of an integrated Liwell flip-flow screen to the separator was also evaluated for 1 mm and 2 mm coal fractions. The two coal samples used in this research was from seam 6 in Illinois and the separation results showed that coal A and B had cut points (SG_{50}) of 1.70 and 1.89 and E_P values of 0.36 and 0.65 respectively. The product ash content of samples A and B were 13.8% and 14.5% while tailing ash contents were 59.7% and 52.9% respectively. The efficiency of the screening for the 1 mm and the 2 mm were 88.7 and 85.1% respectively.

2.4.6. AIR JIG

The dry jig is a deep bed separator unlike the air table, however it works on the same principle of separating gangue from clean coal by employing the difference in density and settling velocities

of particles, which is practically equivalent to the wet jig (Zhao *et al*., 2014; Charan *et* al., 2016; Chagwedera 2017). Although the clean coal and the gangue material move in the same direction, but the separation is achieved with the use of a splitter (Charan *et* al., 2016; Chagwedera, 2017). The air supply into the jig can be achieved through two structures: a consistent air stream and a superimposed pulsated air stream that gives the driving force for stratification (Zhao *et al*., 2014). Stratification is achieved by first delivering constant airflow which helps to unbind or loosen the bed, then the superimposed pulsating air is supplied to boost the stratification sufficiently (Zhao *et al*., 2014; Charan *et al*., 2016). Combining vibration with air supply boosts stratification and transportation of materials across the jigging bed (Honaker, 2007). Sampaio *et al*., (2008) utilized an air jig separator to beneficiate a high ash Brazilian coal from Candiota. This low rank coal with 1.8% sulphur content and 51% ash content was upgraded using this approach. The sulphur and the raw ash content was reduced to 0.7% and 47% respectively in the product with mass yield of approximately 71%.

An air jig which was fabricated by *Allmineral*, with a 50 t/h capacity, was used by Charan *et al*. (2011) to beneficiate an Indian high-ash non-coking coal. With this separator, a clean coal product of 33% ash content was produced from a feed coal of 40% ash at a particle size of -40 + 5 mm. An *Allair* stratification jig was used by Boylu *et al*. (2015) to upgrade a feed coal of (-13+4 mm) particle size fraction and 43% ash content. A clean coal of 17.4% ash and 48.8% mass yield was achieved in this study. Another study was conducted on Barro Branco seam in Brazil using a dry batch jig by Feil *et al*. (2011). The results obtained from this study demonstrated that an effective separation was accomplished when the coal was jigged at a frequency of 88/min, with the uppermost layer having an ash level of 39.1% and the lowest layer 74.93% contrasted with a feed coal of 54.89% ash content.

A recent study was carried out by Kumar and Venugopal, (2020) using a laboratory model of Denver air jig to upgrade coking coal of (-10+3 mm) size fraction. In this study, the coal particle size was split into three size fractions (-10+6.73 mm), (- 6.73+4.73 mm) and (- 4.73+3 mm). The influence of parameters such as the size of the coal particles, the jigging time and the height of the bed were studied to understand their effects on the separator efficiency. The separation results showed that a clean coal product of less than 17% ash content was achieved, which was the targeted ash content for coal particle size of (-5 mm) and 40 mm bed height.

2.4.7. DRY MAGNETIC SEPARATION

The dry magnetic separation is effective in beneficiating coal fines based on the magnetic susceptibility of the coal organic and its inherent minerals (clean coal product and mineral/gangue material). As pointed out by Zhao *et al*. (2014), the dry magnetic separation like the tribo-electrostatic separation technique requires a high degree in the dissociation+ of the feed coal to promote clean coal and mineral matter separation. Separation under high magnetic field occurs owing to the paramagnetic and ferromagnetic properties of mineral matter and the clean coal product which is diamagnetic in nature (Zhao *et al*., 2014; Meshram *et al*., 2015). Zhou *et al*. (1996) carried out an investigation using gravity enhanced magnetic separator (HGMS) separate mineral matter from the clean coal. In this study, a 4T superconducting solenoid magnetic to induce the magnetic field needed for the separation process and results show that optimal separation of the process showed that ash content and pyritic sulphur can be reduced by 44% and 72% respectively, whilst achieving a combustible recovery yield of 95%.

An exhaustive study to de-ash fine coal using the dry magnetic separator was carried out by Jiao *et al*. (2009). A key aim of the study was to ascertain the degree of the magnetic susceptibility, the density of the magnetic field as well as the field's intensity of the coal organic and its mineral content. It was observed in this study that a linear correlation exists between the magnetic field density and magnetic susceptibility. In addition, it was also observed that there exists an opposite polarity in the magnetism of the low- and high-density coal. The results on the separation performance of the coal tested shows that the fine coal was de-ashed and de-sulphurized by 64.41% and 55.52% respectively. Zhang *et al*. (2020) conducted a study on the de-sulphurization of (-0.5 mm) coal using a high gradient magnetic separator. The feed coal utilized was screened into different particle size (-0.5+0.3 mm), (-0.3+0.15 mm), (-0.15+0.074 mm) and the effects of the background field intensity, specific susceptibility and microwave pretreatment time, were investigated for the three coal feed. The experimental results show that 31% sulphur rejection was achieved for the (-0.15+0.074 mm) at a microwave pretreatment time of 240 seconds and a background field of 2750 Gs. In addition, a maximum sulphur rejection of 52% was achieved for (-0.074 mm) coal size fraction at 240 seconds microwave pretreatment time, background field strength of 5000 Gs.

2.4.8. FUHE GANFA XUANMEI (FGX)DRY SEPARATOR

The FGX dry separator is one of the few dry coal separators that has been utilized commercially for the beneficiation of South African coal (de Korte, 2015). The separator was initially designed by a Chinese dry coal specialist, and as of now has a few hundred separators designed (Zhao *et al.*, 2014). It utilizes the separation standards of an autogenous medium and a table concentrator (Charan *et al*., 2016). The deck vibration frequency, feeder frequency, height of baffle plate, longitudinal deck angle, vibration and the air stream all considerably influence the separation efficiency of the separator (Zhao *et al*., 2014). The FGX separator gives a moderately effective separation at high values of separation densities between 1.8 RD to 2.2 RD. Typical value of probable error (E_P) is about 0.25 (Charan *et al*., 2016). Honaker *et al*. (2008) illustrates the principle of operation of the FGX dry separator in figure 2-3 below

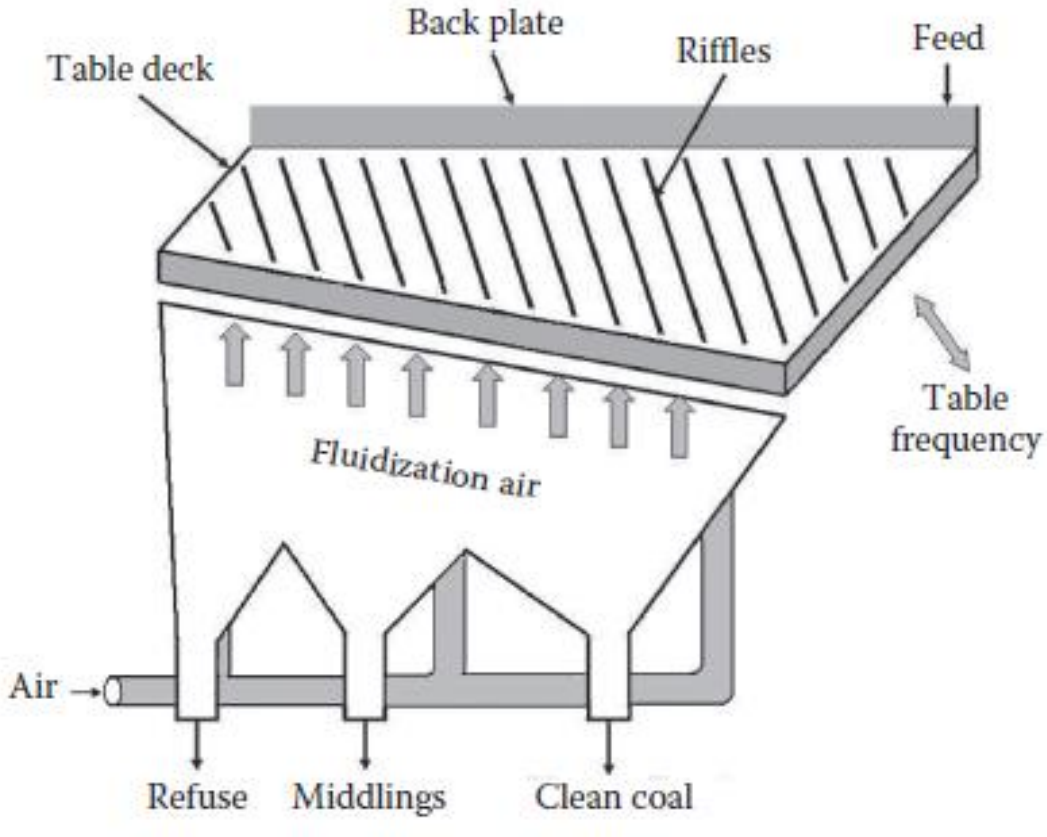


Figure 2 - 5: Schematic diagram of the FGX dry separator and its processing system (Courtesy of FGX Sep. Tech, LLC, USA)

A 5 t/h pilot-scale FGX dry separator was utilized by Honaker *et al*. (2008) to produce clean coal having characteristics that meet contract requirements and improve the measure of rejecting rocks of high-density before transportation and processing of the coal. The results from the separation evidently demonstrate that the FGX can reject more than 70% of rocks of high density from a run-of-mine coal at high separation density estimations of around 1.8-2.2 g/cm^3 with an E_P value of about 0.25. Boylu *et al*. (2015) used an Allair stratification jig to beneficiate a feed coal of 43% ash content and (-13 + 4 mm) particle size fraction. The separation results show a clean coal with a yield of 48.8% and 17.4% ash content. The FGX dry separator was also used by Ling *et al*. (2018) to upgrade run-of-mine coal from Dafeng mine in China. In this study, the FGX-3 dry separator was used to upgrade coal of 80 mm top size. The results from this study shows an ash content of 48.7% in the feed being reduced to 31.28% in the clean coal, with a yield of 65.12%. The author observed that the yield for a cleaner product increased as the size distribution of coal decreased from (-80+50 mm) to (-6+3 mm). In addition, the FGX was found not to be able to beneficiate the -3 mm fraction effectively.

Hacifazlioglu, (2018) used the FGX dry separator to carry out a beneficiation studies on low rank lignite Turkish coal. In this study the FGX dry separator in conjunction with an infra-red (IR) drying to increase the net calorific value of the coal to 10.46 MJ/kg from 6.90 MJ/kg as the minimum energy requirement for lignite coal in Turkish coal market is 10.46 MJ/kg. Optimal result from the FGX dry separator was achieved at operational parameters of 15 mm baffle height, 50% air rate, longitudinal angles of (-1º) and (5º) latitudinal angle, and 48Hz motor frequency. A clean coal product of 70.30% yield with an ash content of 35.20%, combustible recovery of 82.57% and 84.70% organic efficiency was realized from this process. The net calorific value obtained from the clean coal using the coal product from the FGX dry separator was 9.37 MJ/kg and the IR drying process was used to decrease its humidity and thus increase the net calorific value to a saleable benchmark of 10.46 MJ/kg.

2.4.9. TRIBO-ELECTROSTATIC SEPARATOR

The tribo-electrostatic beneficiation process is an advanced coal cleaning process which can upgrade -300 µm particle size fraction feed coal congruously (Dwari and Rao, 2008; Xin-xi *et al*.,

2009; Zhao *et al*., 2014) and Meshram *et al*. (2015) states that this technique can effectively beneficiate fine coal (-74 μm) size fraction. This technique utilizes contrasts in electrical conductivity characteristic of the clean coal and mineral matter in the coal feed (Bada *et al*., 2010). Three key mechanisms involved in the electrostatic separation process as stated by Dwari and Rao, (2007) are conductive induction, tribo-electrification and corona bombardment. Coal feed particles in this technique are charged as they pass through the tribo-electrostatic charger where it gets either positively or negatively charged and the charged particles are subjected to undergo a free fall as they pass through an electrostatic field in the separation chamber, making mineral matter and the clean coal become attracted to opposite plates thus producing clean coal and gangue stream (Chagwedera, 2017; Zhao *et al*., 2014).

It is important to note that this process requires a certain amount of particle dissociation in the feed material, which implies that each particle must be independent of each other so as to allow for deflection to be established when passing through the electro-static field (Zhao *et al*., 2014) and although yield of this technique is low on average, high grade clean coal products with significantly low ash content are realized (Soong *et al*., 2001; Xin-xi *et al*., 2009; Zhao *et al*., 2014). Xin-xi *et al*. (2009) showed the principle of this process in the figure 2-4 below

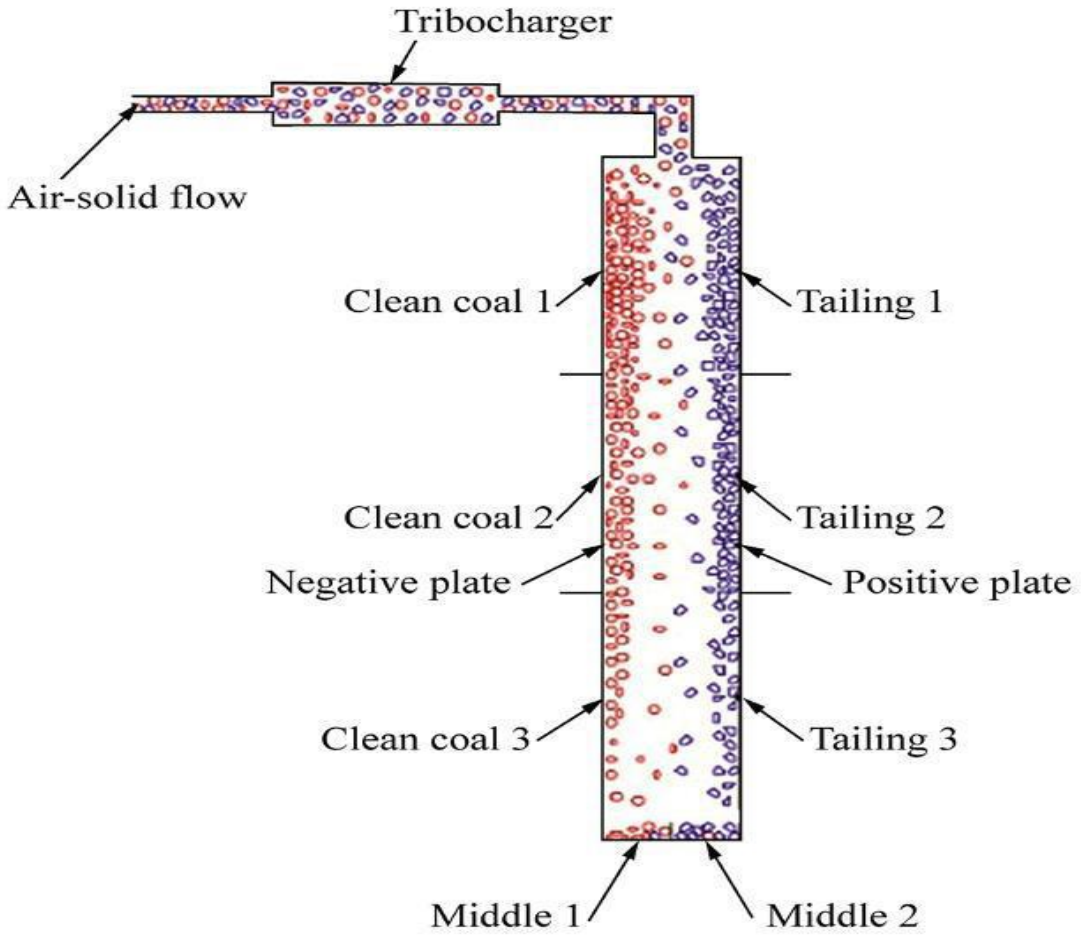


Figure 2 - 6: Principle tribo-electrostatic separator and sampling rule (Xin-xi et al., 2009)

A study was carried out by Soong *et al*. (2001) utilizing the triboelectric separation technique to upgrade three coal samples from Ci'gel, Handlova', and Nova'ky in Slovakia. The feed coals were screened to particle size of (-15 µm) for the Ci'gel coal, (20 µm) for the Handlova coal, while the Nova'ky coal was screened to (-12 µm) size fraction. The result shows that the separation process was unexceptional, with ash contents of 51.58% in the Handlova coal feed reduced to 39% and a combustible recovery of 78%, which can be further reduced to 31% ash content with a corresponding 38% combustible recovery. The Ci'gel coal feed had 48.74% ash content reduced to 40% in the product with a 58% combustible recovery and the ash content can be reduced further to 33% but the combustible recovery drops to 28%. The Nova'ky coal feed with 28.24% ash content was reduced to 22% in the product with combustible recovery of 22%. Dwari and Rao, (2009) also carried out another research utilizing a tribo-electrostatic separator to upgrade Indian

thermal non-coking coal at -300 µm. A clean coal product of 18% ash from 43% feed coal and yield of 30% was achieved.

Xin-xi *et al*. (2009) conducted coal beneficiation using tribo-electrostatic separator on -75 µm particle size fraction of coal. Results from this test shows that 69.31% – 71.27% of quartz, 75.66% – 81.93% of kaolin and 86.74% – 90.52 % of pyrite in coal can be removed. Bada *et al*. (2010) utilized a rotary tribo-electrostatic separator for the separation of South African coal at -177 µm. The investigation was carried out under various process parameters such as air injection velocity, feed rate, applied charging and separating voltage, and splitter position. The results showed that Majuba raw coal of 30% ash content was de-ashed to 14.30% and 10.82% after two stages of separation and at different separating voltage. A coal beneficiation study was conducted by Dwari *et al*. (2015) to upgrade high ash Indian coking coal. In this study, the electrical and chemical properties of the carbon, kaolinite and quartz constituent of the coal sample were investigated, the tribo-charging medium used was copper and the design parameters of the separator such as the plate angle and gap were studied to achieve optimality of the separation performance. It was observed that the carbon, kaolinite and quartz acquired different amounts of absolute charge and as the tribo-charging time increased, the magnitude of charge also increased. Separation results from this research shows that at a 5º plane inclination, the feed coal of 53% ash content could be upgraded to attain 33% ash content in the clean coal with a feasibility of attaining 10% ash content with yield of 61%.

Some unorthodox/innovative techniques for dry coal beneficiation and one of such technique was carried out by Yang *et al*. (2018) utilizing a planar air jet to upgrade coal of (-6+2 mm) size fraction. This separation technique made use of the difference in the densities of the coal particles when traveling through the planar air jet flow field in a horizontal direction. The result obtained from this study shows that the separation process produced a clean coal yield of 56.75% with ash content of 16.61% from feed coal with ash content of 26.92%. Another novel technique was also applied by Dong *et al*. (2019) on coal of two particle size fractions (-100+50 mm) and (-50 mm). The innovative approach for this study entails a combination of two separators; an air dense medium fluidized bed (ADMFB) and an FGX dry separator connected in series. The fluidization characteristics was studied for the AMDFB and for the FGX dry separator, the process of coal transportation and the extent of de-ashing under different vibration parameters (i.e., the vibration

amplitude and vibration frequency) were investigated. The result from the study showed that optimum separation efficiency for the ADMFB was attained at an air velocity of 0.11 m/sec air, yielding a 90.96% clean coal product with a 7.86% ash content. The separation efficiency for the FGX was optimal at a vibration frequency and amplitude of 18 Hz and 2.2 mm respectively with a yield of 90.30% and a 13.28% ash content.

2.5. WIND-SIFTER

This research intends to apply wind sifter technology as a novel approach in the field of dry coal beneficiation. The technology has been utilized in the separation of other minerals and organic materials (Nishinari *et al*., 1992; Krauß *et al*., 2002; Redemann *et al*., 2008; Giani *et al*., 2014; Krüger *et al*., 2014; Evangelopous *et al*., 2018). The technology was also utilized by Redemann *et al*. (2008) in managing ash production in the circulating fluidized bed combustors firing refuse-derived fuel (RDF) and coal. In addition, it was also used in monitoring the transportation of a mixture of fuel and limestone, from a hammer mill, into the combustion chamber. A research using the wind-sifter was conducted by Krüger *et al*. (2014) on the separation of toxic substances from refuse derived fuels by using a fluidized bed. The author utilized a zigzag wind sifter in this study for waste treatment through a sorting processes to remove impurities and achieve a better quality of refuse derived fuel.

A study on the Material Advanced Recovery Sustainable Systems (MARSS), which was funded by the EU Life Plus Program was conducted by Giani *et al*. (2014) in which the wind-sifter was deployed. The research entailed a combination of mechanical and biological treatment of municipal solid wastes (MSWs) and the aim of the research was to obtain biomass fuel to power biomass power plant. A comprehensive characterization program waste was carried out on the municipal solid. The results showed that the biodegradable portions were in the (-40 mm) particle size fraction, with 45% of energy content (calorific value) concentrated in the (-10 mm) fraction and having less than 2% fossil fuel carbon content. From the results, it was recommended that the MSW be sieved with biogenic fabric as further information showed screening the MSWs of (-11.5+4 mm) size fraction will boost the heating value to 13.3MJ/kg. The wind sifter was utilized to partition the heavy inert portion from the lighter desired materials and to obtain the required particle size distribution. Lofti *et al*. (2015) conducted a study to reduce the amount of pollutants

in recycled aggregates for high grade utilization. A combination of smart demolition technologies coupled with innovative techniques to produce high-grade recycled aggregates (RA) with very low pollutants were examined. The wind sifter technology combined with near infrared (NIR) sorting was deployed for this study and results show that although the (+16 mm) fractions of the recycled aggregates still had visibly large fragments of plastic and wood, the (-16+4 mm) size fraction were within the stipulated EU standard. The results overall showed that although the NIR sensor sorting system when used by did not effectively remove small contaminants, however the combination of the wind sifter and the NIR sorting proved to be very valuable for the process.

A study was conducted by Adamčík *et al*. (2017) utilizing the wind-sifter in a rotor air classifier for the classification of particulate material into fine and coarse particles. Operating parameters such as the inlet air velocity, feed rate of the particulate material, the speed of the rotor and their influence on turbulent flow field patterns within the air classifier were investigated. The wind sifter unit in this study was installed together with a centrifugal fan (for air recirculation) and was used for the separation and transportation of particles. De la Fuente *et al*. (2018) also utilized the wind-sifter technology in research which was based on assessing the life cycle decentralized mobile production systems to pellet logging residues under North European conditions. The wind-sifter was used in conjunction with other equipment such as a chipper and a fractioning machine to work as a unit in order to separate contaminants such as gravel and stones after a fractioning process separated fines from wood chips. Another investigation was carried out by Evangelopoulos *et al*. (2018) utilizing the wind-sifter in a pyrolysis process of automotive shredder residue at low temperature to recycle metals for energy recovery. The automotive shredder residue is the leftover fraction, which are the lighter particles from the metal recovery process. The process in this study is based on recovering useful metals from municipal metallic wastes of vehicles which have exhausted their “useful-life”, and the wind sifter was deployed to remove the residue of the shredder in the process.

2.6. THE SOUTH AFRICAN COAL MARKET

A well supplied global market for coal utilization is made possible through commercial mining in more than 50 countries and utilization in 70 or more countries (World Coal Association, 2020). The Republic of South Africa produces an average of 224 million tons of coal on an annual basis (ESKOM, 2021), meeting around 70% of the installed power generation capacity (IEA, 2021). Present coal reserves are deemed to sustain the nation's coal consumption for over a century assuming production rates remain the same (Mineral Council South Africa, 2019), with largest coal deposits in South Africa found in the Ecca deposits, a part of the Karoo super group which covers around two-thirds of the country and contains more than a third of the coal reserves in the entire Gondwanan region (Cairncross 2001; Mining Africa, 2019). The figure below shows nineteen (19) generally accepted coalfields in the nation of South Africa. Present coal reserves are deemed to sustain the nation's coal consumption for over a century assuming production rates remain the same (Mineral Council South Africa, 2019). Largest coal deposits in South Africa are found in the Ecca deposits, a part of the Karoo super group which covers around two-thirds of the country and contains more than a third of the coal reserves in the entire Gondwanan region (Cairncross 2001; Mining Africa, 2019). The figure below shows nineteen (19) generally accepted coalfields in the nation of South Africa.

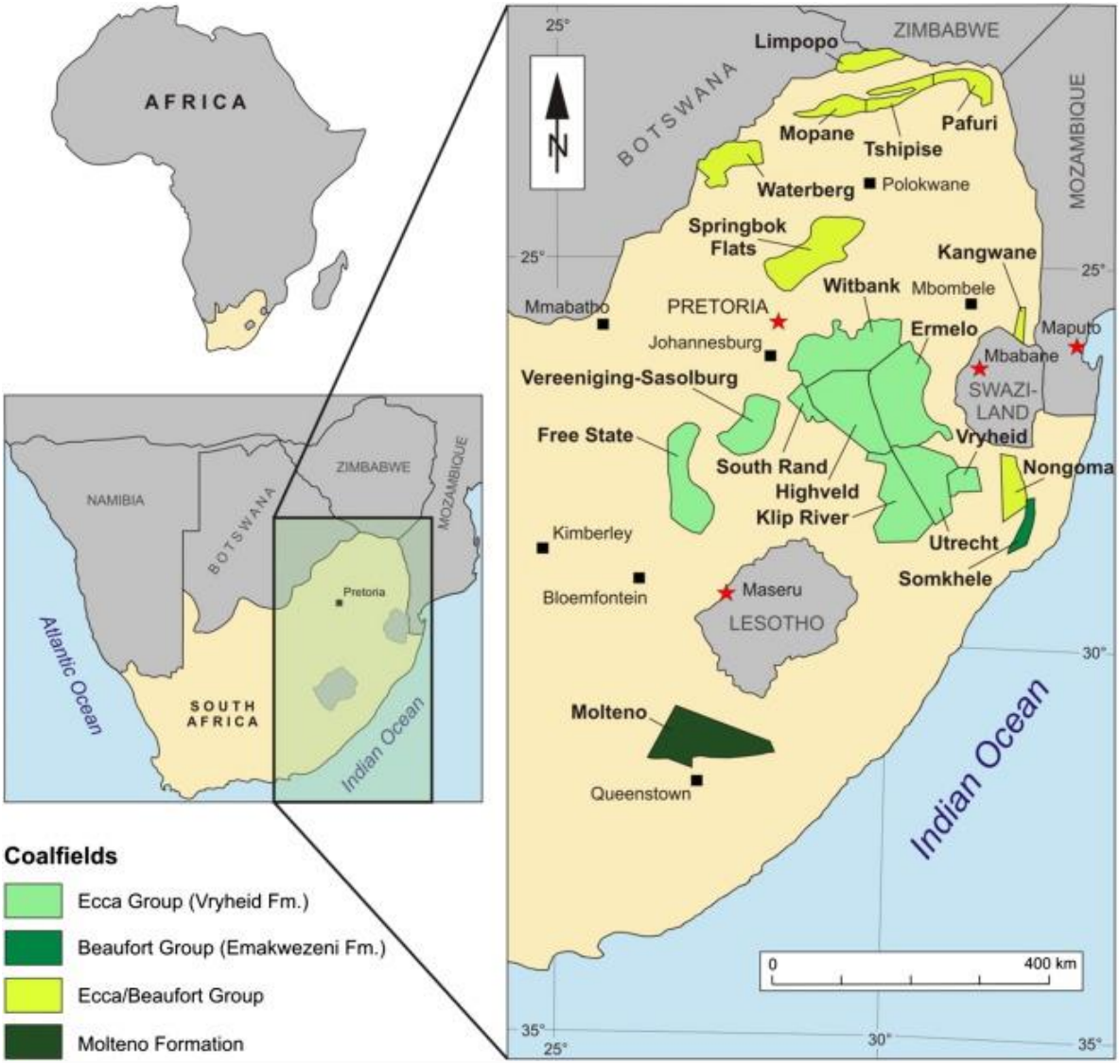


Figure 2 - 7: South African coalfields (taken from Hancox and Götz, 2014)

Of the 19 coalfields, the Highveld coalfield serves as the epicenter of coal mining in South Africa although the Witbank Coalfield (having about 22 collieries) has being the major coal reserves for the nation with approximately 60% of the coal deposits (Africa Mining iQ, 2019). Coal mining interest is beginning to shift to the Waterberg and other coal fields in the Limpopo province owing to the collieries in Emalahleni coalfields are gradually approaching their useful life (mineral council south Africa, 2020).

In 2018, an estimated 1169 million tons of coal was traded on the global stage, accounting for 21% of total coal that was utilized as the lion share of the coal was being consumed locally (World Coal

Association, 2020). In the same 2018, local coal mines in South Africa produced 253 million tonnes of coal (212.52 million tonnes in 2017), putting South Africa in top ten producers of coal (Creamer Media's Coal report, 2019). The year 2017 saw 2% contribution to the South Africa's GDP as the coal mining sector saw a 253 million tons coal production and in the next year, export and local sales of coal when pooled together reached R139.4 billion with about 87,000 people employed by the sector (PRNEWS, 2019). From 1990 to 2017 in South Africa, energy production has increased by 37.39% from 115 to 158 million tons of oil equivalent (Mtoe), total primary energy supply increased by 46.67% from 90 Mtoe, electrical final consumption increased by 45.51% from 156TWh to 227 TWh, and this has also caused 72.95% increase in CO_2 emissions from 244 to 422 million tons (IEA 2020). Some information about the coal industry as pointed out by the Mineral Council South Africa, (2019, 2020) are as follows;

I. The coal industry in 2019 employed 92,230 individuals making 19% of the total employment in the mining industry, employing 86, 647 people in 2018 and 82,248 employed in 2017.
II. About 258.9 million tons (Mt) of coal was produced in 2019, total sales was R139.3 billion. In 2018, 253Mt was produced with total sales of R146 billion.
III. 70-80% of coal produced is consumed locally with more than 70% meeting the electricity demand
IV. R61 billion was spent by the coal industry to procure mostly local goods and services which in turn contributed to job creation and maintenance in other industries.

For the South African coal export market, even though India, South Africa's biggest patron agreed to cut down its economy's dependence on fossil fuel and thus, green-house-gas (GHG) emissions by a margin of 20%-25% from 2005-2020, this really hasn't impacted the export of coal to the nation (Mineral Council South Africa, 2020). In the South-African mining industry, coal accounts for 28% of total sales of minerals during an average year, outpacing other minerals in the mining industry with platinum and gold coming in 2nd and 3rd place with 21% and 15% respectively (Gaille, 2018) and it was ranked the number 1 selling commodity in South-Africa as of June 2019, pulling in an income of R11.64 billion at 26.02% with platinum group metals (PGMs) and Iron ore coming in at 2nd and 3rd with revenue of R11.48 billion at 25.47% and R6.17 at 13.80% while

gold experienced a decline moving to 4th with revenue of R5.87 at 13.13% (South Africa's Mining industry, 2019). South Africa ranks 5th largest thermal coal producer globally as it accounts for 7% of the seaborne market, with a total of around 73.5million tons of coal exported in 2018 according to the Richard Bay Coal Terminal in KwaZulu-Natal (Creamer Media's Coal Report, 2019).

2.7. SUMMARY

The wind sifter has been used in numerous studies for diverse applications however, there has been no literature of this technology in the field of dry beneficiation of coal. The ability of this technique to separate lighter particles from heavier ones is an integral feature which will potentially make this technique a good addition of techniques in the field of dry coal beneficiation. The potential of the wind sifting principles will be meticulously investigated in this study. This will add more to the available literature in the public domain on dry coal beneficiation techniques and provide an insight into the performance of the separator designed, with the possibility of improving the design as well as its operating parameters.

CHAPTER 3: RESEARCH METHODOLOGY

3.1. INTRODUCTION

In this chapter, the procedures and characterization techniques used in analyzing the coal samples utilized in this study, along with the simulation and experimental investigation conducted were outlined. The design and simulation software, the equipment, materials utilized as well as information on the experimental standards utilized are provided.

3.2. EXPERIMENTAL PROCEDURE

The procedures followed in this study is depicted in Figure 3-1, with the designing of the separator being the first of the task outlined conducted. Thereafter, the fabricated separator was used in the beneficiation of the coal at different particle size fractions (-6.7+3.36 mm, -3.36 +1 mm and -1 mm), with the clean coal products obtained under different conditions analyzed for their heat content, ash content, and carbon content etc.

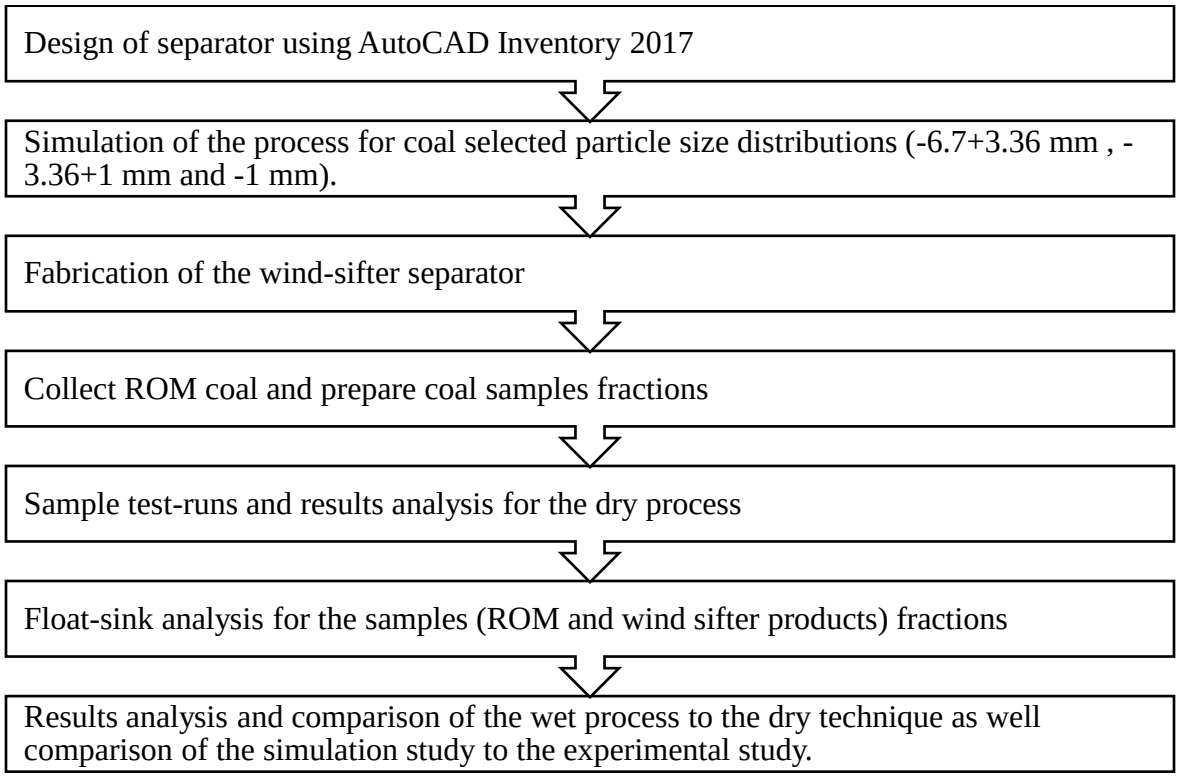


Figure 3 - 1:Summary of Experimental methodology

3.3. DESIGN AND SIMULATION OF THE SEPARATOR

3.3.1. GEOMETRY DESIGN OF THE SEPARATOR

The wind-sifter separator was first generated using AutoCAD Inventory 2017 as can be seen in **Appendix C**, and was then exported into Star-CCM+ for the simulation process. Important factors like the velocity of the airstream, air-jet angle, size and density of the particle, drag force, buoyant force, force of gravity and friction on the wall of the separator were considered as major parameters during the design of the separator. The inter-particle interactions are negligible owing to the minimal mass flowrate, which ensure that a dilute phase of the particles in the air stream was established. The gas phase (airstream) was treated as a continuous phase with the equations below providing the guiding model used in describing the forces experienced by the particles at any location in the separator. The basic equation used arises from the Euler equation that is written below.

$$\begin{cases} \left(\frac{d\rho}{dt} = -\rho\nabla.u\right) & (\text{Equation } 3-1) \\ \left(\frac{du}{dt} = -\nabla\left(\frac{P}{\rho}\right) + \mu\nabla^2 u + g\right) & (\text{Equation } 3-2) \\ \left(\frac{de}{dt} = -\frac{P}{\rho}\nabla.u\right) & (\text{Equation } 3-3) \end{cases}$$

Equations 3-1, 3-2 and 3-3 above show conservation of mass, impulse and energy, respectively, when written in their derived material form. The flow is assumed to be steady state, hence, the velocity is constant and $\nabla u = 0$. This implies that the terms $\frac{d\rho}{dt}$ and $\frac{de}{dt}$ equals zero. The temperature of the air is assumed to be at $20\ ^0$C. This implies that the dynamic viscosity (μ) of air with a value of 1.6×10^{-5} $\text{pascals} - \text{seconds}$ (Pa.s), which is infinitesimal and considered negligible (tends to zero) hence, equations 3-1, 3-2 and 3-3 above can be rewritten as;

$$\begin{cases} \left(\frac{dp}{dt} = -\rho\nabla.u = 0\right) \\ \left(\frac{du}{dt} = -\nabla\left(\frac{P}{\rho}\right) + g\right) \\ \left(\frac{de}{dt} = -\frac{P}{\rho}\nabla u = 0\right) \end{cases}$$

Therefore, the above equation becomes

$$\left(\rho \frac{du}{dt} = -\nabla P + \rho g\right) \qquad \text{(Equation } 3-4\text{)}$$

When explicated, the equation becomes

$$\left(\frac{\partial(\rho\, u)}{dt}\right) + \nabla(\rho\, u\, u) = -\nabla \mathrm{P} + \rho g - F_{ap} \qquad \text{(Equation } 3-5\text{)}$$

where ρ is the fluid density, u is the fluid velocity, e is the specific energy of the fluid, P is pressure of the air, t is time, g is acceleration due to gravity and $F_{a\,p}$ is the total force of the interaction between the fluid and the particles per unit volume of fluid (air). The expression of $F_{a\,p}$ is given in equation 3-6 below as;

$$F_{a\,p} = \sum_{j=1}^{n} \frac{f_{a\,p,j}}{V} \qquad \text{(Equation } 3-6\text{)}$$

where a represents the fluid (air), p_j represents the particle "j", n represents the number of particles considered, V represents volume of particle "j", $f_{a\,p,j}$ is the force of interaction for individual particles which is shown in equation (3-7) below.

$$f_{a\,p,j} = F_B - F_w - F_D \qquad \text{(Equation } 3-7\text{)}$$

According to equations 3-8 and 3-9, the F_B is represented as the buoyant force, ρ is the density of the fluid (air), V is the displaced body volume of the fluid (this is also the volume of the particle since it is fully immersed in air) and g is the acceleration due to gravity.

$$F_B \geq F_W + F_D \qquad \text{(Equation } 3-8\text{)}$$

$$F_B = \rho\, V\, g \qquad \text{(Equation } 3-9\text{)}$$

$$F_W = m \times g \qquad \text{(Equation } 3-10\text{)}$$

In equation 3-10 above, F_W represents the weight of the particle, m is the mass of the particle, and g is the acceleration due to gravity.

$$F_D = \left(\frac{C_D \times A \times \rho \times u^2}{2}\right) \qquad \text{(Equation } 3-11\text{)}$$

In equation 3-11, F_D is the drag force on the particle, C_D denotes the drag coefficient of the particle, A is the cross-sectional area, ρ is the density of the fluid (air), and u is the flow velocity relative to the air.

When $F_B > F_W + F_D$, the particles are being transported in the air stream and when $F_B = F_W + F_D$, this implies that $f_{a\,p,j}$ is zero and the particle velocity in the airstream terminates and the particles fall at constant velocity.

Following the guiding mathematical model derived above, the optimal separator design from the simulation was attained following the steps listed below;

I. The first chamber of the separator assembly was designed using the Autodesk Inventor software and was then imported into the simulation software.
II. Simulation test was then carried out using the assumptions listed in section **3.3.2.**, whilst varying operational parameters like the airstream velocity and the feed rate of the particles.
III. The particle tracks for each relative density were observed and the operational parameters were changed to observe the separation effectiveness of that design at the cut-point of 1.6RD.
IV. Continuous augmentations were made based on the flow tracks observed from each design until an optimal separation was attained in the first chamber.
V. A design of the second chamber was made and the same steps listed above (for the first chamber) was also carried out based on the optimal results achieved through the particle tracks, leading to the design of the separator assembly.

Figure 3-2 and 3-3 below depict the individual chambers and their respective flow boundaries, with $\boldsymbol{A}$ (figure 3-2) representing the air supply inlet into the separation chamber, $\boldsymbol{B}$ denotes the particle inlet into the separation chamber, and $\boldsymbol{C}$ is the outlet of the clean coal particles elutriated by the air stream from the first chamber. $\boldsymbol{D}, \boldsymbol{E}, \boldsymbol{F}$ all represent the collection bins 5, 6, & 7, of particles of the gangue material.

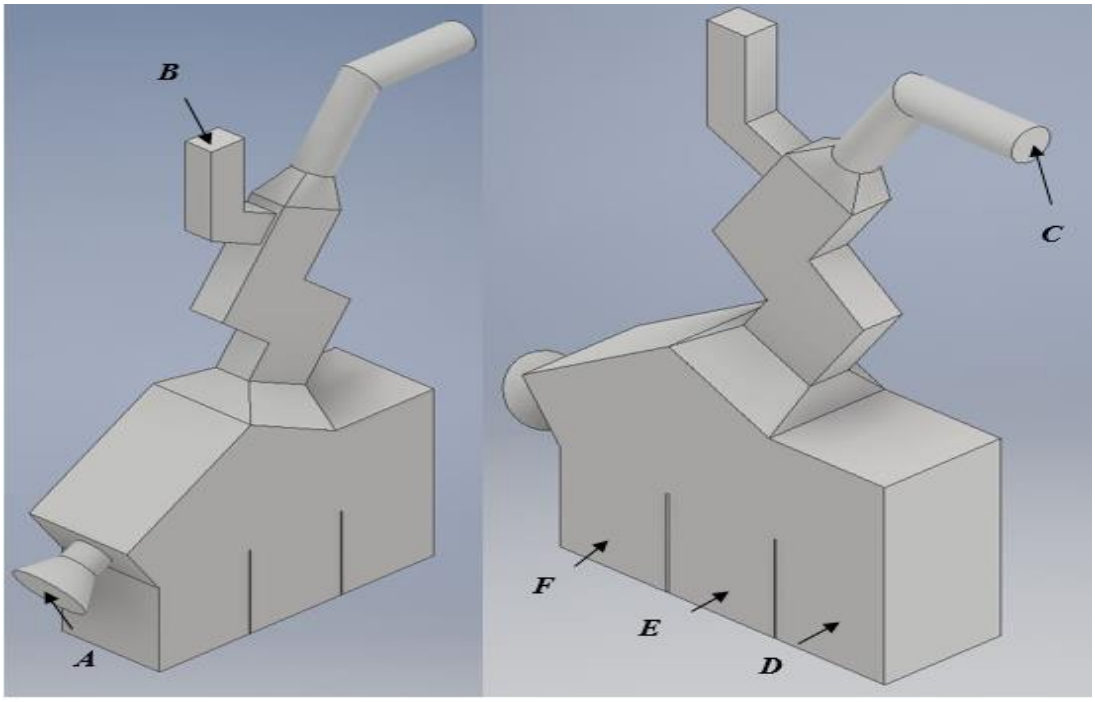


Figure 3 - 2: Flow boundaries of the first chamber with its collection bins

In figure 3-3, ***G*** represents the inlet of the partitioned particles, i.e. through which the lighter particles are transported into the second chamber, while ***H*** is the air outlet from the separator. ***I, J, K and L*** all represent the particle collection bins 1, 2, 3 and 4 respectively. The design of the separator was carried out in such a way to be able to determine the amount of misplacements occurring during the separation process, and figure 3-4 showing the full assembly of the separator.

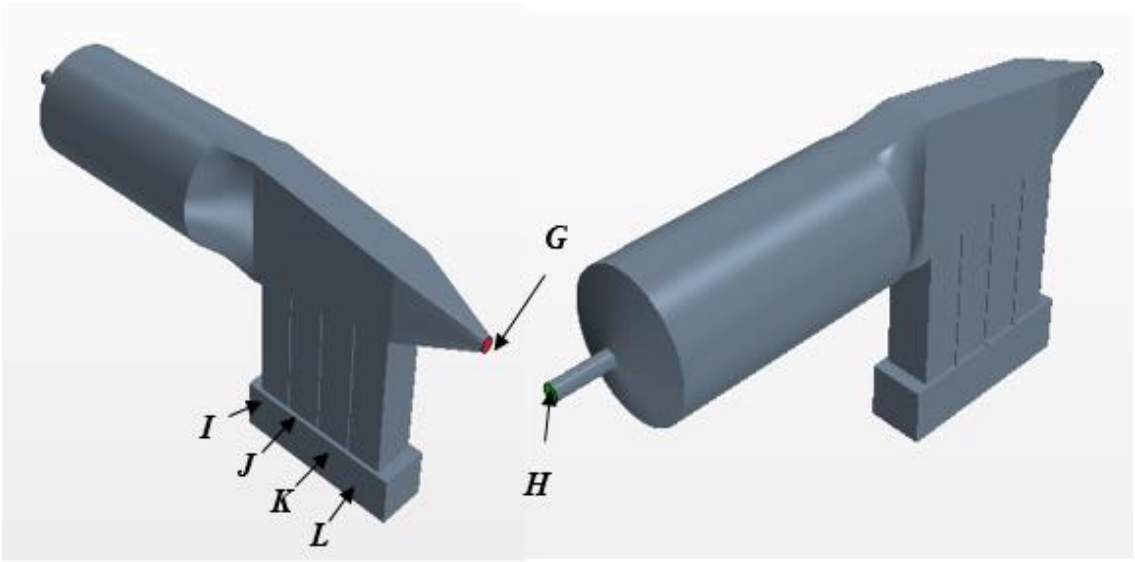


Figure 3 - 3: Flow boundaries of the second chamber with its collection bins

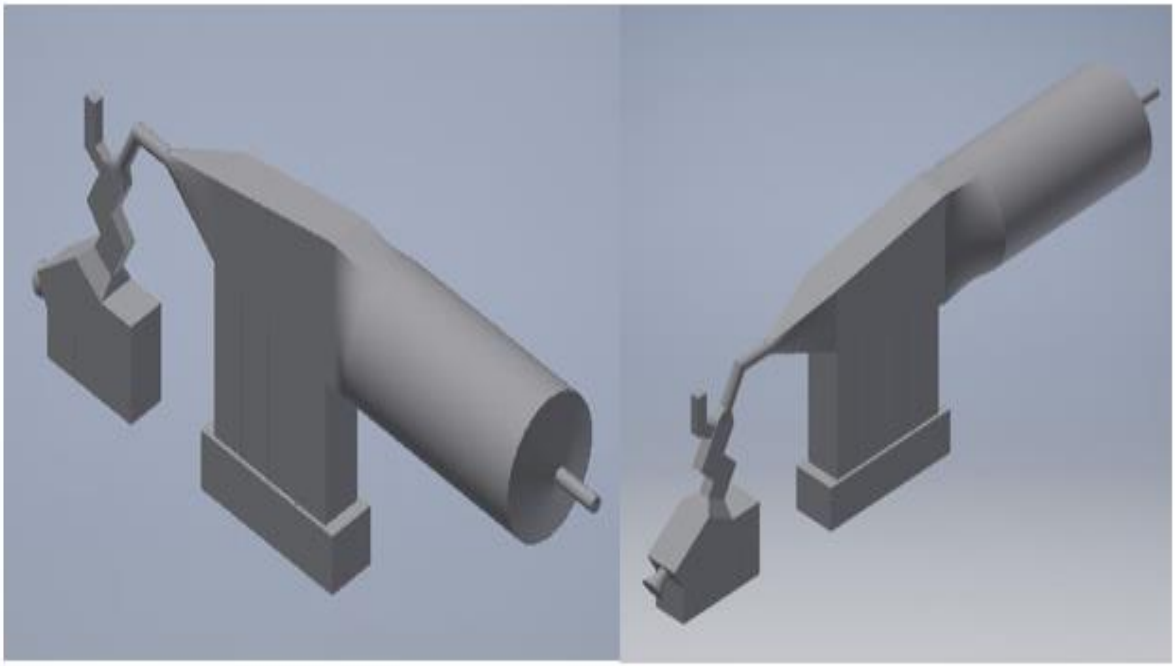


Figure 3 - 4: The full separator assembly

As can be seen from figure 3-5, the upper part of the chamber 1 was designed and then merged with the collecting bins 7, 6 and 5, with the same approach applied to the second chamber design. The merging was done to form a contact region/surface between the two connecting faces when imported into the simulation software. This design approach enabled the determination of the quantity of the particle recovered in each bin. Each of the two chambers was designed as an assembly as shown in figures 3-5 to 3-7.

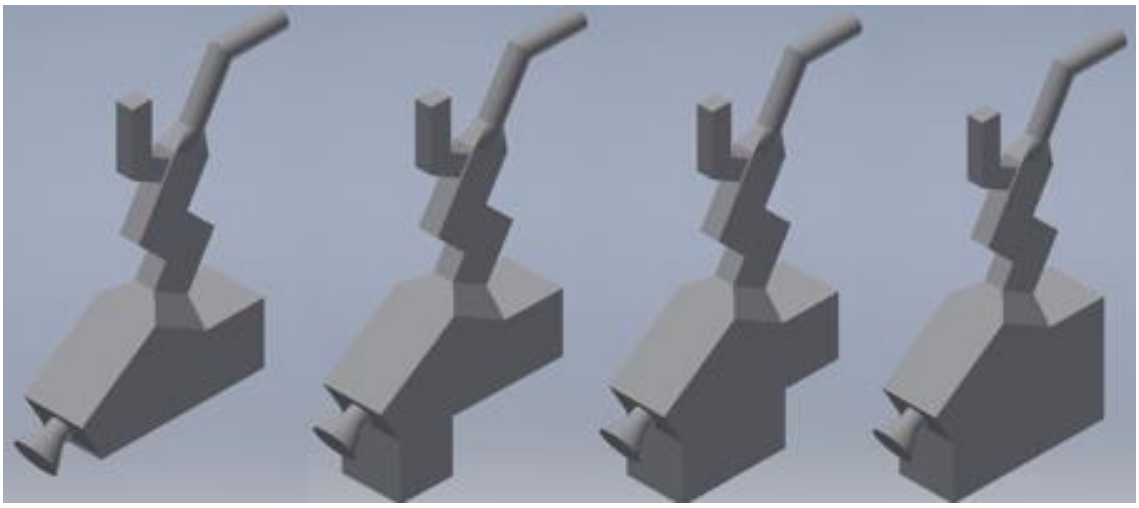


Figure 3 - 2: The designed assembly of chamber 1 to depict contact regions

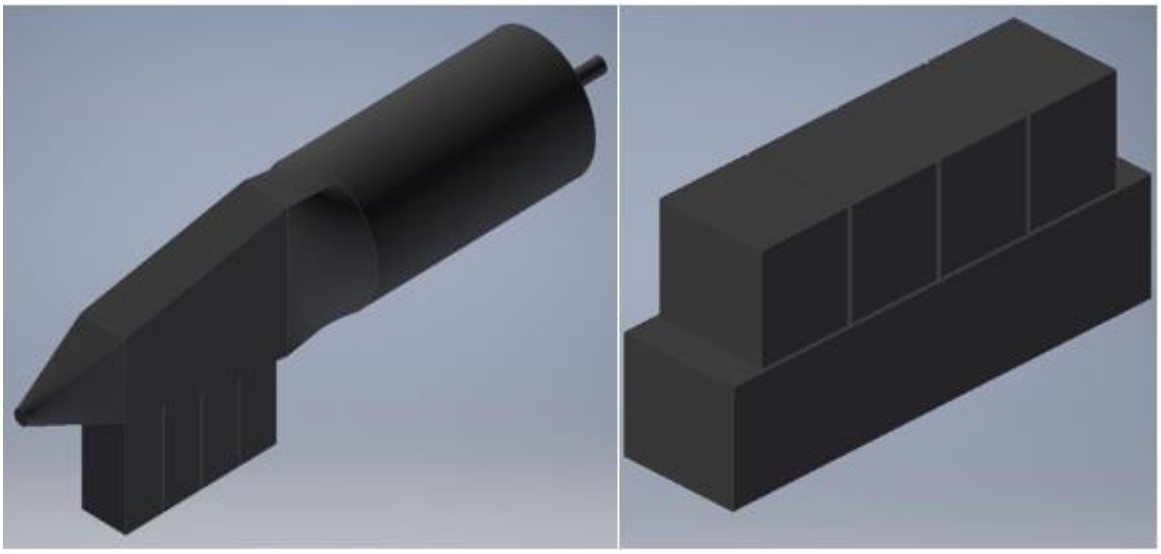


Figure 3 - 3: The designing of the chamber 2

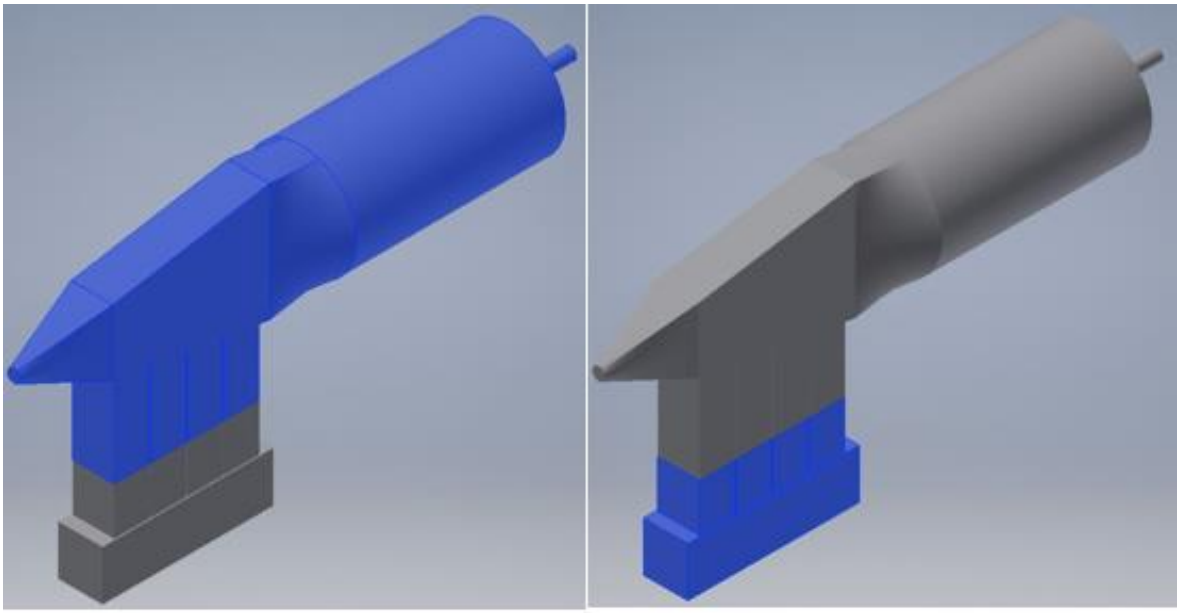


Figure 3 - 4:The designed assembly of chamber 2 to depict contact regions

3.3.2. THE SIMULATION PROCESS

The mesh, which is an integral component of this design was generated for both chambers (1 and 2) to optimize these geometries and obtain a highly accurate measurement. The meshing models used were the *Surface Remesher*, the *Polyhedral Mesher* and the *Prism Layer Mesher*. The surface remesher meshing model is used for improving the overall quality of an existing surface and to optimize it for the volume mesh model, which is the polyhedral mesher, as used in this study. The polyhedral mesher is a volume core mesh model that provides a balanced solution for complex mesh generation as it uses arbitrary polyhedral cell shapes to build the core mesh. The polyhedral mesher was utilized in this design as it is straightforward and requires no further surface preparation unlike the tetrahedral mesher models. It is very effective in the analysis of the simulation and contains approximately five fewer cells when compared to the tetrahedral mesher model.

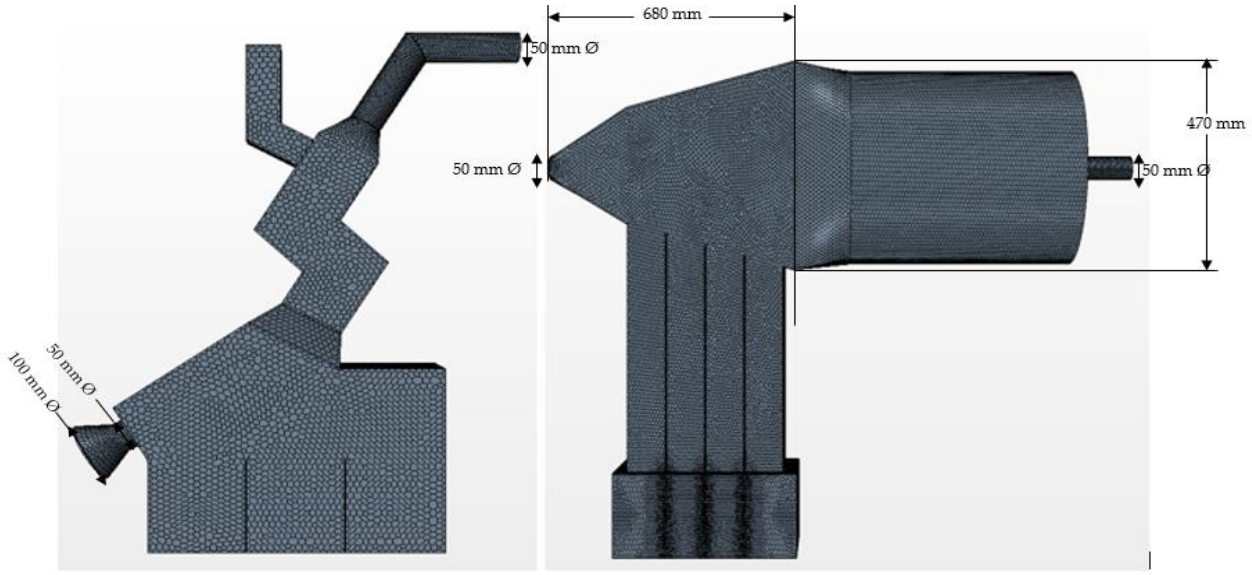


Figure 3 - 5:Mesh generated for chamber 1 and 2, respectively.

The prism layer mesher model was also applied with the core volume mesher (polyhedral mesher). The use of the prism layer model was to generate orthogonal prismatic cells next to the walls (surfaces) of the separator, and to give accurate results in the simulation test runs even with just few prism layers.

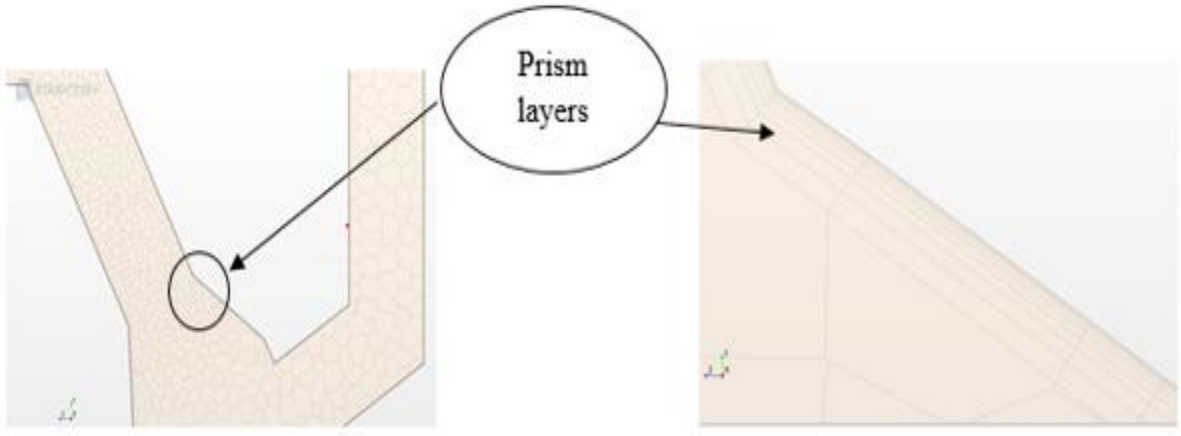


Figure 3 - 6: Prism layer in the first chamber

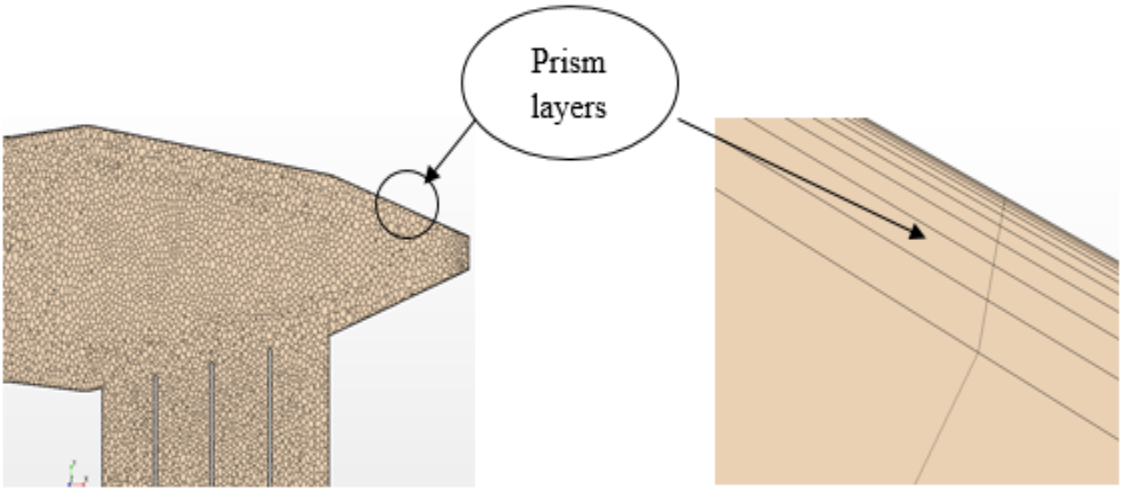


Figure 3 - 7: Prism layers in the second chamber

The contact regions generated were used to determine the amount of particles as well as the relative densities of the particles entering into the individual collecting bins. This also enabled us determine the amount of particles that settled in undesignated bins. Figures 3-11 and 3-12 show the contact regions in the first and second chambers respectively to ascertain the amount of particles entering into each bin as well as the amount of misplacements in both chambers of the separator assembly.

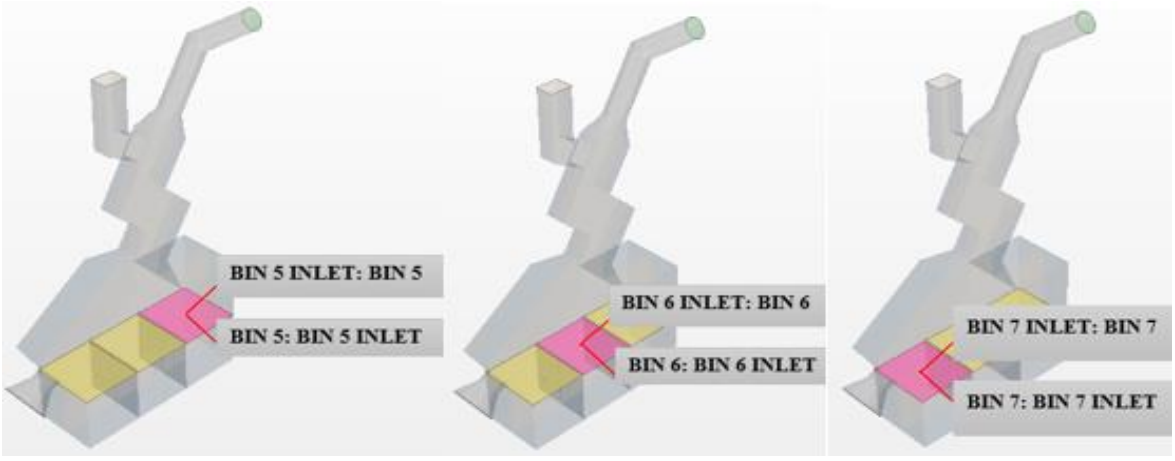


Figure 3 - 8: Contact regions in the first chamber

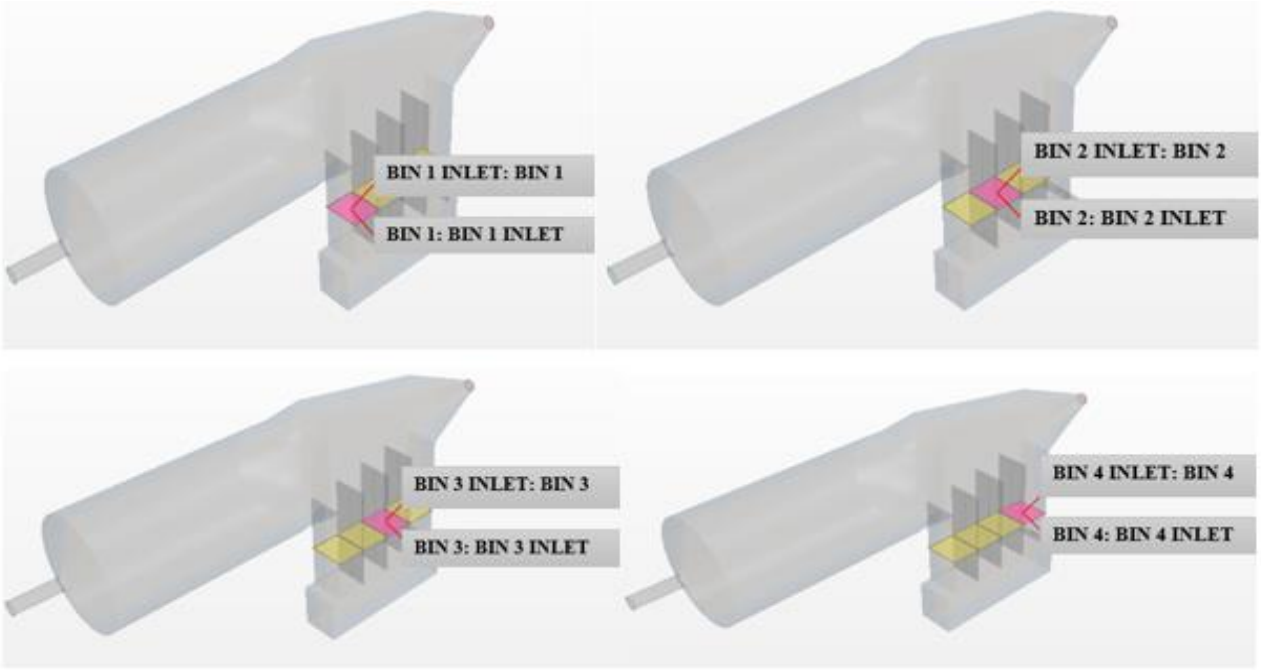


Figure 3 - 9: Contact regions in the second chamber

Physics models are very important in determining primary variables of the process being simulated, a few of such variables include velocity, temperature, pressure, etc. The ***physics*** models to be used in any simulation are dependent on factors such as if the flow is three (3) dimensional, if the flow is steady, unsteady, transient or stationary. In this study, parameters such as flow velocity and the mass flowrate were also considered and the ***physics*** models chosen were ***three dimensional*** model, the ***Time*** model chosen and the ***Steady State***. It is important to point out that steady state flow indicates that properties at every point in the separator remains constant and albeit the flow properties may change at different points, overall properties in the separator do not change. The equation below is the general equation which defines steady flow with respect to density (ρ) and velocity(u):

$$\frac{\partial \rho}{\partial t} = 0 \ , \ \frac{\partial u}{\partial t} = 0 \qquad \text{(Equation 3-12)}$$

The ***Gravity*** and ***Lagrangian*** models were used while air was used as the ***Material*** (continuum) for this simulation study. For the ***Gravity*** model, values of (0, -9.81 m/s, 0) where used in the (x, y, z) dimension to ensure proper action of gravity of the 'negative' y direction in the separator and, seven ***phases*** (given densities of 1.3 g/cm^3 to 1.9g/cm^3) for the ***Lagrangian*** model as particles

which was fed into the computational geometry (separator) via the coal inlet boundary of the first chamber. The following assumptions below were made regarding the simulation test runs.

I. The shape factor of the particles was represented as 1 (particles were perfectly spherical).
II. The particle relative densities are equally represented in terms of mass.
III. Each relative density (RD) within the coal was represented in the simulator and assigned a size (mm) to simplify the simulation, and this can be seen in Table 3-1
IV. Normal and tangential restitution coefficients of the boundary for the wind sifter separator was assumed to be 0.7. This was to account for the inner section of the separator which was lined with linatex rubber HD 60 to prevent the breaking of the coal as it is being transported in the air stream.

Table 3-1: The assigned particle diameters for each particle size fractions per density fraction

Relative Density	(-6.7+3.36 mm)	(-3.36+1.0 mm)	(-1 mm)
1.3	3.36	1.00	0.10
1.4	3.80	1.40	0.25
1.5	4.60	1.80	0.40
1.6	5.40	2.30	0.55
1.7	6.10	2.70	0.70
1.8	6.35	2.90	0.85
1.9	6.70	3.36	1.00

3.4. WIND SIFTER SEPARATOR

The wind-sifter separator separates lighter particles from heavier ones and the separator for this research was fabricated from mild steel, and has a footprint of 400 cm in length, 167 cm in height and 77 cm wide, was used to upgrade coal. The fabricated separator consists of two chambers, with the first chamber having two inlets and an outlet; the top inlet serves as an inlet for the coal, and the other inlet is for the air-stream into the first chamber. The destoning of the coal based on the particle's respective densities occurred in the first chamber. The second chamber only has one inlet to feed the clean coal and an outlet; for the air to exit the separator through the filter compartment. As the clean coal product enters the second chamber, under the differential drag acting on particles in an air stream, the particles were further separated into different bins based on their densities. This chamber was designed under a different principle to that of the first chamber, as seen in figure 3-13.

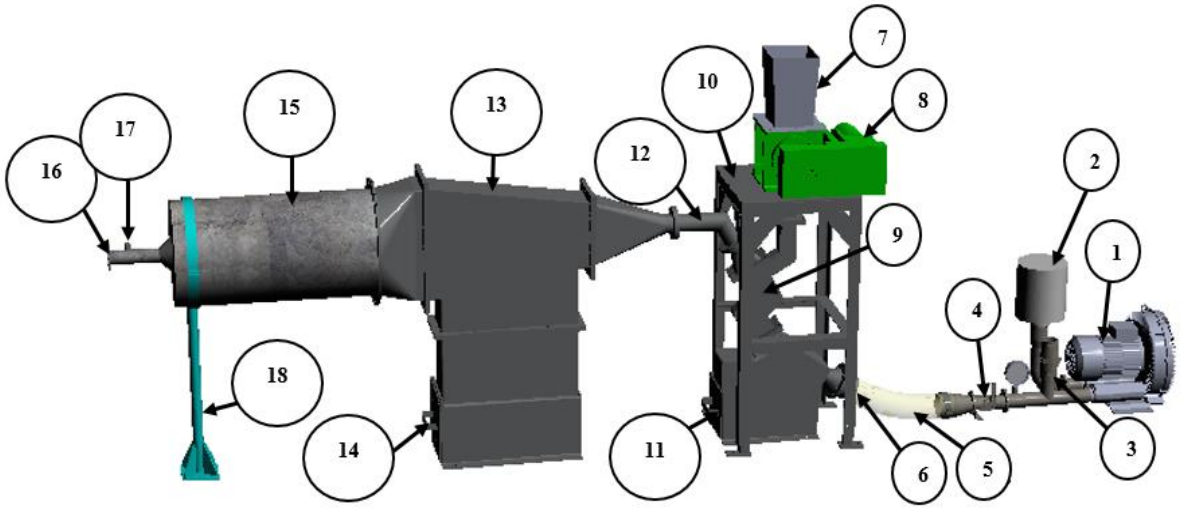


Figure 3 - 10: The proposed wind sifter separator assembly

1- Air Blower

2- Air Filter

3- Safety relief valve

4- Throttle Damper

5- 100 mm diameter flex

6- Air inlet into first chamber

7- Rotary airlock valve for the coal-feed

8- The variable frequency drive motor drive for the rotary hopper valve (coal-feed)

9- The first chamber (the wind-sifter) with the zigzag section

10- Support frame for the wind-sifter

11- Coal bin for the first chamber

12- Exit of the clean coal from the first chamber into the second chamber

13- Second chamber (Diffuser chamber) to collect the clean coal

14- Coal bin for the second chamber (clean coal)

15- Filter section (with filter cartridge) to prevent coal dust from escaping to the environment

16- Air Exit from the separator

17- Velocity measuring port

18- Support stand for the filter compartment

3.4.1. OPERATING PRINCIPLE

Figure 3-13 above shows the fabricated wind-sifter separator. Air is supplied into the separator with the aid of **1**, as the air is drawn into the system through **2**, travels through **4**, **5** and enters the first chamber through **6**. The safety relief value (**3**) served as a measure to depressurize the separator assembly from excessive pressure build up, and is also used in together with **4** when the percentage opening of **4** is reduced for velocity control. The air stream then travels through **9**, **12**, **13**, **15** and then out of the separator through **16**. Coal is then fed into the separator with the aid of a vibratory feeder through **7** when **8** is powered-on, with **10** serving as a support frame for chamber 1 as well as a pedestal for the connection assembly of **7** and **8**. The coal particles then fall into zigzag section (**9)** and as they bounce in this section, some separation occurs as a result of their varying weights. The continuously flowing incoming air then separates the lighter particles from the heavier ones and transports them into the second chamber where they will be collected.

The lighter particles of different densities (clean coal products) transported by the airstream from **9,** through **12** into **13** which is the second separating chamber. The clean coal particles are separated in the bins **(14)** after attaining their settling velocities, while the heavier particles fall through **9** to the coal bins at the base of the wind-sifter section. The efficiency of the wind sifter separator was calculated with the equation below:

$$\%\text{Yield} = \left(\frac{Total\ mass\ of\ coal\ collected\ in\ the\ coal\ bins\ of\ the\ second\ chamber}{Total\ Mass\ of\ Coal\ feed}\right) \times 100 \quad \text{(Equation 3-13)}$$

For the first chamber, there are three bins **(11),** while the second chamber (diffuser chamber) has four coal bins (**14**). Comparisons were made between the simulation test results, the fabricated laboratory scale separator and also that obtained from the float-sink tests. The evaluations were then made in terms of their respective mass yield and separation efficiency and the extent to which the separator can beneficiate (ash content). The control panel which powers both the electric motor driven rotary hopper valve as well as the air blower is shown in figure 3-14 below.

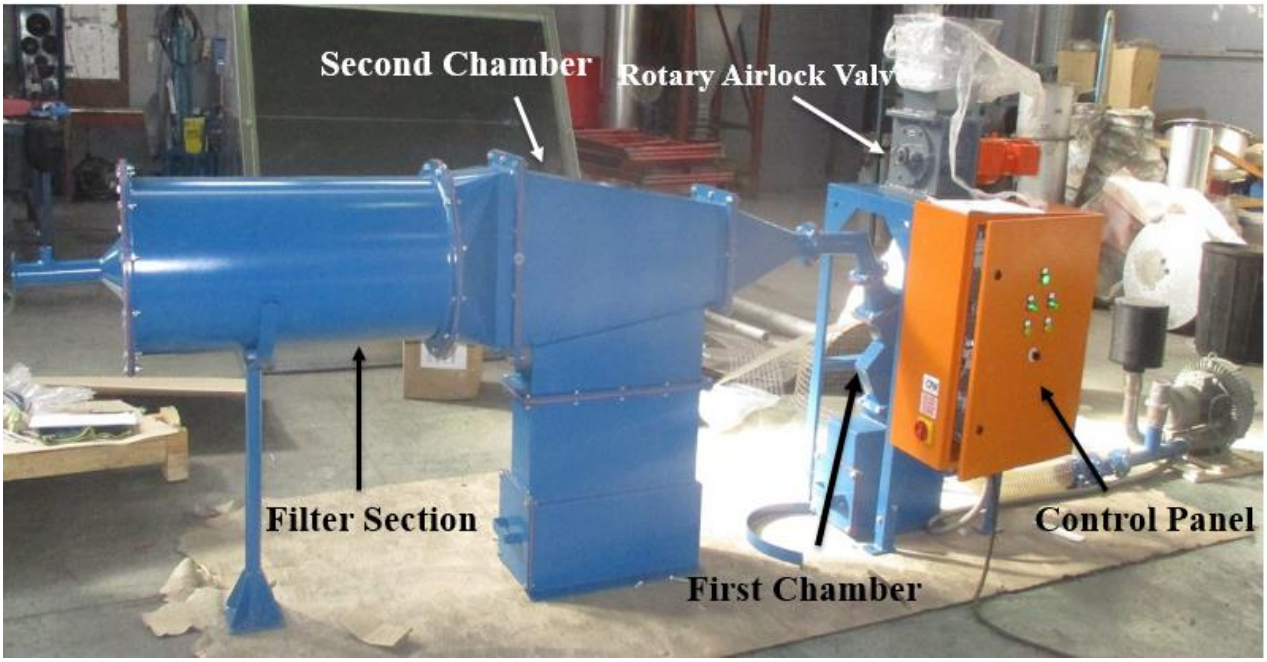


Figure 3 - 11: The Fabricated Wind Sifter Separator

3.4.2. CALIBRATION OF THE COAL FEEDER

A vibratory feeder was used to feed the coal into the separator. It is important to note that the vibratory feeder was calibrated by increasing its "carrier frequency", while 200 g of representative feed coal was fed into the chute of the vibratory feeder assembly as shown in figure 3-13 below.



Figure 3 - 12: The Vibratory feeder Assembly

The time which it takes for the coal to be completely fed into the system is recorded and mass flowrate was derived by dividing the mass of the feed by the time it takes for the feed to be completely fed into the separator. With the changes to the vibration intensity and carrier frequency from the electromagnetic actuator of the feeder, the feed rate of the system can be varied.

3.5. FLOAT AND SINKANALYSIS

The float and sink laboratory scale test, deployed in accordance with ASTM-D4371 and ISO 7936:1992 standards, was used to beneficiate the coal samples at -6.7+3.36 mm, -3.36+1 m and -1 mm at different relative density. The float and sink analysis entails use of a heavy medium solution to partition particles based on the relative density of the solution. Zinc chloride was used as a medium of separation, and the washability data obtained was used as a benchmark for comparison against the designed separator to ascertain its separation efficiency. The test was conducted at six relative densities (RDs) ranging from 1.3 –1.8 (at 0.1 increments), with the sinks in the 1.8 RD solution considered as the sink of the test.

Already prepared Zinc chloride solution ($ZnCl_2$) solutions in six 5 L beaker ranging from 1.3 to 1.8 g/cm^3 at 0.1 intervals were used as the heavy medium for ROM coal samples of 500 g for all

the test work. The density of the solution was determined using a digital density meter with a buffer solution of high concentration, also prepared to account for any decreasing relative density in any of the solutions. The 500 g of run-off-mine coal sample was added stage-wise into the first solution of 1.3RD and 3:1 (medium: ore) was maintained, agitated for few minutes and allowed to stand for separation to take place. As the separation was achieved, the light density particles floating on the medium's surface were collected using a sieve, washed thoroughly to remove the excess zinc chloride and kept separately. The heavy particles at the bottom of the medium were also collected separately and poured into the next beaker of 1.4RD solution whilst maintaining the 3: 1 (medium: ore) ratio. The same process is repeated for each solution with the floats being collected and the sinks poured into the next until the sinks of the 1.9RD solution are obtained.

The results attained were used to construct a washability profile, which is a plot of RDs against the cumulative mass for the individual fractions. Below are the equations used to finding the percentage yield of the clean coal products for the three size fractions.

% Float recovery

$$= \left(\frac{Mass\ of\ recovered\ at\ specific\ relative\ density}{Total\ Mass\ of\ Coal\ feed\ (500\ g)}\right) \times 100 \qquad (\text{Equation } 3-14)$$

Float analysis (wt. %)

$$= \left(\frac{Mass\ of\ \ product\ recovered\ at\ specific\ density\ fraction}{Total\ Mass\ of\ the\ Coal\ product}\right) \times 100 \qquad (\text{Equation } 3-15)$$

Sink analysis (wt. %)

$$= \left(\frac{Mass\ of\ coal\ discard\ at\ specific\ density\ fraction}{Total\ Mass\ of\ Coal\ discard}\right) \times 100 \qquad (\text{Equation } 3-16)$$

% Float of the feed

$$= \left(\frac{Mass\ of\ product\ recovered\ at\ specific\ density\ fraction}{Total\ mass\ of\ coal\ feed}\right) \times 100 \qquad (\text{Equation } 3-17)$$

% Sink of the feed

$$= \left(\frac{Mass\ of\ coal\ discard\ recovered\ at\ specific\ density\ fraction}{Total\ mass\ of\ the\ coal\ feed}\right) \times 100 \qquad (\text{Equation } 3-18)$$

$$\%\ \text{Yield} = \left(\frac{Total\ mass\ of\ the\ Coal\ product}{Total\ Mass\ of\ Coal\ feed}\right) \times 100 \qquad (\text{Equation } 3-19)$$

3.6. ANALYTICAL TECHNIQUES

Coal analyses such is proximate analysis, ultimate analysis and calorific value were conducted to ascertain the physico-chemical properties of the ROM coal and the clean coal products from each bin and from the sink/float fractions.

3.6.1. PROXIMATE ANALYSIS

The inherent moisture, volatile matter, ash content, and the fixed carbon (calculated by the difference) are determined in accordance with ASTM D7582 – 15 standard, in which 1 g of representative sample was added stage-wise in each crucible in the TGA 701 Leco equipment. The proximate analysis entails the use of nitrogen in the first step which is the drying step. The moisture content was determined by mass loss starting from room temperature (around 20^{o}C) to 107 ^{o}C, as the temperature ramps up at a heating rate of 8 ^{o}C /min.

The volatile matter was determined as the mass loss within a temperature range between 107 ^{o}C to 950 ^{o}C, whereas the combustion step that follows, evaluates the mass loss under oxygen between the temperature range of 650 ^{o}C and 750 ^{o}C. The residual mass left after the analysis is then taken as the total ash content in the sample while the fixed carbon is calculated as (100-(Moisture content + Volatile Matter + Ash Content)) %.

3.6.2. ULTIMATE AND TOTAL SULPHUR ANALYSIS

The ultimate (Carbon, Hydrogen, Nitrogen, Sulfur, and Oxygen (by difference)), and total sulphur analyses of all samples were performed according to ASTM D 5373-14:2015 and ASTM D 4239-14:2015 for CHN and sulphur content, respectively using LECO CHN 628 with add on 628 S module. Approximately 0.25 g of the samples was used for the analyses at a temperature up to 1,450 ^{0}C with an analyzing time between 60 – 300 seconds.

3.6.3. CALORIFIC VALUE DETERMINATION

The calorific value is the measure of the heat content in the coal, and was determined in accordance with ASTM D5865-04. This analysis was carried out for some selected samples, in particular the coal samples from bin 1 using a Leco AC 500 bomb calorimeter. The bomb calorimeter calculates

the total amount of heat released from the complete combustion of one-unit mass (1 g) of fuel under the oxygen atmosphere at high pressure of about 3,000 kPa. The temperature was controlled at 25 degrees Celsius by recirculating cooling water in the equipment with the aid of a pump. The system uses an electronic thermometer with an accuracy of 0.0001 0C to measure the temperature every six seconds, with the results obtained within 4.5 to 7.5 minutes.

3.7. SUMMARY

The design of the separator and simulation was carried out to ascertain the dimensions of the separator which then ultimately led to its fabrication. Coal samples used in this study were screened into three particle size fractions (-6.7+3.36 mm, -3.36+1 mm and -1 mm). The proposed experimental tests were carried out on the separator and the results were compared with those from the simulation study. A float and sink test were also carried out to serve as a basis of comparison for the physico-chemical properties of both the wet and dry beneficiation process. The next chapter (Chapter 4) will present the results and discussions of the simulation and experimental investigations that were carried out.

CHAPTER 4: RESULTS AND DISCUSSION

In this chapter, the results which were obtained from the simulation test runs, sink and float tests of the run off mine as well as the dry beneficiation test runs using the fabricated wind sifter separator are presented.

4.1. INTRODUCTION

For the design of the separator, simulation test runs on the effect of air velocity on the three particle size fractions (-6.7 + 3.36 mm, -3.36 + 1 mm and – 1 mm) as well as individual particles in each particle size fractions were investigated. For the experimental studies, the influence of operating parameters such as the air velocity and mass flowrate on the separation performance and quality of the clean coal products based on the sample ash content were investigated. The mass flowrate was kept low as stated in section 3.3.1 to always maintain a dilute phase (low particle to particle interactions) within the separator.

4.2. SIMULATION RESULTS

The influence of factors such as the air velocity and particle size on the separation efficiency of the separator were investigated using a particle feed rate of 420 g/min. Following a study by Santos *et al.* (2011) who utilized a dilute phase of 6 g of particles in 11 g of air, the mass feed rate for the particle size (-6.7+3.36 mm) using the optimal velocity obtained from the simulation can be pushed up to 2,043.36 g/min, whilst still maintaining the dilute phase. Following the above-mentioned conditions, the mass feed-rate of the -3.36 + 1 mm and the -1 mm size fraction can also be pushed up to 1,300.32 g/min and 526.32 g/min, respectively. The density of air used during the simulation process was 1.204 g/cm^3 as the air is assumed to be at room temperature (20^{o}C). The formula for determining the separation efficiency of the separator is given in Equation 4-1, which is similar to Equation 3-6, whereas Equations 4-2 and 4-3 were used to obtain the mass flow rate.

$$Mass\ Yield\ (\%) = \frac{100 \times M_O}{M_I}\ , \qquad \text{(Equation } 4-1\text{)}$$

M_O represents the mass of the lighter particles which flows from the first chamber into the second chamber, and M_I is the total mass of the particles fed into the separator through the separator inlet.

$$Air\ mass\ flowrate = \rho_{air} \times u \times A \qquad \text{(Equation } 4-2\text{)}$$

$$Particle\ mass\ flowrate = Air\ Mass\ flowrate \times \frac{6\ g\ of\ particles}{11\ g\ of\ air} \qquad \text{(Equation } 4-3\text{)}$$

Where ρ_{air} the density of air at 20 ^{0}C, u is the velocity of air entering into the separator and A is the cross-sectional area (with a diameter of 100 mm).

4.2.1. EFFECT OF AIR VELOCITY

To determine the optimal velocity to achieve the optimal mass yield and separation efficiency for each particle size distribution in the simulator, different air inlet velocities were used with other parameters remaining constant. For the (-6.7+3.36 mm) size fraction, using air velocity of 10 m/sec, it was observed that all the particles were carried off in the air stream into the cartridge filter, without dropping into the designated bins according to the particle's RD, and this indicates no separation. Similar results were obtained at 9.5 and 9 m/sec and upon reducing the velocity further, an optimal velocity of 6.0 m/sec was attained for the -6.7 + 3.36 mm fraction as seen in figures 4-1.

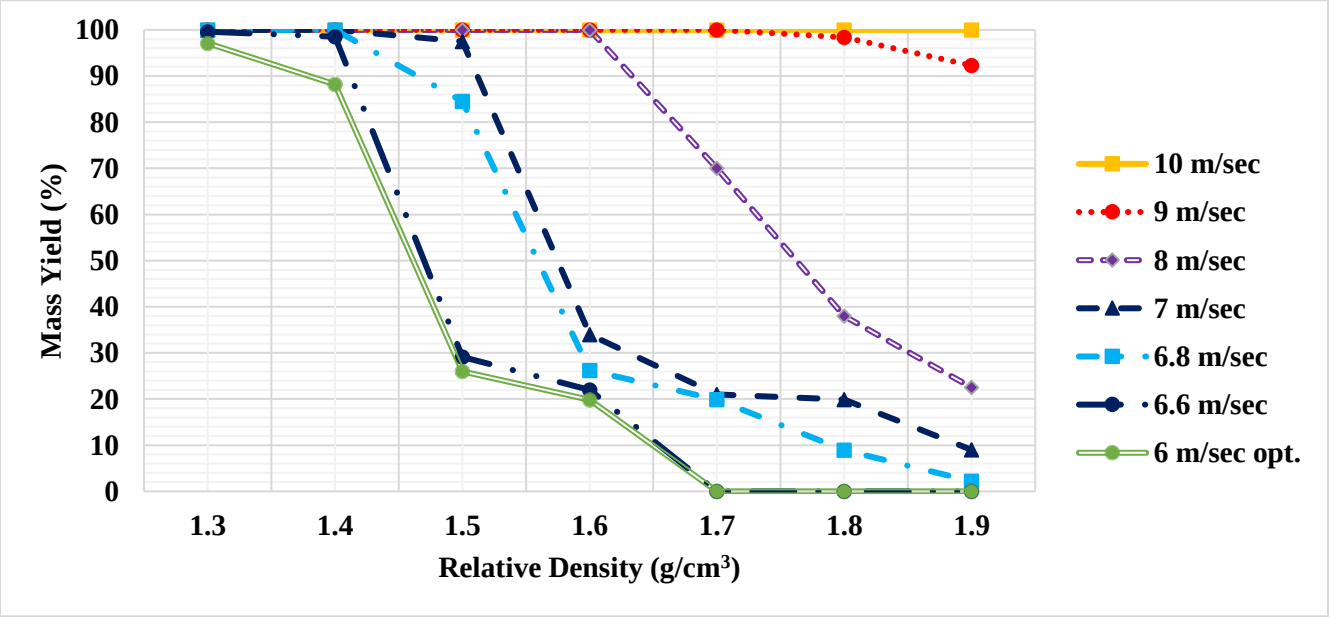


Figure 4 - 1:Effect of Air velocity and optimal velocity determination for (-6.7 + 3.36 mm) size fraction.

A similar process was also conducted for the -3.36 + 1 mm and -1 mm size fractions in figure 4-2 and figure 4-3, until an optimal mass yield at velocities of 4.2 m/sec and 1.7 m/sec, respectively was attained.

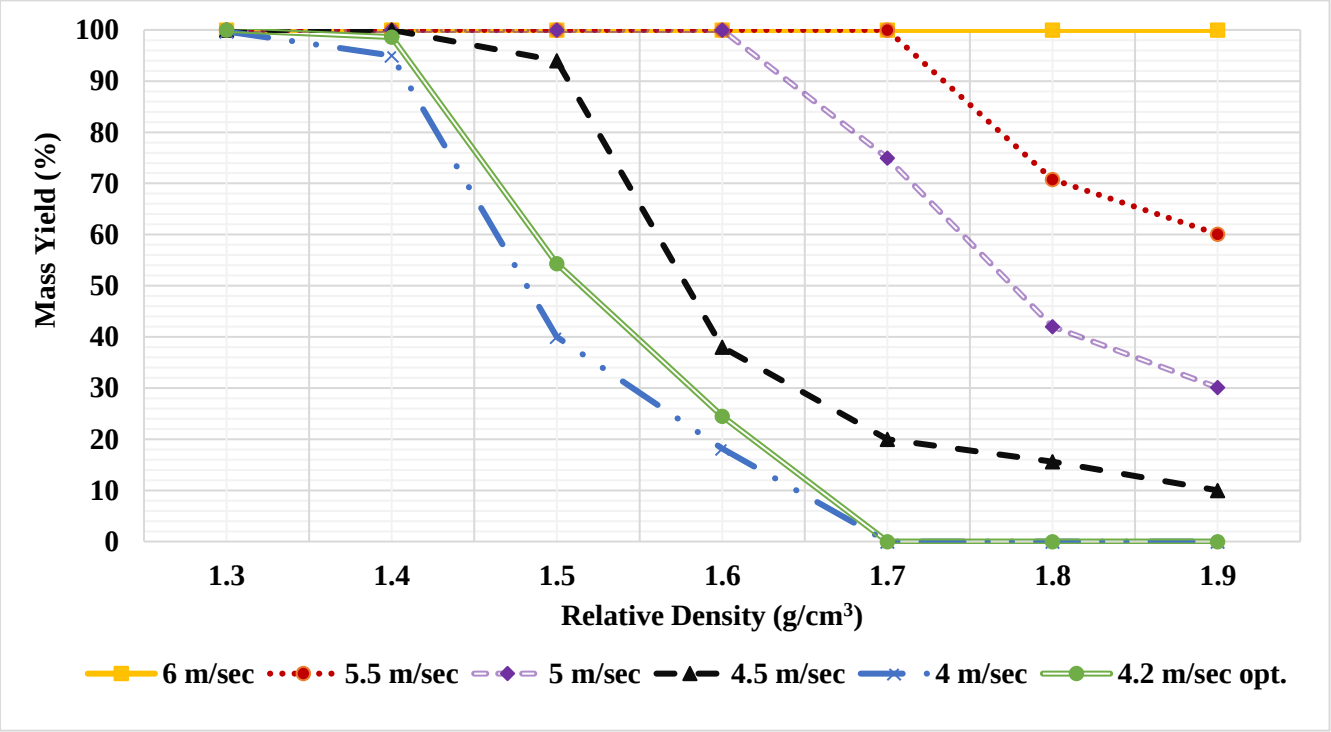


Figure 4 - 2: Effect of Air velocity and optimal velocity determination for (-3.36+1 mm) size fraction

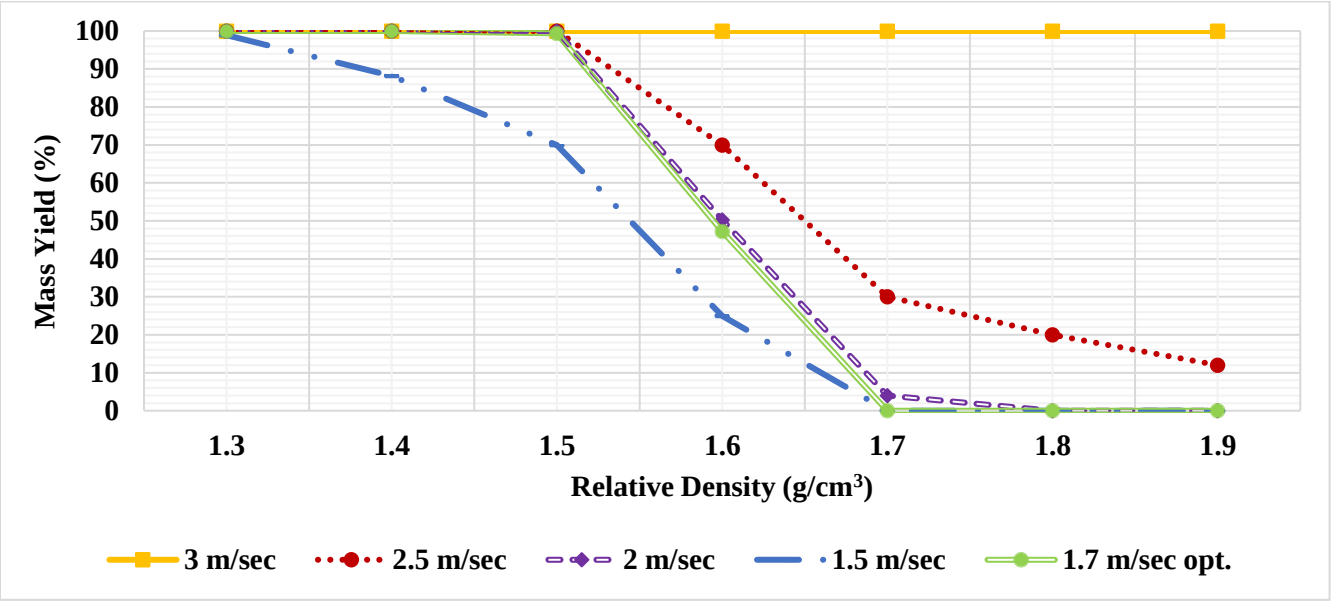


Figure 4 - 3: Effect of Air velocity and optimal velocity determination for (-1 mm) size fraction

From the simulation test runs conducted as shown in figures 4-1 to 4-3, it can be observed that for all the particle size fractions, the optimal velocities were determined and are represented with a green line profile. Figure 4-4 below shows the comparison of the mass yield (%) for the three particle size fractions, as well as for a perfect separation for all particle size distribution. The results show that at the cut off density of 1.6, the -1 mm size fraction has the highest mass recovery of 47.2%, followed by the -3.36+1 mm with a mass recovery of 24.5% and 22% for the -6.7+3.36 mm.

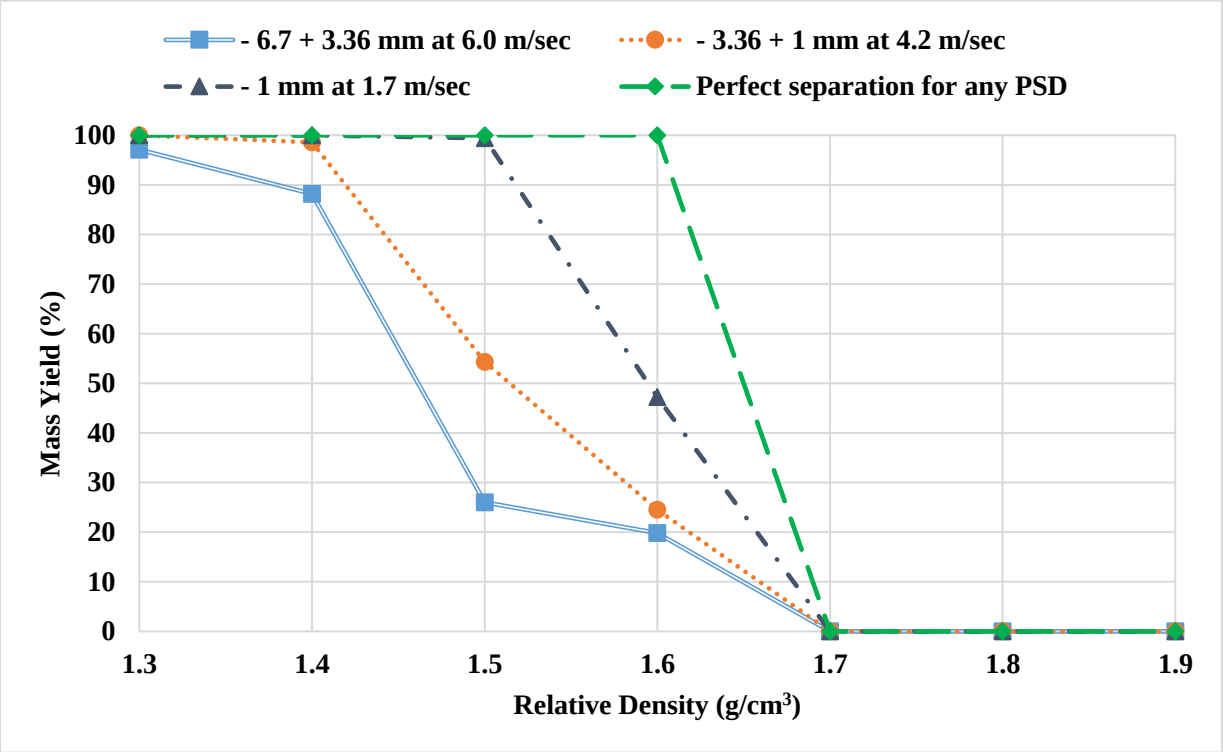


Figure 4 - 4: Mass yields from the 3 particle size fractions at their respective optimal velocities

4.2.2. EFFECT OF INDIVIDUAL PARTICLES WITHIN THE PARTICLE SIZE DISTRIBUTION ON THE MASS YIELD

Further study was also carried out on the simulator to determine the effect of the individual particles within the particle size distribution on the separator efficiency while varying the relative density and keeping the velocity constant. Figure 4-5, depicted the yield obtained from the individual particles present within the -6.7 + 3.36 mm size fraction at different RD and at a constant velocity of 6.0 m/sec. As the individual particle size increases from 3.36 mm to 6.7 mm, the mass

yield decreases from 99.6% to 23.6% at constant velocity. The same trend was also seen for all the (RD), as at 1.9 RD, the yield for 3.36 mm particle size decreased to 0 for 6.35 mm to 6.70 mm fraction.

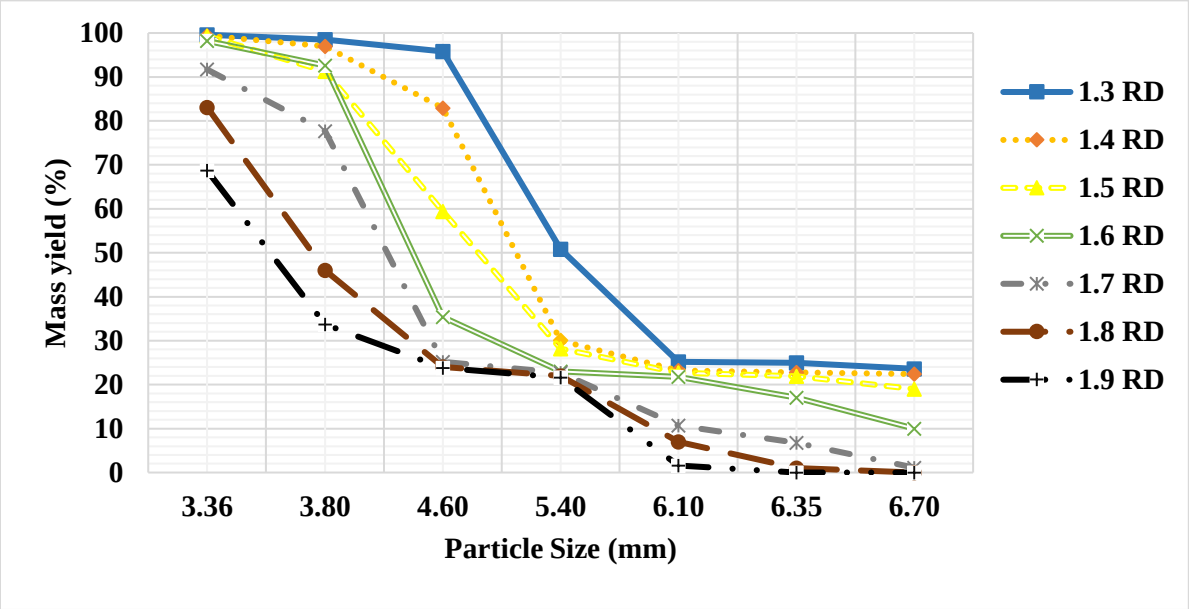


Figure 4 - 5:Mass yield(s) of individual particle in the particle size distribution of (-6.7 + 3.36 mm) as a function of relative density.

Figure 4-6 and 4-7, also depicted the yield obtained for individual particles in the particle size distribution of (-3.36 + 1 mm) and (-1 mm), as a function of relative density. At RD of 1.3 to 1.6, a yield of 100% was achieved for the 1 mm particle size, while at 0.1 mm size, 100% recovery was attained for all the RD tested. These results show that particle size and density play a role in the transportation and separation of particles in an airstream as they influence the drag force and buoyant force experienced by the particles. This is not the case for some dense medium separation process like the float and sink method. The sink and float method partitions the coal particles based on their relative density with minimal influence of shape following Archimedes' principle once the condition of the medium to ore ratio is adhered to.

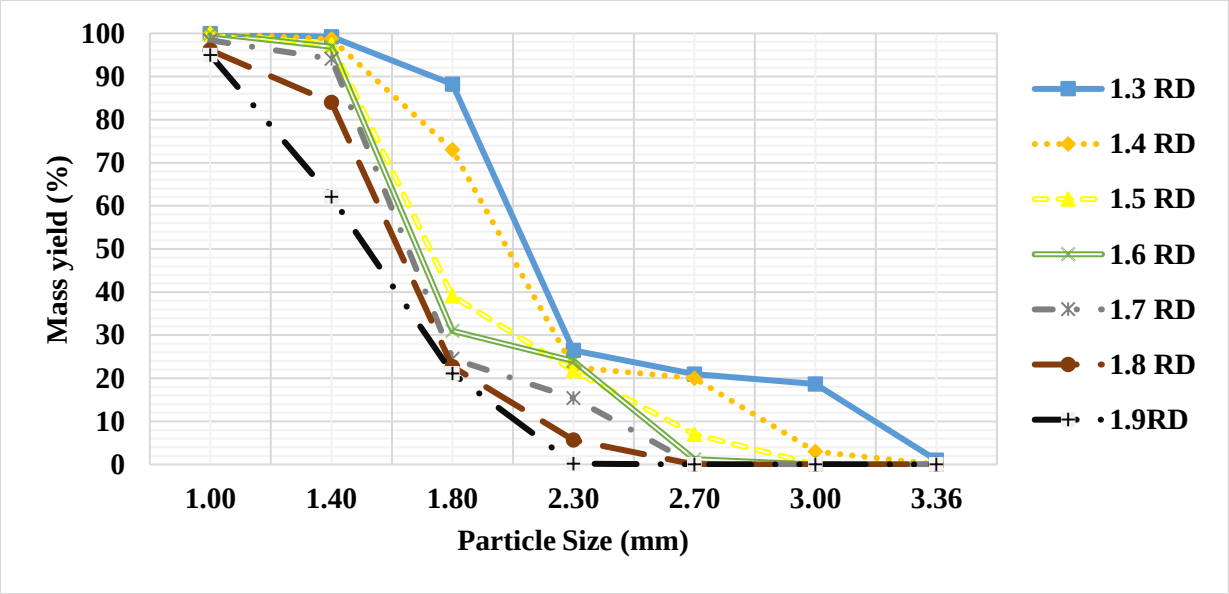


Figure 4 - 6: Mass yield(s) of individual particle at particle size distribution of (-3.36 + 1 mm)

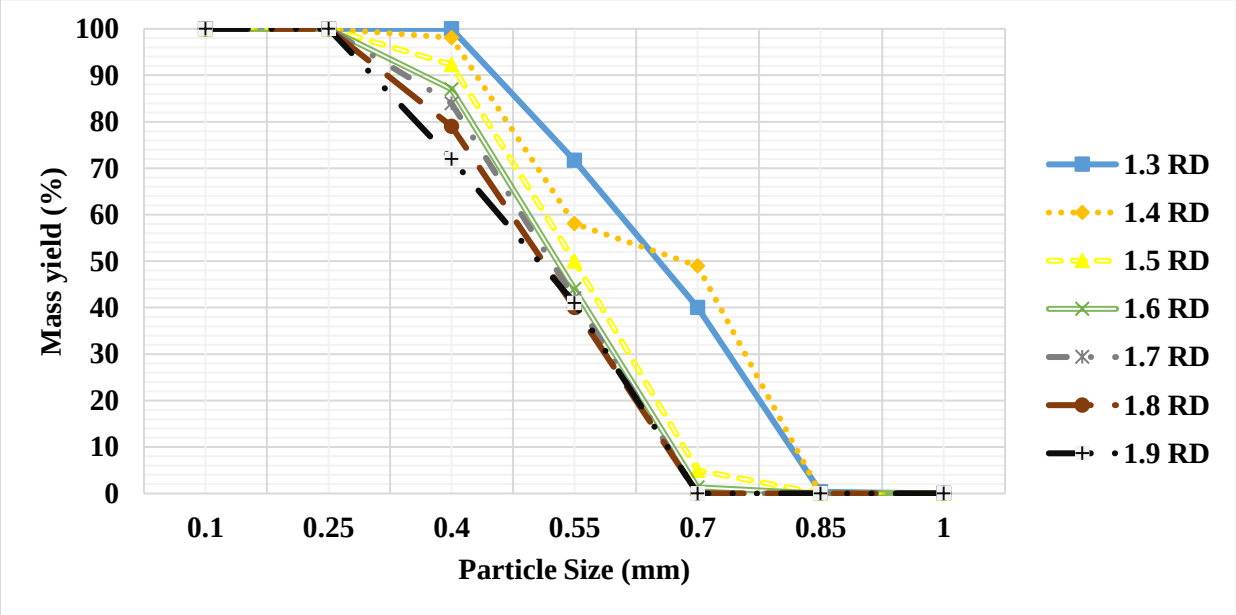


Figure 4 - 7: Mass yield(s) of individual particle at particle size distribution of (-1 mm)

4.2.3. PARTICLE MISPLACEMENT IN THE SEPARATOR

According to the simulation test run, the wind sifter approach showed great flexibility to cut at a specific relative density and particle size. However, a major drawback observed in the simulation study, for all the three particle size fractions was a high tendency of particle misplacement, particularly misplacement of high density particles into the second chamber. This is because in practical application, misplacements of high density particles into second chamber the will influence/reduce the grade of the coal recovered at each of the collecting bin. This phenomenon occurs in both separation chambers and for the three size fractions. Figures 4-8 to 4-11 below shows the particle tracks for the -6.7 + 3.36 mm particle size distribution. From figure 4-8 to 4-10, the amount of particle misplacement observed in bin 5 and 6 of the first chamber, might be because of gravity and constraint in determining an appropriate air-jet angle for effective transportation of all 1.3, 1.4 and 1.5 RD particles respectively into the second chamber.

Although, for particle with RD of 1.3, the lighter particles traveled further in the air stream in comparison to that of 1.4 and 1.5 as shown in the second chamber of the figures 4-8 to 4-10. This is as a result of the delay in the particle attaining its settling velocity as it enters the diffuser chamber. The kinetic energy of the airstream transporting the particles reduces as the particles enter the diffuser section of the 2^{nd} chamber because of the expansion of the air stream channel. As the airstream expands, the trajectory of particle flow tend to also follow the airflow trajectory as they attain their respective settling velocities. The lighter the particles, the further they travel and this makes some of the particles settle in more than one collecting bin as they are being transported by the expanding airstream. This means that the 1.3 RD particles (which is the lightest for this study) will be transported furthest by the transporting airstream and will settle in bins 1 to 4. Following the same logic, the 1.4 RD particles will settle in bins 2 to 4, the 1.5 RD particles will settle in bins 3 and 4, while the 1.6 RD particles settle in bin 4.

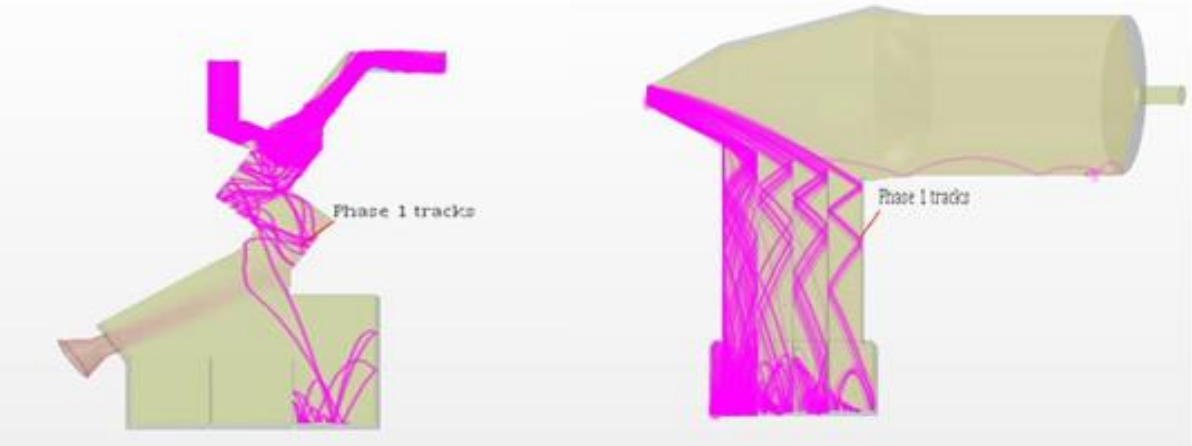


Figure 4 - 8: Particle tracks for -6.7 + 3.36 mm at RD of 1.3 in both chambers at 6.0 m/sec

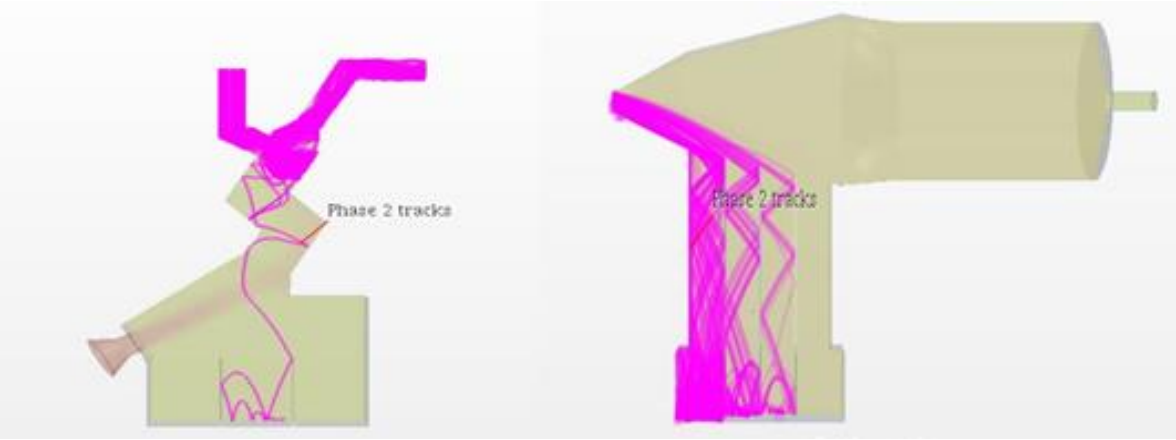


Figure 4 - 9: Particle tracks for -6.7 + 3.36 mm at RD of 1.4 in both chambers at 6.0 m/sec

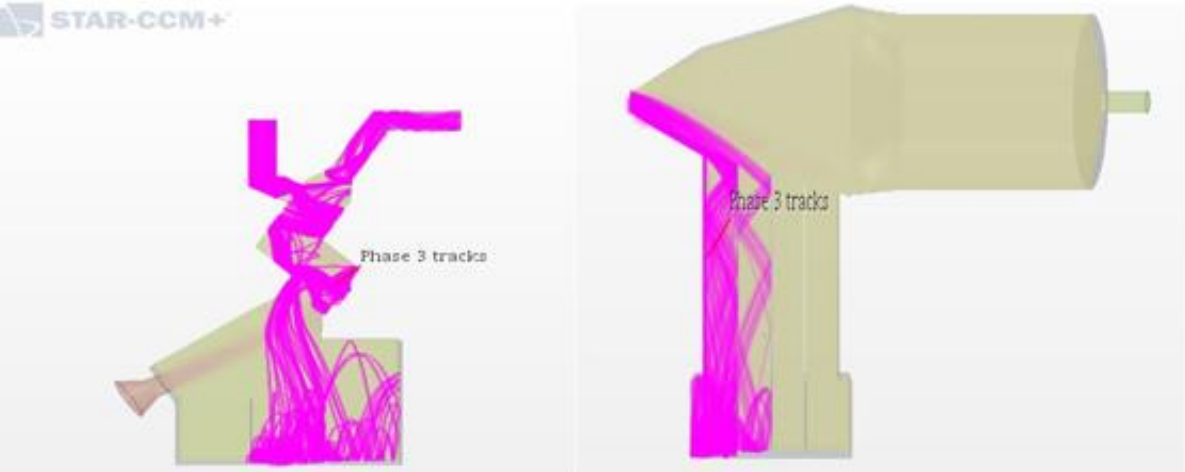


Figure 4 - 10: Particle tracks for -6.7 + 3.36 mm at RD of 1.5 in both chambers at 6.0 m/sec

For the 1.6 RD, as can be seen in the figure 4-11 below, some particle is observed settling in the 3rd bin of the 2nd chamber. This observation might be due to the particles hitting the walls of the separator as well as the particle to particle interactions when they are attaining settling velocity. The same phenomenon with similar trend was also observed for the other two particle size fractions

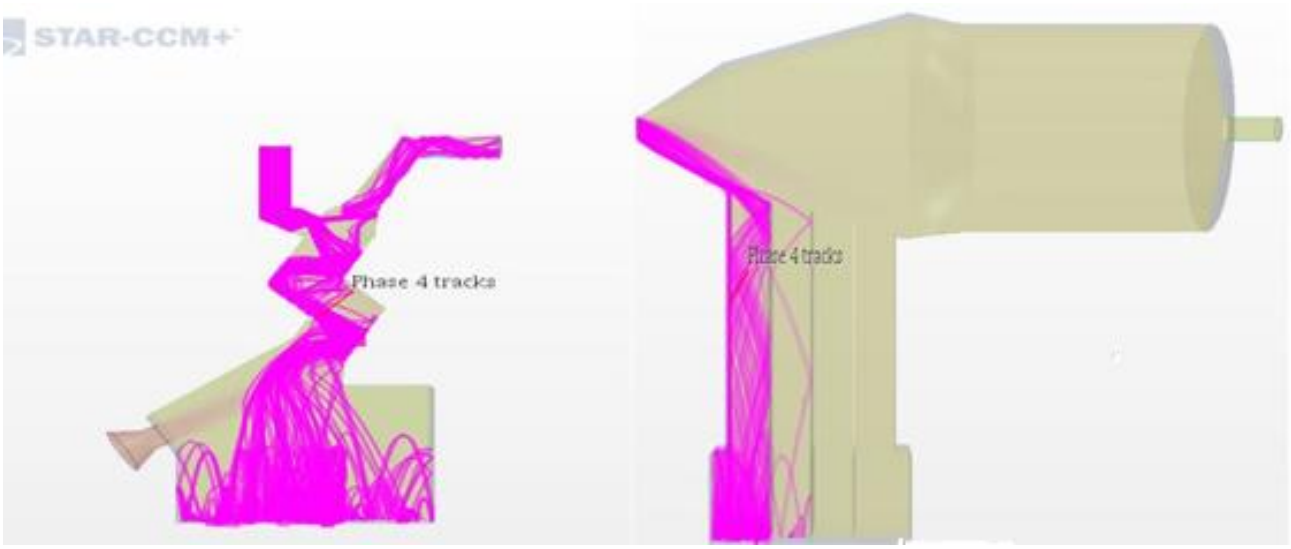


Figure 4 - 11: Particle tracks for -6.7 + 3.36 mm at RD of 1.6 in both chambers at 6.0 m/sec

Figure 4-12 to figure 4-17 shows the recoveries of for each of the relative densities in each of the collecting bins in both chambers, for all three particle size distributions. It can be observed that the majority of the particles that are not transported to the second chamber fall into the 6th bin of the first chamber as can be seen in figures (4-12, 4-14 and 4-16), while the majority of the particles that are transported into the second chamber settled in the 4th bin as can be seen from figures (4-13, 4-15 and 4-17) below.

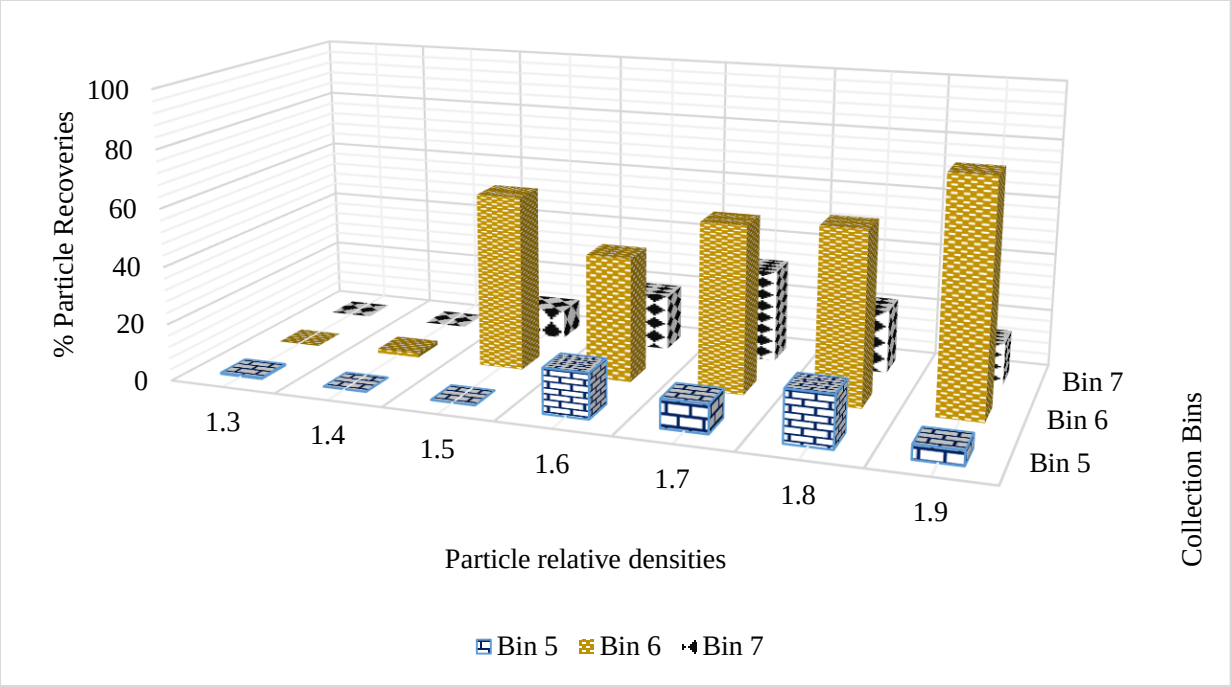


Figure 4 - 12: Particle recoveries in each bin in the first chamber for -6.7+3.36 mm

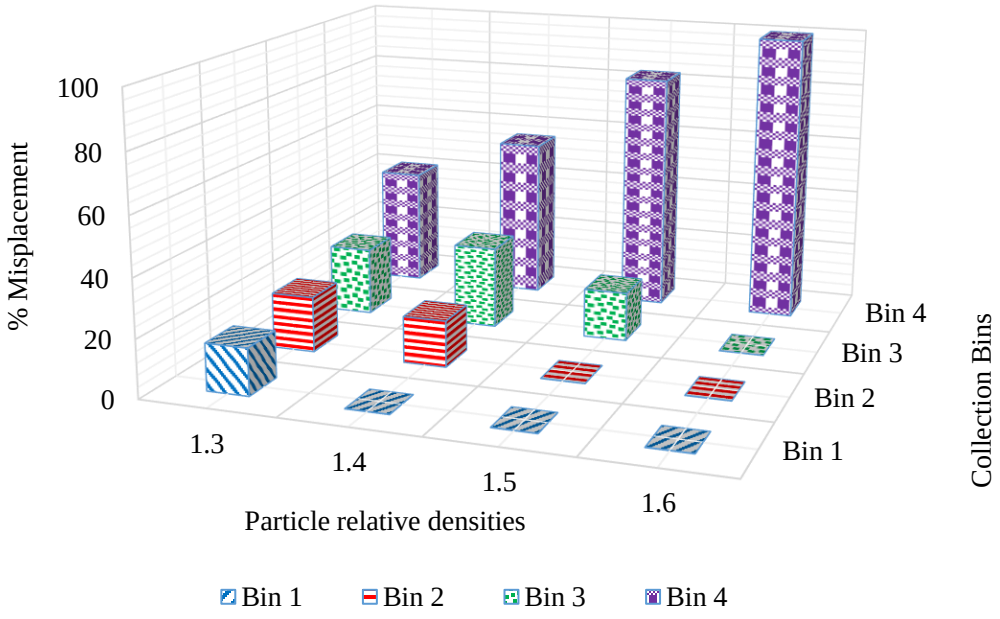


Figure 4 - 13: Particle recoveries in each bin in the second chamber for -6.7 + 3.36 mm

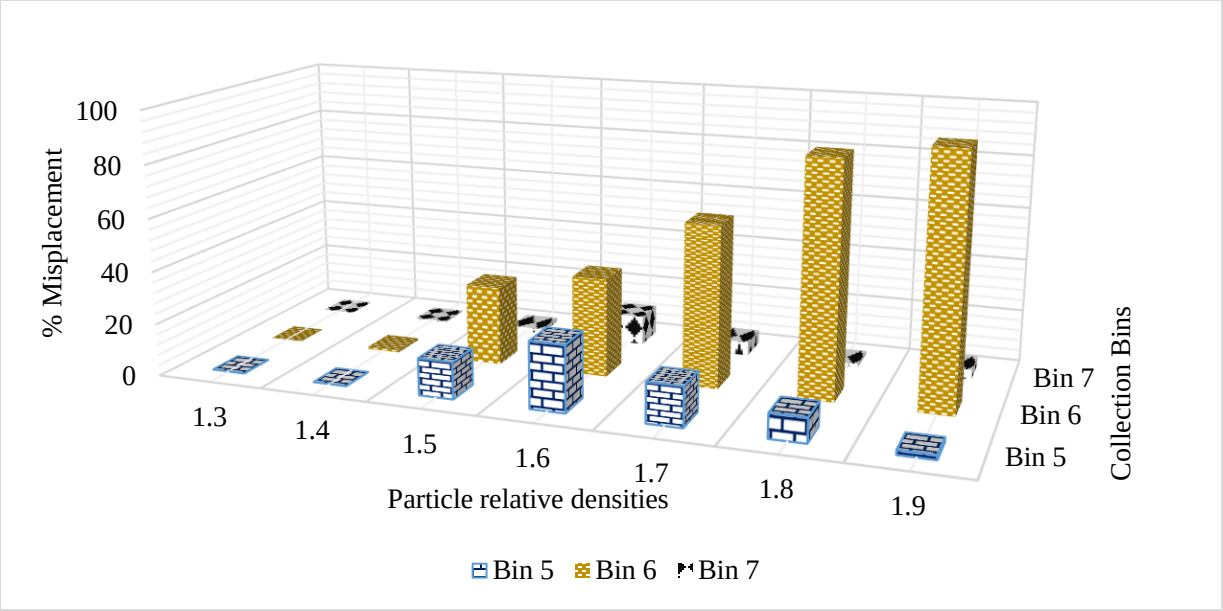


Figure 4 - 14: Particle recoveries in each bin in the first chamber for -3.36 + 1 mm

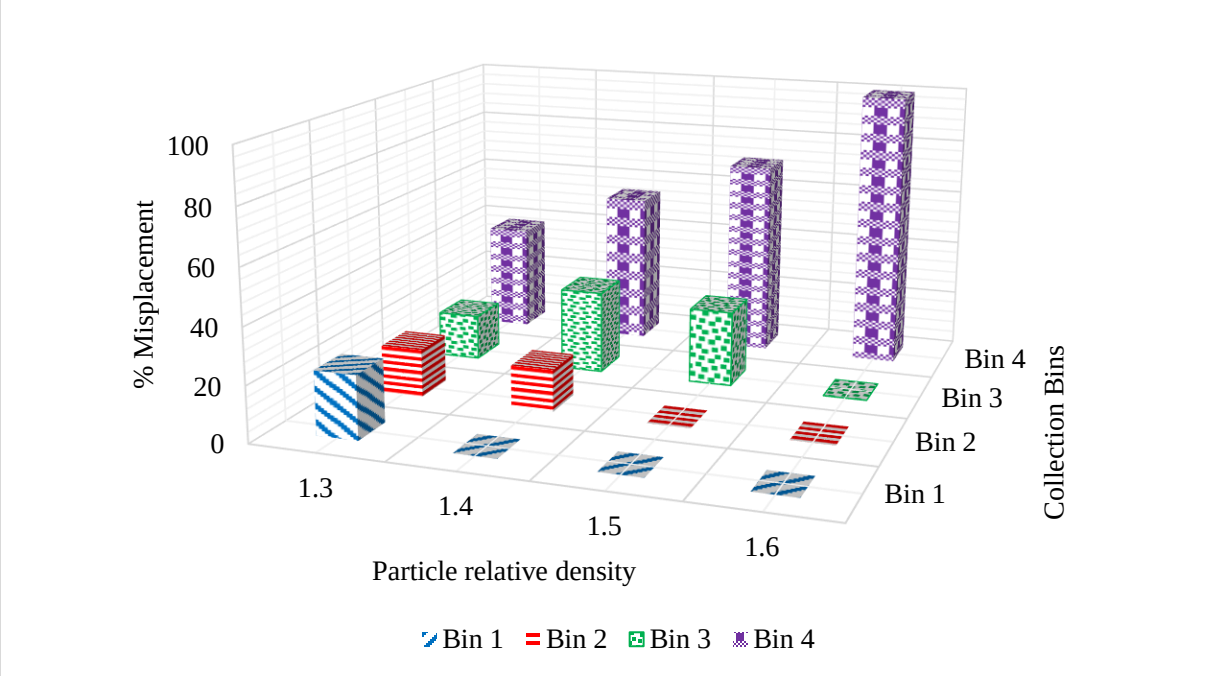


Figure 4 - 15: Particle recoveries in each bin in the second chamber for -3.36 + 1 mm

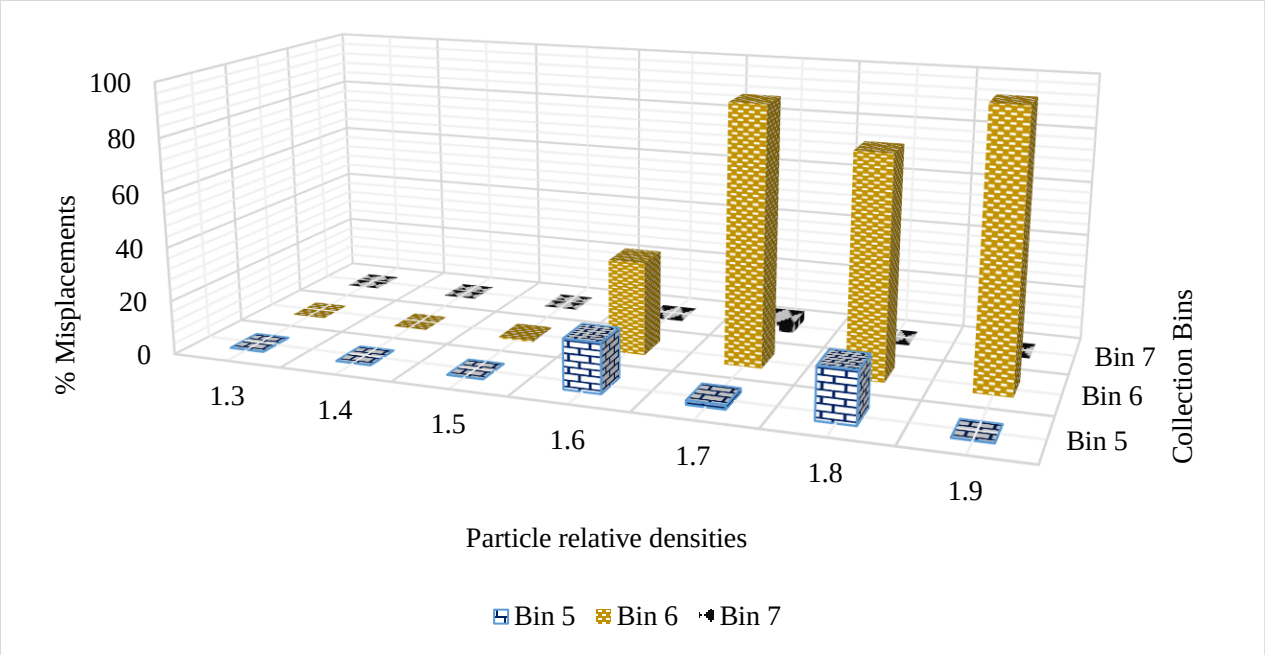


Figure 4 - 16: Particle recoveries in each bin in the first chamber for -1 mm

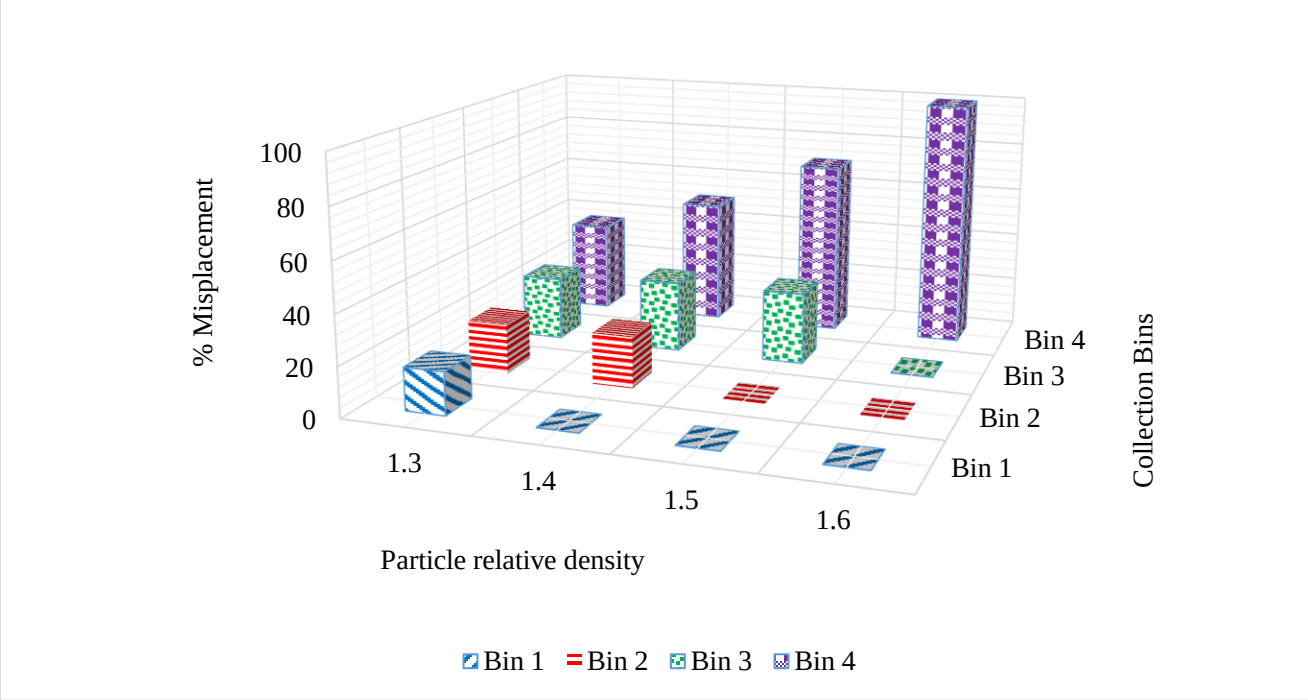


Figure 4 - 17: Particle recoveries in each bin in the second chamber for -1 mm

The result from the simulation study shows that cumulative mass yields (%) at 1.6 RD cut point for the three particle sizes (-6.7 + 3.36 mm; -3.36 + 1 mm; and -1 mm) at optimum conditions were found to be 35.6%, 39.6% and 49.5%, respectively.

4.3. BENEFICIATION RESULTS

4.3.1. CHARACTERIZATION AND WASHABILITY OF THE FEED COAL

The float and sink tests were carried out to beneficiate the as-received feed coal in order to use the results as a basis of comparison to ascertain the separation performance of the wind sifter separator. The washability plot from this test display the cumulative yield at each relative density with their corresponding cumulative ash contents. Table 4-1 presents the physico-chemical properties of the coal utilized.

Table 4- 1: Physico-chemical properties of the feed coal- air dry basis (adb)

Proximate Analysis (%)	Inherent moisture	Volatile Matter	Ash content	Fixed Carbon
	3.02	23.40	30.28	43.29
Calorific Value, MJ/kg	20.94 (adb)			
Elemental Analysis (%)	Total carbon 54.40	Hydrogen 3.13	Nitrogen 1.29	Total sulphur 0.87	Oxygen 6.89

Oxygen: 100- (Total carbon + Hydrogen + Nitrogen + Total sulphur + Ash + Moisture)

A comparison of the cumulative ash % as well as the cumulative weight % from the float and sink analysis are displayed for all three particle size fractions in figure 4-18 and figure 4-19. The figures portray information on the cumulative ash and yields of the coal products at different relative densities. It can be observed in Figure 4-18 below, that the -1 mm sample has the lowest ash content, which can be as result of the liberation of the inorganic minerals from the organic component of the coal. The -3.36 + 1 mm particle size fraction was seen with a high mass yield of 42.45% compared to the other two size fractions.

According to Tables 4-2, 4-3 and 4-4 below, the as-received coal with an ash content of 30.28% was seen improved from a low-quality coal to a high quality coal with an ash content ranging between 4.90% to 5.53% at a RD of 1.3, while at a RD of 1.5, coal product ranging between 11.82 % - 16.15 % ash was achieved, but at a low recovery. It can also be observed from the tables below that as particle size distribution decreases, the ash content also decreases thereby leading to an increase in the grade of the product. This phenomenon might be due to high particle liberation tendency; the smaller the particle size fraction, the higher the likelihood of the liberation of the organic matter from the inorganic mineral matter in the coal.

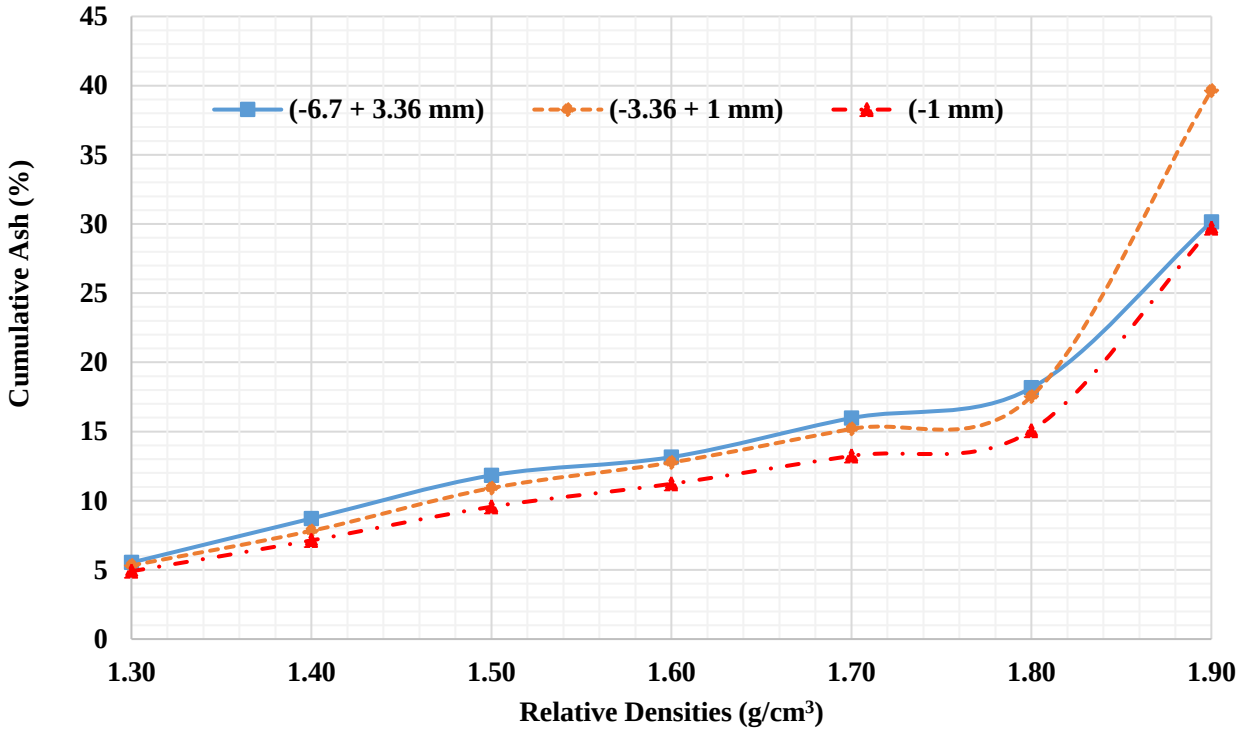


Figure 4 - 18: Relative density versus Cumulative Ash (%) of all three-particle sizes

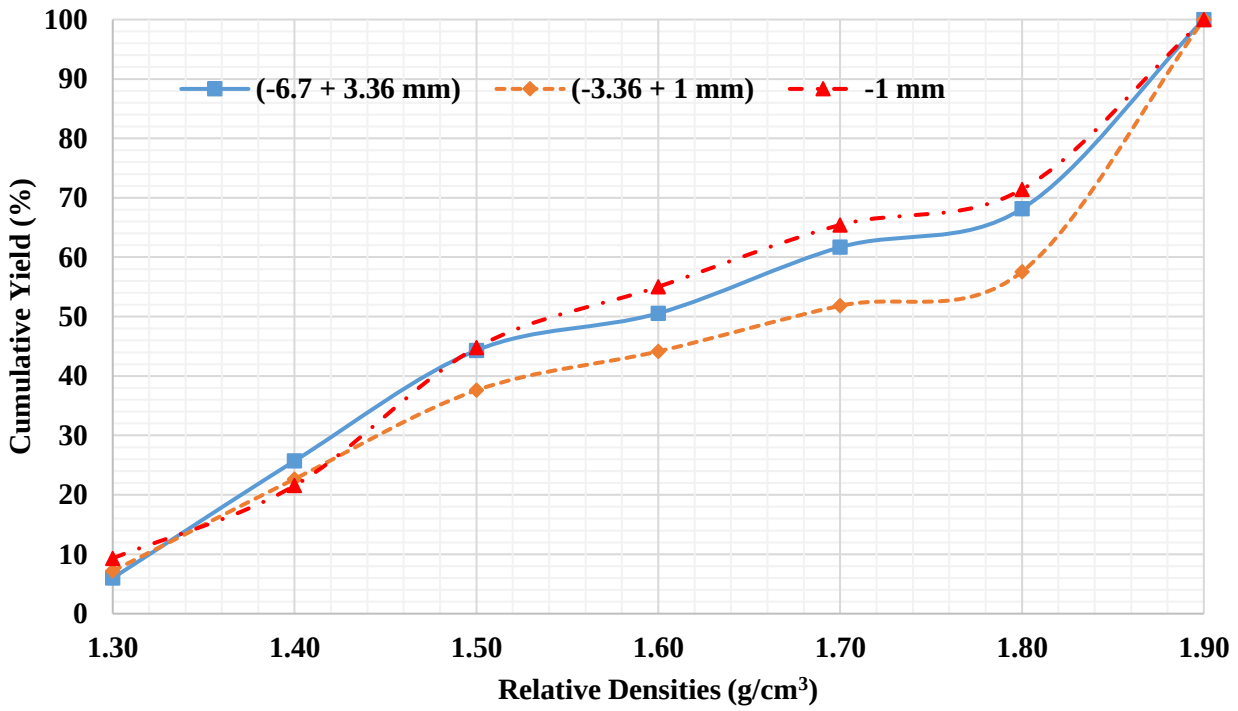


Figure 4 - 19: Relative density versus Cumulative mass (%) of all three-particle sizes

Table 4-2: Results of proximate analysis (adb) for the feed coal of -6.7+3.36 mm particle size fraction

Sample	TM %	VM %	Ash content %	FC %	Specific Mass Yield (%)
Feed	3.02	23.40	30.28	43.29	100
1.30 float	2.29	37.55	5.53	56.64	6.00
1.40 float	2.39	29.71	9.68	58.82	19.71
1.50 float	2.48	23.99	16.15	57.38	18.61
1.60 float	2.40	21.55	22.52	53.52	6.24
1.70 float	2.29	20.66	28.77	48.28	11.12
1.80 float	1.99	18.51	38.95	40.55	6.47
1.80 sink	1.68	17.90	55.85	24.57	21.85

TM: Total Moisture; VM: Volatile matter; FC: Fixed carbon

Table 4-3: Results of proximate analysis (adb) for the feed coal of -3.36 + 1 mm particle size fraction

Sample	TM %	VM %	Ash content %	FC %	Specific Mass Yield (%)
Feed	3.02	23.40	30.28	43.29	100
1.30 float	2.49	36.88	5.32	55.30	7.18
1.40 float	2.29	29.04	8.98	59.70	15.49
1.50 float	2.04	23.28	15.60	59.08	14.94
1.60 float	2.28	21.87	23.29	52.56	6.54
1.70 float	2.61	20.89	29.17	47.33	7.68
1.80 float	2.05	19.50	38.64	39.81	5.72
1.80 sink	1.17	18.66	69.64	10.52	42.45

TM: Total Moisture; VM: Volatile matter; FC: Fixed carbon

Table 4-4: Results of proximate analysis (adb) for the feed coal of -1 mm particle size fraction

Sample	TM %	VM %	Ash content %	FC %	Specific Mass Yield (%)
Feed	3.02	23.40	30.28	43.29	100
1.30 float	2.56	35.48	4.90	57.06	9.31
1.40 float	2.46	27.63	8.82	61.09	12.25
1.50 float	2.09	22.99	11.82	63.10	23.21
1.60 float	2.54	22.10	18.48	56.88	10.24
1.70 float	1.57	20.87	23.90	53.66	10.41
1.80 float	1.90	19.36	35.11	43.63	5.98
1.80 sink	1.29	16.97	66.20	15.54	28.59

TM: Total Moisture; VM: Volatile matter; FC: Fixed carbon

4.3.2. DRY WIND SIFTER SEPARATION TEST

The calibration of the separator was first carried out to determine the mass flowrates at each carrier frequency of the vibratory feeder and to also ascertain the range of sample mass flowrate in which dilute phase can be maintained in the separator. The results from the calibration tests, as seen in figures (4-20) to (4-22) below shows that as the carrier frequency increases from 6 kHz to 14.4 kHz, the time required in feeding the coal (feed coal) into the separator decreases, thus making the mass flowrate simultaneously increase. The particle size fraction was also noted to have an

influence on the mass flow rate, with the – 1 mm size fraction showing lowest mass flow at carrier frequencies between 6 and 8 kHz. However at 8 kHz and above, the mass flowrate of the coal particles into the separator increases from 47.36 g/min to 1000 g/min. The increase noted is due to the increase in the vibration intensity of the feeder leading to the reduction in the clustering of the particles. This trend is also seen in the other particle size distribution where for the – 6.7 + 3.36 mm size fraction, the vibration intensity also leads to an increase in the mass flowrate from 33.43 g/min at 6 kHz to 2400 g/min at 14.4 kHz. For the beneficiation of the -1 mm size fraction in the separator, a carrier frequency of 8.2 kHz resulted in a mass flowrate of 52.2 g/min, while for the – 3.36 + 1 mm, a carrier frequency of 6.1 kHz resulted in a mass flowrate of 46.6 g/min.

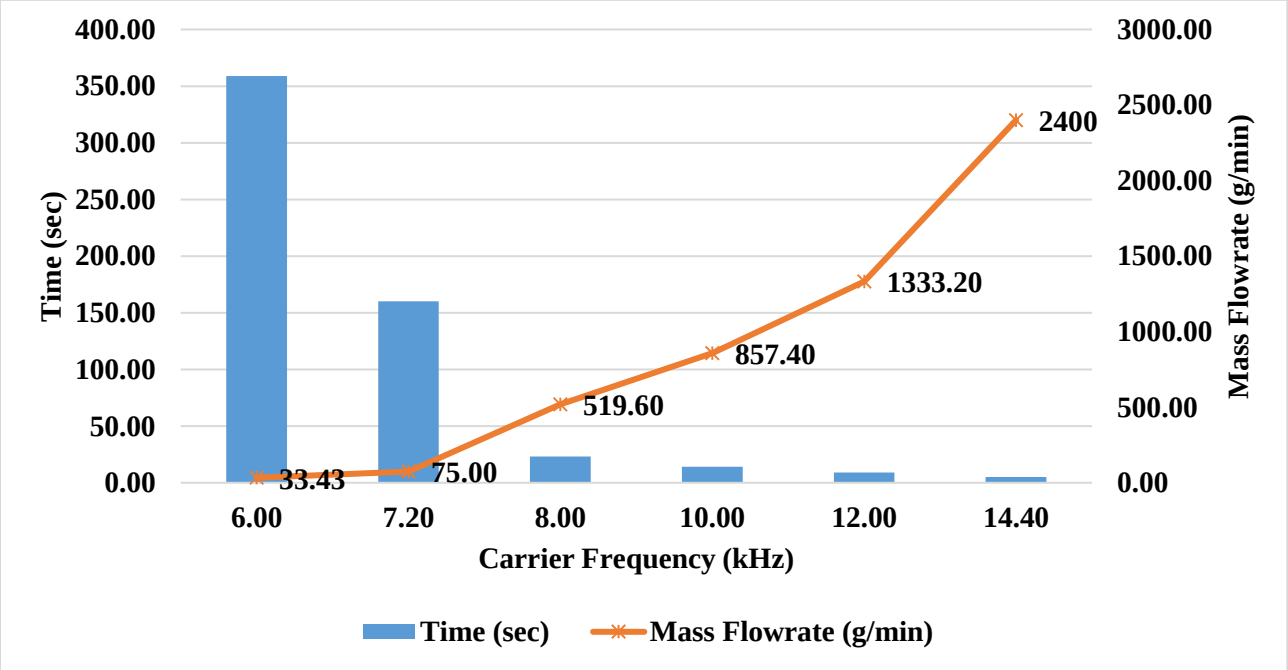


Figure 4 - 20: Calibration of the vibratory feeder for the separation of -6.7+3.36 mm fraction

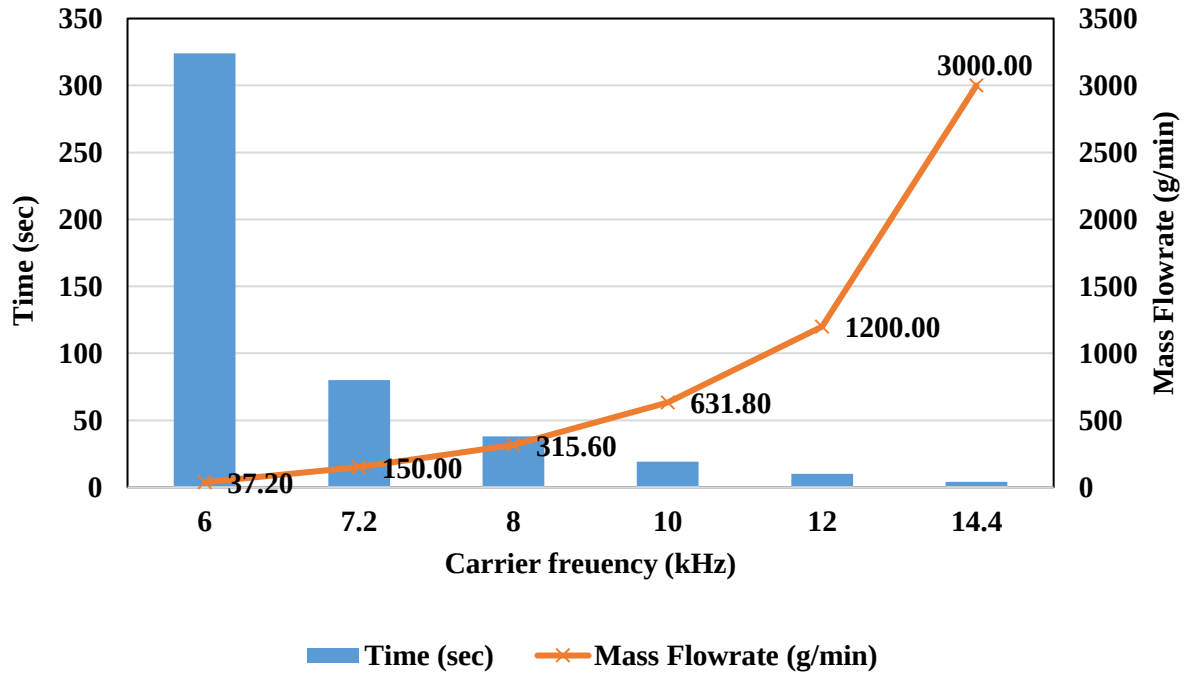


Figure 4 - 21: Calibration of the separator for -3.36+1 mm particle size fraction

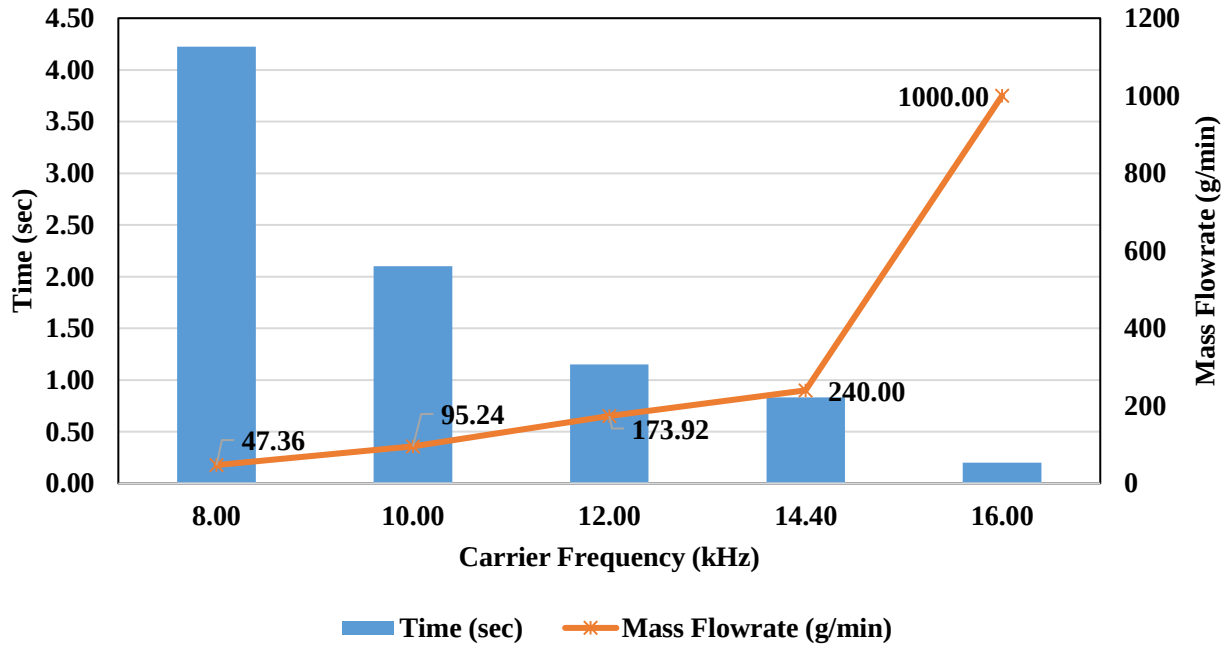


Figure 4 - 22: Calibration of the separator for -1 mm particle size fraction

4.3.3 INFLUENCE OF AIR VELOCITY ON THE WIND SIFTER SEPARATION

4.3.3.1. Influence of air velocity on the separation of -6.7+3.36 mm size fraction

500 g of representative ROM feed coal of – 6.7 + 3.36 mm particle size fraction was fed into the separator at a constant mass flowrate 36 g/min and different air stream velocities of 6.0 m/sec, 4.5 m/sec and 4.0 m/sec. The results show according to Figure 4-23 that as the air velocity reduces, coal with a lower ash content was obtained in the first bin of the diffuser compartment. At 6.0 m/sec, cumulative ash content of 21.95% was achieve in the bins of the second chamber. The cleanest coal product obtained from this size fraction was 16.75% under an air stream of 4.0 m/sec in the first bin. A rapid increase was noted in the cumulative ash content of the coal separated at 4.0 m/sec, and this might be as a result of the drop in the velocity require to transport the coal into the diffuser section. That is, with lower velocity, more of high-density materials rich in mineral matter, dropped into the 6th and 7th bin, and separated out from the lighter particles, which are transported into the 2nd chamber.

According to both Figures (4-23 and 4-24), the separation profiles obtained for individual air stream velocity followed a trend whereby the coal sample separated at 6.0 m/sec has the highest ash content, followed by 4.5 m/sec and lastly 4.0 m/sec at the second bin. Whereas for the cumulative mass yield (Figure 4-24), the coal separated under the 6.0 m/sec velocity was seen with the highest recovery in the second chamber of the separator, which is expected.

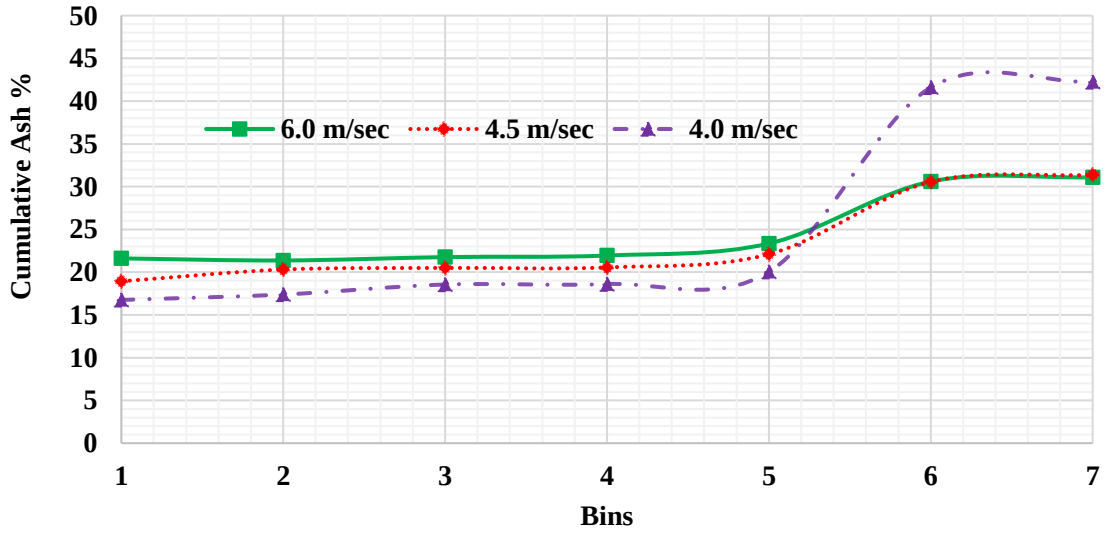


Figure 4 - 23: Cumulative Ash content for – 6.7 + 3.36 mm at different air stream velocities

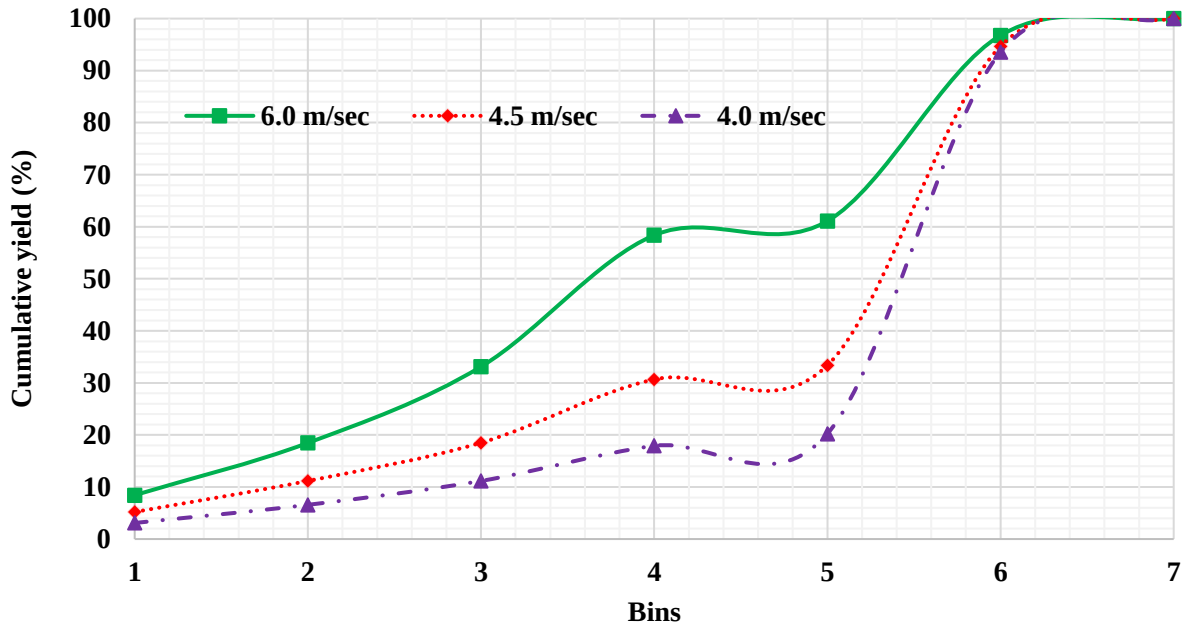


Figure 4 - 24: Cumulative mass yield for – 6.7 + 3.36 mm at different air stream velocities

4.3.3.2. Influence of air velocity on the separation of -3.36+1 mm size fraction

Air stream velocities of 4.2 m/sec, 3.0 m/sec, 2.5 m/sec and 2.0 m/sec were used to upgrade the -3.36 + 1 mm fraction in the separator. The separation of the coal organic from its inorganic also follow similar trend as that of the -6.7 + 3.36 mm fraction. According to Figure 4-25, cumulative ash of 24.61% was obtained from the first bin of the second chamber at the highest air velocity of 4.2 m/sec. As the air stream velocity reduces to 3.0 m/sec, the cumulative ash reduces to 21.89% for the first bin and further produces a much cleaner coal product of 17.63% under an air stream of 2.0 m/sec. Figure 4-26 shows that at a higher air stream velocity, the air stream act as the dominating factor for separation rather than the inherent density of the particles. This resulted in increased sample transport to the second chamber of the separator. The washability data obtained in this test can be seen in **Appendix A** while the tables showing the separation performance for the sink and float as well as the wind sifter can be found in **Appendix B**.

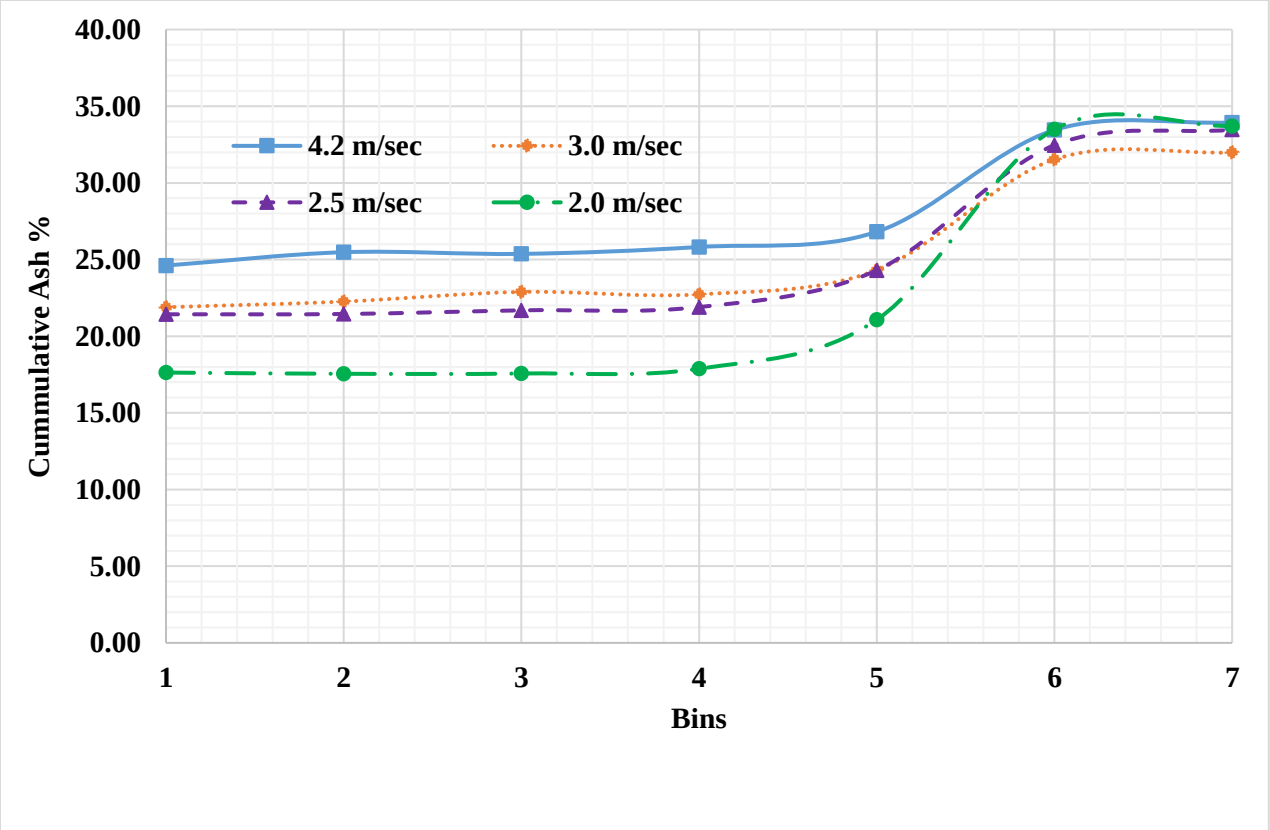


Figure 4 - 25: Cumulative Ash content for – 3.36 + 1 mm at different air stream velocities

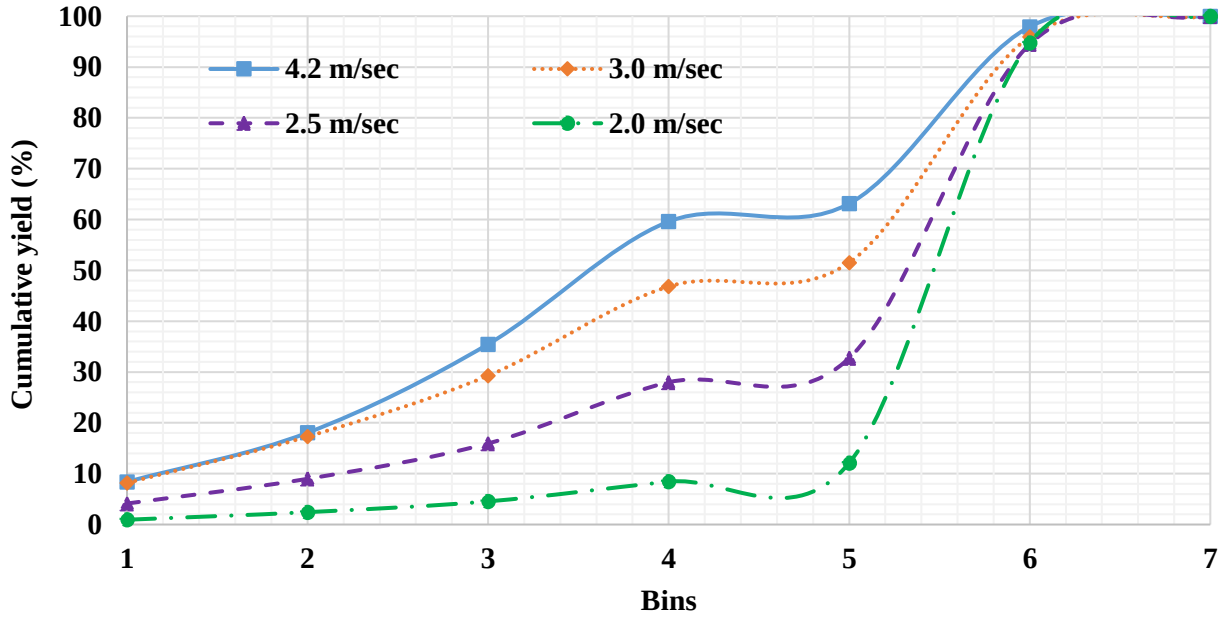


Figure 4 - 26: Cumulative mass yield for – 3.36 + 1 mm at different air stream velocities

4.3.3.3. Influence of air velocity on the separation of -1 mm size fraction

The -1 mm coal size fraction unlike the -6.7+3.36 and the -3.36+1 mm size fractions was not easily beneficiated in the present fabricated wind sifter. More than 50% of the sample are trapped within the separator, as a result of the improper lining of the wall of the separator. In addition, some of the particles are also transported into the cartridge filter, far above the designated bin 1 in the second chamber, which are expected to be of lowest ash content based on the float and sink tests. This test was conducted under air stream velocities of 1.7 m/sec and 1.0 m/sec, and the cumulative ash obtained from this fraction in the first bin was very high compared to other fractions tested. The result obtained from this fraction (Figure 4-27 and 4-28) does not accurately reflect the separator's ability to separate, as observed in the trial and recommendations are therefore made to correct this in Chapter 5 of this thesis.

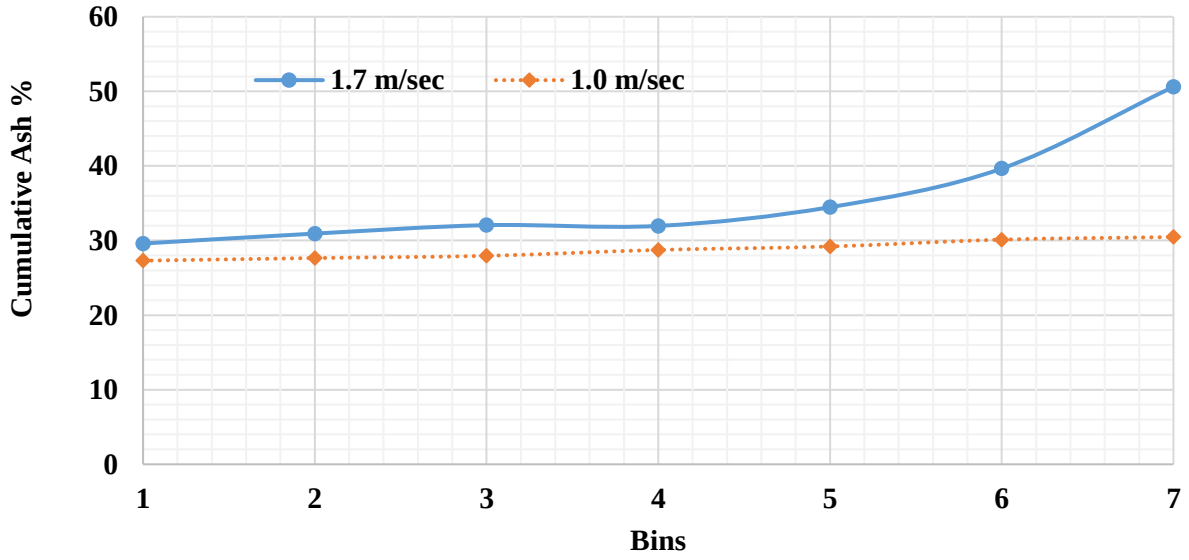


Figure 4 - 27: Cumulative Ash content for – 1 mm at different air stream velocities

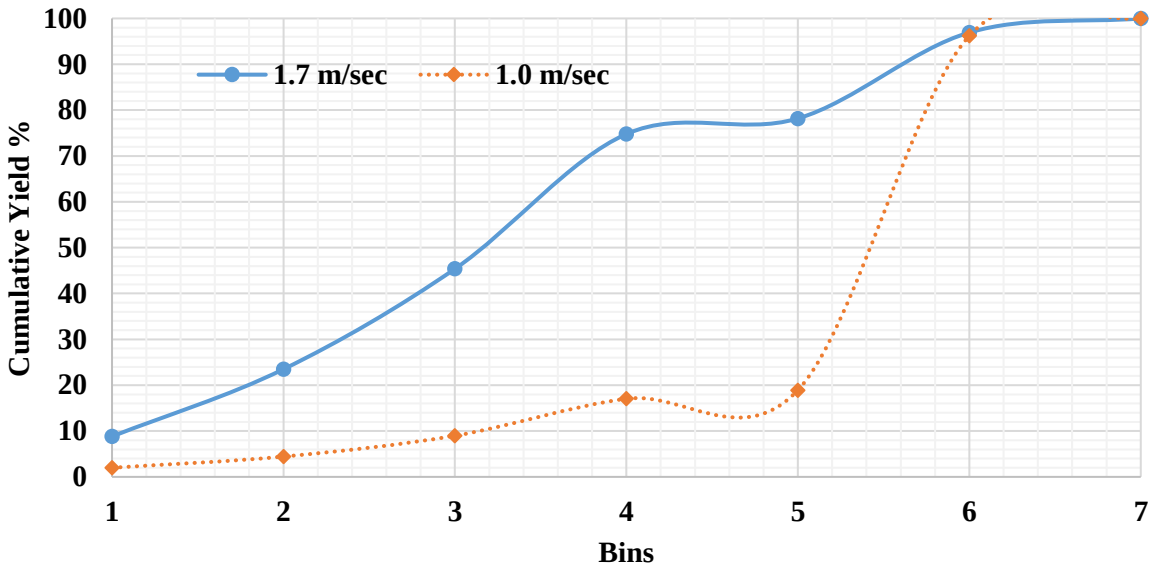


Figure 4 - 28: Cumulative mass yield for – 1 mm at different air stream velocities

4.3.4. REPEATABILITY TESTS AND SAMPLE LOSSES OBSERVED FOR EACH PARTICLE SIZE FRACTION

The repeatability tests were performed for the three particle size fractions using the optimal velocity values obtained from the simulation study to verify the repeatability and consistency in the mass recovery of the separator. It can be observed in Figure 4-29 and Figure 4-30 that the mass recovery for the -6.7 + 3.36 mm and -3.36 + 1 mm size fractions were very repeatable unlike the -1 mm (Figure 4-31), which was inconsistent. The inconsistency in the mass recovery for this size fraction (- 1 mm) was because of the misplacement and trapping of the particles within the linatex used in the lining of the separator wall. This is also responsible for particle accumulation and blockage in the particle stream.

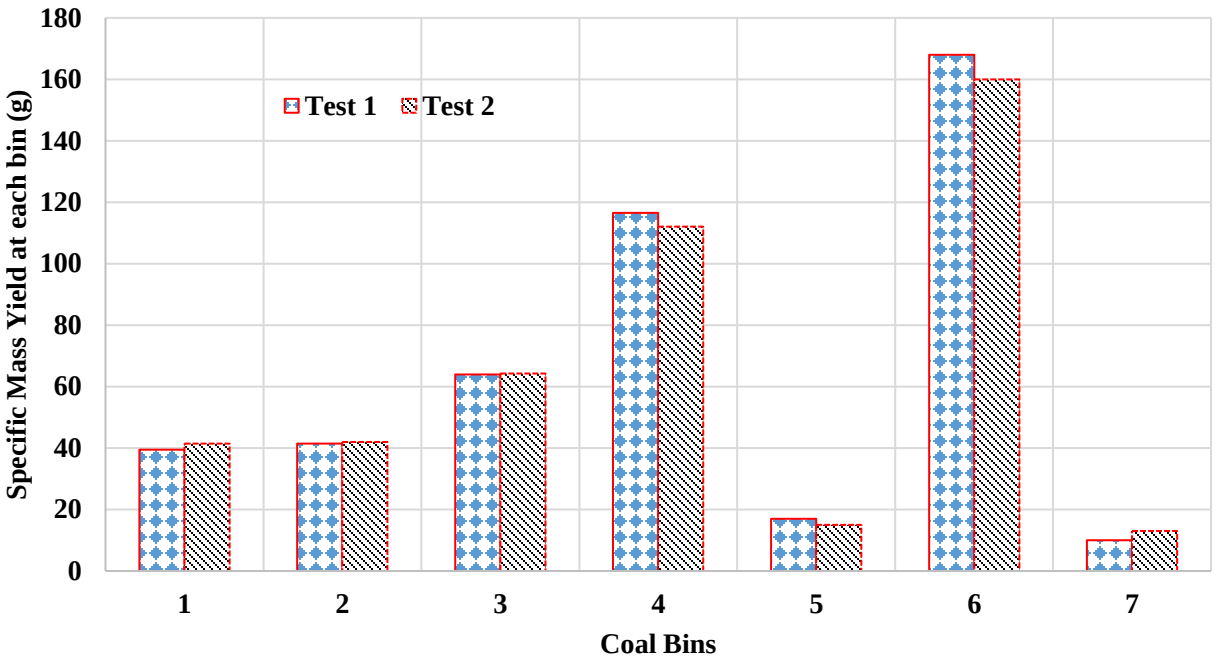


Figure 4 - 29: Repeatability test of -6.7+3.36 mm particle size fraction at 6.0 m/sec

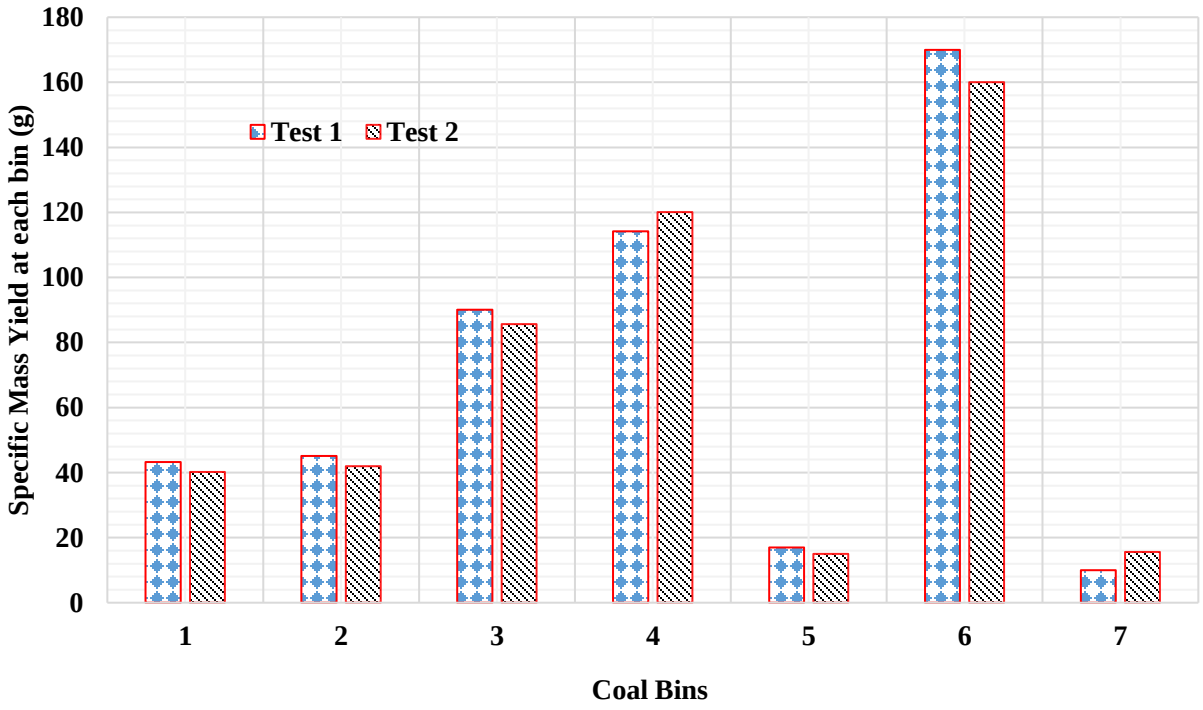


Figure 4 - 30: Repeatability test of -3.36+1 mm particle size fraction at 4.2 m/sec

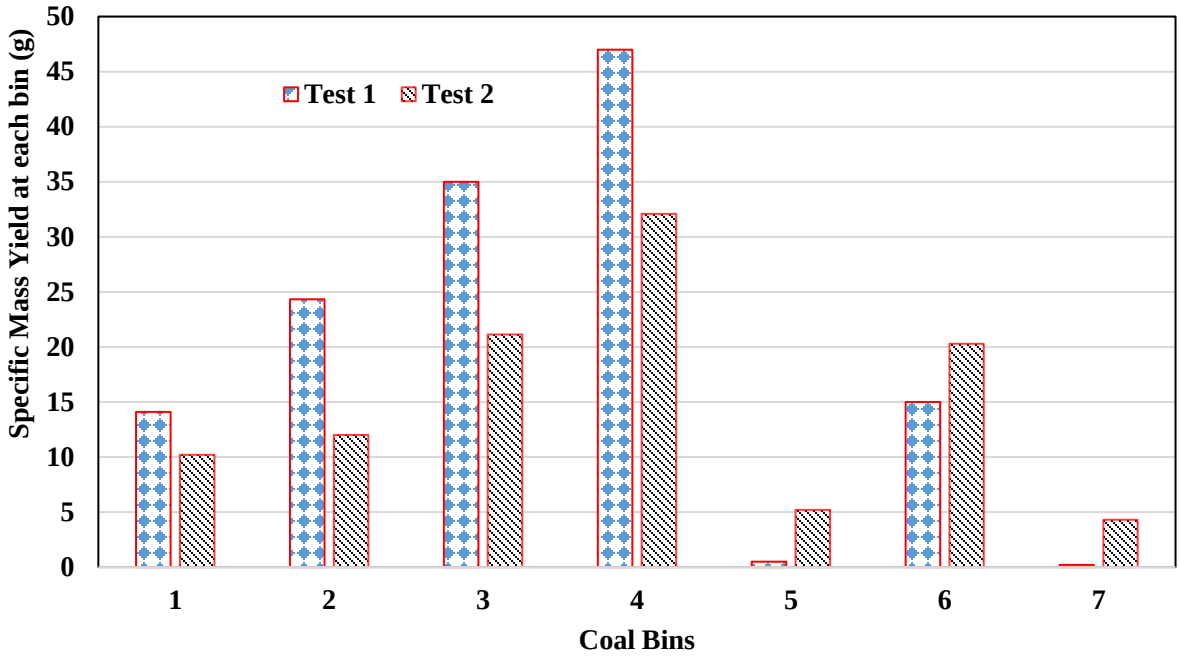


Figure 4 - 31: Repeatability Test of -1 mm particle size fraction at 1.7 m/sec

According to figures 4-32 and 4-33, minimal sample losses were observed for the – 6.7 + 3.36 mm and – 3.36 +1 mm coal fractions. However, there was large amount of the feed sample loss observed for the – 1 mm size fraction. This was because some particles were stuck to the walls of the separator and some were transported into the filter section at the end of the second chamber. With a feed of 500 g fed into the separator and according to figures 4-32 and 4-33 below, it can be observed that in all the seven bins, the cumulative yield for both -6.7+3.36 and -3.36+1 mm, was between 462.85 – 486.85 g (92-97%) of the feed. However for the – 1 mm size fraction, sample loss between 159.84-174.69 g (32-35%) was observed. This shows that the – 1 mm size fraction has a massive loss and hence indicates a need for the optimization of this present separator.

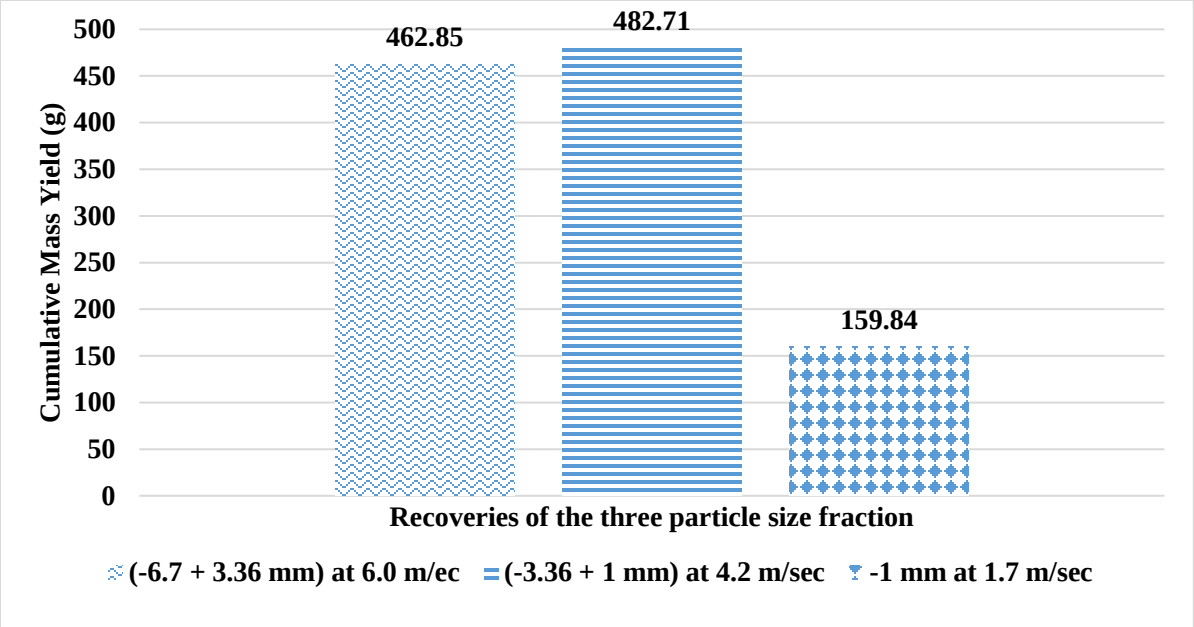


Figure 4 - 32: Cumulative yield (g) of all seven bins for each particle size fractions at their respective highest velocities

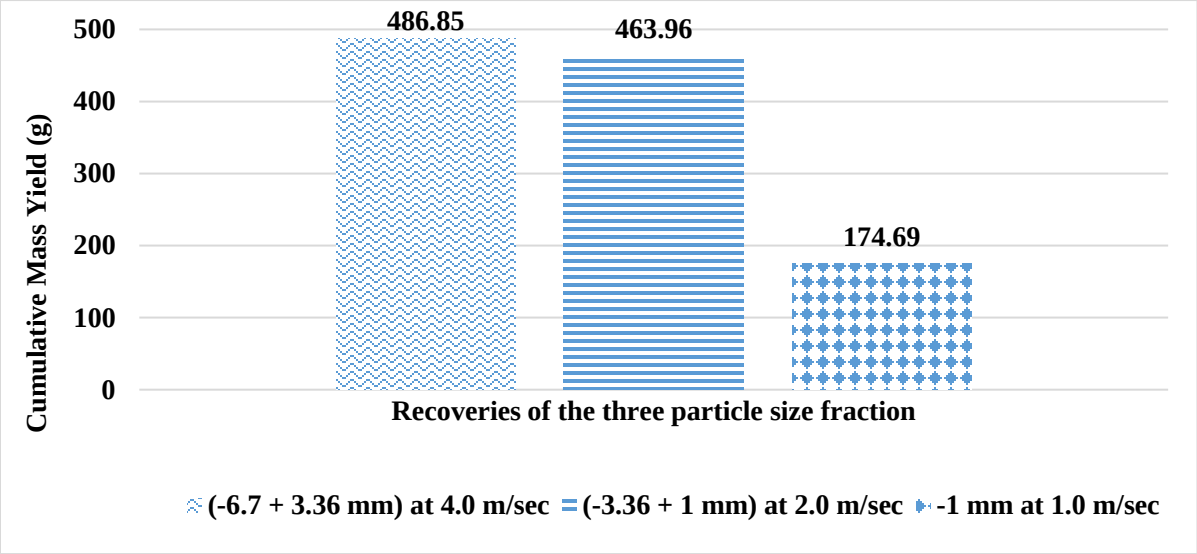


Figure 4 - 33: Cumulative yield (g) of all seven bins for each particle size fractions at their respective lowest velocities

4.3.5. INFLUENCE OF MASS FLOWRATE ON THE WINDSIFTER SEPARATOR

The influence of mass flowrate on – 6.7 + 3.36 mm and – 3.36 + 1 mm coal fractions were also investigated and the results obtained are illustrated in the figures 4-34 to 4-37 below. For the -1 mm as earlier stated, large amount of the feed sample was trapped within the separator and transported into the filter at the end of the second chamber. Owing this occurence, the investigation for this particle size fraction was stopped. The mass flowrates were varied while the airstream velocities were kept constant. The observations made for both size fractions are explained below.

4.3.5.1. INFLUENCE OF MASS FLOWRATE ON -6.7 + 3.36 mm FRACTION

The influence of mass flowrate on -6.7+3.36 mm coal fraction was conducted, and the results obtained illustrated in Figure 4-34. The figure below present results of the cumulative ash content of clean coal products obtained in bins 1 to 4 (in the second chamber) at different sample mass flowrate and constant air stream velocity, while still maintaining dilute phase in the system according to Santos *et al*. (2011). It can be observed from figures (4-34) and (4-35) below that as the mass flowrate increases the cumulative mass yield reduces while the cumulative ash increases. This trend occurs for both particle size fractions and might be as a result of higher tendency of particle to particle interferences as the mass flowrates increase, as well as a reduction in sifting effectiveness of the air stream which will result in some misplacements of mineral rich particles being transported into the second chamber.

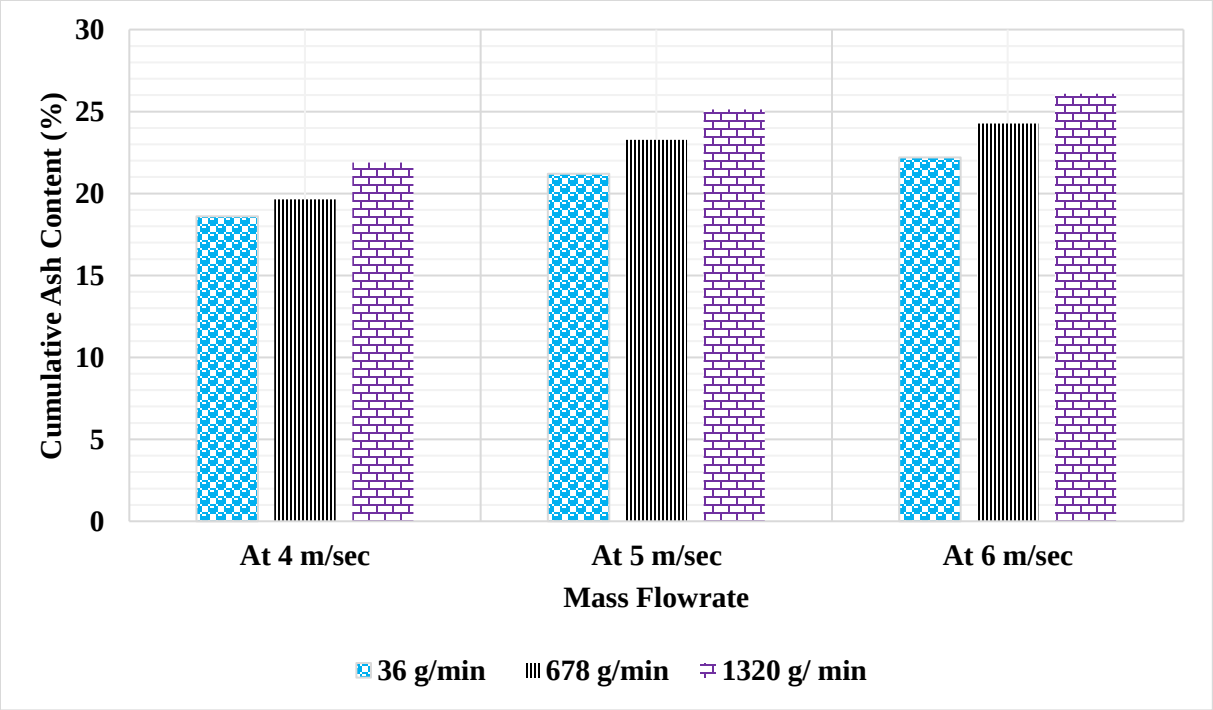


Figure 4 - 34: Cumulative ash content at different mass flowrates and constant air velocity for -6.7+3.36 mm

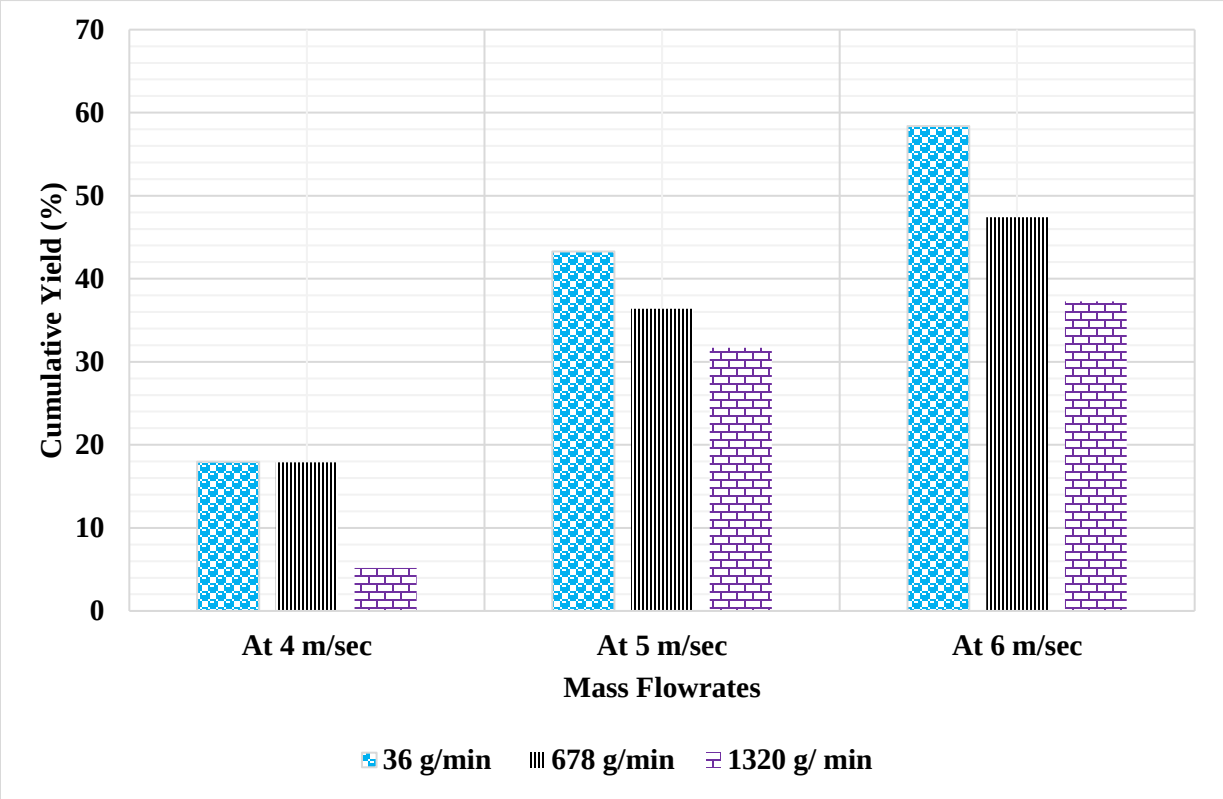


Figure 4 - 35: Cumulative yield at different mass flowrates and constant velocity for -6.7+3.36 mm

4.3.5.2. INFLUENCE OF MASS FLOWRATE ON -3.36 + 1 mm FRACTION

Following the same condition for dilute phase above, similar trend was also observed for both the ash and yield % in the -3.36+1 mm size fraction in figures (4-36) and (4-37), respectively. The cumulative ash at 1200 g/min feed rate was observed to be more at other mass feed rate because of the higher liberation tendency in the -3.36 + 1 mm size fraction.

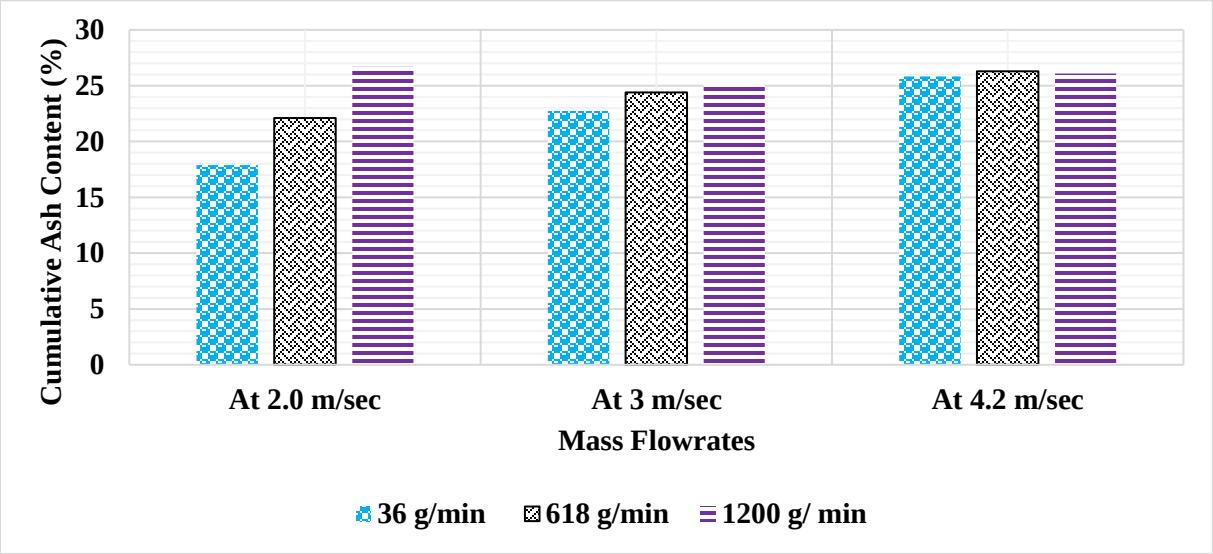


Figure 4 - 36: Cumulative ash content (%) at different mass flowrates for -3.36+1 mm

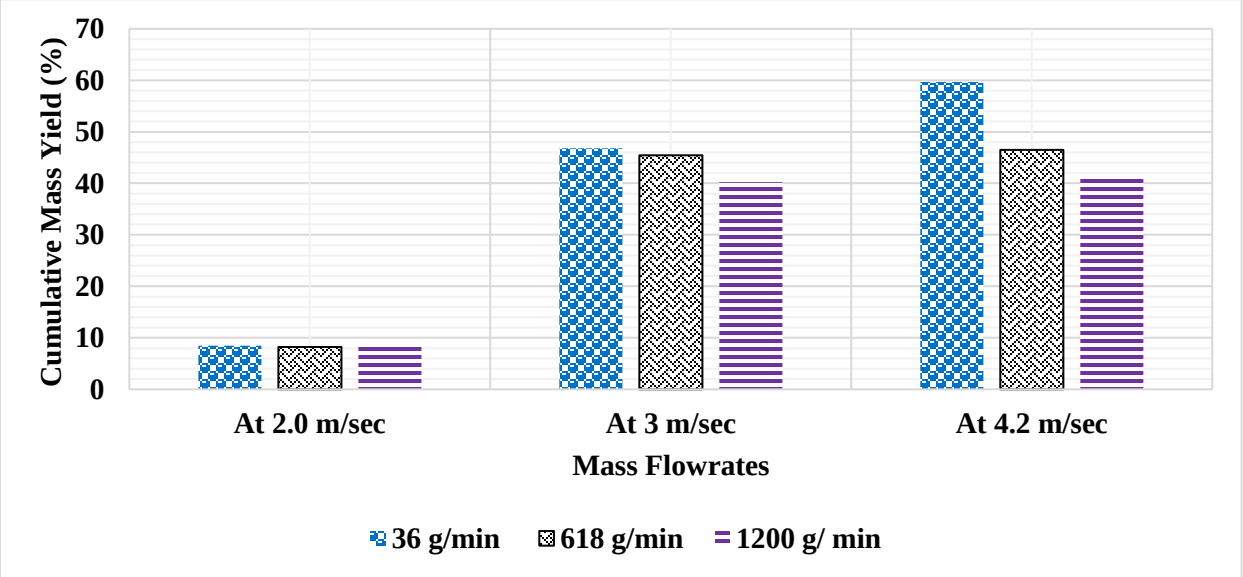


Figure 4 - 37: Cumulative wt. (%) at different mass flowrates for -3.36 + 1 mm

4.4. COMPARISON BETWEEN SIMULATION AND EXPERIMENTAL RESULTS

The simulation and experimental results were compared as can be seen in figure 4-38, by corelating the mass yields at 6.0 m/sec for (-6.7 +3.36 mm), 4.2 m/sec for (-3.36 + 1 mm) and 1.7 m/sec for -1 mm. The result shows that the yield from the experimental study was more than the yield achieved from the simulation study and this might be as a result of the influence of shape. In the simulation study, the particles were assumed to be perfectly spherical, however from the experimental study, the flat shaped coals which are expected to have lower coefficeint of drag were realized in the second chamber. This flat shaped coals are observed to have vitrain bands which denotes that they are of high grade. To account for the differences in the yields for both the simulation and experimental studies, a particle shape analysis will be conducted in the doctoral study leading to the optimization of this present separator.

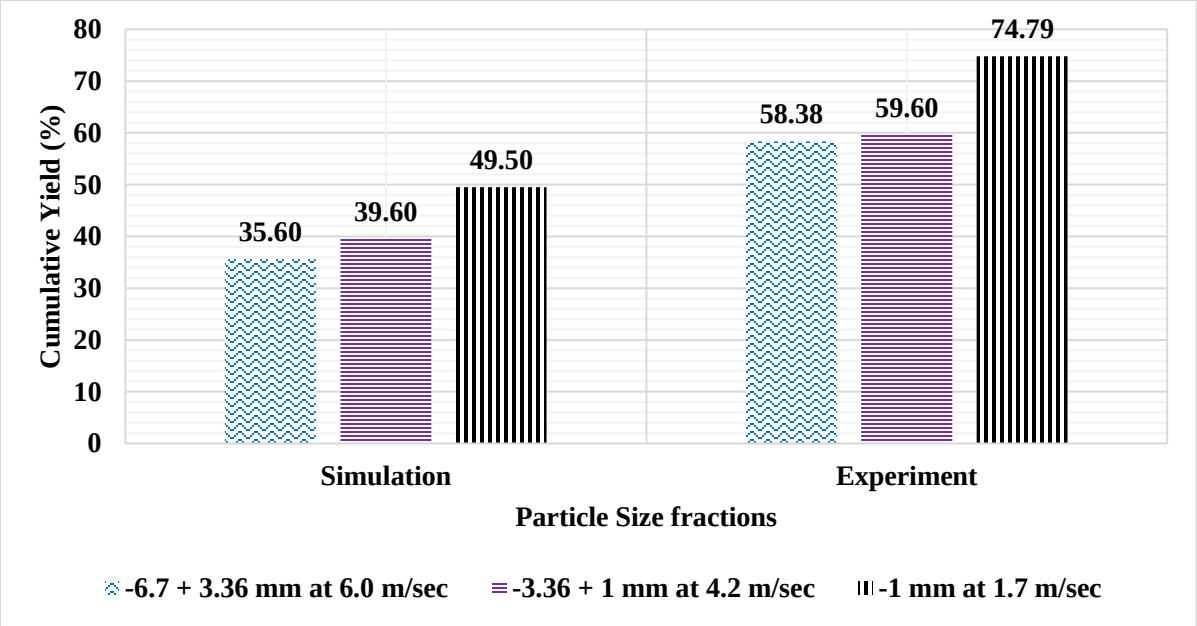


Figure 4 - 38: Comparison between the Simulation and Experimental results

The cleanest coal in this research was recovered from bin 1 of the -6.7+3.36 mm particle size fraction at 36 g/min mass flowrate and air velocity of 4.0 m/sec with an ash content of 16.75% and a calorific value of 27.00 MJ/kg. In addition, the other washability data from the wind-sifter beneficiation test can be seen in **Appendix A**.

4.5. SUMMARY

High ash South African ROM coal from Witbank coalfield was used in this study and screened at three particle size distributions (-6.7+3.36 mm; -3.36+1 and -1 mm). The wind sifter separator designed and fabricated in this study was used to upgrade all the three particle size fractions and result obtained compared with the data from the float and sink analysis of the same coal fractions. The results show that the separator could upgrade the -6.7 + 3.36 and -3.36 + 1 mm size fractions, as well as the -1 mm, but not as effective as the dense medium separation. Based on the challenges faced in the running of the separator, there is potential for an improvement to this present design. The challenges observed will be investigated in a doctoral study to optimize this present design of the separator. With the present design, the cleanest coal product achieved in this research was 16.75% ash content, which is a higher specification to the average coal used in the South African power plants.

CHAPTER 5: CONCLUSION AND RECOMMENDATION

5.1. CONCLUSION

The principle of wind sifting was used in the designing and fabricating a wind sifter separator used in the beneficiation of high ash coal screened at three different particle sizes. The separator was fabricated based on the results obtained from the simulation process. Experimental study which includes sink and float analysis, as well as the dry beneficiation test run was carried out to ascertain the present separation capability of this invention. From this study, the following were achieved:

I. From the simulation results, we were able to predict that the highest sample recoveries would be realized in bin 6 (in the first chamber) and bin 4 (in the second chamber), as can be seen in figures 4-12 to 4-14 in the first chamber and figures 4-15 to 4-17 in the second chamber.

II. A lower product yield was achieved from the simulation test run compared to that yield from the experimental runs, and this might be as a result of the assumption that the particles in the simulation study were perfectly spherical, which is not the case for actual coal particles.

III. It was observed that parameters such as the air stream velocity, particle size, and particle density, influenced the separation of particles within the separator.

IV. For each particle size distribution used in this study, reducing the air stream velocity led to a decrease in ash content of the product recovered, however, the yield also reduced as well. This is due to the lower air stream velocities being able to carry the lighter particles (predominantly coal), but not the heavier mineral rich particles.

V. For the -6.7 + 3.36 mm particle size fraction, at air velocity of 6.0 m/sec, cumulative product yield of 58.38% was obtained from chamber 2 with cumulative ash content of 21.95%, and when reduced to 4.0 m/sec, product yield of 17.97% with cumulative ash of 18.61% was recovered.

VI. For coal of -3.36 + 1 mm size fraction, cumulative product yield of 59.60% with 25.62% cumulative ash was achieved, and when reduced to 2.0 m/sec air velocity, cumulative yield of 8.44% and cumulative ash content of 17.88% was recovered.

VII. The -1 mm particle size fraction, are seen trapped on the walls of the separator, leading to a significant loss; a cumulative product yield of 74.79% with cumulative ash of

31.51% was realized at 1.7 m/sec air velocity and when reduced to 1.0 m/sec, cumulative yield of 17.05% was recovered with a cumulative product ash of 28.74%.

A wind sifter separator incorporating the first chamber of the *Trennso Wind-sifter luchtscheiding* as earlier stated in the chapter 1 of this dissertation has been modified, in terms of the re-configuration to the air jet angle of the first chamber for the Trennso from 180 degrees horizontal, to 150 degrees vertical and 60 degrees horizontal, respectively. In addition, a newly designed diffuser with four collection bins was integrated as the second chamber for separating lighter particles. This chamber has a filter connected in tandem with it to filtered coal dust particles along with the air exiting the separator.

5.2. RECOMMENDATIONS

The present study has portrayed that the wind sifter technique is able to upgrade run of mine coal however, this present design will be optimized in a doctoral study, in order to reduce the challenges faced when using this current separator. For this to be done, the separator must be redesigned and re-simulated using software tools which include Autodesk Inventor and Star CCM respectively. The optimal values from the simulation results can then be used to rework and optimize the present fabricated separator to prevent particle build up as seen in figure 5-1. Major reasons why this has to be done is to;

I. To account for differences in particle shape, rather than assuming all particles are spherical during simulation.
II. To account for the presence of swirls in the air flow profile at lower velocities and reduce them.
III. To deal with the problems of sample loss observed for the – 1 mm size fraction as can be seen in section **4.3.4.**, for better separation performance.
IV. To account for the misplacement of particles in both chambers by working on the air-jet angle of the air inlet in the first chamber, which is denoted as ***A*** in figure 5-2 below and reduce air reflux in the area represented as ***B***.
V. To eliminate the settling of particles in the inlet section of the second chamber, denoted as ***C*** in 5-2 below.

VI. To account for the particles that travel further than bin 1 in the second chamber and particularly travelled further towards the air filter section denoted as ***D*** in the figure 5-2 below, by extending the coal collection bins in the second chamber.

VII. To account for clogging of filter which will ultimately result in backpressure build-up in the separator.

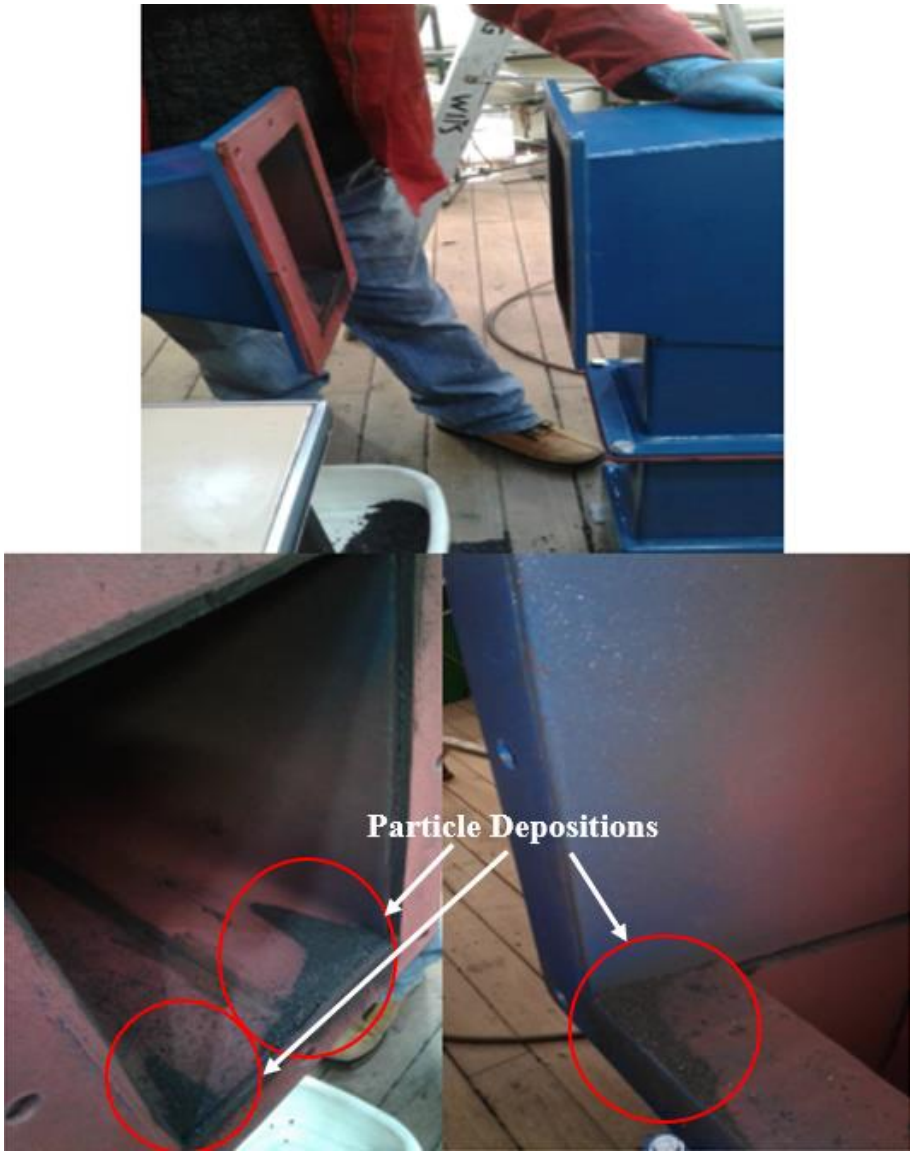


Figure 5 - 1: The particles deposition observed during repeatability testing

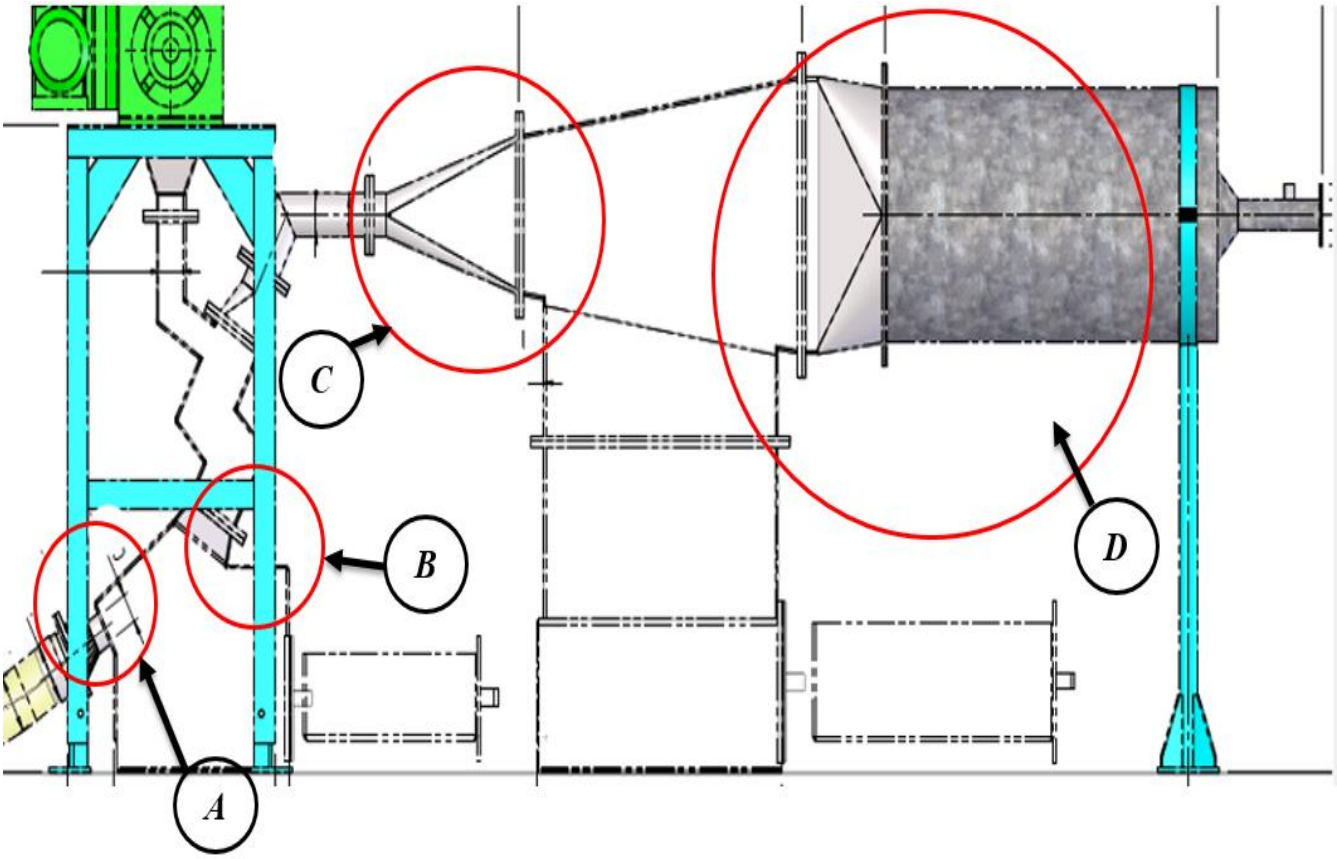


Figure 5 - 2: Identified areas in the wind sifter pointed out for optimization

REFERENCES

Adamčík, M., Svěrák, T. and Peciar, P., 2017. Parameters effecting forced vortex formation in blade passageway of dynamic air classifier.

Africa Mining IQ, 2019. "Coal Mining in South Africa". URL: https://www.projectsiq.co.za/coal-mining-in-south-africa.htm#mining-companies. [Accessed May 20th, 2020]

Akbari, H., Ackah, L. and Mohanty, M., 2017. Performance optimization of a new air table and flip-flow screen for fine particle dry separation. *International Journal of Coal Preparation and Utilization*, pp.1-23.

Aktaş, Z., Karacan, F. and Olcay, A., 1998. Centrifugal float–sink separation of fine Turkish coals in dense media. *Fuel Processing Technology*, *55*(3), pp.235-250.

Andersson, B., Andersson, R., Håkansson, L., Mortensen, M., Sudiyo, R. and Van Wachem, B., 2011. *Computational fluid dynamics for engineers*. Cambridge University Press.

Annexure, Q., 2017. South African Coal. Center for Environmental Rights.

URL: https://cer.org.za/wp-content/uploads/2017/12/Annexure-Q.pdf. [Accessed October 17th, 2018]

Ashish, A., Perminder, S., and Nikkam, S., 2011.Use of jigs in coal and mineral industries – an overview, *XII International Conference on Mineral Processing Technology*, CP 24 1271.

Atesok, G., Perek, K.T., Dincer, H. and Celik, M.S., 1999. Reduction of Ash and Sulfur Contents of Low-RankTurkish Semicoked Lignite by High Intensity Dry Magnetic Separation. *Coal Perparation*, *20*(3-4), pp.179-190.

Azimi, E., Karimipour, S., Rahman, M., Szymanski, J. and Gupta, R., 2013. Evaluation of the performance of air dense medium fluidized bed (ADMFB) for low-ash coal beneficiation. Part 1: Effect of operating conditions. *Energy & Fuels*, *27*(10), pp.5595-5606.

Azimi, E., Karimipour, S., Rahman, M., Szymanski, J. and Gupta, R., 2013. Evaluation of the performance of air dense medium fluidized bed (ADMFB) for low-ash coal beneficiation. Part 2: Characteristics of the beneficiated coal. *Energy & Fuels*, *27*(10), pp.5607-5616.

Bada, S.O., Falcon, L.M., Falcon, R., Du Cann, V.M., 2012. Qualitative analysis of fine coals obtained from triboelectrostatic separation. *Journal of the Southern African Institute of Mining and Metallurgy Vol 112*, 55–62.

Bada, S. O., Tao, D., Honaker, R., Falcon, L., Falcon, R., 2010. Parametric study of electrostatic separation of South African fine coal. *Mining Science and Technology Vol 20*, 0535–0541. doi.org/10.1016/S1674-5264(09)60239-8

Bada, S.O., Tao, D., Honaker, R.Q., Falcon, L.M., Falcon, R.M.S., 2010. A study of rotary tribo-electrostatic separation of South African fine coal. *International Journal of Coal Preparation and Utilization Vol 30,* 154–172. doi.org/10.1080/19392699.2010.497100

Bao, Y., Lin, S. and Weng, L., 2008, October. Three-Dimensional Computer Aided Design of a Vertical Winnower. In *International Conference on Computer and Computing Technologies in Agriculture* (pp. 1497-1503). Springer, Boston, MA.

Boylu, F., Çinku, K., Çetinel, T., Karakaş, F., Güven, O., KaraağaçlIoğlu, I.E. and Çelik, M.S., 2015. Effect of coal moisture on the treatment of a lignitic coal through a semi-pilot-scale pneumatic stratification jig. *International Journal of Coal Preparation and Utilization*, *35*(3), pp.143-154.

Cairncross, B., 2001. An Overview of the Permian (Karoo) Coal Deposits of southern Africa. *Journal of African Earth Sciences Vol 33,* 529–562. doi.org/10.1016/S0899-5362(01)00088-4.

Campbell, Q.P., Le Roux, M. and Smith, I.G.T., 2015. Water-only laboratory coal fractionation using the reflux classifier. *Minerals Engineering*, *83*, pp.59-63.

Çetinkaya, Z. and Bayat, O., 2020. Upgrading low-rank coals (Çan, Çanakkale/Turkey) by float-sink separation in dense media. *Energy Sources, Part A: Recovery, Utilization, and Environmental Effects*, *42*(1), pp.113-120.

Chagwedera, K.M., 2017. Cost evaluation of different medium solids for Air Dense Medium Fluidized Bed coal separation.

Chagwedera, K.M., Bada, S.O. and Falcon, R.M.S., 2018. Evaluation of alternative solid media for coal beneficiation using an air dense-medium fluidized bed. *Journal of the Southern African Institute of Mining and Metallurgy*, *118*(8), pp.883-890.

Chalavadi, G. and Das, A., 2015. Study of the mechanism of fine coal beneficiation in air table. *Fuel*, *154*, pp.207-216.

Charan, T.G., Chattopadhyay, U.S., Singh, K.M.P., Kabiraj, S.K. and Haldar, D.D., 2011. Beneficiation of high-ash, Indian non-coking coal by dry jigging. *Mining, Metallurgy & Exploration*, *28*(1), pp.21-23.

Charan, T.G., Riazi M. R., Gupta, R., 2016. Coal Beneficiation, in: Coal Production and Processing Technology. *Taylor & Francis Group*, LLC CRC Press.

Chen, H., Chen, Y., Hsieh, H.T. and Siegel, N., 2007. Computational fluid dynamics modeling of gas-particle flow within a solid-particle solar receiver.

Cheng, G., Cao, Y., Zhang, C., Jiang, Z., Yu, Y. and Mohanty, M.K., 2020. Application of novel flotation systems to fine coal cleaning. *International Journal of Coal Preparation and Utilization*, *40*(1), pp.24-36.

Choung, J., Mak, C. and Xu, Z., 2006. Fine coal beneficiation using an air dense medium fluidized bed. *Coal Preparation*, *26*(1), pp.1-15.

Çicek, T. (2008) Dry Cleaning of Turkish Coal. *Energy Sources, Part A: Recovery, Utilization, and Environmental Effects Vol 30,* (7) 593–605.

Creamer Media's Coal Report, 2019. Coal 2019: A review of South Africa's coal sector. URL: https://www.creamermedia.co.za/article/coal-2019-a-review-of-south-africas-coal-sector-pdf-report-2019-10-21. [Accessed January 25th, 2020]

Dave, P.C., 2012. Dry Cleaning of Coal by a Laboratory Continuous Air Dense Medium Fluidised Bed Separator.

De Korte, G.J., 2010. Coal preparation research in South Africa. *Journal of the Southern African Institute of Mining and Metallurgy*, *110*(7), pp.361-364.

De Korte, G.J., 2015. Processing low-grade coal to produce high-grade products. *Journal of the Southern African Institute of Mining and Metallurgy 115,* 569–572. doi.org/10.17159/2411-9717/2015/v115n7a2

De Korte, J., Jeffrey, L., 2016. URL: http://www.fossilfuel.co.za/conferences/2016/IPP/de-Korte-Johan-and-Jeffrey-Lesley.pdf [Accessed November 16th, 2018]

De la Fuente, T., Bergström, D., González-García, S. and Larsson, S.H., 2018. Life cycle assessment of decentralized mobile production systems for pelletizing logging residues under Nordic conditions. *Journal of cleaner production*, *201*, pp.830-841.

Diedericks, E.S., Le Roux, M., Campbell, Q.P. and Hughes, N., 2020. Beneficiation of small South African coal using an air dense medium fluidized bed. *International Journal of Coal Preparation and Utilization*, pp.1-14.

Dong, L., Wang, Z., Zhou, E., Wang, X., Li, G., Fan, X., Zhang, B., Duan, C., Chen, Z., Luo, Z. and Jiang, H., 2019. A novel dry beneficiation process for coal. *International Journal of Coal Preparation and Utilization*, pp.1-21.

Duan, C., Yuan, W., Cai, L., Lv, K., Zhao, Y., Zhang, B., Dong, L. and Lv, P., 2015. Characteristics of fine coal beneficiation using a pulsing air dense medium fluidized bed. *Powder technology*, *283*, pp.286-293.

Dwari, R.K., Mohanta, S.K., Rout, B., Soni, R.K., Reddy, P.S.R. and Mishra, B.K., 2015. Studies on the effect of electrode plate position and feed temperature on the tribo-electrostatic separation of high ash Indian coking coal. *Advanced Powder Technology*, *26*(1), pp.31-41.

Dwari, R.K. and Rao, K.H., 2007. Dry beneficiation of coal – A review. *Mineral Processing & Extractive Metall. 28:*177-234.

Dwari, R.K. & Rao, K.H. 2009. Fine coal preparation using novel tribo-electrostatic separator. *Minerals Engineering*, *22*(2), pp.119-127.

Eberhard, A., 2011. The future of South African coal: Market, investment and policy challenges. *Program on energy and sustainable development*, pp.1-44.

England, T., Hand, P.E., Michael, D.C., Falcon, L.M., Yell, A.D., 2002. Rank and Types of Coal, in: Coal Prepararion in South Africa. pp. 8–13.

Ericsson, M., 1991. Minerals and metals production technology. *Resources Policy Vol 17,* 284–300. doi.org/10.1016/0301-4207(91)90014-M

ESKOM, 2021. Avaliable Online: https://www.eskom.co.za/AboutElectricity/ElectricityTechnologies/Pages/Coal_Power.aspx. [Accessed July 25th, 2021]

Eskom, Integrated Report, 2018. https://www.eskom.co.za/IR2018/Pages/default.aspx [Accessed July 25th, 2021]

Evangelopoulos, P., Sophonrat, N., Jilvero, H., Yang, W., 2018. Investigation on the low-temperature pyrolysis of automotive shredder residue (ASR) for energy recovery and metal recycling. *Waste Management Vol 76*, 507–515. doi.org/10.1016/j.wasman.2018.03.048.

Falcon, R.M.S., 1986. A brief review of the origin, formation and distribution of coal in Southern Africa. *Mineral Deposits of Southern Africa*, *2*, pp.1879-1898.

Fan, M., Chen, Q., Zhao, Y., Tao, D., Luo, Z., Zhang, X., Tao, X. and Yang, G., 2006. Fine coal dry classification and separation. *Mining, Metallurgy & Exploration*, *23*(1), pp.17-21.

Fan, X., Zhou, C., Dong, L., Duan, C. and Zhao, Y., 2020. Coal Beneficiation via the Tapered Fluidized Bed Using Magnetite with a Wide Size Range. *Mining, Metallurgy & Exploration*, pp.1-11.

Feil, N.F., Sampaio, C.H. and Wotruba, H., 2012. Influence of jig frequency on the separation of coal from the Bonito seam—Santa Catarina, Brazil. *Fuel Processing Technology*, *96*, pp.22-26.

FLSmidth Reflux Classifier, 2021. URL: https://video.flsmidth.com/flsmidth-reflux-classifier. [Accessed on June 22nd, 2021]

Fu, Z., Zhu, J., Barghi, S., Zhao, Y., Luo, Z. and Duan, C., 2019. Dry coal beneficiation by the semi-industrial air dense medium fluidized bed with binary mixtures of magnetite and fine coal particles. *Fuel*, *243*, pp.509-518.

Fu, Z., Zhao, Y., Yang, X. and Duan, C., 2017. Spontaneous segregation behavior in a vibrated gas-fluidized bed for fine lignite dry cleaning. *Separation Science and Technology*, *52*(12), pp.2017-2028.

Fu, Z., Zhao, Y., Yang, X., Luo, Z. and Zhao, J., 2016. Fine coal beneficiation via air-dense medium fluidized beds with improved magnetite powders. *International Journal of Coal Preparation and Utilization*, *36*(1), pp.55-68.

Gaille, B., 2018. 17 South African Coal Mining Industry Statistics, Trends & Analysis: www.brandongaille.com/17-south-african-coal-mining-industry-statistics-trends-analysis/.pdf [Accessed on June 2nd, 2019]

Galvin, K.P., Callen, A.M. and Spear, S., 2010. Gravity separation of coarse particles using the Reflux Classifier. *Minerals Engineering*, *23*(4), pp.339-349.

Giani, H., Feil, A., Hornsby, K., Clausen, A. and Pretz, T., 2014. Processing concept for the production of biomass fuel from mixed municipal solid waste.

Hacifazlioglu, H., 2018. Production of Merchantable Coal from Low Rank Lignite Coal by Using FGX and Subsequent IR Drying. *International Journal of Coal Preparation and Utilization*, pp.1-8.

Han, C., 1983. *COAL CLEANING BY FROTH FLOTATION (IOWA)* (Doctoral dissertation, Iowa State University).

Hancox, P.J. and Götz, A.E., 2014. South Africa's coalfields—A 2014 perspective. *International Journal of Coal Geology*, *132*, pp.170-254.

He, J., Zhao, Y., He, Y.Q., Luo, Z. and Duan, C.L., 2013. Separation performance of raw coal from South Africa using the dense gas-solid fluidized bed beneficiation technique. *Journal of the southern African Institute of Mining and Metallurgy*, *113*(7), pp.01-08.

He, J., Zhao, Y., Huang, G. and Liu, C., 2018. Evaluation of the separation performance of an air dense medium gas-solid fluidized bed for coal cleaning: Effect of the binary dense media. *Advanced Powder Technology*, *29*(12), pp.3265-3273.

He, J., Zhao, Y., Zhao, J., Luo, Z., Duan, C. and He, Y., 2015. Separation performance of fine low-rank coal by vibrated gas–solid fluidized bed for dry coal beneficiation. *Particuology*, *23*, pp.100-108.

He, Y., Xie, W., Zhao, Y., Li, H. and Wang, S., 2017. Triboelectrostatic separation of pulverized fuel of coal power plant based on mineralogical analyses. *International Journal of Mineral Processing*, *166*, pp.7-12.

Ho, S.H., Rosario, L. and Rahman, M.M., 2010. Numerical simulation of temperature and velocity in a refrigerated warehouse. *International Journal of Refrigeration*, *33*(5), pp.1015-1025.

Honaker, R.Q., 2007, August. Coarse dry coal cleaning. In *Workshop on Coal Beneficiation and Utilization of Rejects* (pp. 22-24)

Honaker, R.Q., Saracoglu, M., Thompson, E., Bratton, R., Luttrell, G.H., Richardson, V., 2008. Upgrading Coal Using a Pneumatic Density-Based Separator. *International Journal of Coal Preparation and Utilization Vol 28*, 51–67. doi.org/10.1080/19392690801934054.

Honaker, R.Q., Singh, N. and Govindarajan, B., 2000. Application of dense-medium in an enhanced gravity separator for fine coal cleaning. *Minerals Engineering*, *13*(4), pp.415-427.

IEA, 2018, "Market Report Series: Coal 2018". https://webstore.iea.org/market-report-series-coal-2018. [Accessed May 16th, 2019]

IEA. 2019, "Coal 2019", IEA, Paris. https://www.iea.org/reports/coal-2019. [Accessed on July 22nd, 2020]

IEA Coal South Africa, 2020. https://www.iea.org/countries/south-africa. [Accessed on December 28th, 2020]

IEA Coal South Africa, 2021. https://www.iea.org/countries/south-africa. [Accessed on April 25th, 2021]

IEEJ Outlook, 2020. https://thecoalhub.com/wp-content/uploads/2020/02/IEEJ.pdf. [Accessed on December 28th, 2020]

Isaac, K. and Bada, S.O., 2020. The co-combustion performance and reaction kinetics of refuse derived fuels with South African high ash coal. *Heliyon*, *6*(1), p.e03309.

Iveson, S.M., Price, A. and Galvin, K.P., 2019. Separation of coal with a top size of up to 6 mm in a full-scale REFLUX™ Classifier. *International Journal of Coal Preparation and Utilization*, pp.1-21.

James, P., 1982. Coal: Origins and Exploitation, in: The Future of Coal. *The Macmillan Press Ltd.*

Jeffrey, L.S., 2005. Characterization of the coal resources of South Africa. *Journal of the Southern African Institute of Mining and Metallurgy*, Vol 105(2), pp.95-102.

Jeffrey, R., Falcon, R., Kinghorn, A., 2014. The Benefits and Challenges Associated with Coal In South Africa. *Society and Culture* 66–70.

Jiao, H.G., Cui, J.Y., Liu, P., Chen, Q.R. And Tie, Z.X., 2009. Experimental Study of Magnetic Property and Dry Magnetic Separation of Fine Coal [J]. *Journal of China University of Mining & Technology*, *38*(1), 131–134+148.

Killmeyer, R.P., Hucko, R.E. and Jacobsen, P.S., 1992. Centrifugal float-sink testing of fine coal: an interlaboratory test program. *Coal Preparation*, *10*(1-4), pp.107-118.

Ko, A.S. and Chang, N.B., 2008. Optimal planning of co-firing alternative fuels with coal in a power plant by grey nonlinear mixed integer programming model. *Journal of environmental management*, *88*(1), pp.11-27.

Kopparthi, P., Awasthi, A., Sachinraj, D. and Mukherjee, A.K., 2019. Beneficiation of coal fines using the Reflux™ Classifier. *Minerals Engineering*, *136*, pp.110-119.

Korte (2014) *Dry Processing of Coal – Status update*. COALTECH.

Kumar, S. and Venugopal, R., 2020. Coal cleaning using jig and response surface approach for determination of quality of clean coal. *International Journal of Coal Preparation and Utilization*, *40*(2), pp.107-115.

Krauß, G., Kübler, J. and Trentini, E., 2002. Preparation and properties of pressureless infiltrated SiC and AlN particulate reinforced metal ceramic composites based on bronze and iron alloys. *Materials Science and Engineering: A*, *337*(1-2), pp.315-322.

Kretzschmar, S., 2010. *Dry beneficiation of coal using an air dense-medium fluidised bed separator* (Doctoral dissertation).

Krüger, B., Mrotzek, A. and Wirtz, S., 2014. Separation of harmful impurities from refuse derived fuels (RDF) by a fluidized bed. *Waste management*, *34*(2), pp.390-401.

Kumar, S. and Venugopal, R., 2017. Performance analysis of jig for coal cleaning using 3D response surface methodology. *International Journal of Mining Science and Technology*, *27*(2), pp.333-337.

Levi, P.G. and Cullen, J.M., 2018. Mapping global flows of chemicals: from fossil fuel feedstocks to chemical products. *Environmental science & technology*, *52*(4), pp.1725-1734.

Lin, S., Chen, B., Chen, W., Li, W. and Wu, S., 2012. Study on clean coal technology with oil agglomeration in Fujian Province. *Procedia Engineering*, *45*, pp.986-992.

Ling, X., He, Y., Li, G., Tang, X. and Xie, W., 2018. Separation performance of different particle sizes using an industrial FGX dry separator. *International Journal of Coal Preparation and Utilization*, *38*(1), pp.30-39.

Lotfi, S., Di Maio, F., Xia, H., Serranti, S., Palmieri, R. and Bonifazi, G., 2015. Assessment of the contaminants level in recycled aggregates and alternative new technologies for contaminants recognition and removal. *EMABM 2015: Proceedings of the 15th Euroseminar on Microscopy Applied to Building Materials, Delft, The Netherlands, 17-19 June 2015*.

Luo, Z., Fan, M., Zhao, Y., Tao, X., Chen, Q. and Chen, Z., 2008. Density-dependent separation of dry fine coal in a vibrated fluidized bed. *Powder Technology*, *187*(2), pp.119-123.

Luo, Z.F., Zhu, J.F., Fan, M.M., Zhao, Y.M. and Tao, X.X., 2007. Low density dry coal beneficiation using an air dense medium fluidized bed. *Journal of China University of Mining and Technology*, *17*(3), pp.306-309.

Lynch, A. J., N. W. Johnson, E. V. Manlapig, and C. G. Thome., 1981. Mineral and Coal Flotation Circuits. Vol. 3. *Elsevier Scientific Publishing Co.*, New York.

Mackinnon, W.L.A. and Swanson, A.R., 2010. Strategies for Washing Australian Coals. *International Journal of Coal Preparation and Utilization*, *30*(2-5), pp.69-82.

Ma, G., Bu, X., Xie, G., Peng, Y., Sha, J., Xia, W. and Wu, E., 2018. Comparative study of separation performance of a spiral and dense-medium cyclone on cleaning coal. *International Journal of Coal Preparation and Utilization*, pp.1-9.

Maharaj, A., 2014. *Experimental and numerical studies of air preheater leakage* (Doctoral dissertation).

Meshram, P., Purohit, B.K., Sinha, M.K., Sahu, S.K. and Pandey, B.D., 2015. Demineralization of low grade coal–A review. *Renewable and Sustainable Energy Reviews*, *41*, pp.745-761.

Meyer, E.J. and Craig, I.K., 2010. The development of dynamic models for a dense medium separation circuit in coal beneficiation. *Minerals Engineering*, *23*(10), pp.791-805.

Mills, S., 2016. Low Quality Coals—Key Commercial, Environmental and Plant Considerations. *IEA Clean Coal Centre*.

Mineral Council South Africa, 2018. Coal Strategy 2018 (National Coal Strategy for South Africa).www.mineralscouncil.org.za/component/jdownloads/send/25-downloads/535-coal-strategy-2018. [Accessed May 16th, 2019]

Mineral Council South Africa, 2020. Coal-Mineral Council South Africa. www.mineralscouncil.org.za/sa-mining/coal. [Accessed on April 25th, 2020]

Mining Africa, 2019. Coal Mining in Africa.https://www.miningafrica.net/natural-resources-africa/coal-mining-in-africa/. [Accessed January 7th, 2020].

Muscolino, J., 2010. Mechanical Centrifugal Air Classifiers - Chemical Chemical Engineering. URL : www.chemengonline.com/mechanical-centrifugal-air-classifiers.[Accessed November 16th, 2018].

Napier-Munn, T., 2018. The dense medium cyclone–past, present and future. *Minerals Engineering*, *116*, pp.107-113.

Ndou, N.R., Bada, S.O., Falcon, R.M.S. and Weiersbye, I.M., 2020. Co-combustion of Searsia lancea and Tamarix usneoides with high ash coal. *Fuel*, *267*, p.117282.

Nishinari, K., Williams, P.A. and Phillips, G.O., 1992. Review of the physico-chemical characteristics and properties of konjac mannan. *Food hydrocolloids*, *6*(2), pp.199-222.

Norton, T. and Sun, D.W., 2006. Computational fluid dynamics (CFD)–an effective and efficient design and analysis tool for the food industry: a review. *Trends in Food Science & Technology*, *17*(11), pp.600-620.

Norton, T., Sun, D.W., Grant, J., Fallon, R. and Dodd, V., 2007. Applications of computational fluid dynamics (CFD) in the modelling and design of ventilation systems in the agricultural industry: A review. *Bioresource technology*, *98*(12), pp.2386-2414.

Onifade, M., Lawal, A.I., Aladejare, A.E., Bada, S. and Idris, M.A., 2019. Prediction of gross calorific value of solid fuels from their proximate analysis using soft computing and regression analysis. *International Journal of Coal Preparation and Utilization*, pp.1-15.

Oruç, F., Özgen, S. and Sabah, E., 2010. An enhanced-gravity method to recover ultra-fine coal from tailings: Falcon concentrator. *Fuel*, *89*(9), pp.2433-2437.

Özgen, S., Malkoç, Ö., Doğancik, C., Sabah, E. and Şapçi, F.O., 2011. Optimization of a multi gravity separator to produce clean coal from Turkish lignite fine coal tailings. *Fuel*, *90*(4), pp.1549-1555.

Ozmak, M. and Aktas, Z., 2006. Coal froth flotation: Effects of reagent adsorption on the froth structure. *Energy & fuels*, *20*(3), pp.1123-1130.

Patil, D.P. and Parekh, B.K., 2011. Beneficiation of fine coal using the air table. *International Journal of Coal Preparation and Utilization*, *31*(3-4), pp.203-222.

Parnaby Cyclones, 2015. Dense Medium Cyclones. URL: https://www.parnaby.co.uk/equipmen-dense-medium-cyclone-plant/?doing_wp_cron=1626956547.4211859703063964843750. [Accessed on June 22nd, 2021]

Pettinari, M., Simone, A., 2015. Effect of crumb rubber gradation on a rubberized cold recycled mixture for road pavements. *Materials & Design Vol 85*, 598–606. doi.org/10.1016/j.matdes.2015.06.139

Polat, M., Polat, H. and Chander, S., 2003. Physical and chemical interactions in coal flotation. *International Journal of Mineral Processing*, *72*(1-4), pp.199-213.

Prashant, D., Xu, Z., Szymanshki, J., Gupta, R., Boddez, J., 2010. Dry cleaning of coal by a laboratory continuous air dense medium fluidized bed separator, in: Dry Coal Cleaning. Presented at *The international Coal Preparation Congress 2010 Conference*, Honaker RQ (ed), Society for Mining, Metallurgy & Exploration, Lexington, pp. 608–616.

Prevost, X.M., 2003. SA coal resources and reserves, a present-day outlook. *Application of Computers and Operations Research in the Minerals Industries (APCOM)*, pp.14-16.

PRNEWSWIRES, 2019. South Africa Coal Mining Report 2019 including Coal Testing and Laboratories. URL: https://www.prnewswire.com/news-releases/south-africa-coal-mining-report-2019-including-coal-testing-and-laboratories-300945607.html[Accessed February 4th, 2020].

Ragaert, K., Delva, L., Van Geem, K., 2017. Mechanical and chemical recycling of solid plastic waste. *Waste Management Vol 69*, 24–58. doi.org/10.1016/j.wasman.2017.07.044

Rao, K.N. and Vidyadhar, A., 2006. Comparative Studies between Jigging and HMS for Lowering of Ash in a Coal Sample from Assam.

Ratshomo, K. and Nembahe, R., 2018. South African energy sector report. *Department of Energy–Republic of South Africa, November*.

Rautenbach, R., Strydom, C.A., Bunt, J.R., Matjie, R.H., Campbell, Q.P. and Van Alphen, C., 2019. Mineralogical, chemical, and petrographic properties of selected South African power stations' feed coals and their corresponding density separated fractions using float-sink and reflux classification methods. *International Journal of Coal Preparation and Utilization*, *39*(8), pp.421-446.

Redemann, K., Hartge, E.-U., Werther, J., 2008. Ash management in circulating fluidized bed combustors. *Fuel 87*, 3669–3680. doi.org/10.1016/j.fuel.2008.07.002

Reid, I. (PhD), 2017. Coal Beneficiation. *IEA Clean Coal Centre*.

Riazi, M.R. and Gupta, R., 2015. *Coal production and processing technology*. CRC press.

Rio Suerte, 2021. Available Online: https://riosuerte.com/in-the-beginning-there-was-gold/day-75-placer-gold-recovery-methods-xv-a-review/ [Accessed July 27th, 2021]

Rotich, N., Tuunila, R. and Louhi-Kultanen, M., 2013. Modeling and simulation of gravitational solid–solid separation for optimum performance. *Powder technology*, *239*, pp.337-347.

Sahoo, S.K., Suresh, N. and Varma, A.K., 2020. Flotation production of vitrinite maceral concentrate and its optimization using response surface approach. *International Journal of Coal Preparation and Utilization*, *40*(3), pp.155-174.

Santos, S.M., Tambourgi, E.B., Fernandes, F.A.N., Moraes Júnior, D. and Moraes, M.S., 2011. Dilute-phase pneumatic conveying of polystyrene particles: pressure drop curve and particle distribution over the pipe cross-section. Brazilian Journal of Chemical Engineering, 28(1), pp.81-88.

Schobert, H.H. and Song, C., 2002. Chemicals and materials from coal in the 21st century. *Fuel*, *81*(1), pp.15-32.

Scholtz, J., Du Plessis, K., Roche, R., Cresswell, M., Toerin, L., Voges, J., Reddy, D., De Korte, J., Craddock, M., Lok, G., McMillian, K., Buthelezi, V., Darley, P., Jacobs, Jakes, Campbell, Q., Jacobs, Jayson, 2015. Section2: Geology, in: Coal Preparation in Southern Africa. p. 17.

Scott, G. and Richardson, P., 1997. The application of computational fluid dynamics in the food industry. *Trends in Food Science & Technology*, *8*(4), pp.119-124.

Shi, C., Cheng, G. and Wang, S., 2019. Optimization of Coal Washery Tailings by Flotation Process. *Energies*, *12*(20), p.3956.

Singh, J.P., Kumar, S. and Mohapatra, S.K., 2020. Chemical treatment of low-grade coal using Taguchi approach. *Particulate Science and Technology*, *38*(1), pp.73-80.

Song, S., Zhao, Y., Luo, Z., Tang, L. (2012a) Motion Behavior of Particles in Air–Solid Magnetically Stabilized Fluidized Beds for Separation. *International Journal of Mining Science and Technology*. **22**(5), 725–729.

Soong, Y., Link, T.A., Schoffstall, M.R., Gray, M.L., Fauth, D.J., Knoer, J.P., Jones, J.R. and Gamwo, I.K., 2001. Dry beneficiation of Slovakian coal. *Fuel processing technology*, *72*(3), pp.185-198.

Song, S.L., Zhao, Y.M., Jia, Z.F., Tang, L.G. and Yang, X.L., 2012b. Fine coal particles separation by air solid magnetic fluidization. *Journal of China Coal Society*, *37*(9), pp.1586-1590.

South Africa's Mining Industry, August 2019. Mining, Commodities and Employment | South Africa's Mining industry. URL: www.southafricanmi.com/south-africas-mining-industry.html [accessed January 9th, 2020].

Statistical Review of World Energy, 2021. URL: https://www.bp.com/content/dam/bp/business-sites/en/global/corporate/pdfs/energy-economics/statistical-review/bp-stats-review-2021-full-report.pdf. [Accessed August 7th, 2021]

Suresh, P.D., Kumar, V., Sripriya, R., Chakraborty, S. and Meikap, B.C., 2010. Performance characteristics of pilot plant dense media hydrocyclone for beneficiation of coal and 3-D CFD simulation. *Chemical engineering science*, *65*(16), pp.4661-4671.

Tran, Q.A., Stanger, R., Xie, W., Lucas, J., Yu, J., Stockenhuber, M., Kennedy, E. and Wall, T., 2016. Maceral separation from coal by the Reflux Classifier. *Fuel processing technology*, *143*, pp.43-50.

Trennso Technik, **2018**. URL: https://www.trennsotechnik.de/en/machinesandrecyclingmodul-e/#SCREENINGTECHNOLOGY. [Accessed April 4th, 2021]

Tripathy, A., Panda, L., Sahoo, A.K., Biswal, S.K., Dwari, R.K. and Sahu, A.K., 2016. Statistical optimization study of jigging process on beneficiation of fine size high ash Indian non-coking coal. *Advanced Powder Technology*, *27*(4), pp.1219-1224.

Terblanche, A.N., 2013. *Dry beneficiation of fine coal using a fluidized dense medium bed* (Doctoral dissertation).

Tu, J.Y. and Liu, G.H., C., 2008. Computational Fluid Dynamics: A Practical Approach.

Wang, C., S. Wu, Q. Lv, X. Liu, W. Chen, and D, Che. 2017. Study on correlations of coal chemical properties based on database of real-time data. Applied Energy 204:1115–1123.

Vegter.I., 2019. Why Mining Still Matters. URL https://irr.org.za/reports/occasional-reports/files/01-2014-page-1-21-2014-why-mining-still-matters-11-03-2019.pdf. [Accessed March 16th, 2020].

Wang, T.-J., Jin, Y., Tsutsumi, A., Wang, Z., Cui, Z. (2000) Energy Transfer Mechanism in a Vibrating Fluidized Bed. *Chemical Engineering Journal*. **78**(2), 115–123.

Wang, Y., Luo, Z., Huang, G., Ren, B. (2016) Effect of Agitation on the Characteristics of Air Dense Medium Fluidization. *International Journal of Mining Science and Technology*. **26**(3), 383–387.

WCA (World Coal Association), 2015. The Coal Resource: What is coal: Coal Formation www.worldcoal.org/coal/what-coal. [Accessed November 6th, 2018].

WCA (World Coal Association), 2020. Coal Trade: Coal Marketing and Pricing. URL: https://www.worldcoal.org/coal/coal-market-pricing. [Accessed February 6th, 2021].

World Coal Association, 2020. https://www.worldcoal.org/coal-facts/coals-contribution/. [Accessed August 6th, 2021].

World Coal Association, 2021. https://www.worldcoal.org/coal-facts/. [Accessed July 25th, 2021]

Williams, J.C. and Rahman, M.A., 1972. Prediction of the performance of continuous mixers for particulate solids using residence time distributions Part I. Theoretical. *Powder Technology*, *5*(2), pp.87-92.

Wills, B.A. and Napier-Munn, T.J., 2006. An introduction to the practical aspects of ore treatment and mineral recovery. *Wills' Mineral Processing Technology.* pp. 267-352.

Workman, D., August 2020. Coal Exports by Country. World's Top Exports. URL http://www.worldstopexports.com/coal-exports-country/ [accessed November 20th 2020].

Xia, B. and Sun, D.W., 2002. Applications of computational fluid dynamics (CFD) in the food industry: a review. *Computers and electronics in agriculture*, *34*(1-3), pp.5-24.

Xia, W., Xie, G. and Peng, Y., 2015. Recent advances in beneficiation for low rank coals. *Powder Technology*, *277*, pp.206-221.

Xin-xi, Z., Dai-yong, D., Bing, T., Jin-song, W., Feng, D., Hai-sheng, L. and Rui-xin, M., 2009. Research on the triboelectrostatic separation of minerals from coal. *Procedia Earth and Planetary Science*, *1*(1), pp.845-850.

Xuliang, Y., Yuemin, Z., Gongmin, L., Zhenfu, L., Zengqiang, C. and Chuncheng, L., 2012. Establishment and evaluation of a united dry coal beneficiation system. *International Journal of Coal Preparation and Utilization*, *32*(2), pp.95-102.

Yang, X.L., Zhao, Y.M., Luo, Z.F., Chen, Z.Q., Song, S.L. And Duan, C.L., 2013a. Energy transfer mechanism of vibro-fludization and its separation for fine coal. *Journal of China University of Mining & Technology*, *2*.

Yang, X., Zhao, Y., Luo, Z., Song, S., Duan, C. and Dong, L., 2013b. Fine coal dry cleaning using a vibrated gas-fluidized bed. *Fuel Processing Technology*, *106*, pp.338-343.

Yang, Y., Ge, L., He, Y., Xie, W., Ge, Z., 2017. Mechanism and fine coal beneficiation of a pulsating airflow classifier. *International Journal of Coal Preparation and Utilization Vol 39*, 20–32. doi.org/10.1080/19392699.2017.1288622.

Yang, X., Wang, S., Zhang, Y., Zhao, Y., Luo, Z., 2018. Dry beneficiation of fine coal using planar air jets. *Powder Technology Vol 323*, 518–524. doi.org/10.1016/j.powtec.2017.10.042

Yu, X., Luo, Z., Yang, X., Jiang, H., Zhou, E., Zhang, B. and Dong, L., 2016. Oil shale separation using a novel combined dry beneficiation process. *Fuel*, *180*, pp.148-156. doi.org/10.1016/j.fuel.2016.04.036

Zhang, B., Akbari, H., Yang, F., Mohanty, M.K. and Hirschi, J., 2011. Performance optimization of the FGX dry separator for cleaning high-sulfur coal. *International Journal of Coal Preparation and Utilization*, *31*(3-4), pp.161-186.

Zhang, B., Zhao, Y., Luo, Z., Song, S., Li, G. and Sheng, C., 2014. Utilizing an air-dense medium fluidized bed dry separating system for preparing a low-ash coal. *International Journal of Coal Preparation and Utilization*, *34*(6), pp.285-295.

Zhang, B., Zhao, Y., Zhou, C., Duan, C. and Dong, L., 2015. Fine coal desulfurization by magnetic separation and the behavior of sulfur component response in microwave energy pretreatment. *Energy & Fuels*, *29*(2), pp.1243-1248.

Zhang, L., Xia, X. and Zhang, J., 2014. Improving energy efficiency of cyclone circuits in coal beneficiation plants by pump-storage systems. *Applied energy*, *119*, pp.306-313.

Zhang, Q., Tian, Y., Qiu, Y., Cao, J. and Xiao, T., 2011. Study on the washability of the Kaitai coal, Guizhou Province China. *Fuel Processing Technology*, *92*(3), pp.692-698.

Zhang, Y., Jia, Y., Xu, J., Wang, J., Duan, C., Ge, W. and Zhao, Y., 2020. CFD intensification of coal beneficiation process in gas-solid fluidized beds. *Chemical Engineering and Processing-Process Intensification*, *148*, p.107825.

Zhang, Z., Yan, G., Zhu, G., Zhao, P., Ma, Z. and Zhang, B., 2020. Using microwave pretreatment to improve the high-gradient magnetic-separation desulfurization of pulverized coal before combustion. *Fuel*, *274*, p.117826.

Zhao, Y., Fu, Z., Yang, X., Luo, Z., Duan, C., Song, S. and Cai, L., 2015. Fine coal dry cleaning using an air dense medium fluidized bed with improved magnetite medium. *Procedia engineering*, *102*, pp.1133-1141.

Zhao, Y., Li, G., Luo, Z., Zhang, B., Dong, L., Liang, C. and Duan, C., 2017. Industrial application of a modularized dry-coal-beneficiation technique based on a novel air dense medium fluidized bed. *International Journal of Coal Preparation and Utilization*, *37*(1), pp.44-57.

Zhao, Y., Tang, L., Luo, Z., Liang, C., Xing, H., Wu, W. and Duan, C., 2010. Experimental and numerical simulation studies of the fluidization characteristics of a separating gas–solid fluidized bed. *Fuel Processing Technology*, *91*(12), pp.1819-1825.

Zhao, Y., Yang, X., Luo, Z., Duan, C., Song, S., 2014. Progress in developments of dry coal beneficiation. *International Journal of Coal Science & Technology Vol 1*, 103–112. doi.org/10.1007/s40789-014-0014-5

Zhao, Y.M., Li, G.M., Luo, Z.F., Liang, C.C., Tang, L.G., Chen, Z.Q. and Xing, H.B., 2011. Modularized dry coal beneficiation technique based on gas-solid fluidized bed. *Journal of Central South University of Technology*, *18*(2), pp. 374-38

Zhou, C., Fan, X., Duan, C. and Zhao, Y., 2019. A method to improve fluidization quality in gas–solid fluidized bed for fine coal beneficiation. *Particuology*, *43*, pp.181-192.

APPENDIX A: WASHABILITY DATA OF ALL THREE PARTICLE SIZE FRACTION FOR FLOAT AND SINK ANALYSIS AND DRY BENEFICIATION PROCESS

Table A-1: Float and sink test result for -6.7+3.36 mm size fraction of the feed coal

Specific Gravity (g/cm^3)	Mass (Wt) g	Fractional Yield (Wt) %	Cum. Wt %	Ash Content %	Cum. Ash Content (%)	Combustible Recovery (%)	Ash Rejection (%)	Separation Efficiency (%)
1.3 float	29.58	6.00	6.00	5.53	5.53	8.12	98.90	7.02
1.4 float	97.11	19.71	25.71	9.68	8.71	33.61	92.57	26.18
1.5 float	91.72	18.61	44.32	16.15	11.83	55.95	82.61	38.56
1.6 float	30.75	6.24	50.56	22.52	13.15	62.87	77.95	40.82
1.7 float	54.78	11.12	61.68	28.77	15.97	74.21	67.34	41.55
1.8 float	31.86	6.47	68.15	38.95	18.15	79.86	58.99	38.85
1.8 sink	156.96	31.85	100.00	55.86	30.16	100.00	0.00	0.00
Total	492.76	100.00		30.16				

Table A-2: Wind sifter separation test result for -6.7+3.36 mm size fraction at 6.0 m/sec

Bin Number	Mass (Wt) g	Fractional Yield (Wt) %	Cum. Wt %	Ash Content %	Cum. Ash Content (%)	Combustible Recovery (%)	Ash Rejection (%)	Separation Efficiency (%)
1	39.00	8.43	8.43	21.61	21.61	9.59	94.14	3.73
2	46.50	10.05	18.47	21.17	21.37	21.08	87.31	8.39
3	67.80	14.65	33.12	22.24	21.76	37.61	76.83	14.44
4	116.90	25.26	58.38	22.20	21.95	66.13	58.80	24.93
5	12.60	2.72	61.10	51.27	23.25	68.06	54.31	22.37
6	165.10	35.67	96.77	43.19	30.60	97.47	4.77	2.24
7	14.95	3.23	100.00	45.93	31.10	100.00	0.00	0.00
Total	462.85	100.00		31.10				

Table A-3: Wind sifter separation test result for -6.7+3.36 mm size fraction at 4.5 m/sec

Bin Number	Mass (Wt) g	Fractional Yield (Wt) %	Cum. Wt %	Ash Content %	Cum. Ash Content (%)	Combustible Recovery (%)	Ash Rejection (%)	Separation Efficiency (%)
1	24.68	5.20	5.20	18.94	18.94	6.14	96.86	3.00
2	28.35	5.97	11.17	21.51	20.31	12.97	92.77	5.74
3	34.81	7.33	18.50	20.78	20.55	21.44	87.91	9.35
4	57.82	12.18	30.68	20.66	20.56	35.52	79.89	15.41
5	12.73	2.68	33.37	39.71	22.10	37.87	76.50	14.37
6	291.00	61.30	94.67	35.16	30.56	95.80	7.80	3.60
7	25.32	5.33	100.00	45.90	31.38	100.00	0.00	0.00
Total	474.71	100.00		31.38				

Table A-4: Wind sifter separation test result for -6.7+3.36 mm size fraction at 4.0 m/sec

Bin Number	Mass (Wt) g	Fractional Yield (Wt) %	Cum. Wt %	Ash Content %	Cum. Ash Content (%)	Combustible Recovery (%)	Ash Rejection (%)	Separation Efficiency (%)
1	15.04	3.09	3.09	16.75	16.75	4.45	98.78	3.23
2	16.94	3.48	6.57	17.95	17.39	9.40	97.30	6.70
3	22.36	4.59	11.16	20.23	18.56	15.74	95.10	10.84
4	33.13	6.80	17.97	18.71	18.61	25.32	92.09	17.41
5	11.00	2.26	20.23	31.42	20.04	28.01	90.41	18.41
6	357.00	73.33	93.55	47.54	41.60	94.63	7.91	2.54
7	31.38	6.45	100.00	51.88	42.26	100.00	0.00	0.00
Total		100.00		42.66				

Table A-5: Float and sink test result for -3.36+1 mm size fraction of the feed coal

Specific Gravity (g/cm^3)	Mass (Wt) g	Fractional Yield (Wt) %	Cum. Wt %	Ash Content %	Cum. Ash Content (%)	Combustible Recovery (%)	Ash Rejection (%)	Separation Efficiency (%)
1.3 float	35.14	7.18	7.18	5.32	5.32	11.26	99.04	10.30
1.4 float	75.82	15.49	22.67	8.98	7.82	34.62	95.53	30.15
1.5 float	73.13	14.94	37.60	15.60	10.91	55.51	89.65	45.16
1.6 float	32.04	6.54	44.15	23.39	12.76	63.82	85.79	49.61
1.7 float	37.59	7.68	51.83	29.17	15.19	72.83	80.14	52.97
1.8 float	27.99	5.72	57.55	38.68	17.53	78.64	74.56	53.21
1.9 float	207.83	42.45	100.00	69.64	39.65	100.00	0.00	0.00
Total	489.54	100.00		39.65				

Table A-6: Wind sifter separation test result for -3.36+1 mm size fraction at 4.2 m/sec

Bin Number	Mass (Wt) g	Fractional Yield (Wt) %	Cum. Wt %	Ash Content %	Cum. Ash Content (%)	Combustible Recovery (%)	Ash Rejection (%)	Separation Efficiency (%)
1	40.50	8.39	8.39	24.61	24.61	9.58	93.92	3.49
2	46.70	9.67	18.06	26.23	25.48	20.38	86.44	6.82
3	84.00	17.40	35.47	25.26	25.37	40.07	73.49	13.55
4	116.51	24.14	59.60	26.49	25.82	66.93	54.65	21.57
5	17.00	3.52	63.12	43.51	26.81	69.94	50.13	20.07
6	168.00	34.80	97.93	45.49	33.45	98.65	3.49	2.14
7	10.00	2.07	100.00	57.11	33.94	100.00	0.00	0.00
Total	482.71	100.00		33.94				

Table A-7: Wind sifter separation test result for -3.36+1 mm size fraction at 3.0 m/sec

Bin Number	Mass (Wt) g	Fractional Yield (Wt) %	Cum. Wt %	Ash Content %	Cum. Ash Content (%)	Combustible Recovery (%)	Ash Rejection (%)	Separation Efficiency (%)
1	36.60	8.18	8.18	21.89	21.89	9.40	94.40	3.80
2	41.66	9.31	17.50	22.59	22.26	20.00	87.82	7.82
3	52.70	11.78	29.28	23.83	22.89	33.19	79.05	12.24
4	78.51	17.55	46.83	22.45	22.73	53.21	66.73	19.94
5	21.02	4.70	51.53	40.07	24.31	57.35	60.84	18.19
6	198.66	44.42	95.95	39.51	31.35	96.85	5.98	2.83
7	18.13	4.05	100.00	47.20	31.99	100.00	0.00	0.00
Total	447.28	100.00		31.99				

Table A-8: Wind sifter separation test result for -3.36+1 mm size fraction at 2.5 m/sec

Bin Number	Mass (Wt) g	Fractional Yield (Wt) %	Cum. Wt %	Ash Content %	Cum. Ash Content (%)	Combustible Recovery (%)	Ash Rejection (%)	Separation Efficiency (%)
1	17.52	4.13	4.13	21.43	21.43	4.88	97.36	2.23
2	20.62	4.86	8.99	21.47	21.45	10.61	94.24	4.85
3	29.52	6.96	15.95	22.00	21.69	18.77	89.67	8.44
4	51.04	12.03	27.98	22.17	21.90	32.84	81.70	14.54
5	20.20	4.76	32.74	38.44	24.30	37.25	76.23	13.48
6	262.00	61.75	94.49	36.78	32.46	95.93	8.38	4.30
7	23.40	5.51	100.00	50.85	33.47	100.00	0.00	0.00
Total	424.30	100.00		33.47				

Table A-9: Wind sifter separation test result for -3.36+1 mm size fraction at 2.0 m/sec

Bin Number	Mass (Wt) g	Fractional Yield (Wt) %	Cum. Wt %	Ash Content %	Cum. Ash Content (%)	Combustible Recovery (%)	Ash Rejection (%)	Separation Efficiency (%)
1	4.36	0.94	0.94	17.63	17.63	1.17	99.51	0.68
2	6.90	1.49	2.43	17.50	17.55	3.02	98.74	1.76
3	9.87	2.13	4.55	17.60	17.57	5.66	97.63	3.29
4	18.03	3.89	8.44	18.23	17.88	10.46	95.92	5.98
5	17.01	3.67	12.11	28.41	21.07	14.42	92.43	6.85
6	383.50	82.66	94.76	35.32	33.50	95.07	5.83	0.90
7	24.29	5.24	100.00	37.54	33.71	100.00	0.00	0.00
Total	463.96	100.00		33.71				

Table A-10: Float and sink test result for -1 mm size fraction of the feed coal

Specific Gravity	Mass (Wt) g	Fractional Yield (Wt) %	Cum. Wt %	Ash Content %	Cum. Ash Content (%)	Combustible Recovery (%)	Ash Rejection (%)	Separation Efficiency (%)
1.3 float	41.39	9.31	9.31	4.90	4.90	12.59	98.46	11.05
1.4 float	54.49	12.25	21.56	8.82	7.13	28.48	94.82	23.30
1.5 float	103.23	23.21	44.78	11.82	9.56	57.60	85.58	43.18
1.6 float	45.53	10.24	55.02	18.48	11.22	69.47	79.21	48.67
1.7 float	46.30	10.41	65.43	23.90	13.24	80.47	70.82	51.56
1.8 float	26.60	5.98	71.41	35.11	15.07	86.26	63.75	50.01
1.9 float	127.13	28.59	100.00	66.20	29.69	100.00	0.00	0.00
Total	444.67	100.00		29.69				

Table A-11: Wind sifter separation test result for -1 mm size fraction at 1.7 m/sec

Bin Number	Mass (Wt) g	Fractional Yield (Wt) %	Cum. Wt %	Ash Content %	Cum. Ash Content (%)	Combustible Recovery (%)	Ash Rejection (%)	Separation Efficiency (%)
1	14.1	8.82	8.82	29.60	29.60	1.17	99.51	0.68
2	23.44	14.66	23.49	30.93	30.43	3.02	98.74	1.76
3	35.00	21.90	45.38	32.06	31.22	5.66	97.63	3.29
4	47.00	29.40	74.79	31.96	31.51	10.46	95.92	5.98
5	5.4	3.38	78.17	34.47	31.64	14.42	92.43	6.85
6	30.00	18.77	96.93	39.65	33.19	95.07	5.83	0.90
7	4.9	3.07	100.00	50.61	33.72	100.00	0.00	0.00
Total	159.84	100.00		33.72				

Table A-12: Wind sifter separation test result for -1 mm size fraction at 1.0 m/sec

Bin Number	Mass (Wt) g	Fractional Yield (Wt) %	Cum. Wt %	Ash Content %	Cum. Ash Content (%)	Combustible Recovery (%)	Ash Rejection (%)	Separation Efficiency (%)
1	3.47	1.99	1.99	27.30	27.30	2.08	98.22	0.30
2	4.27	2.44	4.43	27.94	27.65	4.61	95.98	0.59
3	7.95	4.55	8.98	28.23	27.95	9.31	91.76	1.07
4	14.10	8.07	17.05	29.63	28.74	17.48	83.91	1.39
5	3.25	1.86	18.91	33.38	29.20	19.26	81.88	1.13
6	135.00	77.28	96.19	30.35	30.12	96.67	4.90	1.57
7	6.65	3.81	100.00	39.20	30.47	100.00	0.00	0.00
Total	174.69	100.00		30.47				

APPENDIX B: WASHABILITY PLOTS OF ALL THREE PARTICLE SIZE FRACTION FOR FLOAT AND SINK ANALYSIS AND DRY BENEFICIATION PROCESS

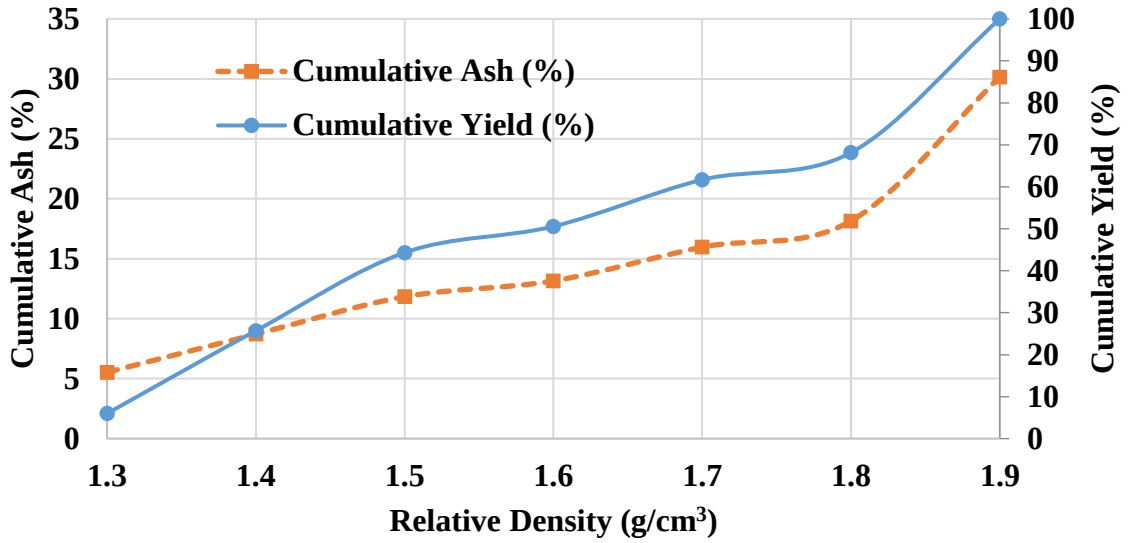


Figure B - 1: Washability plot for the float and sink analysis of (-6.7+3.36 mm) size fraction of feed coal

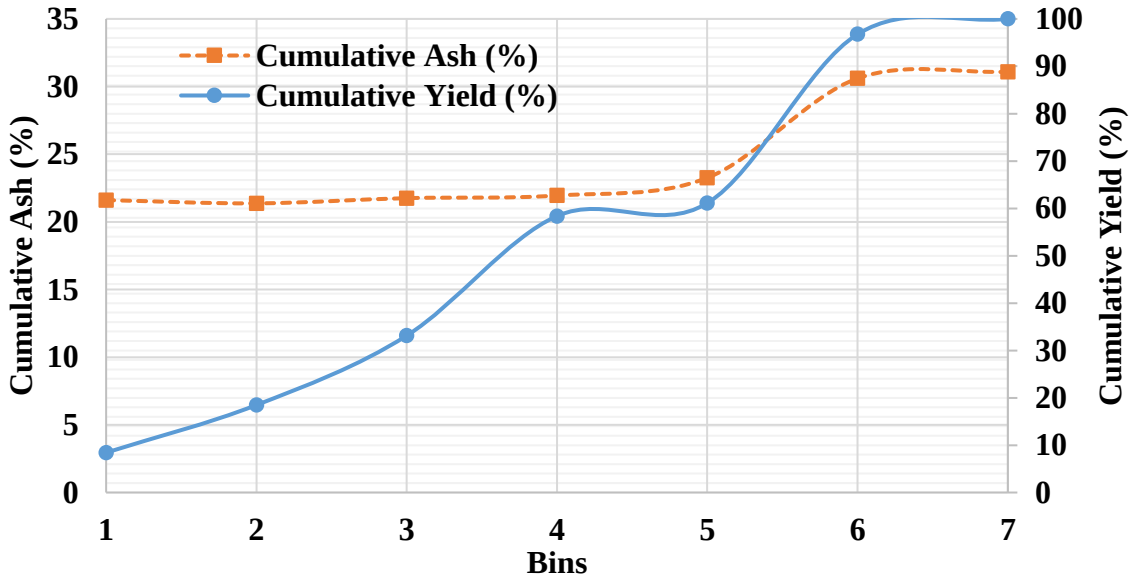


Figure B - 2: Washability plot for the dry process of (-6.7+3.36 mm) size fraction at 6.0 m/sec

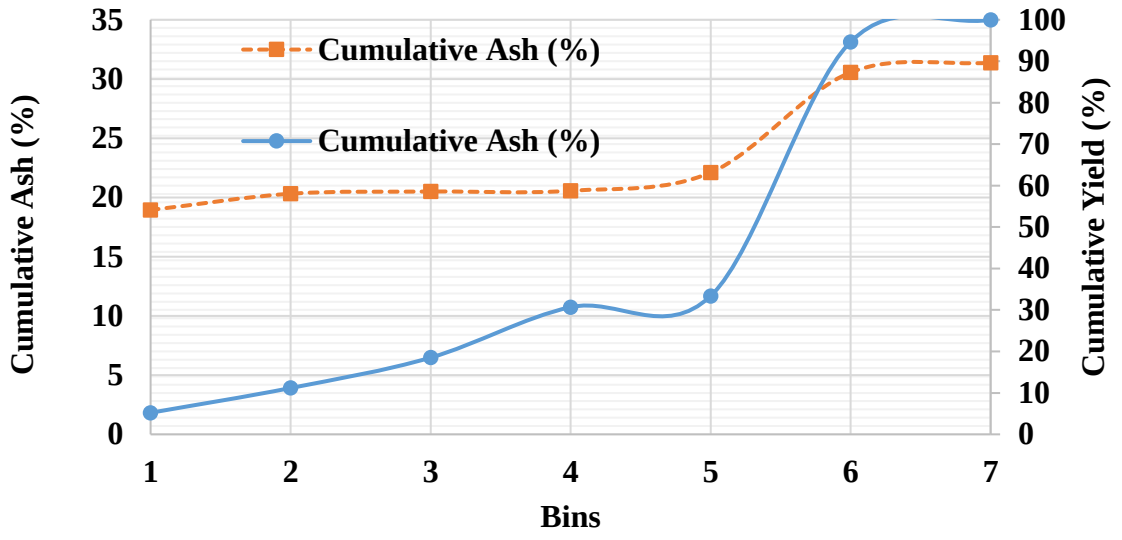


Figure B - 3: Washability plot for the dry process of (-6.7+3.36 mm) size fraction at 4.5 m/sec

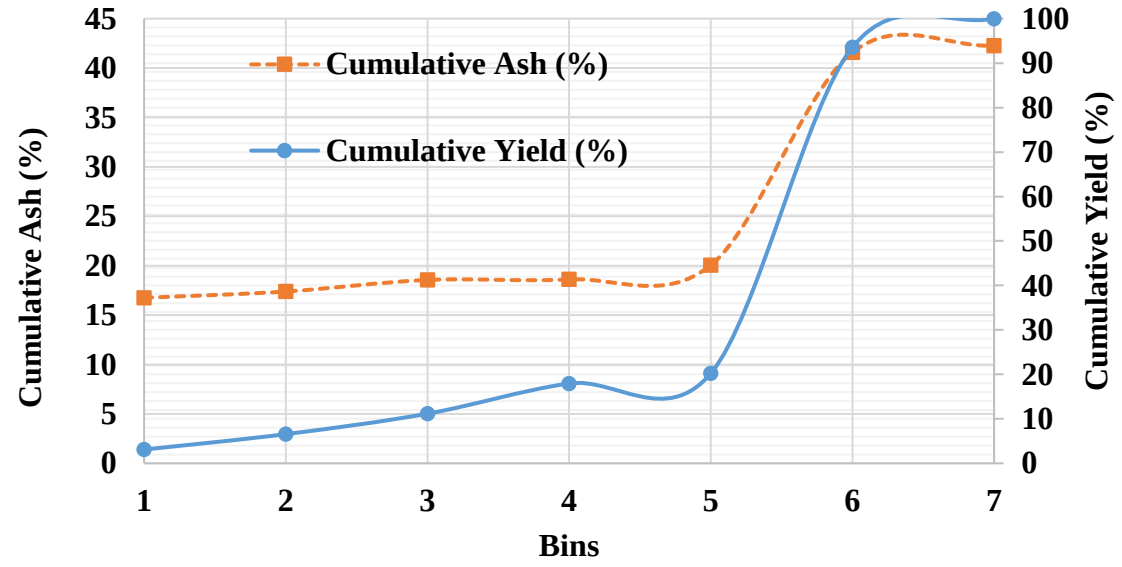


Figure B - 4: Washability plot for the dry process of (-6.7+3.36 mm) size fraction at 4.0 m/sec

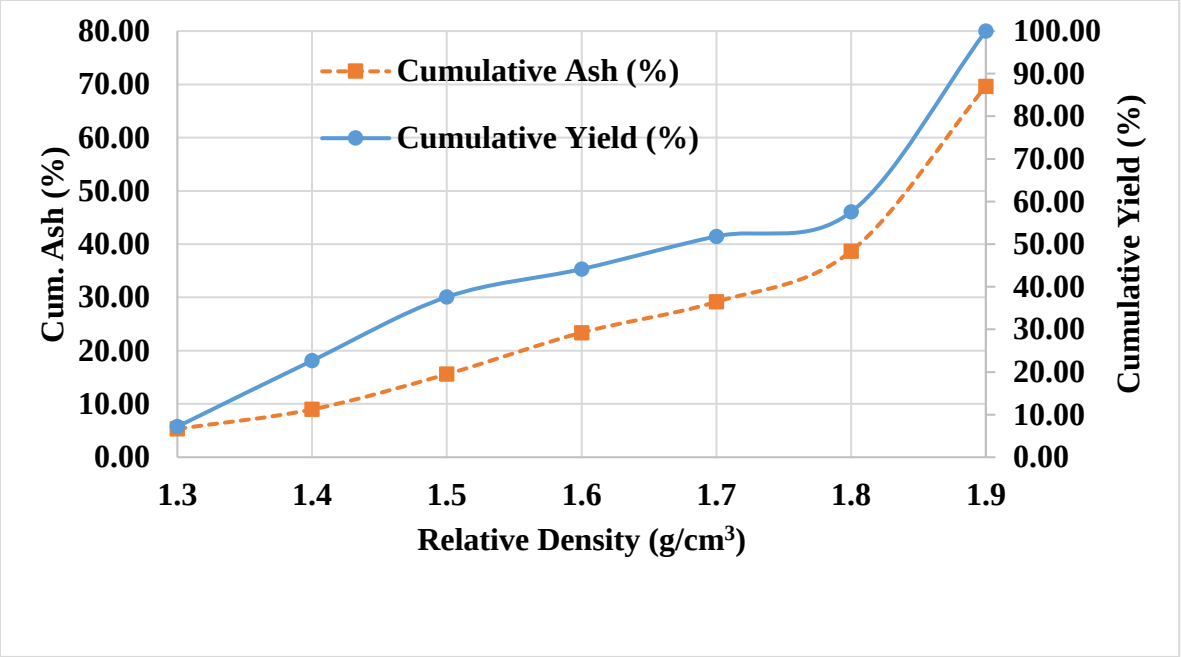


Figure B - 5: Washability plot for the float and sink analysis of (-3.36+1 mm) size fraction of feed coal

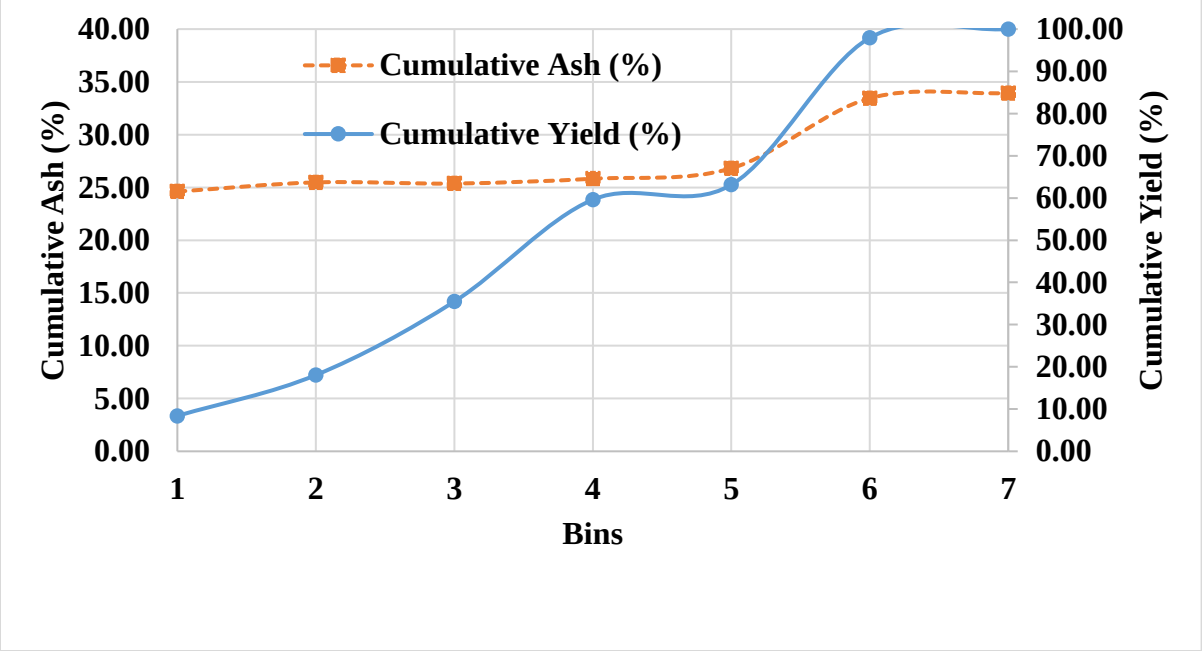


Figure B - 6: Washability plot for the dry process of (-3.36+1 mm) size fraction at 4.2 m/sec

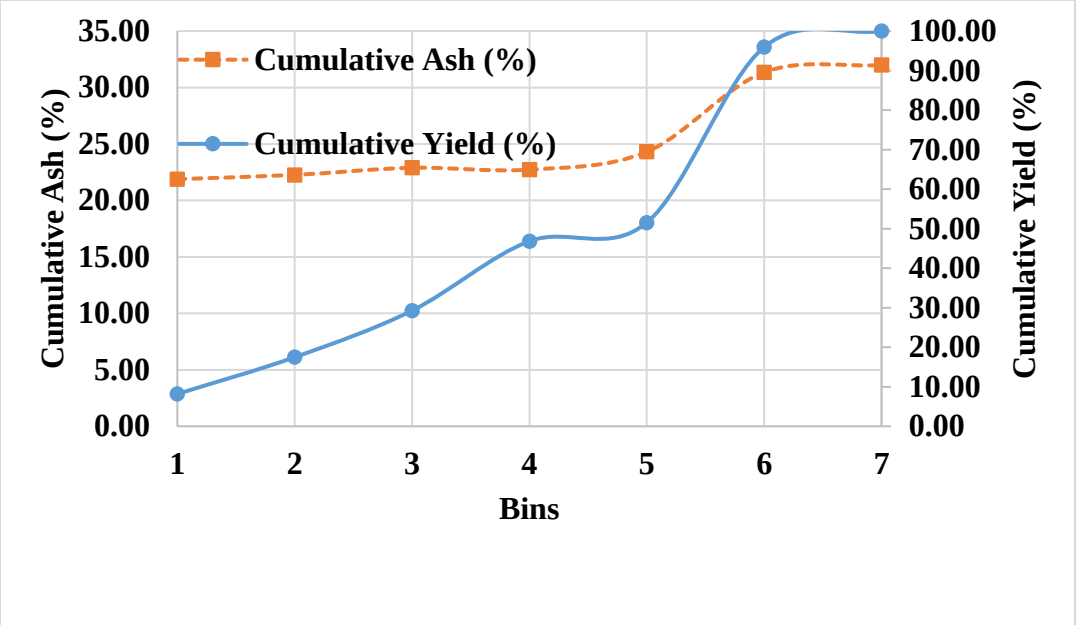


Figure B - 7: Washability plot for the dry process of (-3.36+1 mm) size fraction at 3.0 m/sec

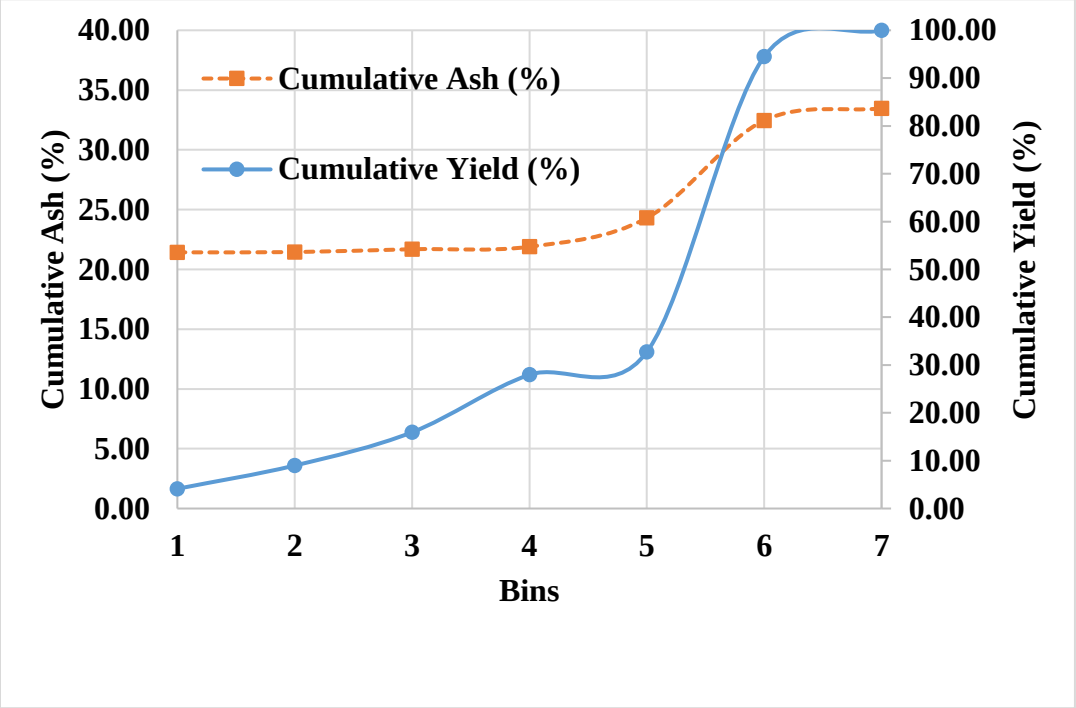


Figure B - 8: Washability plot for the dry process of (-3.36+1 mm) size fraction at 2.5 m/sec

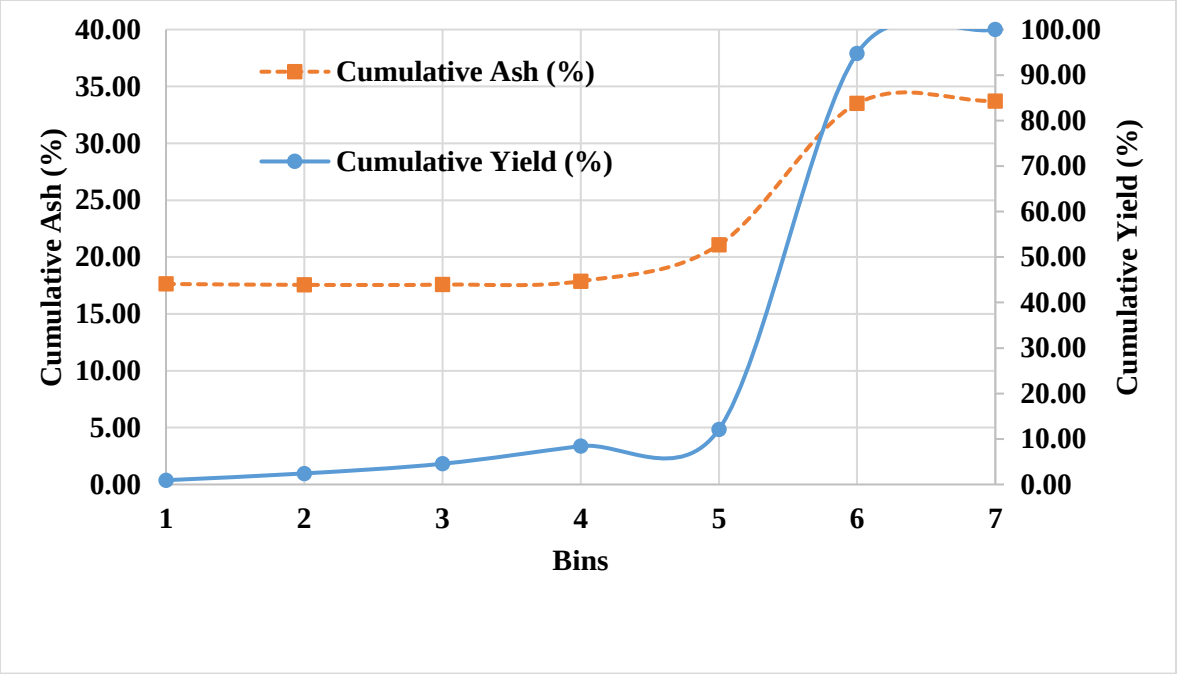


Figure B - 9: Washability plot for the dry process of (-3.36+1 mm) size fraction at 2.0 m/sec

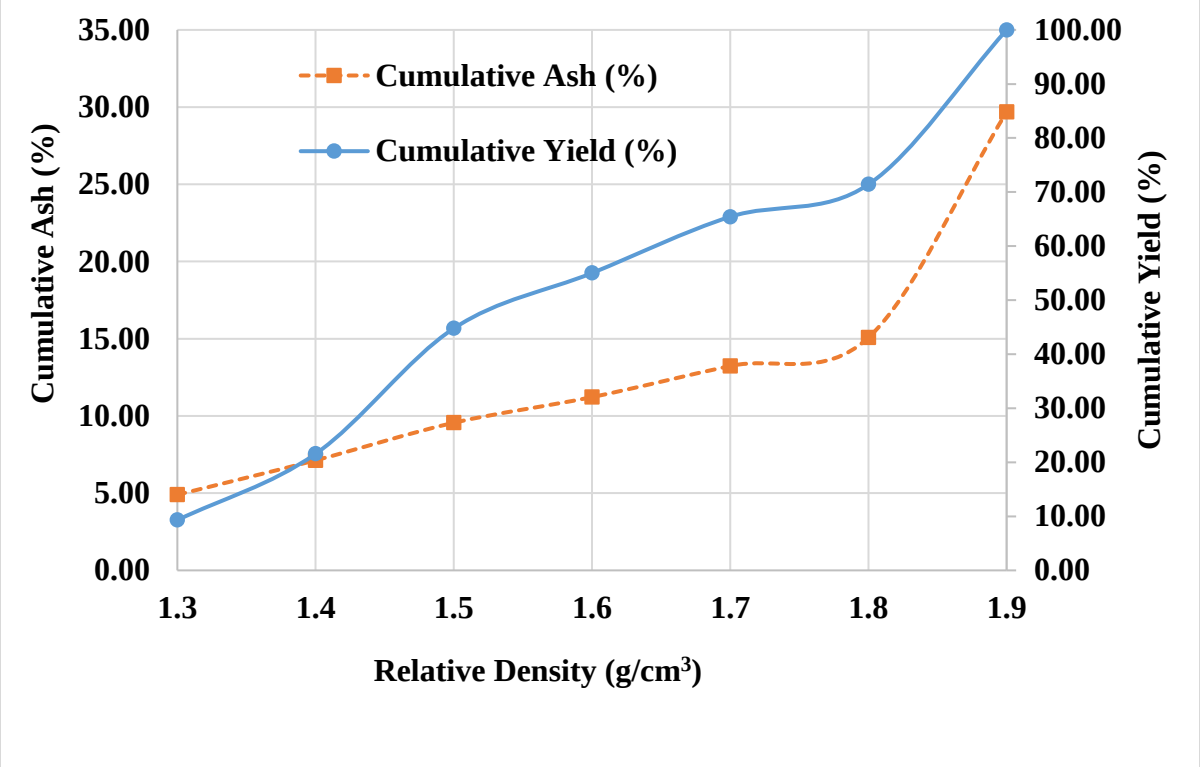


Figure B - 10: Washability plot for the float and sink analysis of (-1 mm) size fraction of feed coal

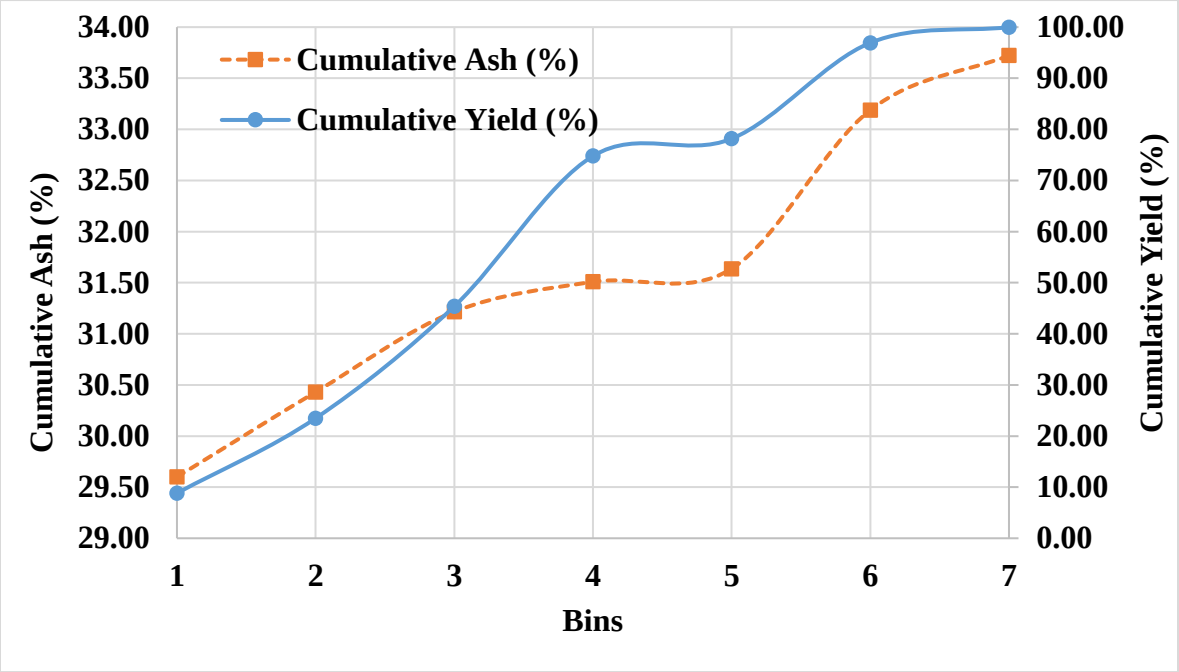


Figure B - 11: Washability plot for the dry process of (-1 mm) size fraction at 1.7 m/sec

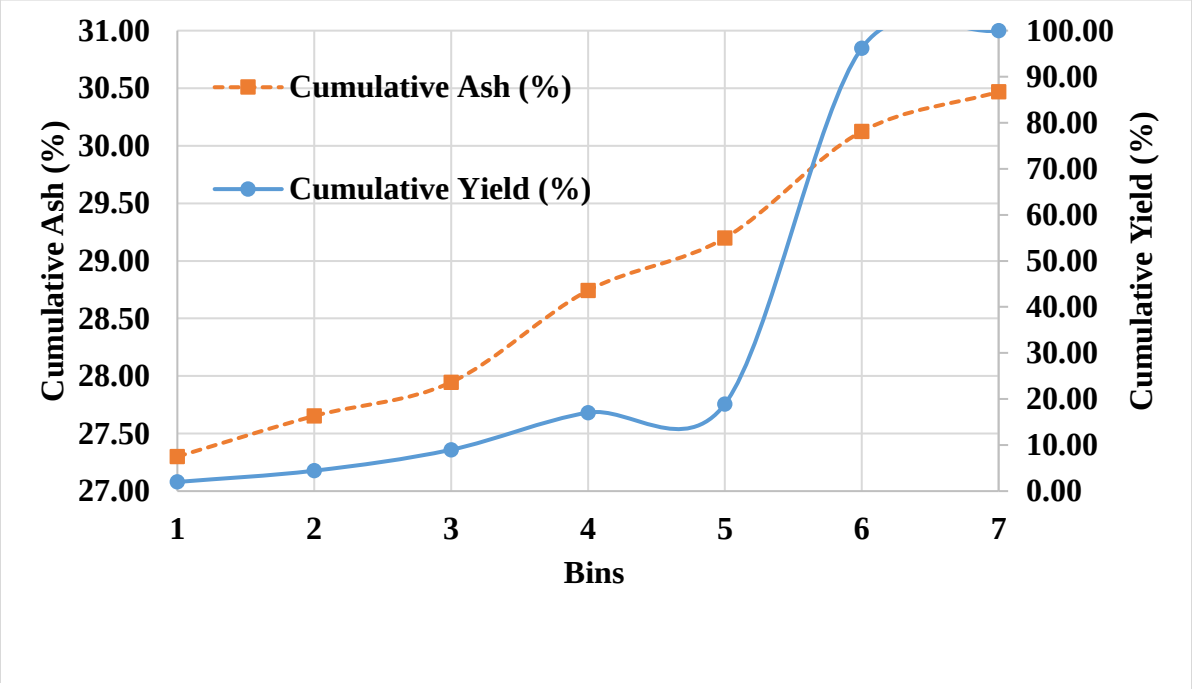


Figure B - 12: Washability plot for the dry process of (-1 mm) size fraction at 1.0 m/sec

APPENDIX C: DESIGN OF THE WIND-SIFTER SEPARATOR FROM AUTODESK INVENTOR SOFTWARE.

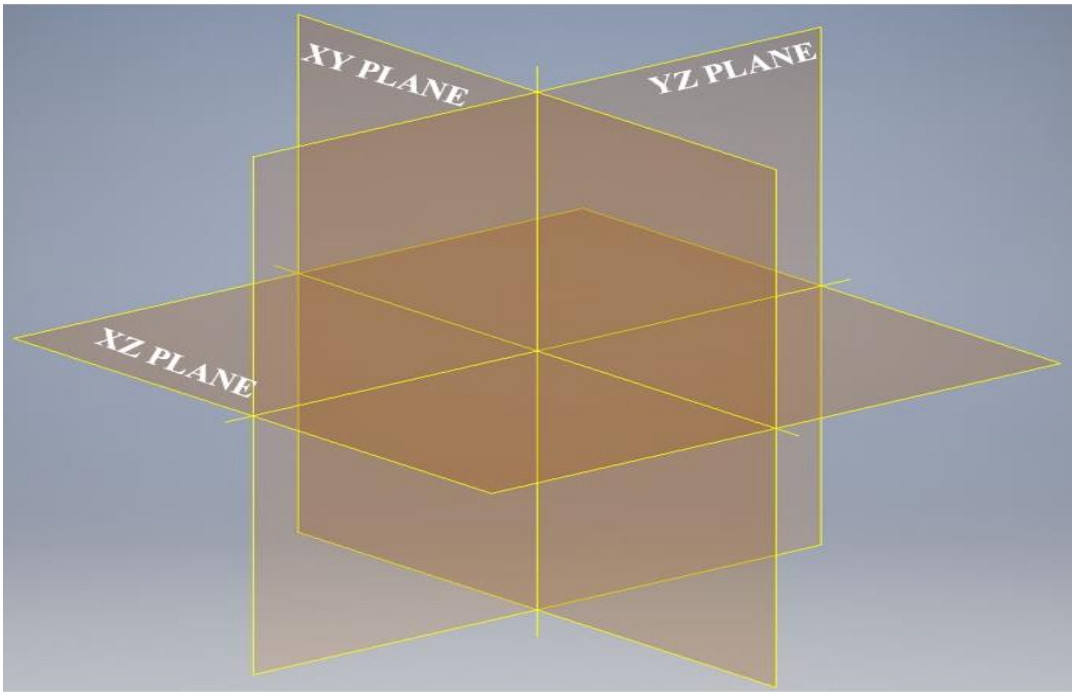


Figure C - 1: The three-dimensional Cartesian planes when starting a new drawing

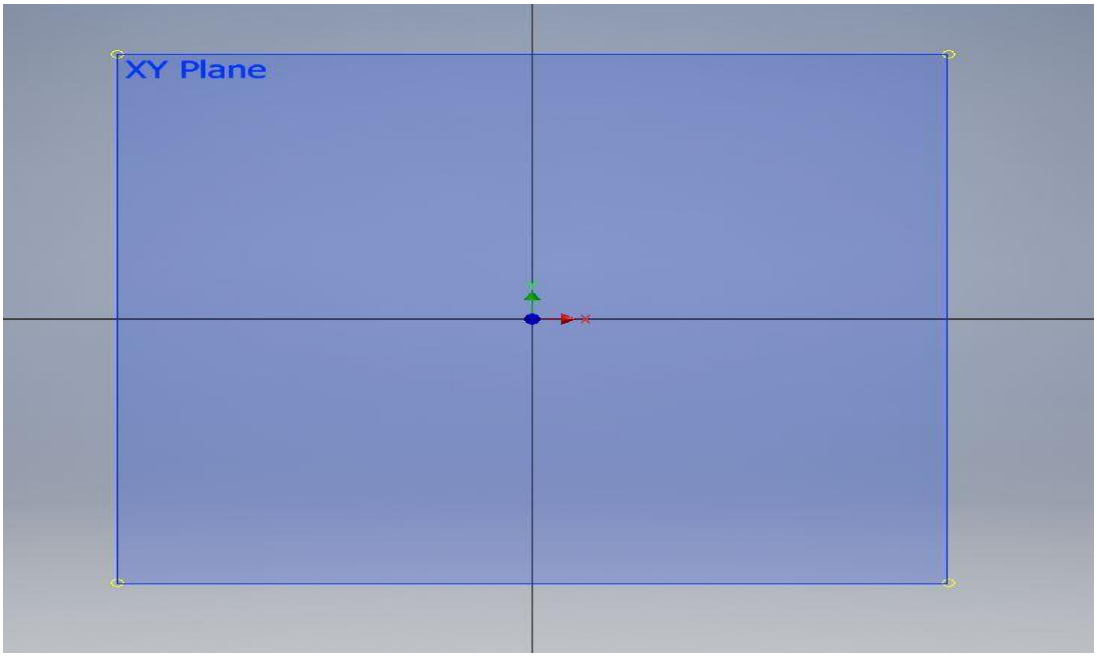


Figure C - 2: XY plane slected to draw the first chamber

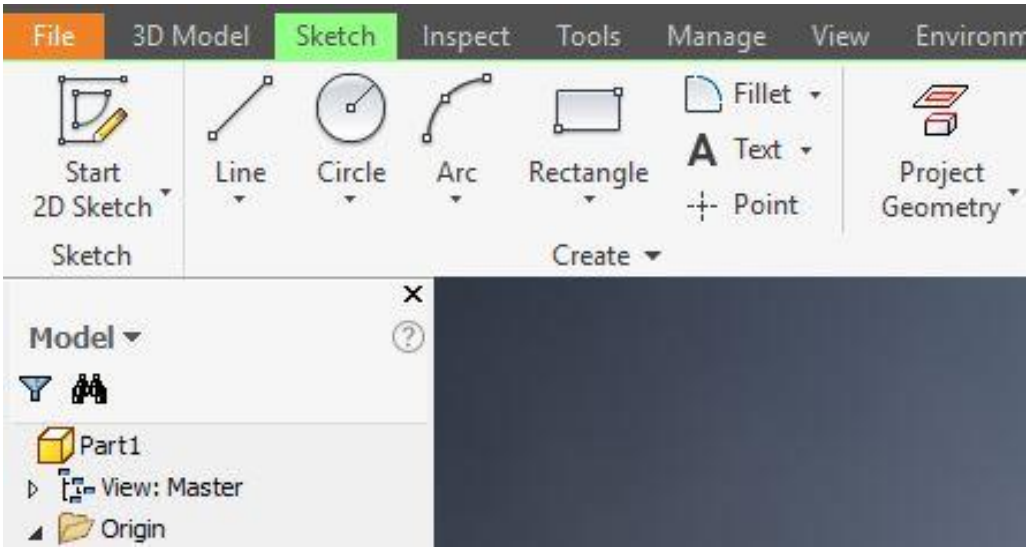


Figure C - 3: Selecting the “Sketch” tab and then “Circle”to draw the first circle

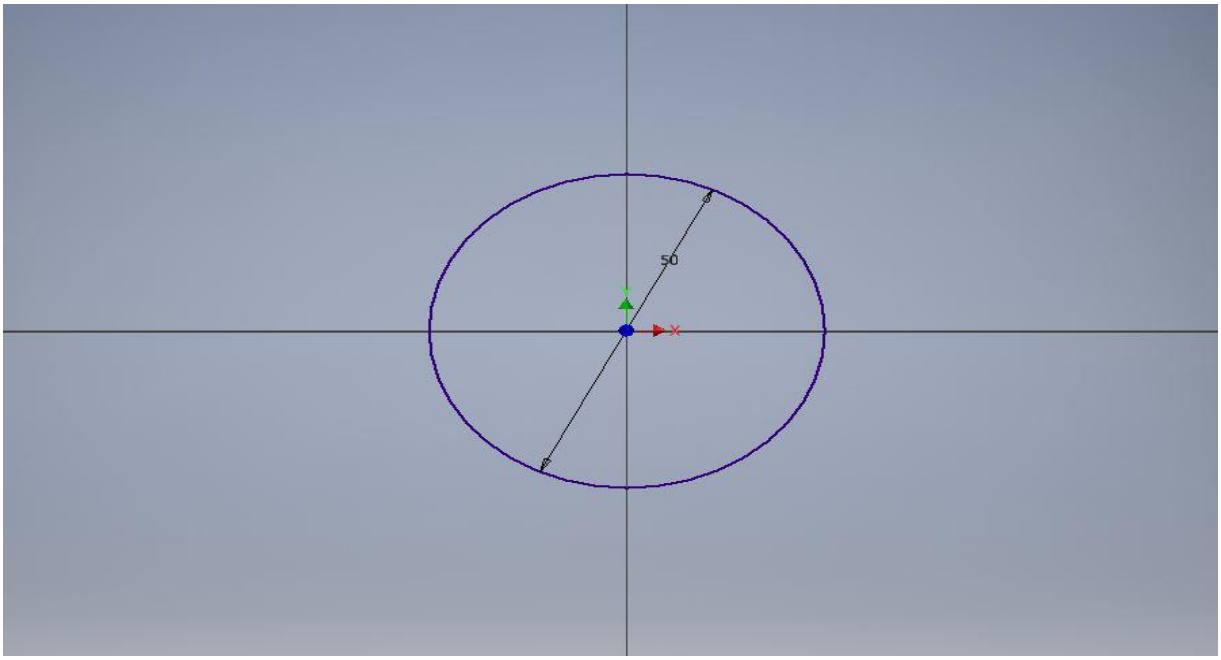


Figure C - 4: The first circle of 50 mm in dimension, representing the outlet of the first chamber 1 drawn on the XY plane.

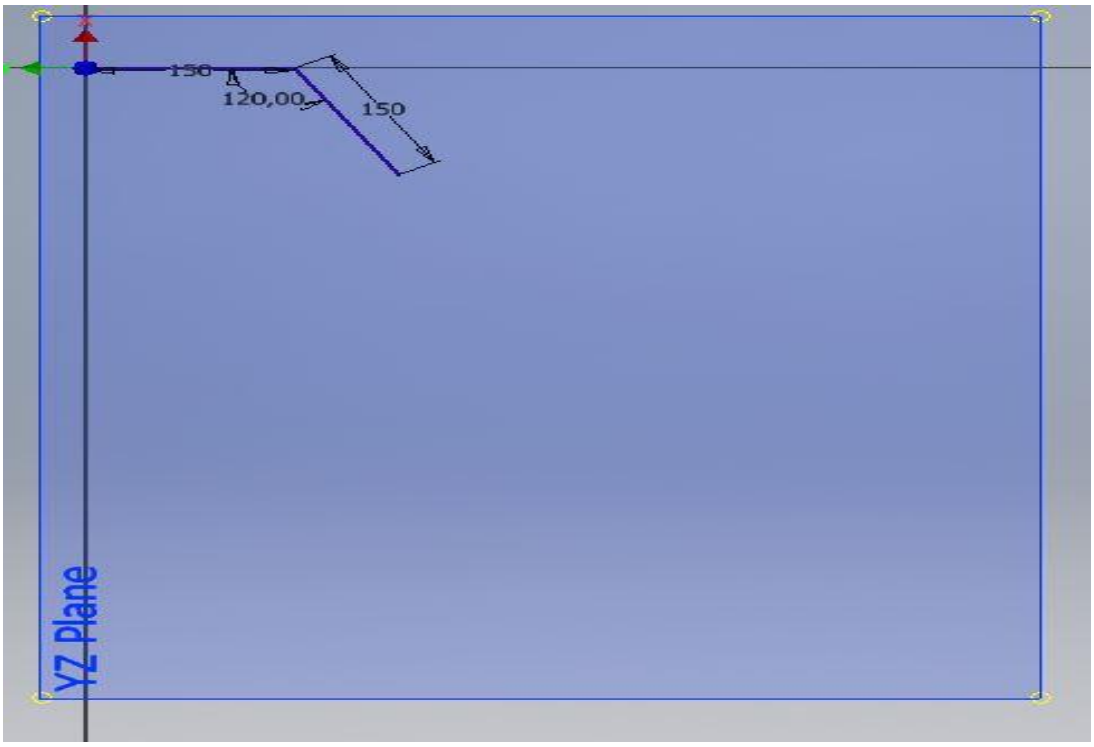


Figure C - 5: lines drawn on the YZ plane to represent the outlet pipe.

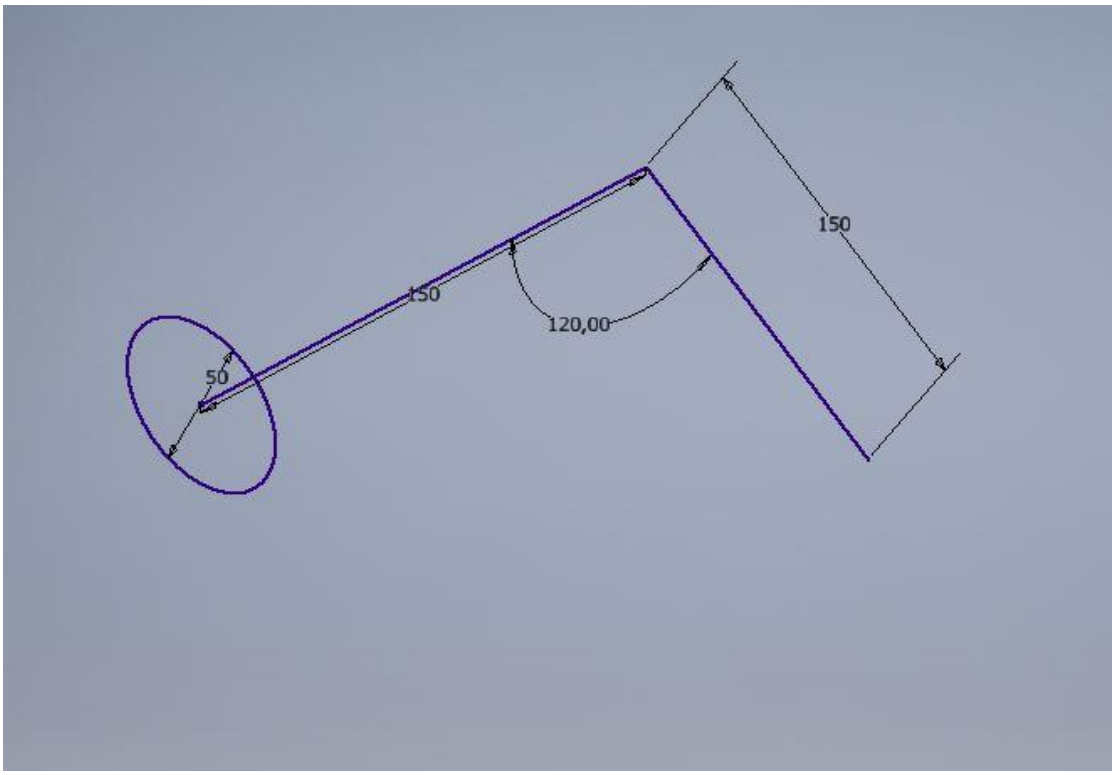


Figure C - 6: The circle and the line drawn to create the outlet pipe of chamber 1

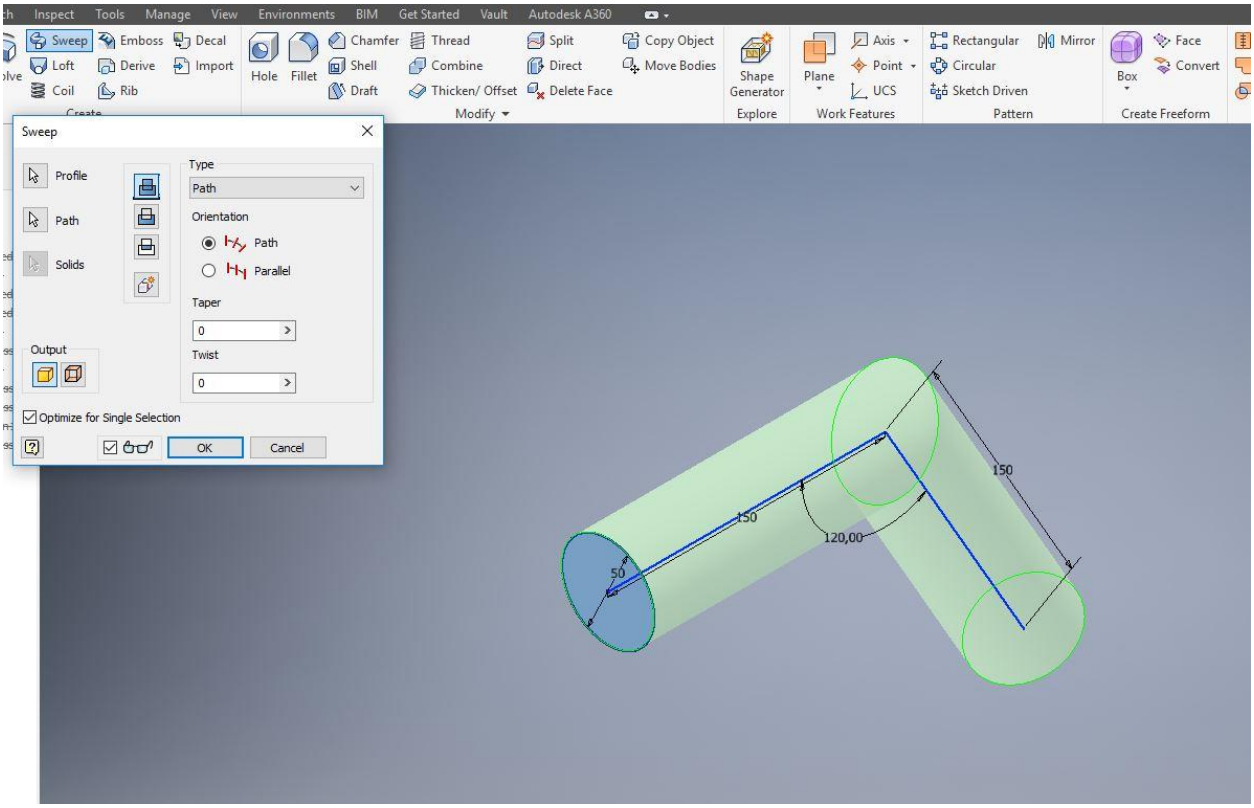


Figure C - 7: Creating the outlet of the first chamber using the “Sweep” tool

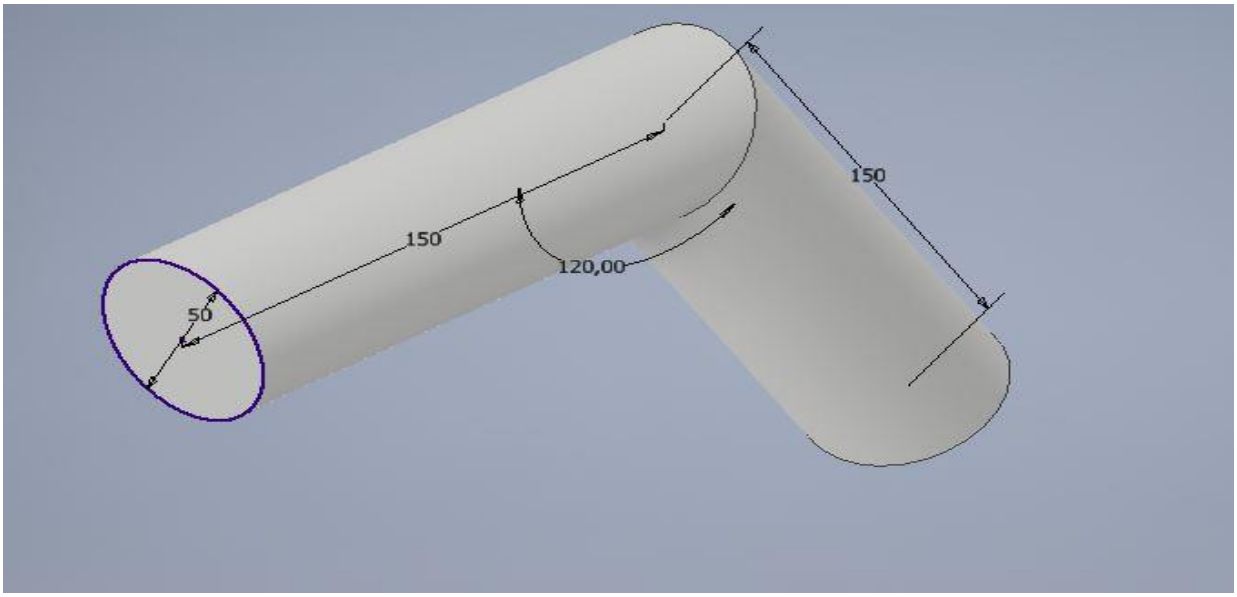


Figure C - 8: Outlet pipe created

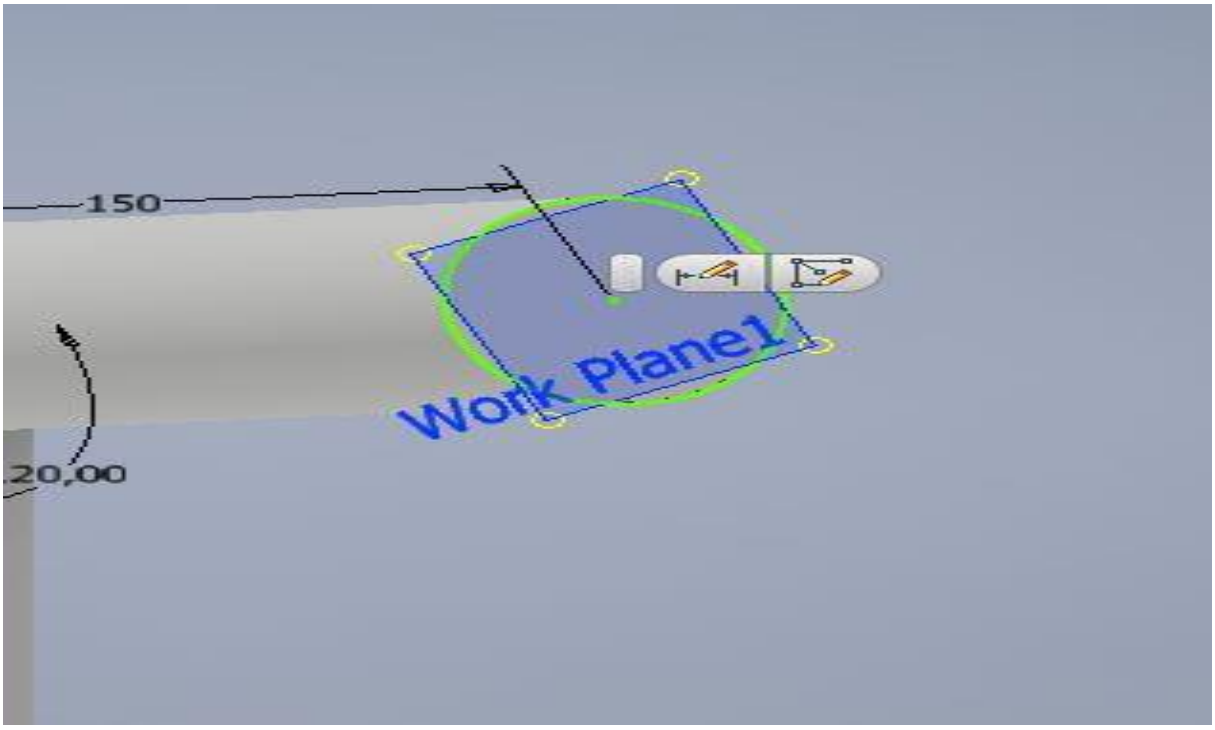


Figure C - 9: Base part of the Chamber 1-outlet pipe is lifted to draw the design transition piece.

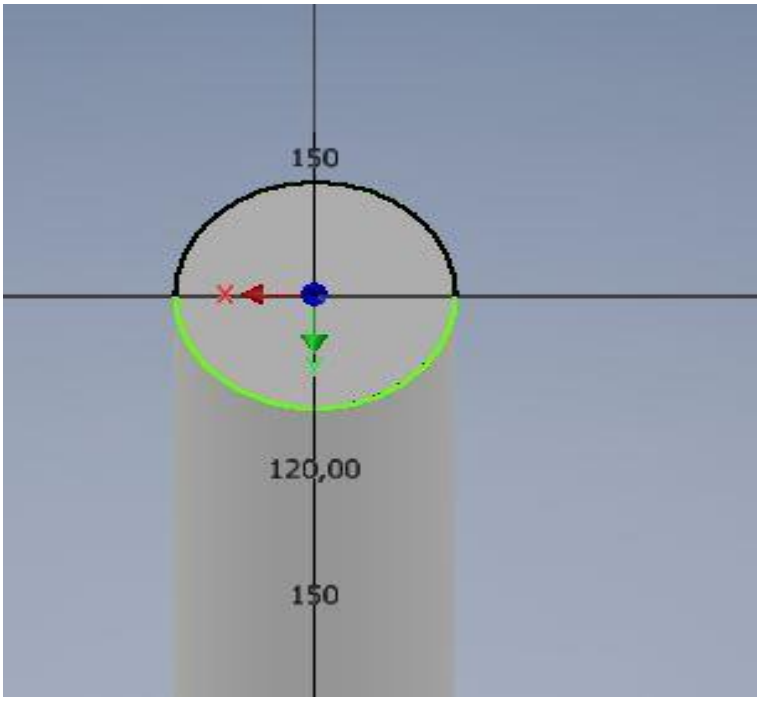


Figure C - 10: Circle drawn and the base of the Outlet Pipe

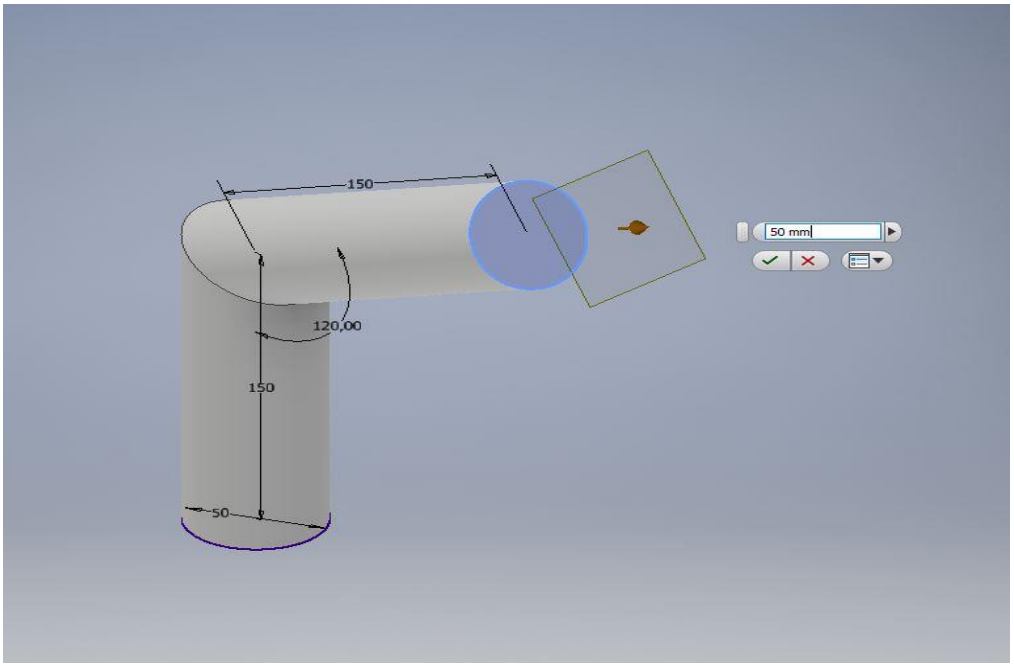


Figure C - 11: Another work plane to draw the base part of the transition piece

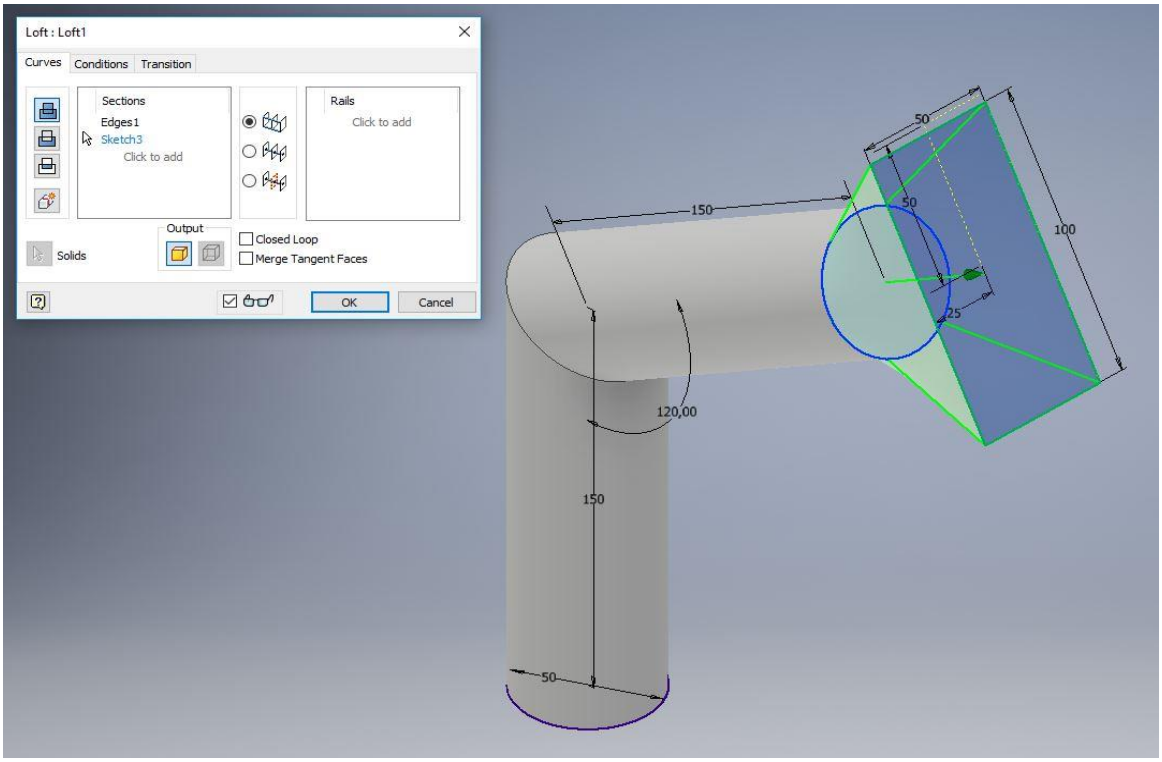


Figure C - 12: The first nozzle-transition piece designed using the “Loft” tool.

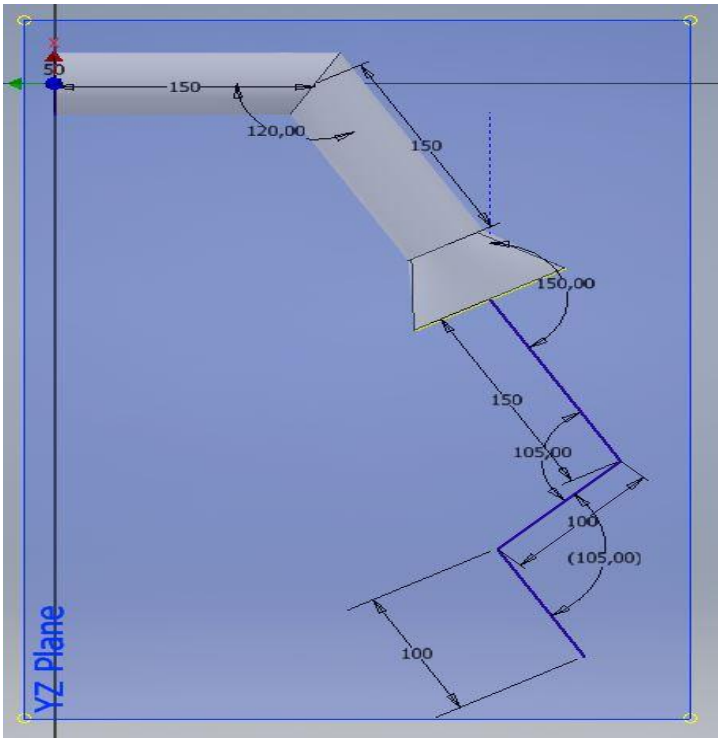


Figure C - 13: Line drawn to create the zigzag section

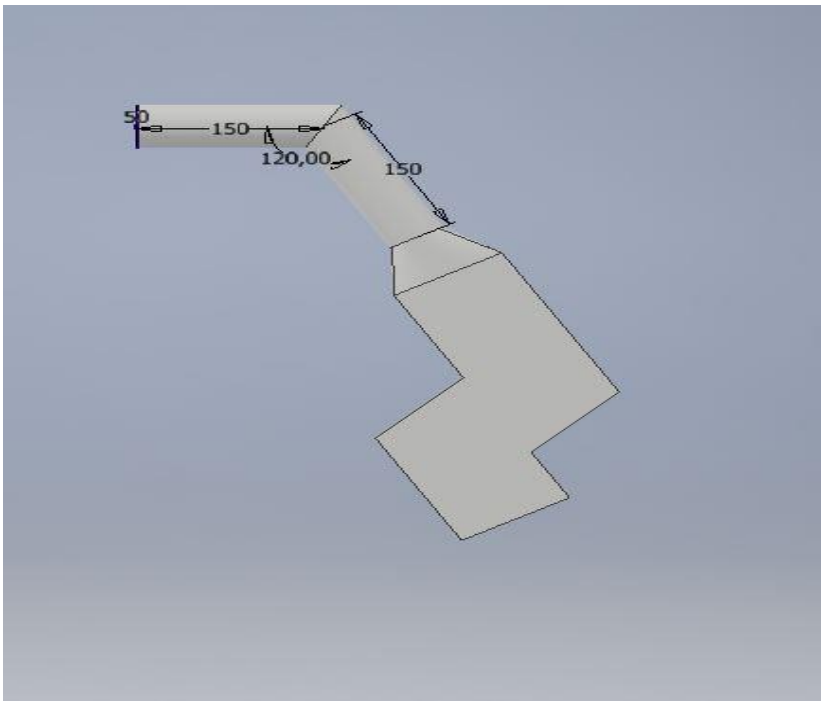


Figure C - 14: The zigzag section once the sweep is completed

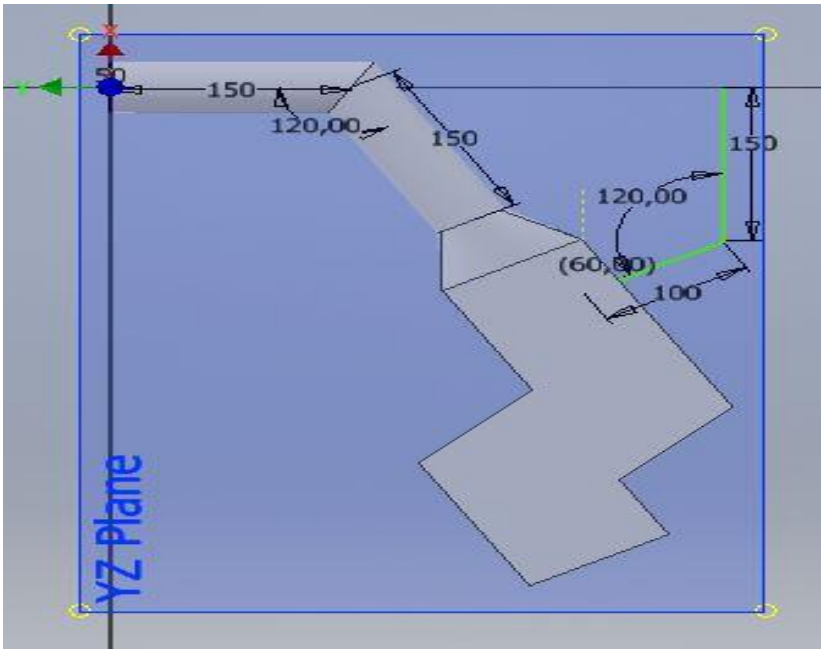


Figure C - 15: Line for the raw coal-feed inlet

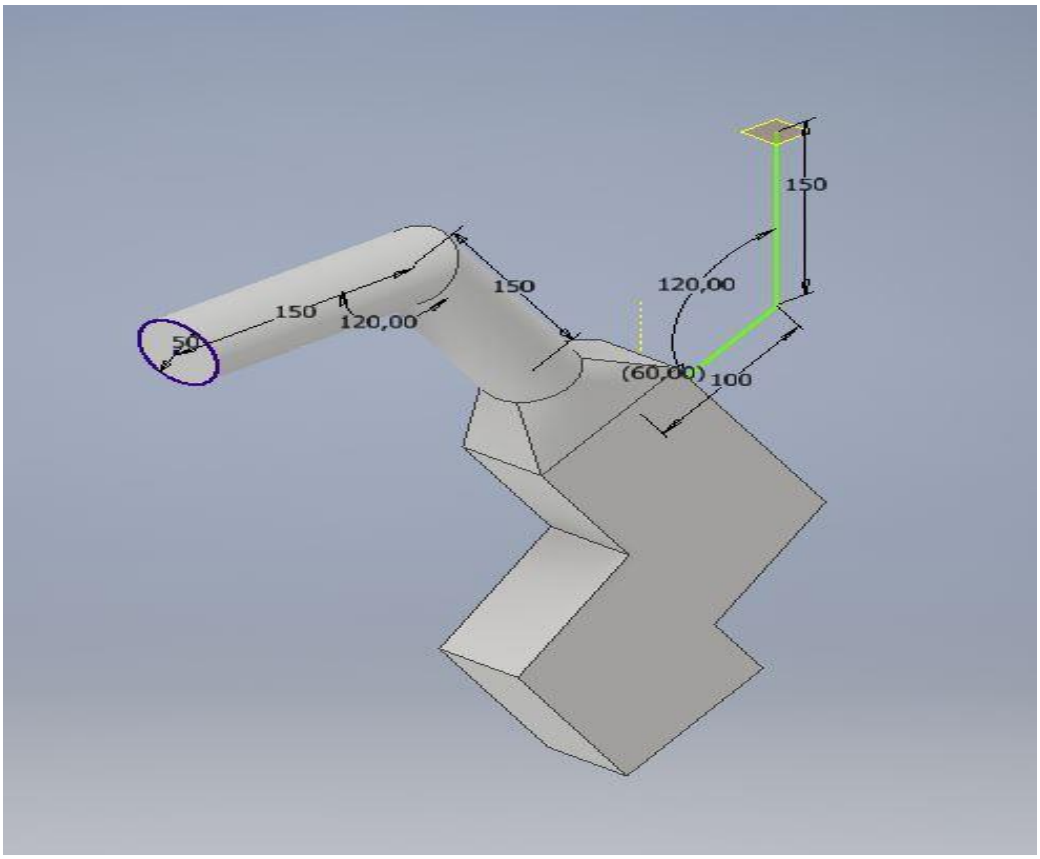


Figure C - 16: Customized workplane to draw for the raw coal inlet

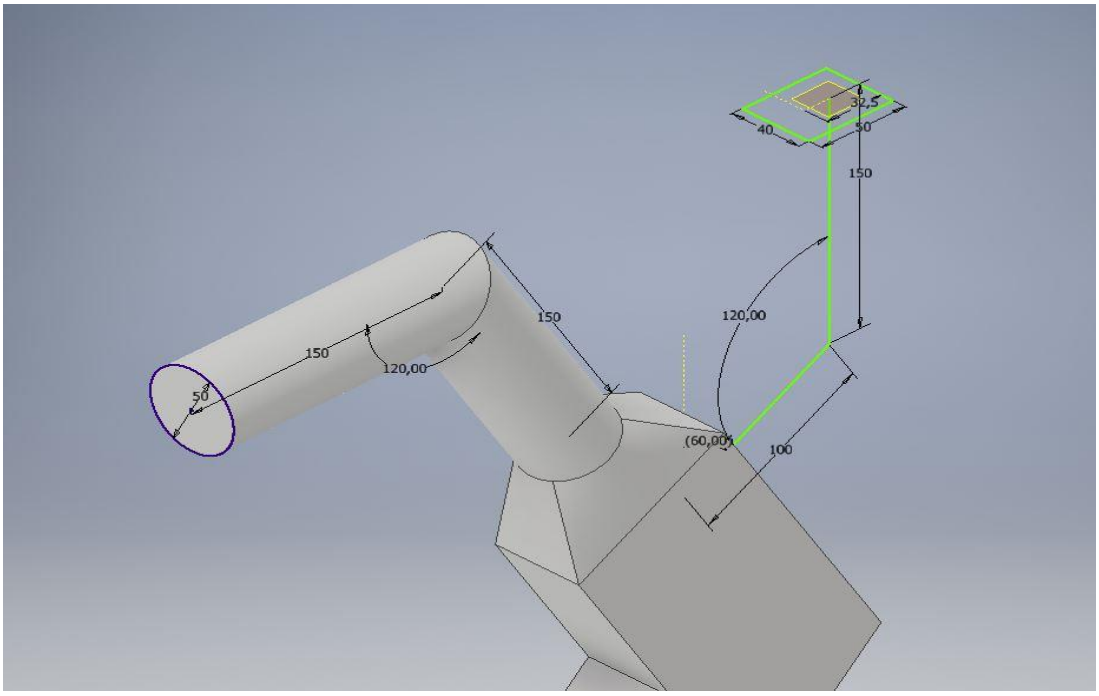


Figure C - 17: Square drawn on a work plane to serve as raw coal inlet

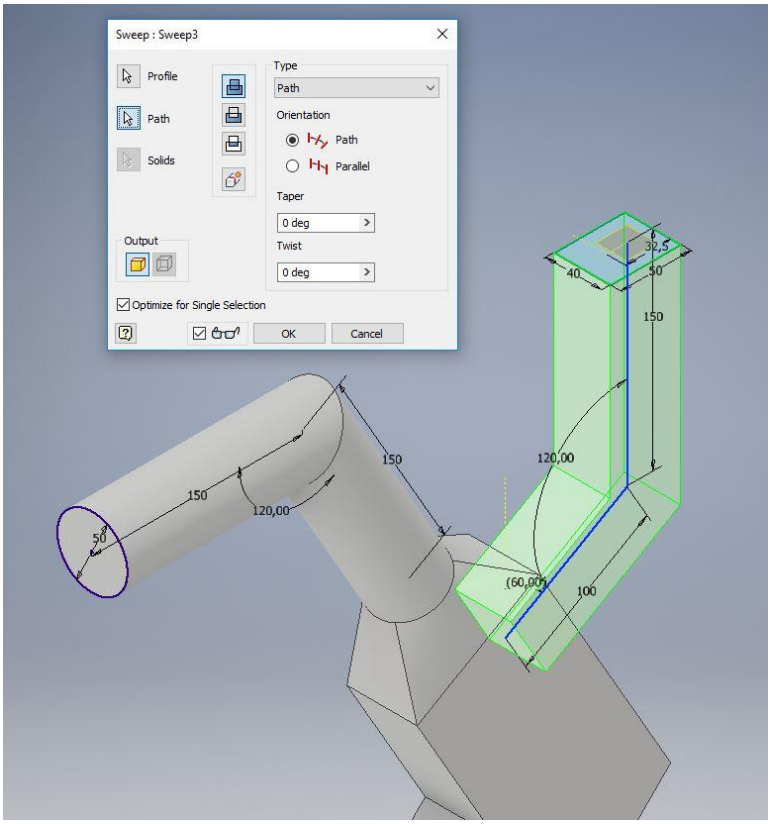


Figure C - 18: The Design of the inlet pipe for the coal feed using the “Sweep” tool.

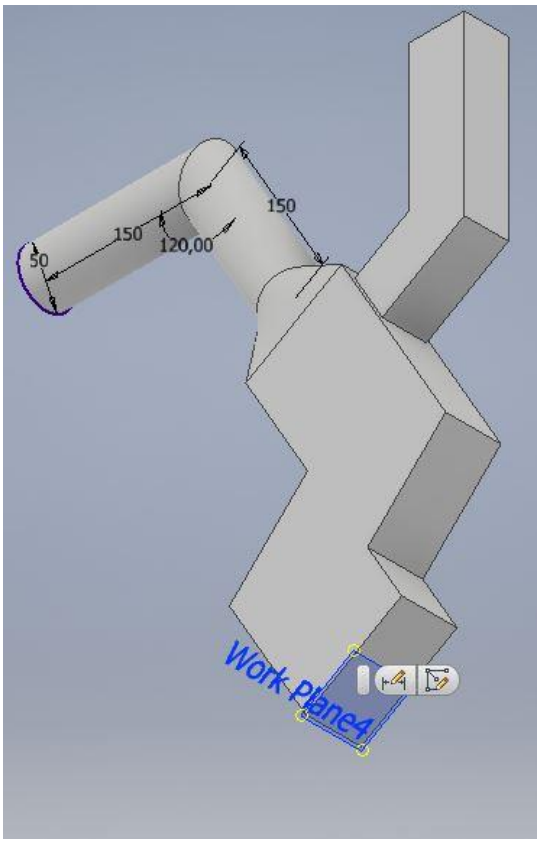


Figure C - 19: Work plane to create the second nozzle-transition piece

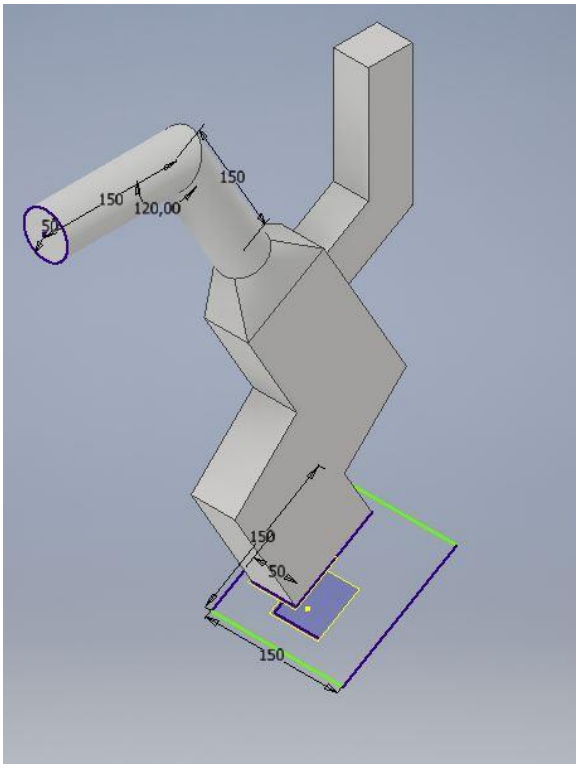


Figure C - 20: The second part of the second second nozzle for chamber 1

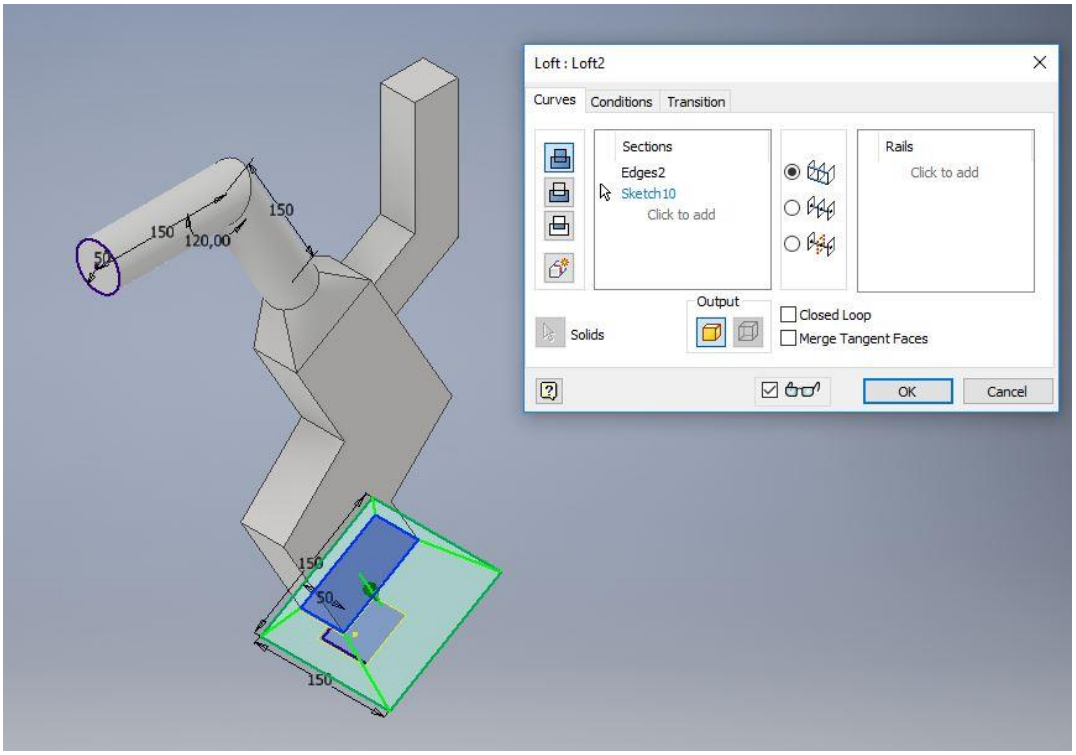


Figure C - 21: Second loft completed for the second nozzle transition piece

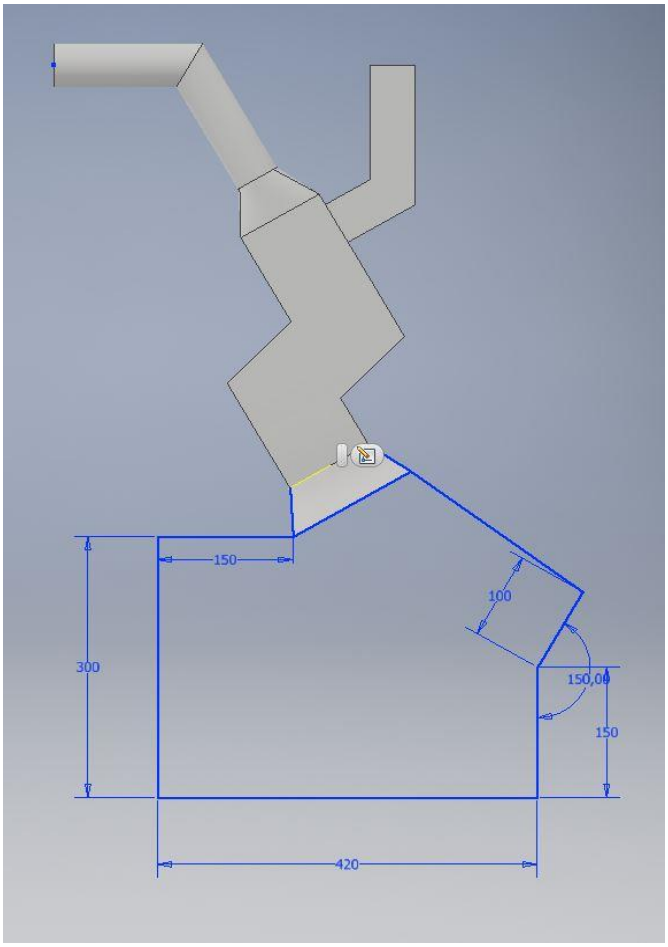


Figure C - 22: The line for the bin compartment of chamber 1

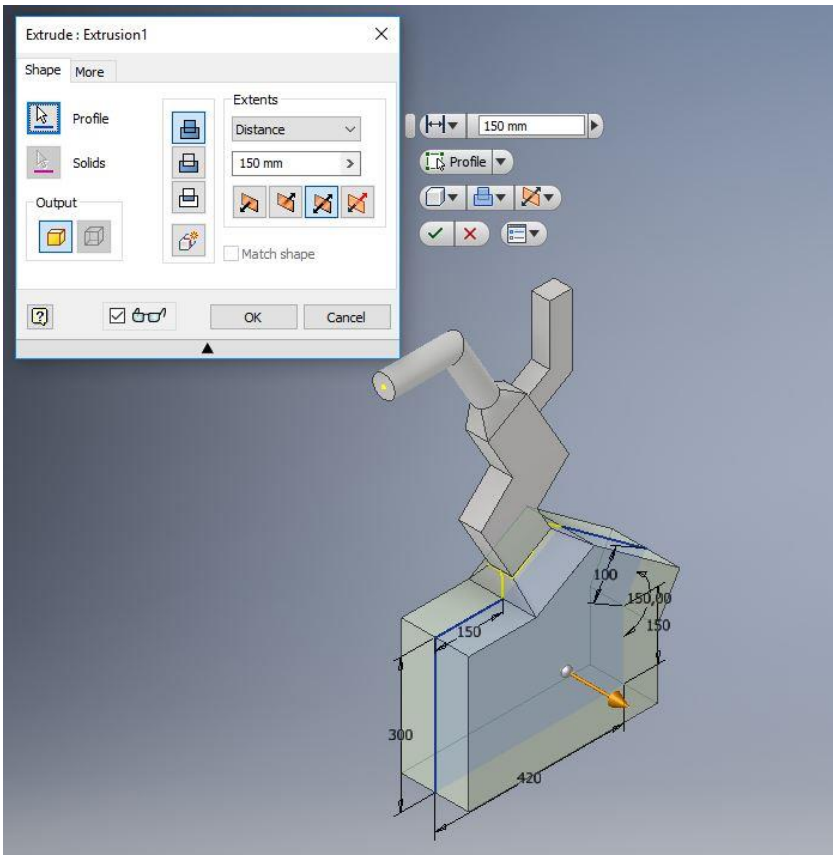


Figure C - 23: The bin compartment for chamber 1 using “Extrusion” tool

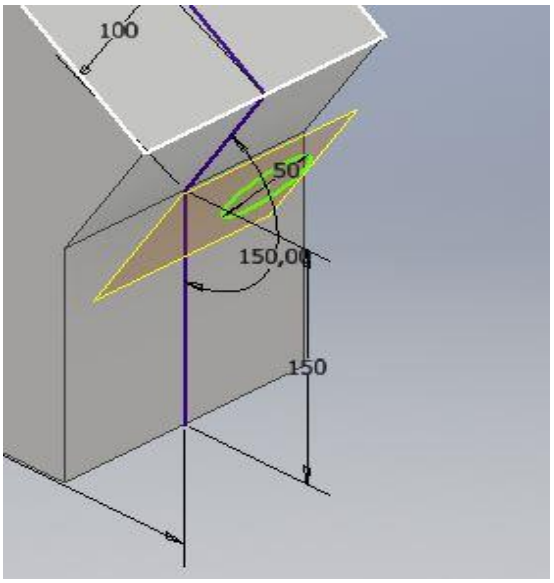


Figure C - 24: Drawing of the Air-Inlet into the separator

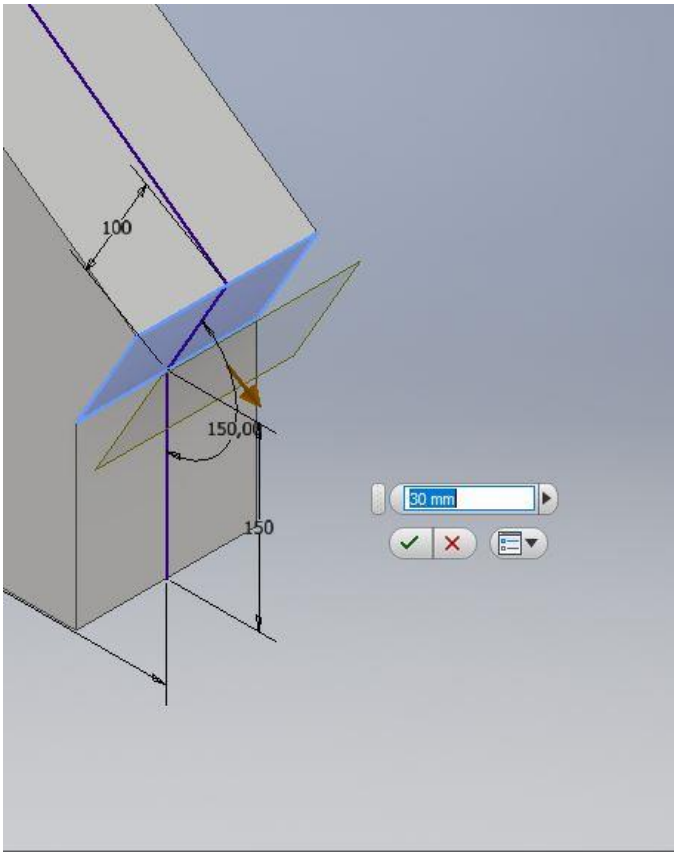


Figure C - 25: Work plane for the designing of the inner section

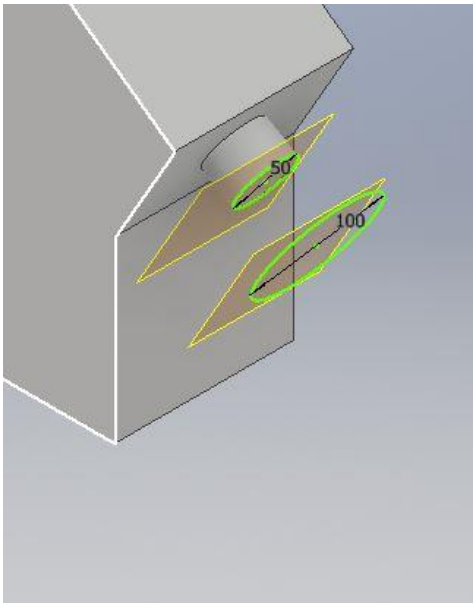


Figure C - 26: The circle on the work plane extruded backwards and the circle for the inlet

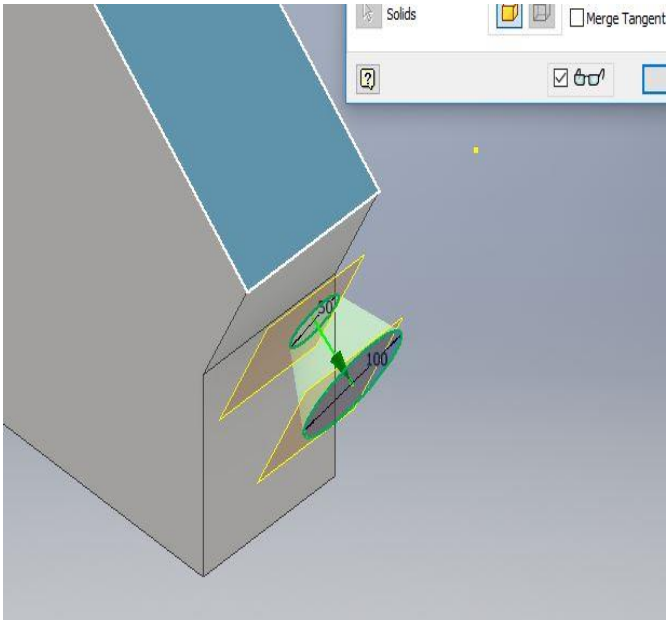


Figure C - 27: Using the “loft” tool to design the Air inlet nozzle

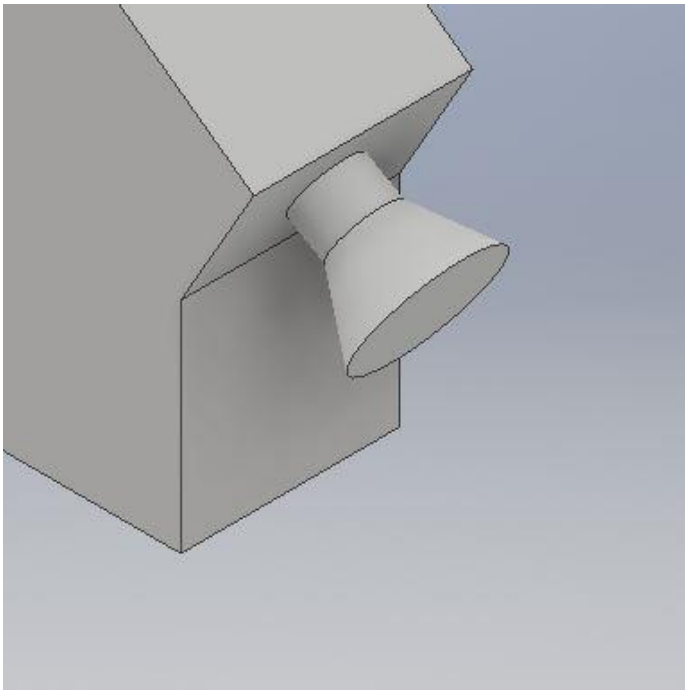


Figure C - 28: The completed Air inlet section

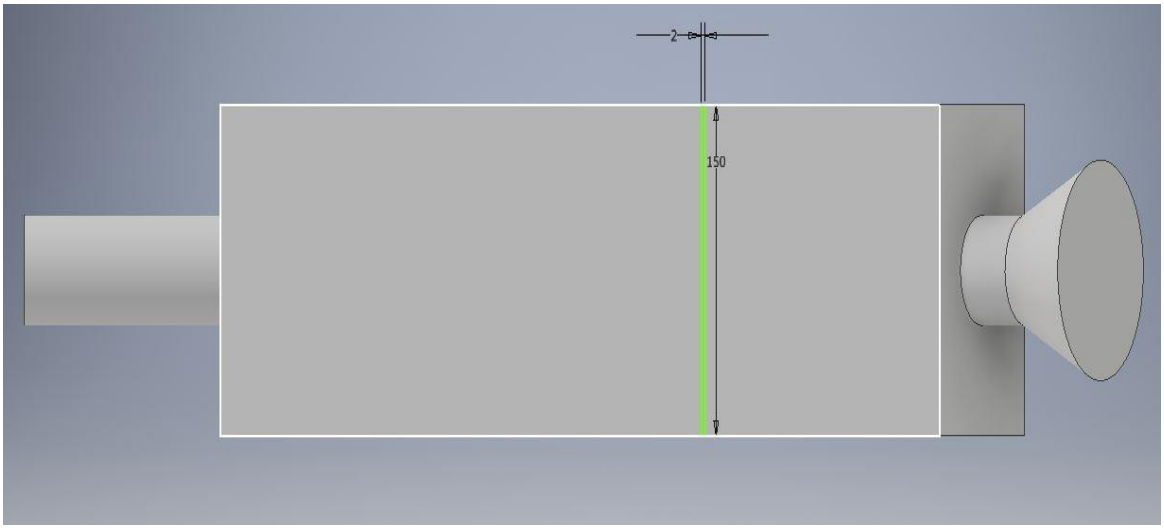


Figure C - 29: The Drawing of the bin compartment at the base of the first chamber (Upside down view of the Chamber 1)

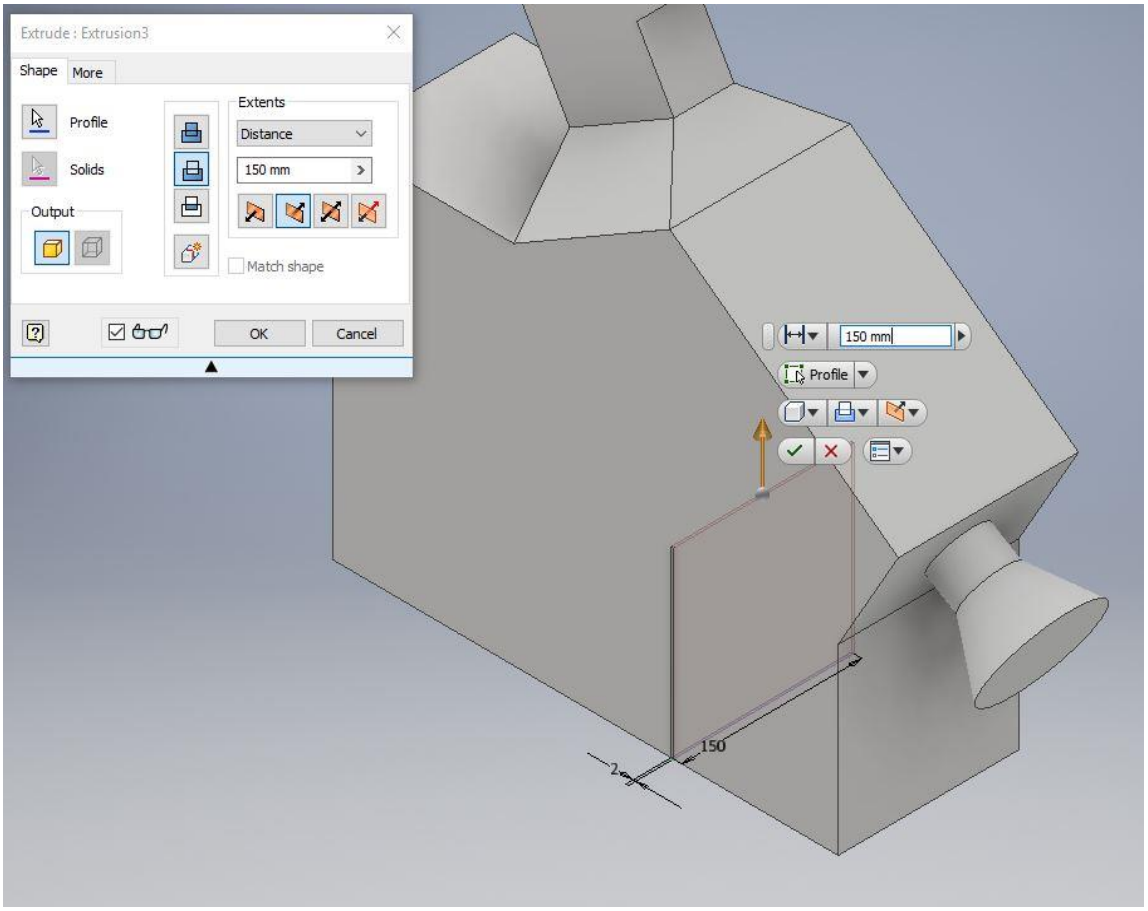


Figure C - 30: Extruding the drawn line inwards

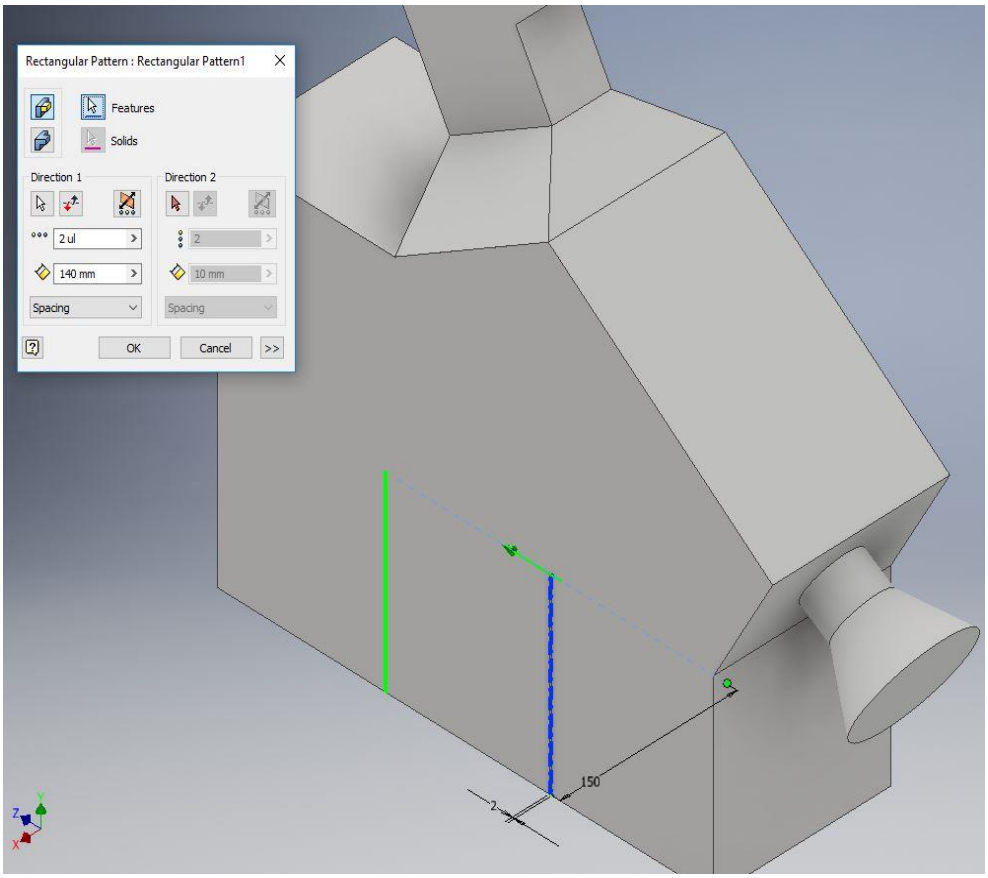


Figure C - 31: Creating the remaining bin section using the “Repeated Rectangular Pattern” tool

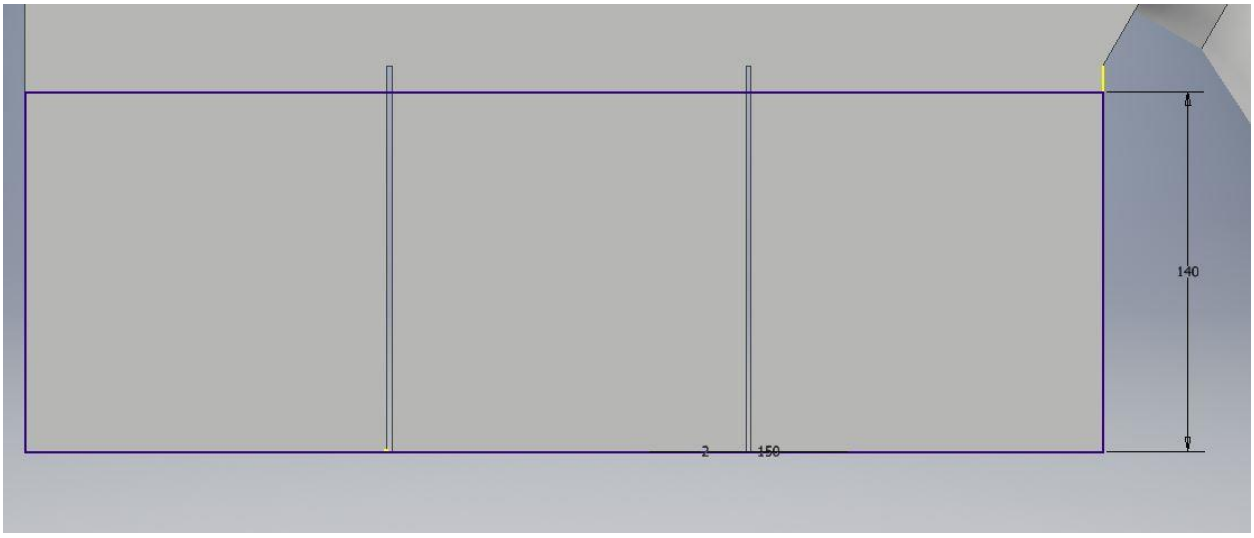


Figure C - 32: Drawing a section to cut the base part away and then attach the collecting bins.

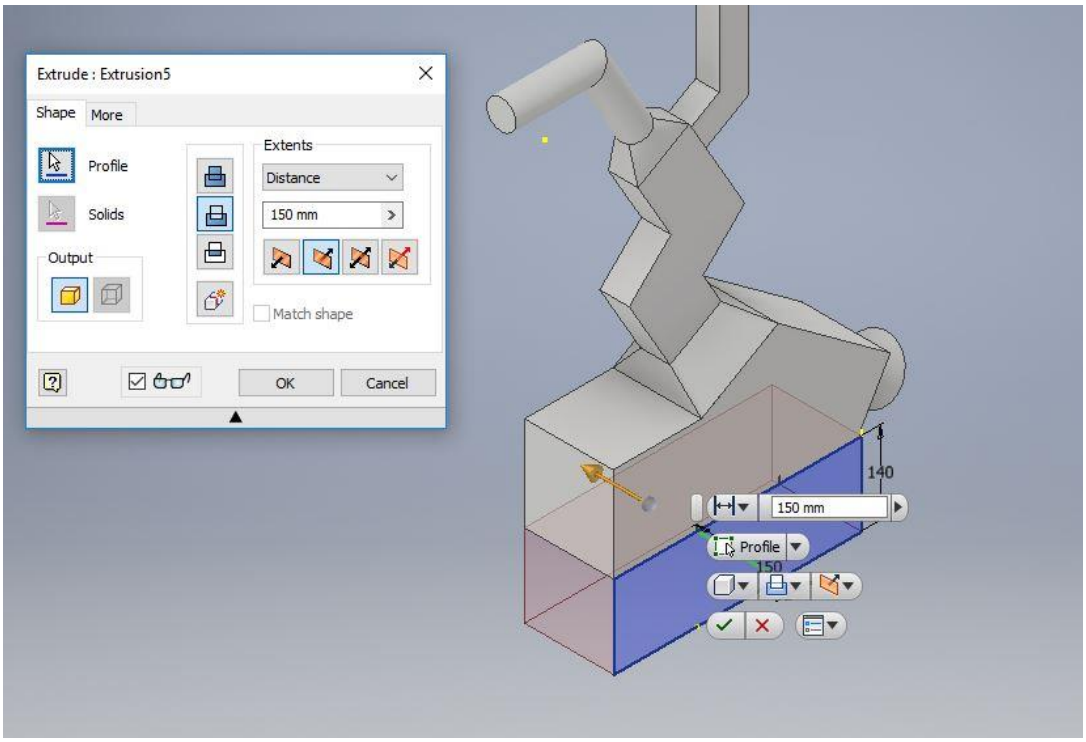


Figure C - 33: Cutting away the base part of the bin compartment to attach the bins

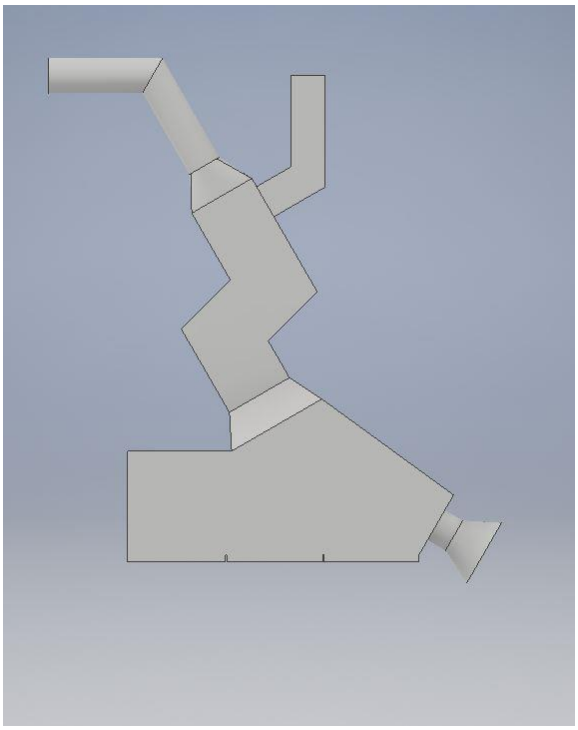


Figure C - 34: The first chamber, cut off to attach the collection bins 5, 6 and 7.

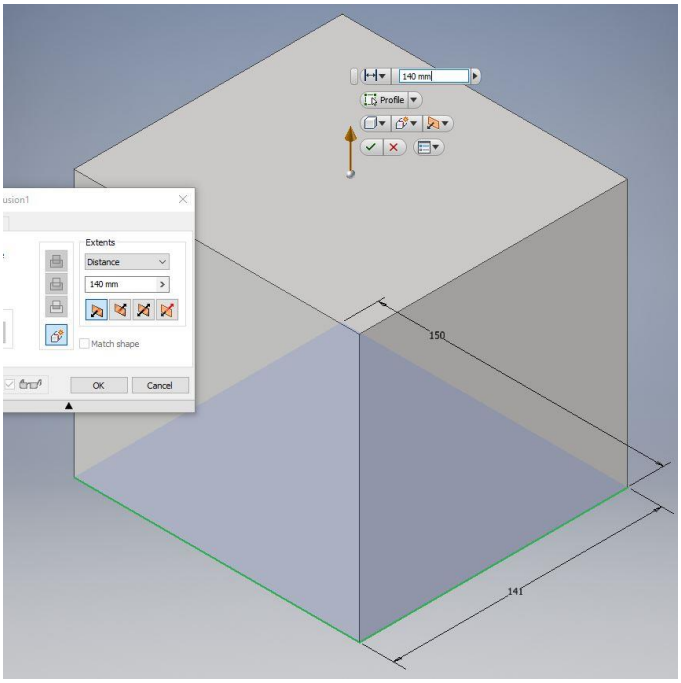


Figure C - 35: Drawing of Each collecting bin to attach to the cut-off version and create contact regions

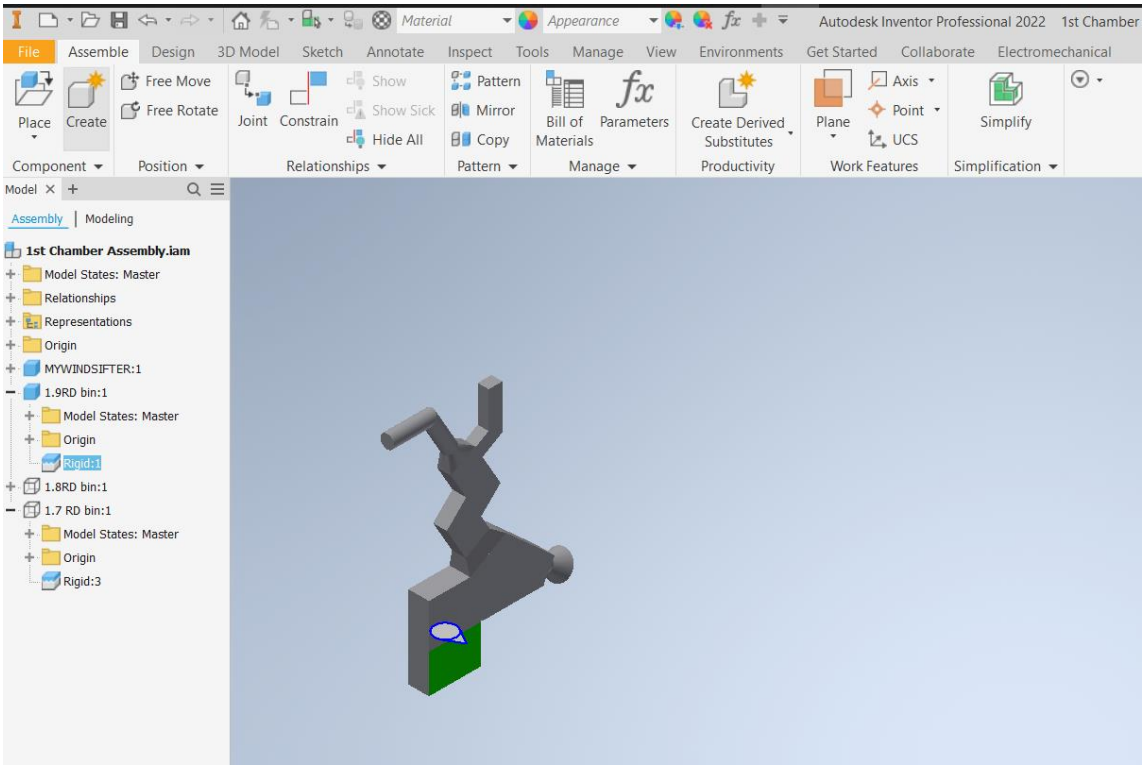


Figure C - 36: Attaching the bins as an assembly



Figure C - 37: The completed chamber 1

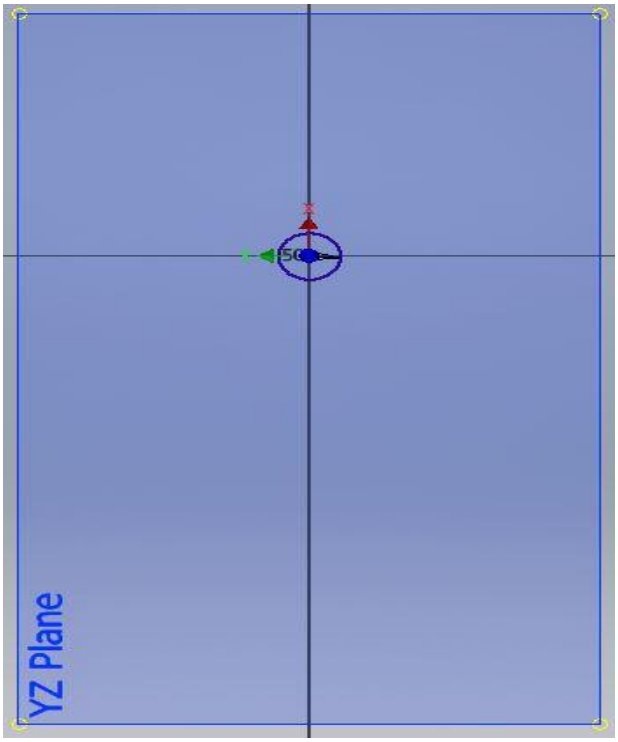


Figure C - 38: Circle of 50 mm for the Inlet Diffuser for the second chamber

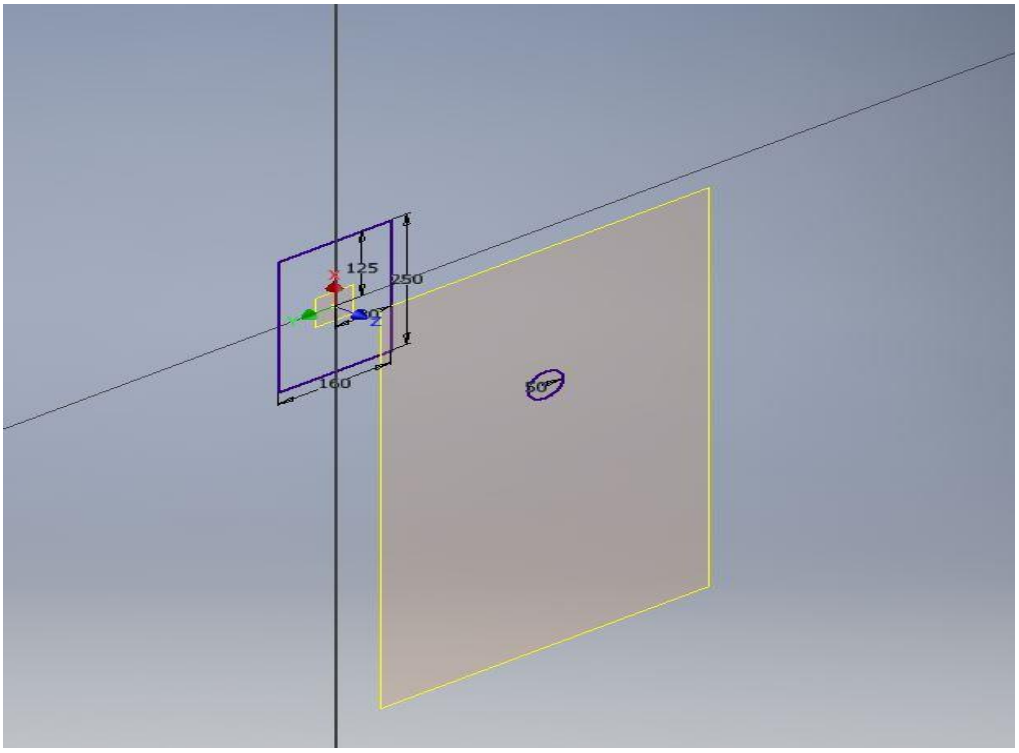


Figure C - 39: Drawing of the Inlet diffuser-transition piece of the second chamber

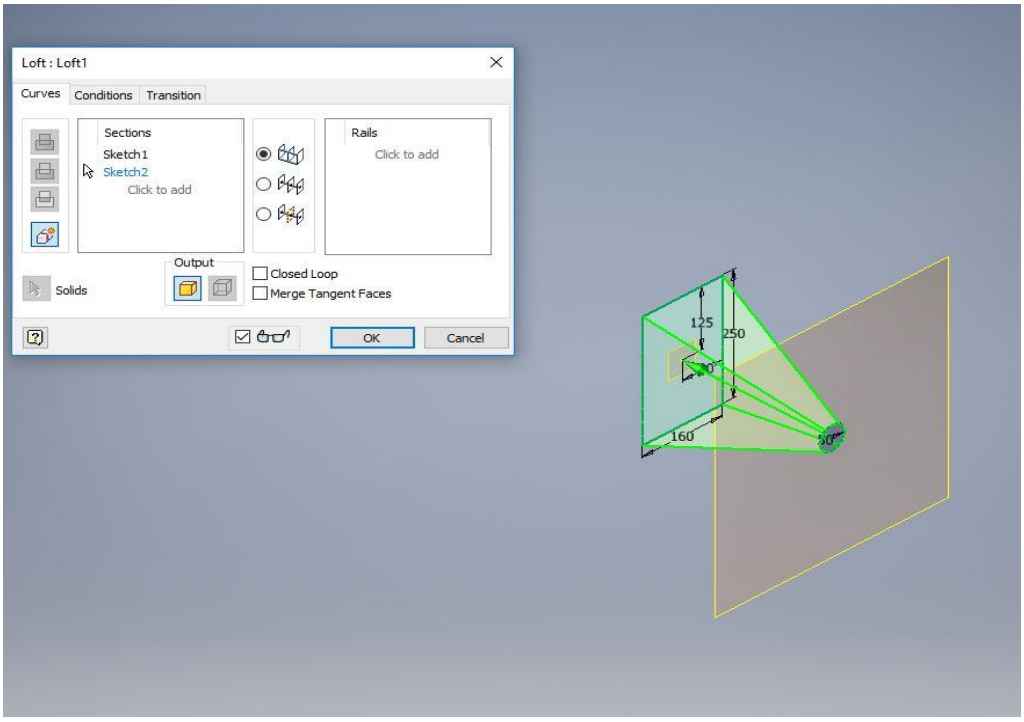


Figure C - 40: First diffuser transition piece created using the “loft” tool

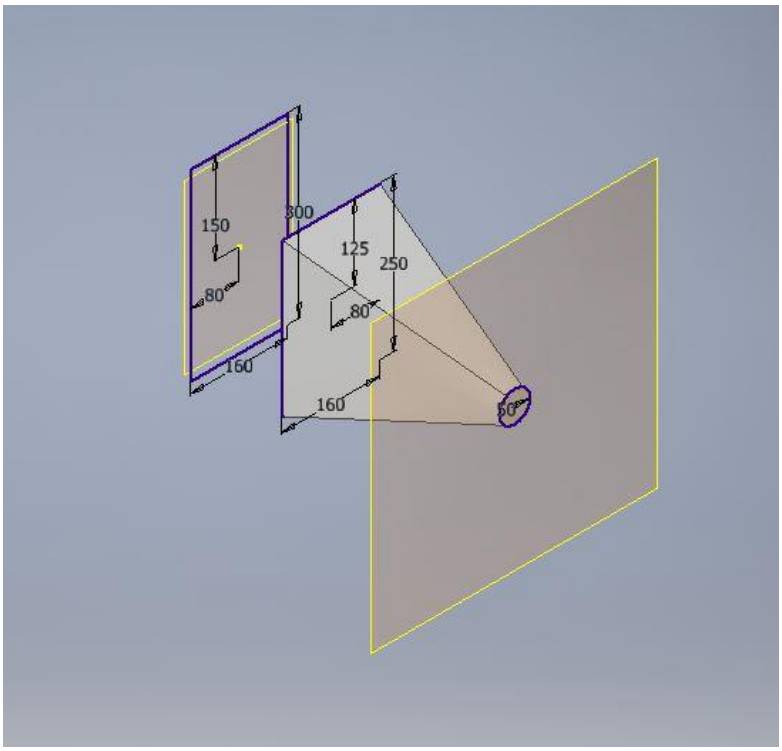


Figure C - 41: Drawing the first loft of the second chamber

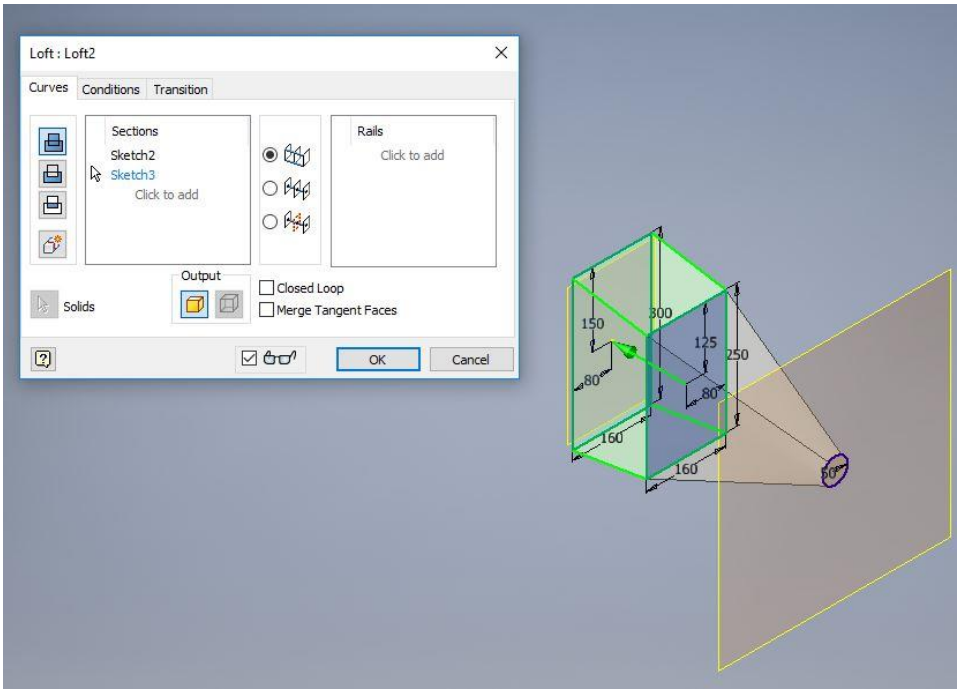


Figure C - 42: Second loft for second chamber

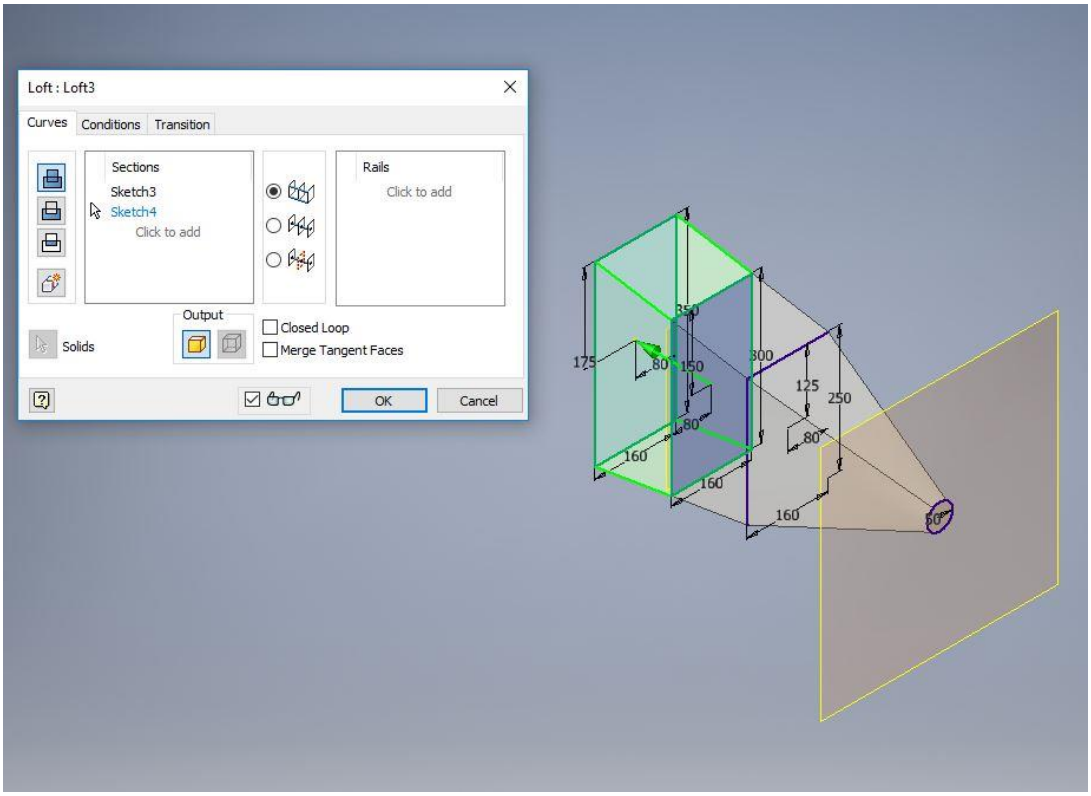


Figure C - 43: Third loft for the second chamber

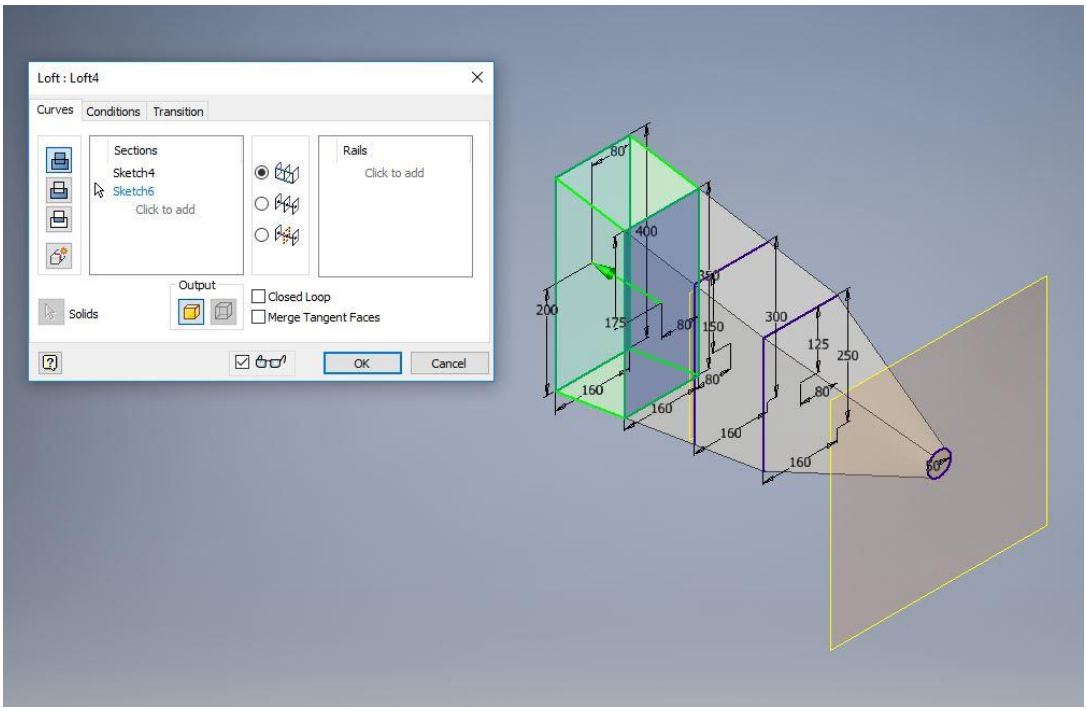


Figure C - 44: Fourth loft for the second chamber

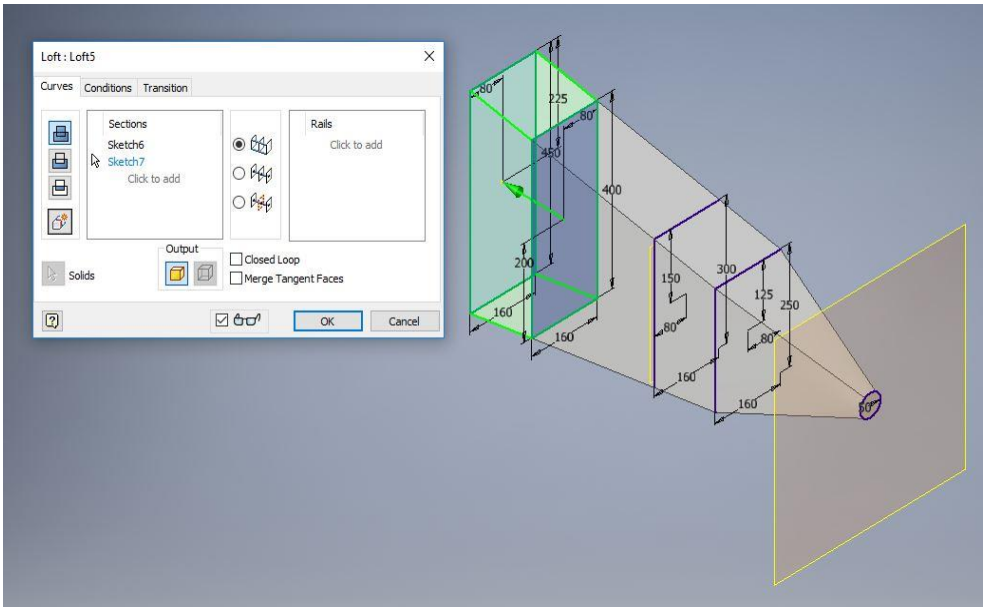


Figure C - 45: Fifth loft for the second chamber

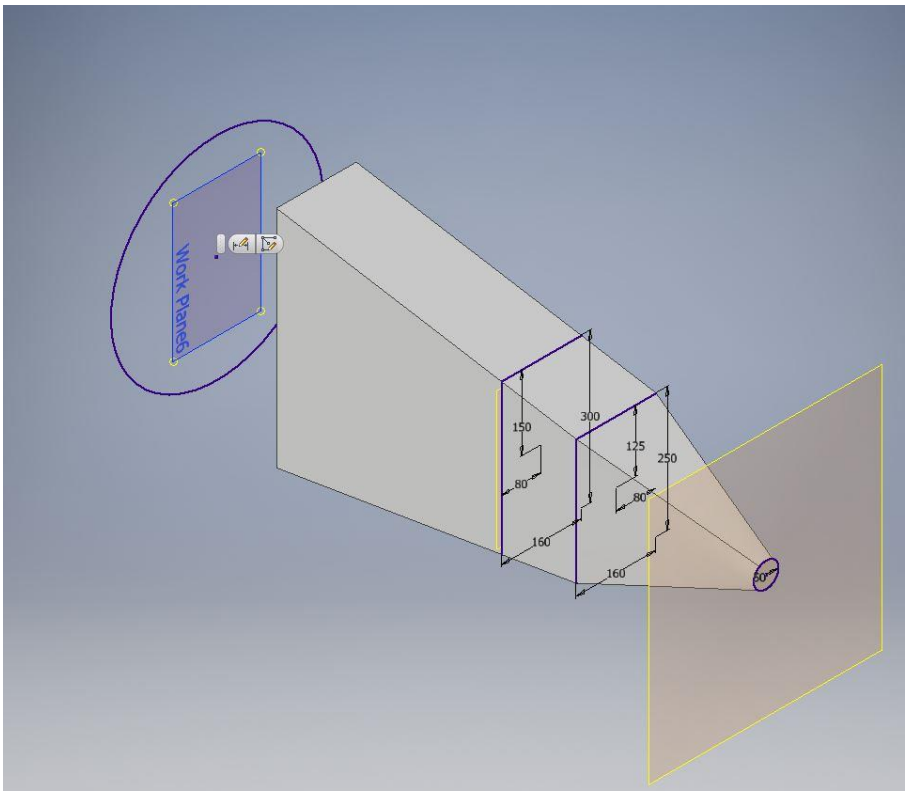


Figure C - 46: Circular Outline for the circular transition piece in the second chamber

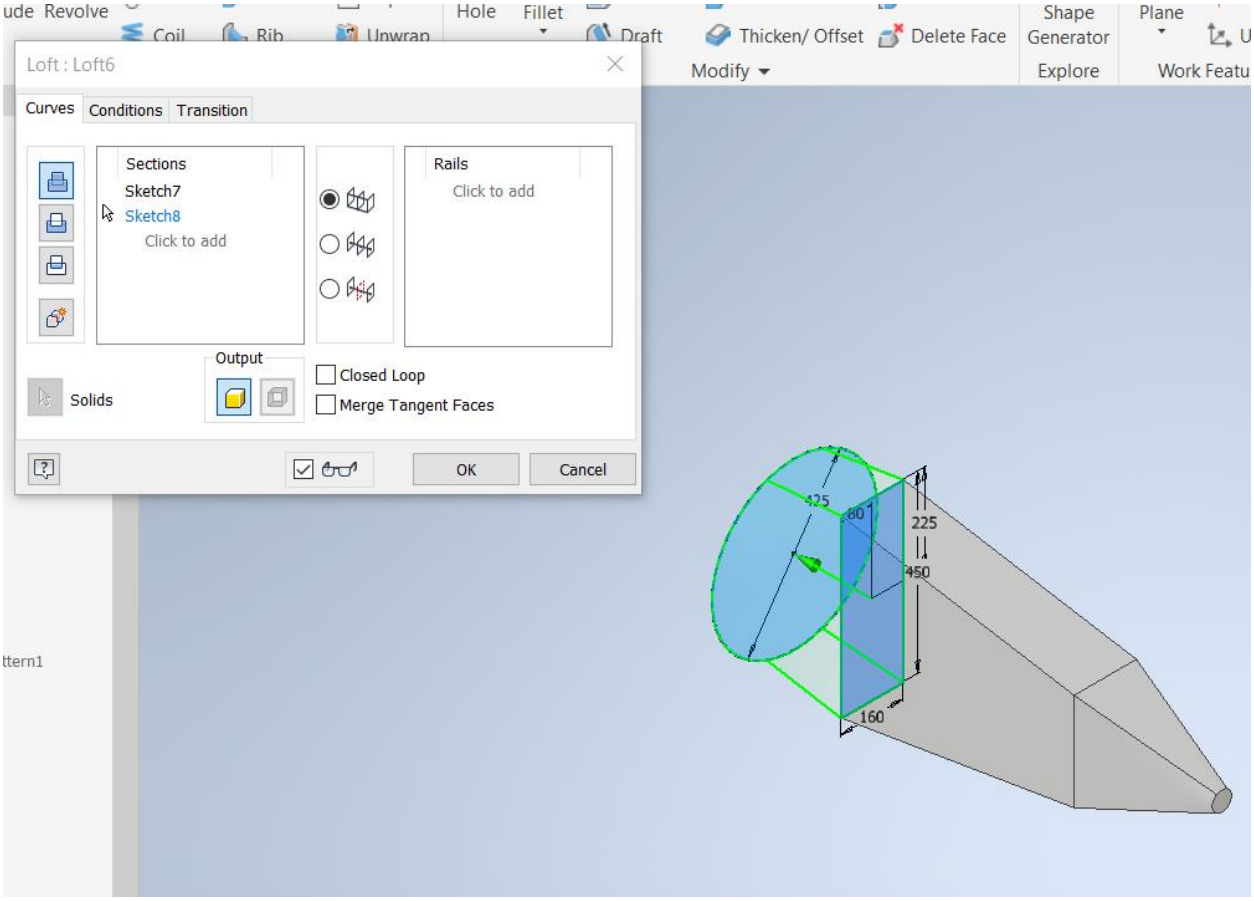


Figure C - 47: Circlular loft for the second chamber

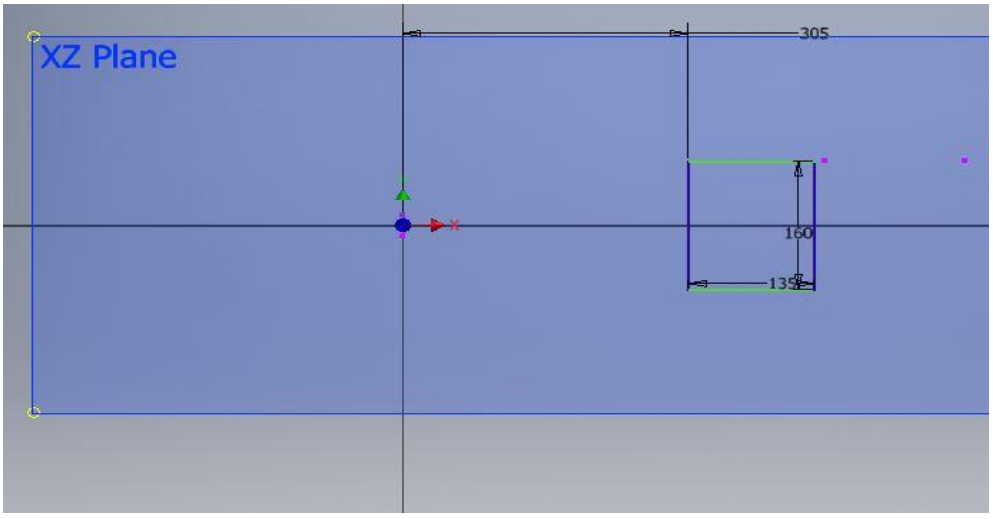


Figure C - 48: XZ plane selected to draw the pipes of the second chamber

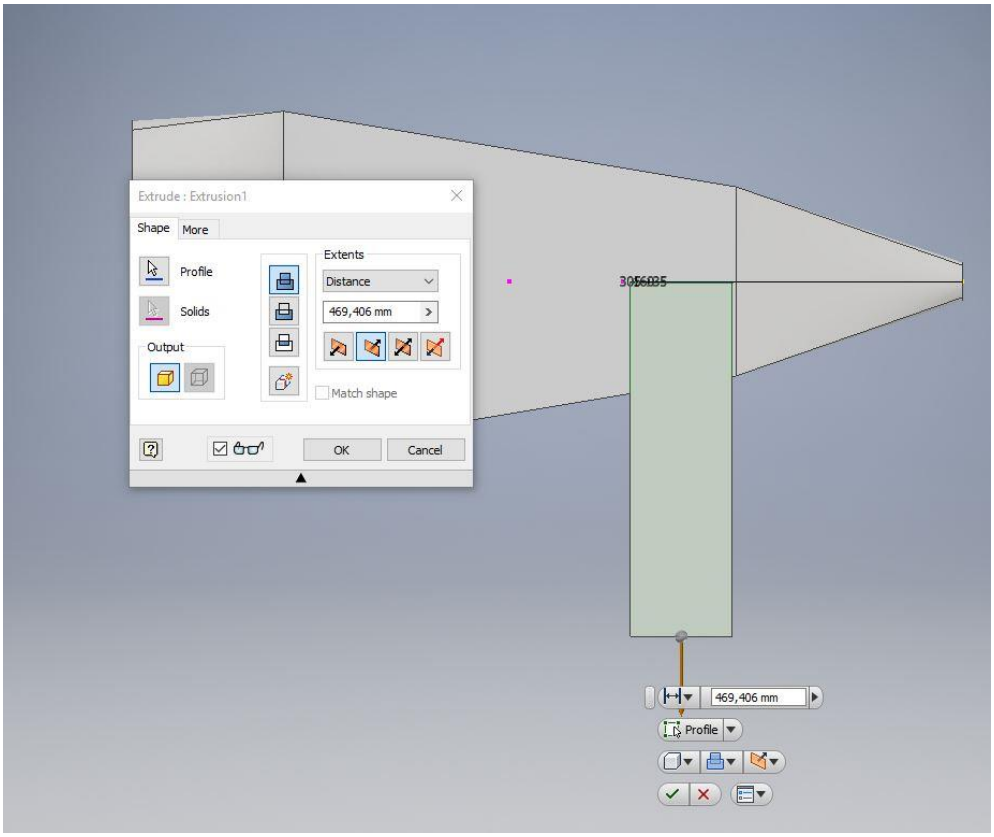


Figure C - 49: Extrusion of the pipe for the collection bin of the second chamber

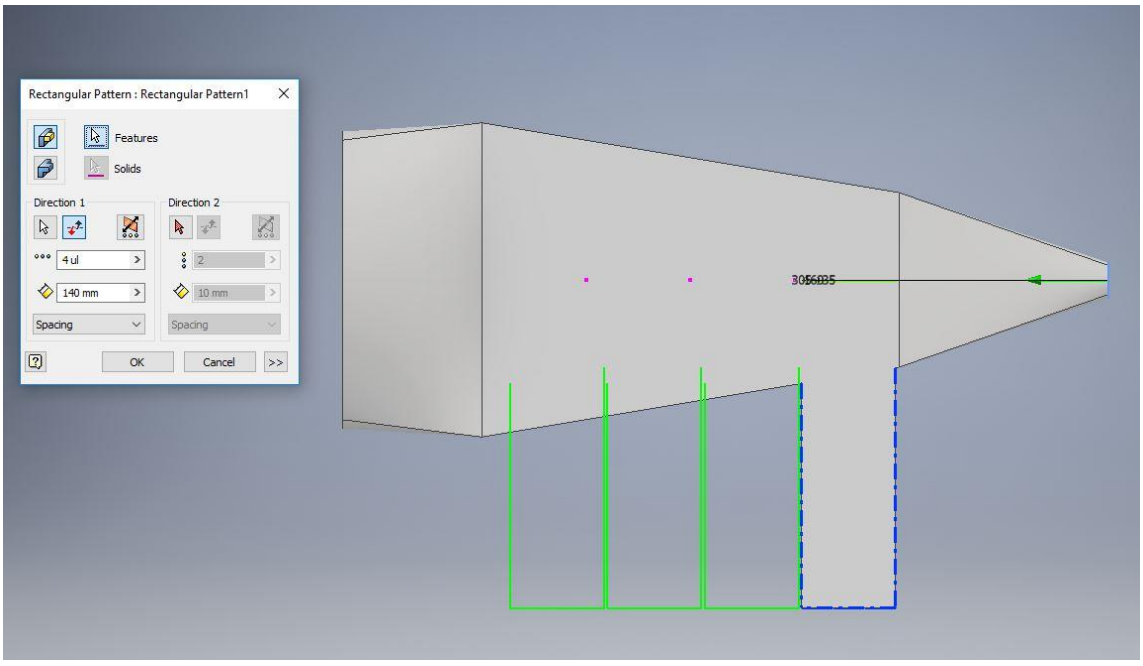


Figure C - 50: Using “Repeated Pattern” tool to design the remaining pipes for the collection bins

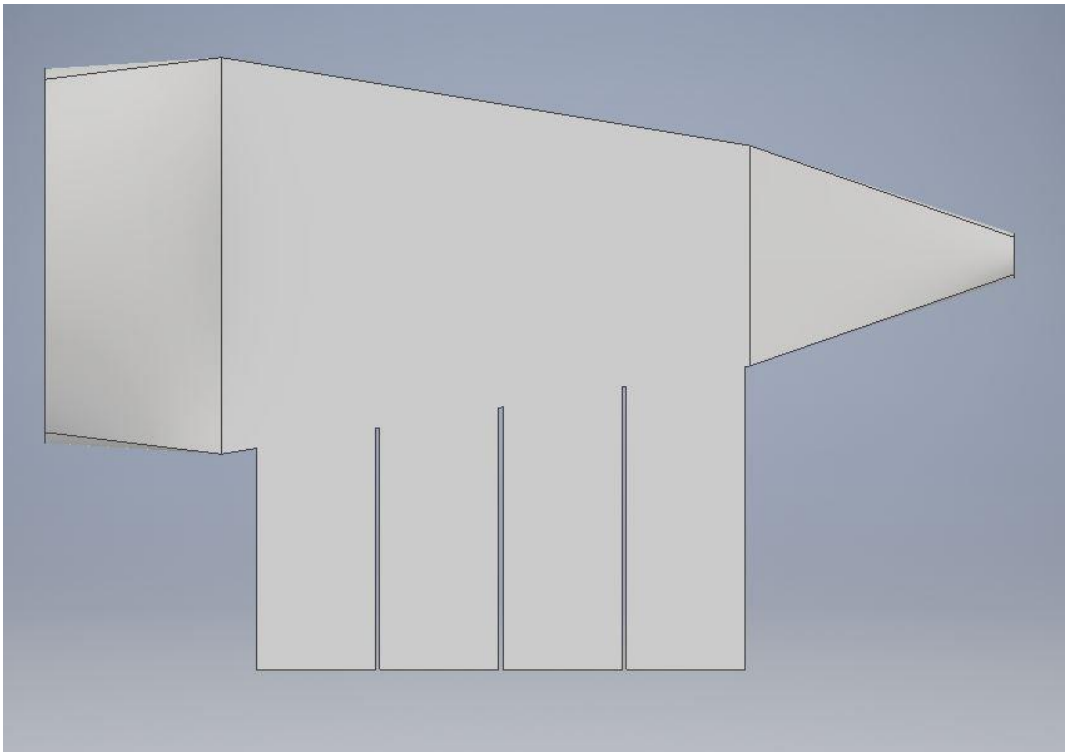


Figure C - 51: The partly completed section of the second chamber

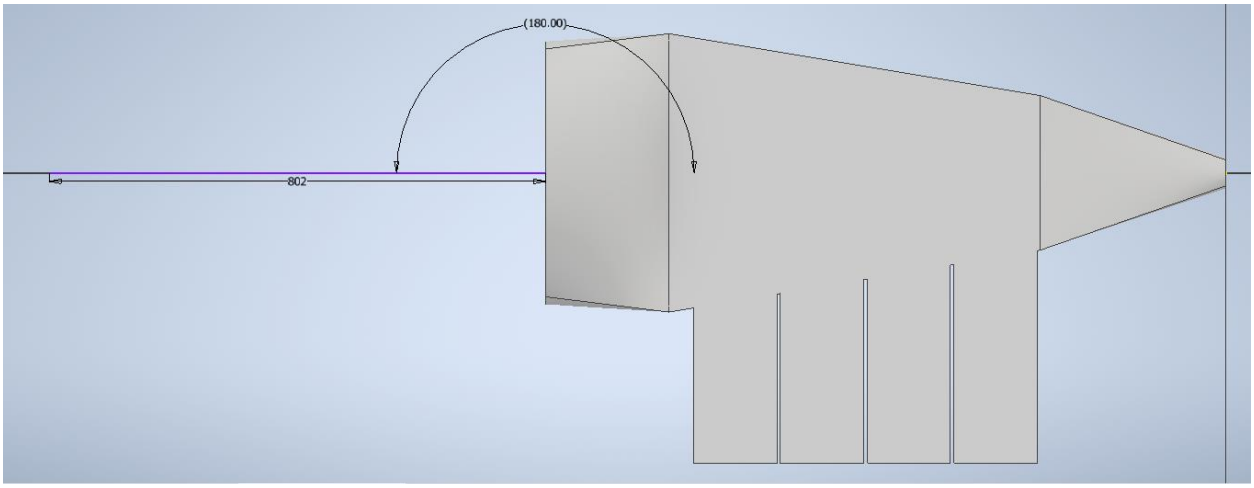


Figure C - 52: Drawing of the filter section

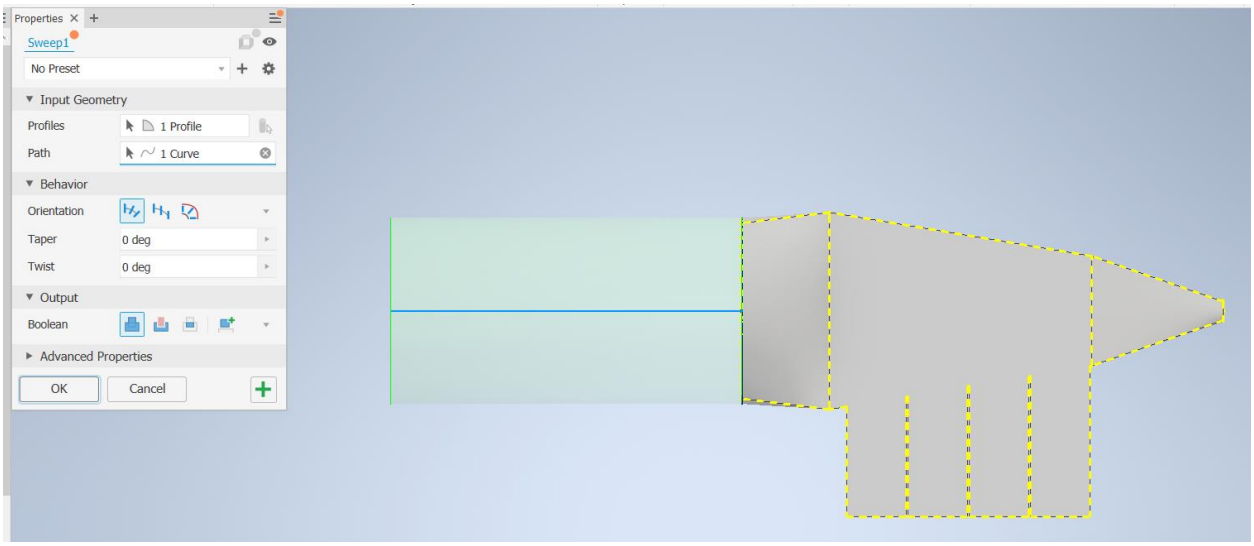


Figure C - 53: Completing the filter section using the “Sweep” tool.

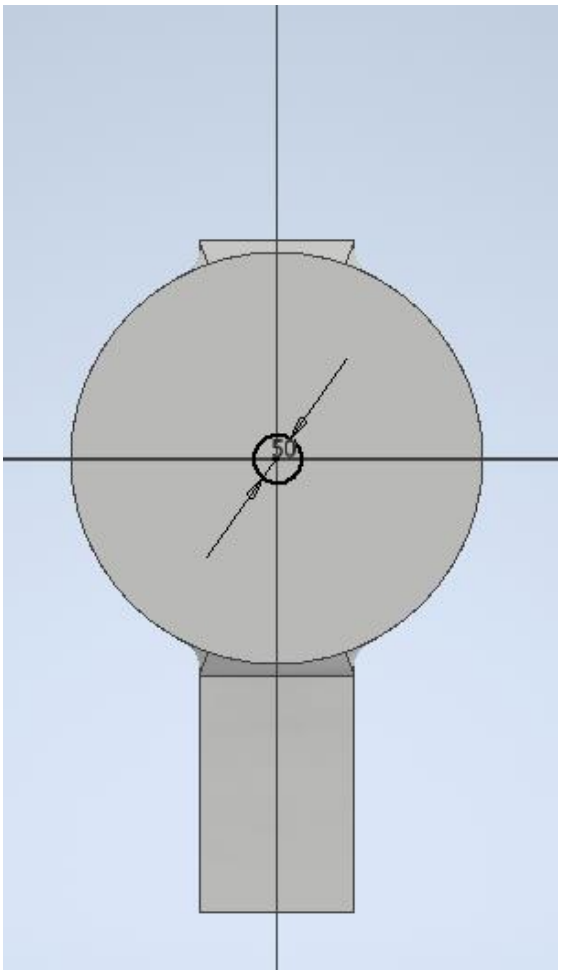


Figure C - 54: Designing the nozzle-transition piece for the Air outlet

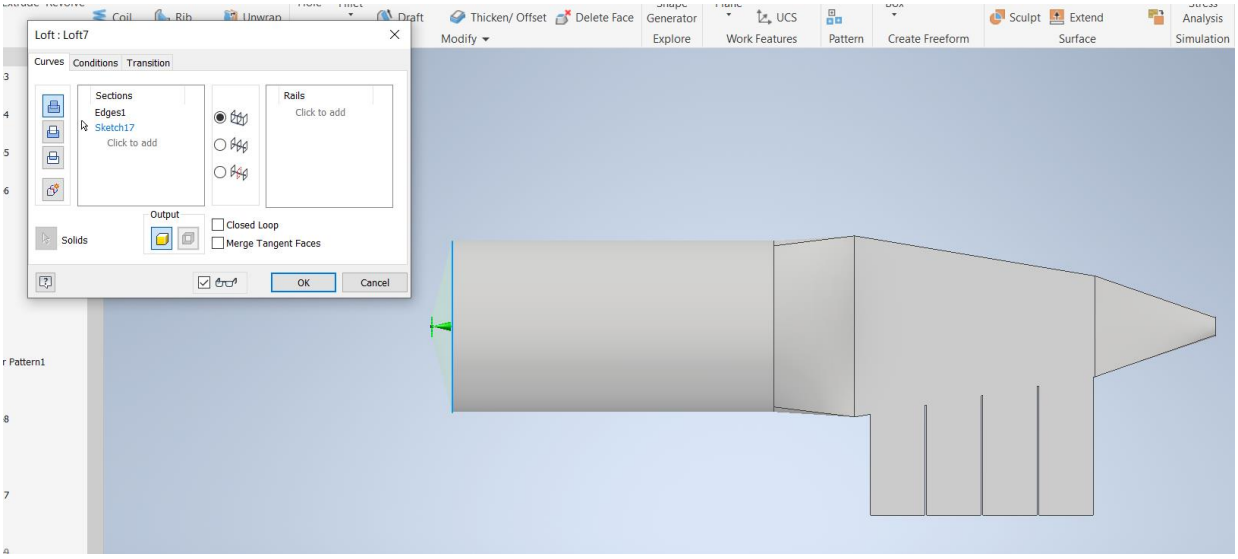


Figure C - 55: Completing the nozzle-transition piece for the Air outlet

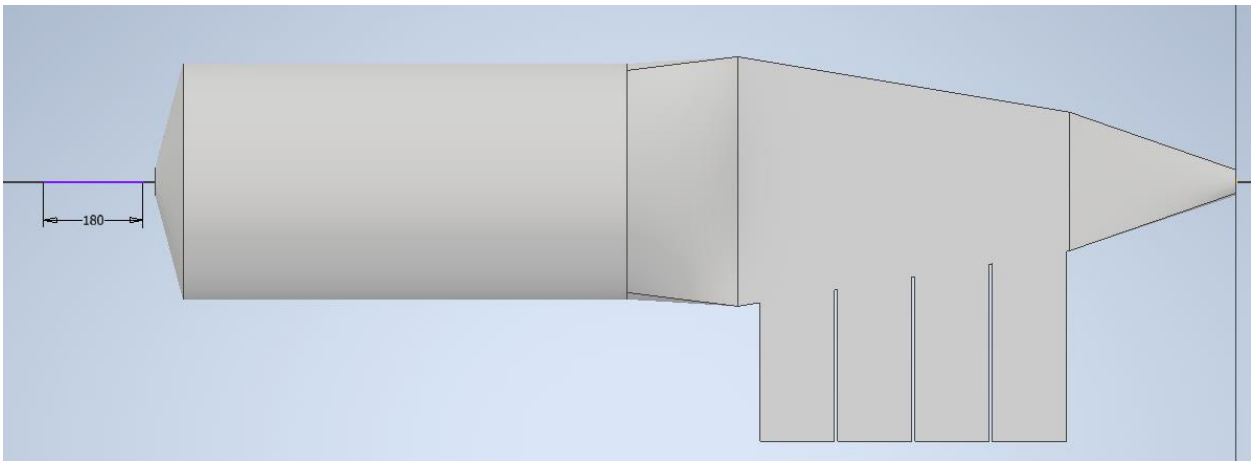


Figure C - 56: Designing outlet port

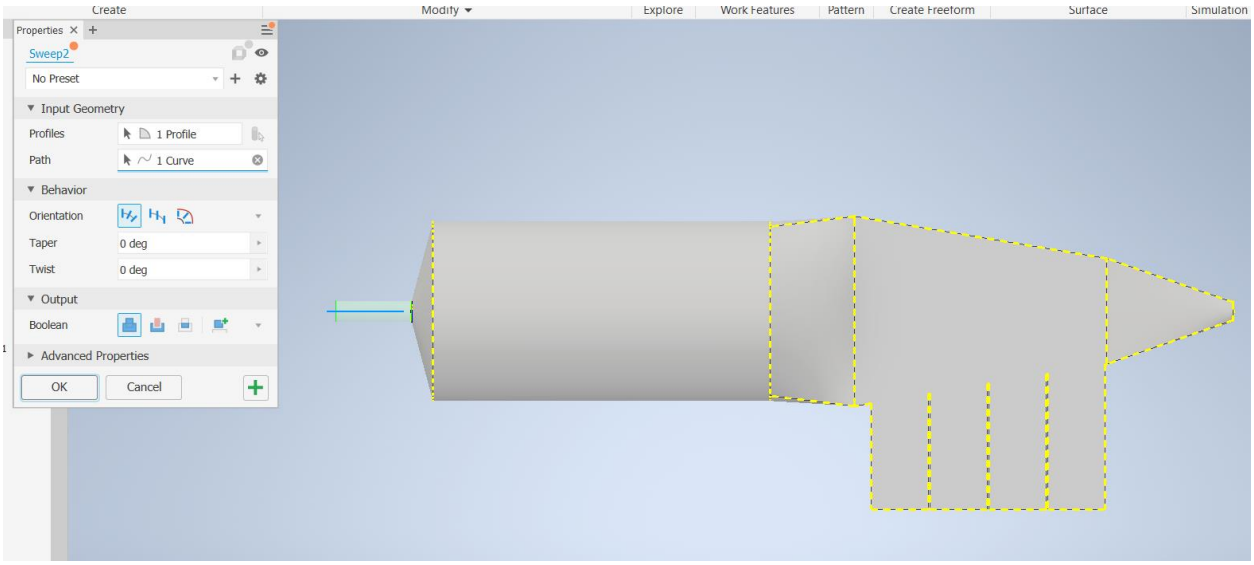


Figure C - 57:Completing the outlet port using the “Sweep” tool.

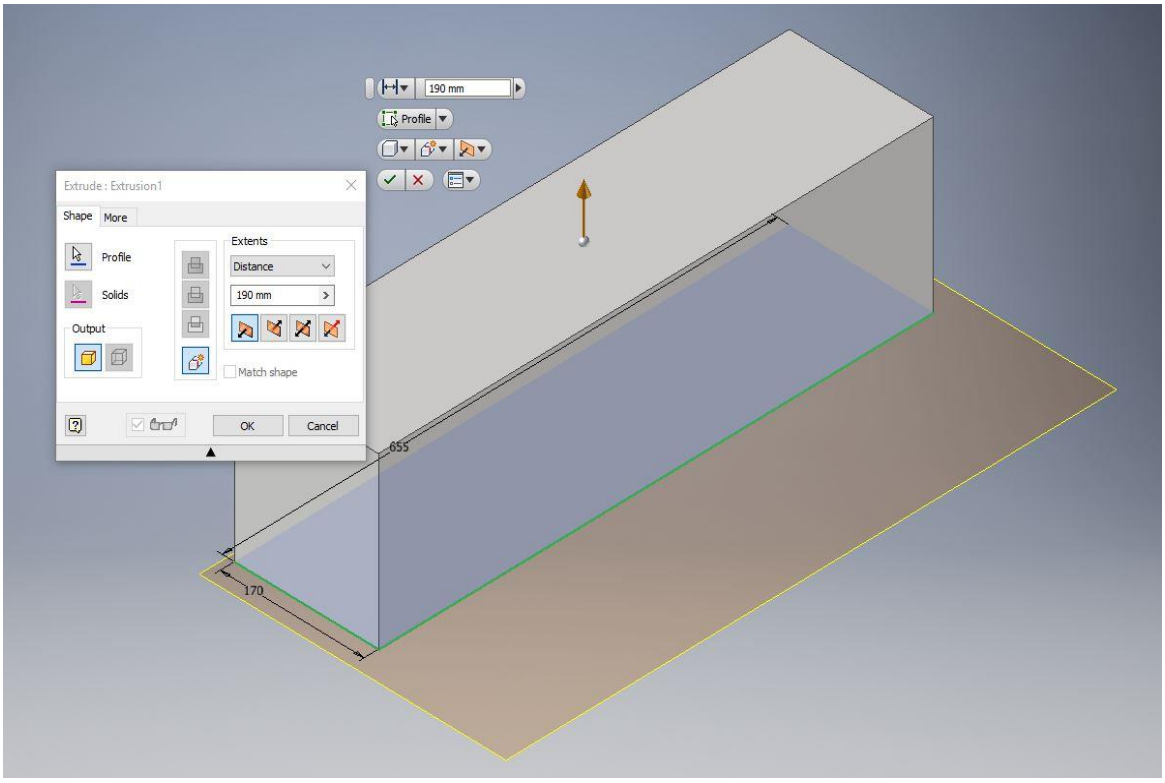


Figure C - 58: Designing the base section of the collecting bins

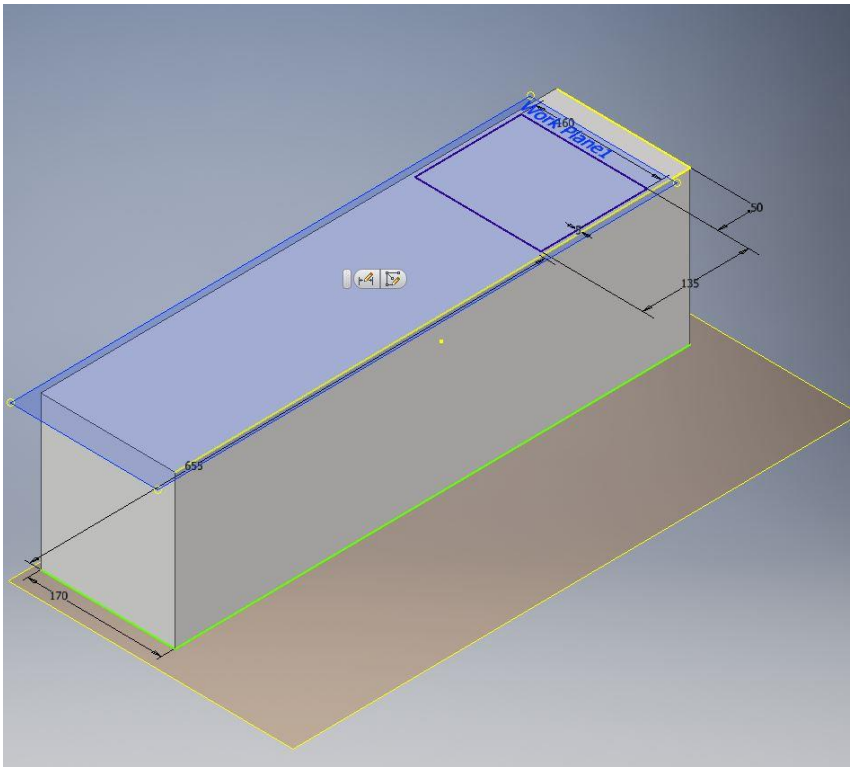


Figure C - 59: Outline for the connecting pipes of the base section

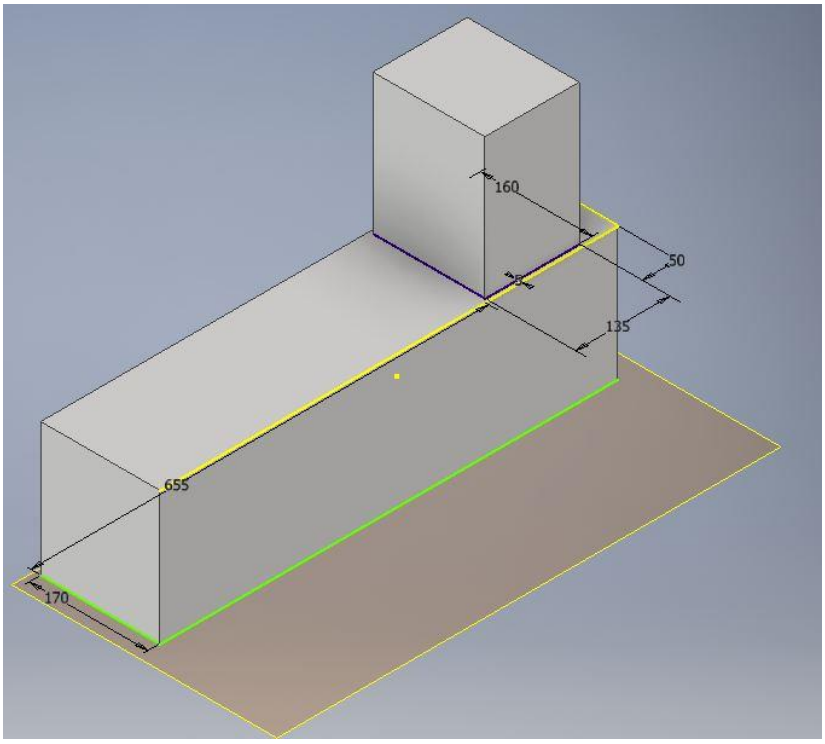


Figure C - 60: The Extruded outline

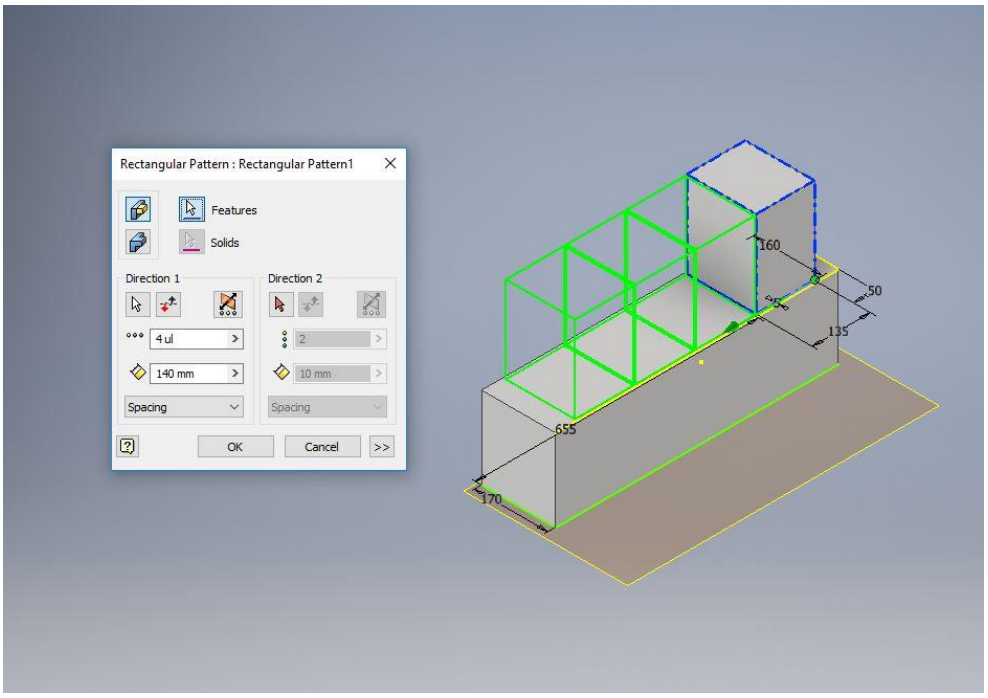


Figure C - 61:Drawing of the remaining connecting pipes using the “Rectangular Pattern”

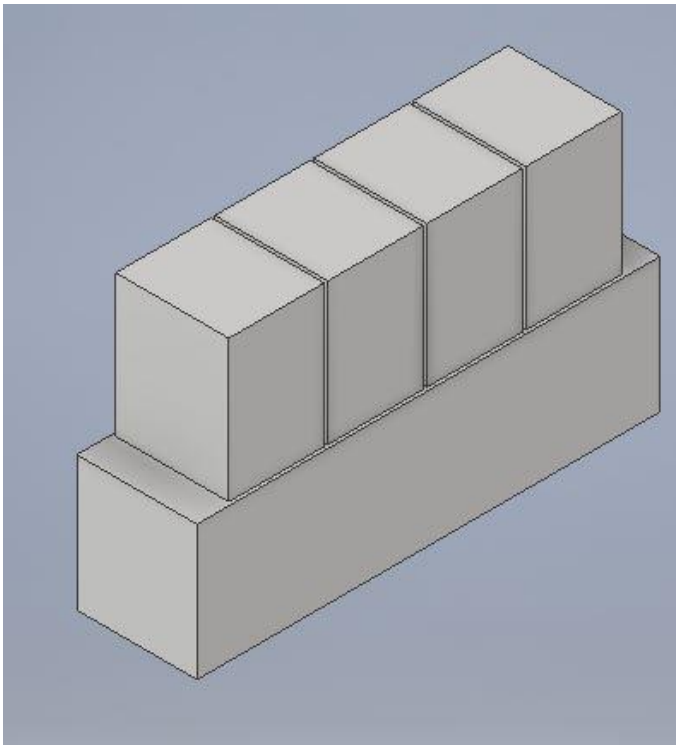


Figure C - 62: The completed bottom section for the second chamber

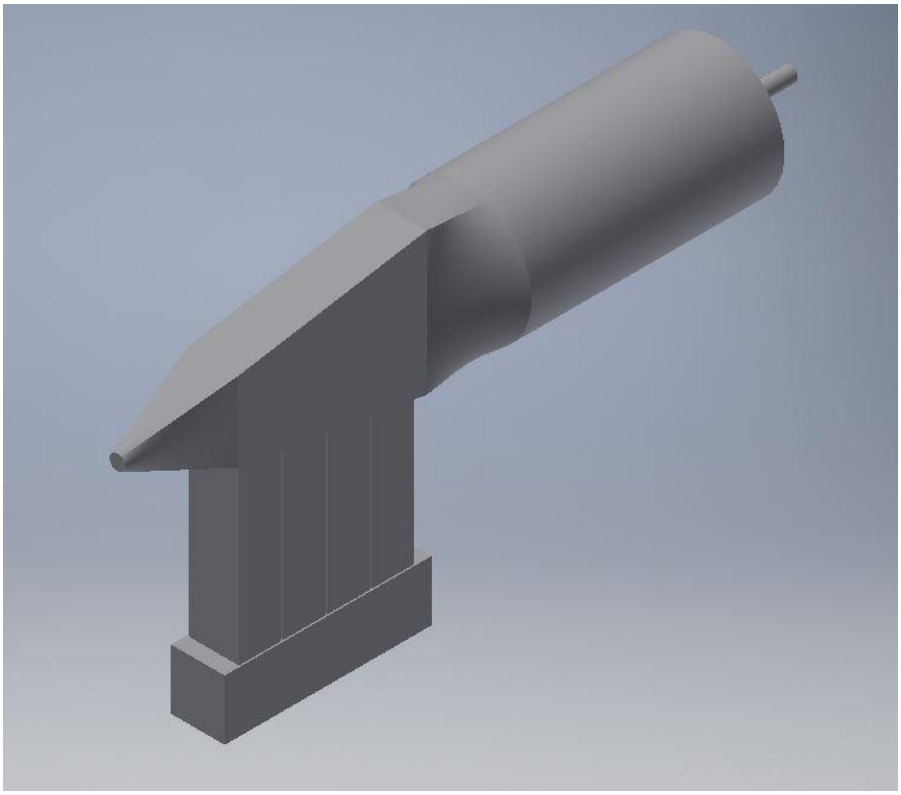


Figure C - 63: The second chamber after assembling